

THE APPLICATION OF ELECTROCHEMISTRY AND ORGANIC
CHEMISTRY IN POLYMER SYNTHESIS AND BATTERY ELECTRODE
DESIGN

A Dissertation

Presented to the Faculty of the Graduate School
of Cornell University

In Partial Fulfillment of the Requirements for the Degree of
Doctor of Philosophy

by

Brian Mark Peterson

August 2020

© 2020 Brian Mark Peterson

THE APPLICATION OF ELECTROCHEMISTRY AND ORGANIC
CHEMISTRY IN POLYMER SYNTHESIS AND BATTERY ELECTRODE
DESIGN

Brian Mark Peterson, Ph. D.

Cornell University 2020

The following chapters detail the use of electrochemistry in synthesizing multiblock copolymers from a single solution and the application of organic polymer cathodes as high-rate cathode materials. Chapter two focuses on the development of a cationic polymerization of isobutyl vinyl ether, utilizing an electric stimulus to control polymer initiation, propagation and reversible termination. Chapters three and four pair electrochemically-controlled cationic polymerizations with photocontrolled radical polymerizations and report methods to synthesize block copolymers of vinyl ethers and methyl acrylate. In chapters six through eight, organic polymer cathodes are reported which can tolerate high charge and discharge rates. In chapter nine, a relationship between polymer crystallinity and charge storage mechanism in organic cathodes is proposed, wherein disrupting ordering in the charge storage material results in less diffusion-limited charge storage processes.

BIOGRAPHICAL SKETCH

My story begins in Milwaukee, Wisconsin where I was born and found my love for all things Wisconsin. I completed my bachelor's degree across state at the University of Wisconsin – La Crosse on the Mississippi River. I continued to study chemistry at Cornell University. The following contains my findings over my course of study at Cornell.

ACKNOWLEDGMENTS

My family is my greatest source of strength. Throughout my life, my family has always stood with me. Thank you Mom and Dad, for always teaching me what parts of life lead to joy and happiness and which are distractions. Thank you for working every day to provide for me, Brad, Katie and Ali. Thank you to my brother Brad, and my cousin Ryan, for teaching me to hate losing, this has made me stronger. Thank you to my sister Katie for caring for my health and holding me accountable for my health. Thank you to my brother-in-law Colin for guiding my growth out of college and into adulthood. Thank you to my sister Ali for our morning conversations, for listening and for sharing. You and your family made 1200 miles feel like a much small distance. Thank you to my brother-in-law, Jason, for being an archetype of a good father and husband, for putting up with my faults over the years, and for being a good friend. Thank you to my Aunt Jolyn for being an outlet for help when I needed it. Thank you to my Grandmother for my ten aunts and uncles and over 50 cousins. Thank you for being the matriarch and teaching us how to live through faith and love.

Thank you to my advisor, Professor Brett P. Fors. Thank you for your leadership and mentorship, both academically and in life. I learned to believe in myself in all circumstances, familiar or unfamiliar. By your example, I learned to discard fear and ego in learning new things. I am lucky to have worked with you, and learned from you over the last five years. Thank you to my co-advisors, Professor Héctor D. Abruña and Professor Geoff W. Coates. Thank you for your support and thank you for being approachable and helpful when I needed guidance.

Thanks to all of my lab mates in the Fors lab. I was fortunate to have

directly worked with four undergraduates Yu-Chi Mason Wu, Gerickson Lopez, Kirkland Sugrim, and Colleen Trainor. I hope that you learned as much from me as I learned from working with each of you. I am especially thankful to Dillon Gentekos, Parker Singleton, Quentin Michaudel, Renee Sifri, Stephanie Rosenbloom, and Erin Stache. You each have been particularly impactful in helping me through graduate school. Thank you Dillon for being normal and helping me keep perspective. Thank you Parker for being unique and challenging my preconceived notions. Thank you Quentin for your enthusiasm for chemistry, for getting me out of lab, and for teaching me about finding a good life-balance. Thank you Renee for promoting my growth and taking on personal challenges together. Thank you Stephanie for making me feel valued when I didn't value myself. Thank you Erin for being a good friend and for being a fan of the Green Bay Packers.

Thank you to my incoming class of PhD candidates and all those that I relied on in my first year at Cornell. I had an outstanding group surrounding me through classes (Omar, Paden, Matt, Sean, Keith, Parker, Max). From homework on football Sundays to Pi-Farm parties, you all had a massive impact on my transition from undergrad to graduate school. Thank you all for your friendship and support during that challenging transition. Thank you Omar Valez-Padilla for being a great friend during challenges in my life over the last five years. A special thank you to Alicia Cintora for being a great listener, helping me stay grounded, and keep perspective. Thank you to my friends Bryce, Mike, Greg, and Alex. You were all a fresh reminder to enjoy myself and golf more. Thank you to Grace. Thank you for your support and love, you are my partner and I love growing with you.

TABLE OF CONTENTS

List of Figures	x
List of Tables	xvii
1. Introduction of Method Development of Electrochemical Polymerizations and Switching Polymerization Mechanisms	1
1.1. Introduction	1
1.2. State of the Field	2
1.3. References	5
2. Electrochemically Controlled Cationic Polymerization of Vinyl Ethers	8
2.1. Abstract	8
2.2. Introduction	8
2.3. Results and Discussions	10
2.4. Conclusion	19
2.5. References	19
2.6. Appendix	23
3. On Demand Switching of Polymerization Mechanism and Monomer Selectivity with Orthogonal Stimuli	58
3.1. Abstract	58
3.2. Introduction	59
3.3. Results and Discussion	62
3.4. Conclusion	72
3.5. References	73
3.6. Appendix	79
4. Dual Stimuli Switching: Interconverting Cationic and Radical Polymerization with Electricity and Light	102
4.1. Abstract	102

4.2.	Introduction _____	103
4.3.	Results and Discussion _____	106
4.4.	Conclusion _____	115
4.5.	References _____	116
4.6.	Appendix _____	119
5.	Introduction to the Design and Performance of Amorphous Organic Electrodes _____	164
5.1.	Introduction _____	164
5.2.	Discussion _____	165
5.3.	References _____	177
6.	Phenothiazine-Based Polymer Cathode Materials with Ultra-High Power Densities for Lithium Ion Batteries _____	184
6.1.	Abstract _____	184
6.2.	Introduction _____	184
6.3.	Results and Discussion _____	187
6.4.	Conclusion _____	195
6.5.	References _____	195
6.6.	Appendix _____	198
	6.6.1. Appendix References _____	222
7.	Elucidation of the Electrochemical Behavior of Phenothiazine-Based Polyaromatic Amines _____	228
7.1.	Abstract _____	228
7.2.	Introduction _____	228
7.3.	Results and Discussion _____	231
	7.3.1. Synthesis of Redox Active Small Molecule _____	231
	7.3.2. Electropolymerization of Thin-Film P2-TF _____	233

7.3.3.	Electrochemical Quartz Crystal Microbalance _____	236
7.4.	Conclusion _____	241
7.5.	References _____	241
7.6.	Experimental _____	244
7.7.	Appendix _____	249
8.	Cross-Linking Effects on Performance Metrics of Phenazine-Based Polymer Cathodes _____	266
8.1.	Abstract _____	266
8.2.	Introduction _____	266
8.3.	Results and Discussion _____	269
8.4.	Reference _____	289
8.5.	Appendix _____	293
9.	The Effects of Ordering and Morphology on Charge Storage Mechanism in Organic Cathode Materials _____	330
9.1.	Introduction _____	330
9.2.	Experimental Section _____	333
9.3.	Results and Discussion _____	334
9.4.	Conclusion _____	345
9.5.	Reference _____	346

LIST OF FIGURES

Figure 2.1	10
Figure 2.2	11
Figure 2.3	14
Figure 2.4	15
Figure 2.5	17
Figure 2.6	18
Figure 2.7	28
Figure 2.8	30
Figure 2.9	32
Figure 2.10	32
Figure 2.11	33
Figure 2.12	33
Figure 2.13	34
Figure 2.14	36
Figure 2.15	36
Figure 2.16	37
Figure 2.17	38
Figure 2.18	39
Figure 2.19	40
Figure 2.20	41
Figure 2.21	42
Figure 2.22	43
Figure 2.23	44
Figure 2.24	45
Figure 2.25	46

Figure 2.26	47
Figure 2.27	48
Figure 2.28	49
Figure 2.29	53
Figure 2.30	54
Figure 2.31	54
Figure 2.32	56
Figure 3.1	61
Figure 3.2	63
Figure 3.3	66
Figure 3.4	68
Figure 3.5	70
Figure 3.6	71
Figure 3.7	83
Figure 3.8	84
Figure 3.9	85
Figure 3.10	86
Figure 3.11	87
Figure 3.12	88
Figure 3.13	90
Figure 3.14	91
Figure 3.15	92
Figure 3.16	95
Figure 3.17	96
Figure 3.18	98
Figure 3.19	99

Figure 4.1	105
Figure 4.2	107
Figure 4.3	111
Figure 4.4	112
Figure 4.5	114
Figure 4.6	123
Figure 4.7	128
Figure 4.8.a	130
Figure 4.8.b	130
Figure 4.9.a	131
Figure 4.9.b	131
Figure 4.10.a	132
Figure 4.10.b	132
Figure 4.11.a	133
Figure 4.11.b	133
Figure 4.12.a	134
Figure 4.12.b	134
Figure 4.13.a	135
Figure 4.13.b	135
Figure 4.14.a	136
Figure 4.14.b	136
Figure 4.15	139
Figure 4.16	142
Figure 4.17	143
Figure 4.18	144
Figure 4.19	146

Figure 4.20	147
Figure 4.21	149
Figure 4.22	149
Figure 4.23	151
Figure 4.24	152
Figure 4.25	154
Figure 4.26	154
Figure 4.27	156
Figure 4.28	157
Figure 4.29	159
Figure 4.30	159
Figure 4.31	162
Figure 4.32	162
Figure 6.1	186
Figure 6.2	188
Figure 6.3	189
Figure 6.4	192
Figure 6.5	193
Figure 6.6	194
Figure 6.7	202
Figure 6.8	203
Figure 6.9	203
Figure 6.10	204
Figure 6.11	204
Figure 6.12	205
Figure 6.13	205

Figure 6.14	219
Figure 6.15	220
Figure 6.16	220
Figure 6.17	221
Figure 6.18	221
Figure 7.1	231
Figure 7.2	232
Figure 7.3	234
Figure 7.4	237
Figure 7.5	252
Figure 7.6	253
Figure 7.7	254
Figure 7.8	255
Figure 7.9	256
Figure 7.10	257
Figure 7.11	258
Figure 7.12	260
Figure 7.13	262
Figure 7.14	263
Figure 7.15	264
Figure 7.16	265
Figure 8.1	271
Figure 8.2	273
Figure 8.3	279
Figure 8.4	281
Figure 8.5	283

Figure 8.6	301
Figure 8.7	302
Figure 8.8	304
Figure 8.9	305
Figure 8.10	306
Figure 8.11	307
Figure 8.12	308
Figure 8.13	309
Figure 8.14	310
Figure 8.15	311
Figure 8.16	311
Figure 8.17	312
Figure 8.18	312
Figure 8.19	313
Figure 8.20	314
Figure 8.21	315
Figure 8.22	316
Figure 8.23	317
Figure 8.24	318
Figure 8.25	318
Figure 8.26	319
Figure 8.27	320
Figure 8.28	320
Figure 8.29	321
Figure 8.30	322
Figure 8.31	323

Figure 8.32	323
Figure 8.33	324
Figure 8.34	325
Figure 8.35	327
Figure 8.36	328
Figure 9.1	335
Figure 9.2	336
Figure 9.3	337
Figure 9.4	340
Figure 9.5	342
Figure 9.6	345

LIST OF TABLES

Table 2.1	12
Table 2.2	16
Table 2.3	34
Table 2.4	51
Table 2.5	55
Table 2.6	55
Table 3.1	65
Table 3.2	82
Table 3.3	101
Table 4.1	109
Table 4.2	127
Table 4.3	129
Table 4.4	142
Table 6.1	206
Table 6.2	206
Table 8.1	272
Table 8.2	274
Table 8.3	277
Table 8.4	303
Table 8.5	316
Table 8.6	326
Table 9.1	338

PREFACE

This thesis was predominantly adapted from the following published articles co-written by the author:

Peterson, B. M.; Lin, S.; Fors, B. P. Electrochemically Controlled Cationic Polymerization of Vinyl Ethers. *J. Am. Chem. Soc.* **2018**, *140*, 2076.

Peterson, B. M.; Kottisch, V.; Supej, M. J.; Fors, B. P. On Demand Switching of Polymerization Mechanism and Monomer Selectivity with Orthogonal Stimuli. *ACS Cent. Sci.* **2018**, *4*, 1228.

Supej, M. J.; Peterson, B. M.; Fors, B. P. Dual Stimuli Switching: Interconverting Cationic and Radical Polymerizations with Electricity and Light. *Chem.* Accepted.

Peterson, B. M.; Ren, D.; Shen, L.; Wu, Y-C. M.; Ulgut, B.; Coates, G. W.; Abruña, H. D.; Fors, B. P. Phenothiazine-Based Polymer Cathode Materials with Ultrahigh Power Densities for Lithium Ion Batteries. *ACS Appl. Energy Mater.* **2018**, *1*, 3560.

Peterson, B. M.; Shen, L.; Lopez, G. J.; Gannett, C. N.; Ren, D.; Abruña, H. D.; Fors, B. P. Elucidation of the electrochemical behavior of phenothiazine-based polyaromatic amines. *Tetrahedron*, **2019**, *75*, 4244.

Gannett, C. N.; Peterson, B. M.; Shen, L.; Seok, J.; Fors, B. P.; Abruña, H. D. Cross-linking Effects on Performance Metrics of Phenazine-Based Polymer Cathodes. *ChemSusChem* **2020**, *13*, 2428.

Chapters 1 of this thesis was written as an introduction to the use of external stimuli to synthesize block copolymers.

Chapter 5 of this thesis was adapted from a review in preparation in collaboration with Cara N. Gannett, Luis Melecio-Zombrano, Monica Jo Theibault. The review was adapted to serve as an introduction to battery electrode materials and factors affecting energy density and power density.

Chapter 9 of this thesis was adapted from a manuscript in preparation in collaboration with Cara N. Gannett.

CHAPTER 1

INTRODUCTION TO METHOD DEVELOPMENT OF ELECTROCHEMICAL POLYMERIZATIONS AND SWITCHING POLYMERIZATION MECHANISMS

1.1 Introduction

While 'living' polymerizations are known for their ability to provide control over molecular weights (M_n) and dispersity (\mathcal{D}), their most prominent use is in the design of complex macromolecules such as multi-block copolymers. The living nature of the polymer allows each chain end to be extended upon exposure to additional monomer leading to complex macromolecular structure.¹ Szwarc and coworkers provided one of the first examples of a living polymerization, wherein the poly(styrene-*b*-isoprene) was synthesized through an anionic mechanism, by treating styrene with sodium naphthalamide in tetrahydrofuran, followed by chain extension with isoprene.²

Block copolymers can be synthesized by a number of controlled polymerizations, including controlled radical polymerization (i.e. nitroxide mediated polymerizations (NMP), atom-transfer radical polymerizations (ATRP), and random-addition fragmentation chain-transfer polymerizations (RAFT)), single-site metal catalyzed olefin polymerization, and ring opening polymerizations. However, the scope of block copolymers synthesized by sequential addition of is restricted to monomers which can be polymerized by a given polymerization mechanism (cationic, radical, anionic). Herein, the

development of new methodologies to expand the scope of block copolymer synthesis through the use of external stimuli to control polymerization mechanism is reported.

External stimuli can be used to control initiation, propagation, and reversible termination in polymerizations.³ Light, electric potential, force, and temperature can all provide impetus to a polymerization in real time. Synthesis of complex multiblock structure can be achieved by alternating application and removal of at least two separate stimuli.⁴ By controlling the length of time each stimulus is applied, the length of each block can be precisely controlled. Additionally, the number of times the stimuli are alternated dictates the number of segments found within a given block copolymer. The following section provides the current state of external stimuli controlled polymerizations to synthesize multiblock copolymers and the subsequent chapters detail the contributions my coworkers and I have made to this expanding field.

1.2 State of the Field

Block copolymers can be synthesized by changing the selectivity or reactivity of a metal catalyst towards monomer classes by the controlling the redox state of a metal catalyst. In 2011, Diaconescu and coworkers reported a salen-based cerium catalyst, wherein the reactivity towards lactide polymerization could be activated or deactivated by reduction or oxidation with cobaltocene or ferrocene respectively.⁵ This work expanded in 2014, using group IV metal catalysts, such as titanium, with ferrocene-based ligands.⁶ The

ferrocene-based ligands can be chemically oxidized or reduced, providing a handle to change the reactivity of the active titanium center. In the reduced state, the titanium based catalyst was activated for *L*-Lactide polymerization and deactivated for ϵ -caprolactone polymerization. When oxidized with a ferrocenium salt, the catalyst became deactivated for *L*-lactide polymerization and activated for ϵ -caprolactone polymerization. Taking advantage of a chemical stimulus, the selectivity of the catalyst for the incorporation of either monomer could be controlled and multiblock copolymers of lactide, lactones, and caprolactone could be synthesized.⁷

In a similar manner, Byers and coworkers utilized a bis(imino)pyridine iron catalyst to generate block copolymers through the ring opening polymerization of epoxides and lactones.⁸ The iron(II) catalyst is selective for the lactide ring opening polymerization. When oxidized to iron(III), the catalyst is deactivated towards lactide ring opening polymerization and selectively polymerizes epoxides. By alternating redox states, through chemical stimuli, block copolymers can easily be synthesized. More recently, Byers and coworkers demonstrated that redox states could be alternated via electric potential and block copolymers could be synthesized from a single solution by varied application of electric potential.⁹ However, the challenge in generating block copolymers by controlling the oxidation states of metal catalysts lies in the difficulty of identifying catalysts with selectivity that entirely alternate monomer selectivity with redox states. There are still many opportunities to develop

methodology which allow control over the block structure of polymer branching, insertion mechanism, and stereocenters.

Switching between a radical RAFT polymerization mechanism and an ionic polymerization mechanism allows selectivity to be determined by the propagating species. Additionally, this approach can provide the synthesis of multiblock copolymers consisting of traditionally incompatible monomer pairings. You and coworkers successfully demonstrated switching between reaction mechanisms by combining a PET-RAFT and an anionic ring opening polymerization, controlled by photoirradiation and heat, respectively, to synthesize undecablock copolymers from a telechelic chain transfer agents.¹⁰ More recently, Boyer, Kamigaito, and Satoh reported the synthesis of block copolymers by pairing PET-RAFT polymerization with an acid-catalyzed cationic polymerization.¹¹ They demonstrate the ability to control the amount of propagating cations and radicals by exposing the reaction to different wavelengths of light irradiation. However, no formal switching between reaction mechanism was demonstrated.

These methodologies can lead to the discovery of new thermoplastic elastomers, push the frontiers of phase separation in block copolymers, and find application in advanced technologies like 3-D printing.¹² However, much more work is needed to expand the mechanisms and types of external stimuli that can be used for *in situ* polymer switching. Herein are presented contributions to the field in developing electrochemically controlled cationic polymerizations and the

pairing of the polymerizations with PET-RAFT mechanisms. This work was inspired by the development of acid-catalyzed cationic polymerizations developed by Kamigaito and Sugihara, as well as work done by Veronika Kottisch in photocontrolled cationic polymerizations.^{13,14}

1.3 References

- (1) Szwarc, N. *Nature* **1956**, *178*, 1168.
- (2) Szwarc, N.; Levy, M.; Milkovich, R. *J. Am. Chem. Soc.* **1956**, *78*, 2656.
- (3) Leibfarth, F. A.; Mattson, K. M.; Fors, B. P.; Collins, H. A.; Hawker, C. J. *Angew. Chem., Int. Ed.* **2013**, *52*, 199.
- (4) Bates, F. S.; Hillmyer, M. A.; Lodge, T. P.; Bates, C. M.; Delaney, K. T.; Fredrickson, G. H. *Science*, **2012**, *336*, 434.
- (5) Broderick, E. M.; Guo, N.; Wu, T.; Vogel, C. S.; Xu, C.; Sutter, J.; Miller, J. T.; Meyer, K.; Cantat, T.; Diaconescu, P. L. *Chem. Commun.*, **2011**, *47*, 9897.
- (6) Wang, X.; Thevenon, A.; Brosmer, J. L.; Yu, I.; Khan, S. I.; Mehrkhodavandi, P.; Diaconescu, P. L. *J. Am. Chem. Soc.* **2014**, *136*, 11264.
- (7) (a) Quan, S. M.; Wang, X.; Rongjia, Z.; Diaconescu, P. L. *Macromolecules* **2016**, *49*, 6768. (b) Lowe, M. Y.; Shu, S.; Quan, S. M.; Diaconescu, P. L. *Inorg. Chem. Front.* **2017**, *4*, 1798. (c) Dai, R.; Diaconescu, P. L. *Dalton Trans.* **2019**, *48*, 2996

- (8) (a) Biernesser, A. B.; Li, B.; Byers, J. A. *J. Am. Chem. Soc.* **2013**, *135*, 16553. (b) Biernesser, A. B.; Delle Chiaie, K. R.; Curley, J. B.; Byers, J. A. *Angew. Chem. Int. Ed.* **2016**, *55*, 5251. (c) Ortuño, M. A.; Dereli, B.; Delle Chiaie, K. R.; Biernesser, A. B.; Qi, M.; Byers, J. A.; Cramer, C. C. *Inorg. Chem.* **2018**, *57*, 2064.
- (9) Qi, M.; Dong, Q.; Wang, D.; Byers, J. A. *J. Am. Chem. Soc.* **2018**, *140*, 5686.
- (10) Zhang, Z., Zeng, T., Xia, L., Hong, C., Wu, D., and You, Y. *Nat. Commun.* **2018**, *9*, 2577.
- (11) Satoh, K., Sun, Z., Uchiyama, M., Kamigaito, M., Xu, J., and Boyer, C. *Polym. J.* **2020**, *52*, 65.
- (12) (a) Dolinski, N. D.; Page, Z. A.; Callaway, E. B.; Eisenreich, F.; Garcia, R. V.; Chavez, R.; Bothman, D. P.; Hecht, S.; Zok, F. W.; Hawker, C. J. *Adv. Mater.* **2018**, *30*, 1800364. (b) Schwartz, J. J.; Boydston, A. J. *Nat. Commun.* **2019**, *10*, 791.
- (13) (a) McKenzie, T. G.; Fu, Q.; Uchiyama, M.; Satoh, K.; Xu, J.; Boyer, C.; Kamigaito, M.; Qiao, G. G. *Adv. Sci.* **2016**, *3*, 1500394. (b) Aoshima, H., Uchiyama, M., Satoh, K., Kamigaito, M. *Angew. Chem. Int. Ed.* **2014**, *53*, 10932. (c) Uchiyama, M.; Satoh, K.; Kamigaito, M. *Angew. Chem., Int. Ed.* **2015**, *54*, 1924. (d) Sugihara, S.; Konegawa, N.; Maeda, Y. *Macromolecules* **2015**, *48*, 5120. (e) Sugihara, S.; Konegawa, N.;

Maeda, Y. *Macromolecules* **2015**, *48*, 5120. (f) Zhu, Q.; Gentry, E. C.; Knowles, R. R. *Angew. Chem., Int. Ed.* **2016**, *55*, 9969.

- (14) (a) Kottisch, V.; Michaudel, Q.; Fors, B. P. *J. Am. Chem. Soc.* **2016**, *138*, 15535. (b) Michaudel, Q.; Chauviré, T.; Kottisch, V.; Supej, M. J.; Stawiasz, K. J.; Shen, L.; Zipfel, W. R.; Abruña, H. D.; Freed, J. H.; Fors, B. P. *J. Am. Chem. Soc.* **2017**, *139*, 15530.

CHAPTER 2

ELECTROCHEMICALLY CONTROLLED CATIONIC POLYMERIZATION OF VINYL ETHERS

2.1 Abstract

Control of polymer initiation, propagation and termination is important in the development of complex polymer structures and advanced materials. Typically, this has been achieved chemically, electrochemically, photochemically, or mechanochemically. Electrochemical control has been demonstrated in radical polymerizations; however, regulation of a cationic polymerization has yet to be achieved. Through the reversible oxidation of a polymer chain end with an electrochemical mediator, temporal control over polymer chain growth in cationic polymerizations was achieved. By subjecting a stable organic nitroxyl radical mediator and chain transfer agent to an oxidizing current, control over polymer molecular weight and dispersity is demonstrated and excellent chain end fidelity allows for the synthesis of block copolymers.

2.2 Introduction

Recently there has been a significant push to develop polymerizations where polymer chain growth is controlled by a chemical,¹ electrochemical,² photochemical,³ or mechanochemical⁴ stimulus. The spatiotemporal control offered by these stimuli give an additional means to precisely regulate polymer structure and, hence, function.⁵ Of these stimuli, electrochemistry offers unique

advantages because both applied voltage and current can be modified and monitored throughout the polymerization process.⁶ Taking advantage of this, Matyjaszewski developed an electrochemically mediated atom transfer radical polymerization (eATRP),⁷ which has proved powerful in a number of applications.⁸ More recently, Matyjaszewski⁹ and Yan¹⁰ independently reported electrochemically mediated reversible addition fragmentation chain transfer processes (eRAFT). However, to date, mediation of controlled polymerizations electrochemically has been restricted to radical mechanisms and its implementation in other polymerization types remains a challenge.^{1,2} In this study, we address this challenge and disclose a controlled cationic polymerization where chain growth is electrochemically regulated.

Recently, our group developed a cationic polymerization of vinyl ethers that was controlled by light.¹¹ By selectively oxidizing a dithiocarbamate polymer chain end with an appropriate photoredox catalyst, we were able to reversibly form a propagating carbocation that participated in a controlled cationic RAFT process.^{11,12} In an analogous strategy, we hypothesized that we could reversibly form the carbocation in this process with electrical potential instead of light, which would give a system where chain growth would be regulated electrochemically (Figure 2.1).

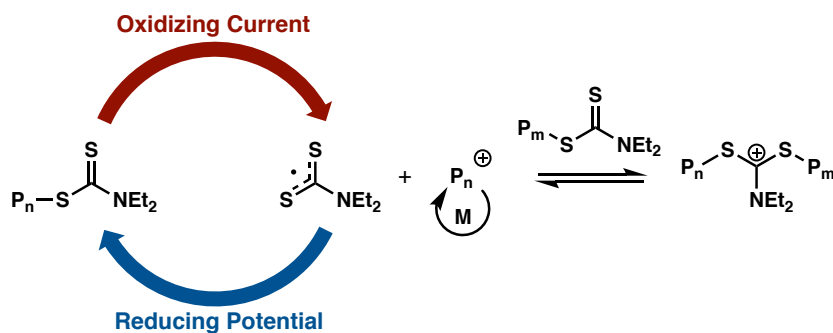


Figure 2.1. Proposed mechanism for electrochemically mediated cationic polymerization of vinyl ethers

2.3 Results and Discussion

Our group has previously shown that upon photochemical oxidation of a dithiocarbamate chain transfer agent (CTA), **1**, mesolytic cleavage occurs to generate an oxocarbenium ion and a stabilized dithiocarbamate radical.^{11c} Cyclic voltammetry (CV) of **1** showed that an irreversible oxidation was occurring, suggesting that a similar oxidation followed by mesolytic cleavage process could be occurring at the electrode surface (Figure 2.2.a). To test our hypothesis that this oxidation/mesolytic cleavage at the anode would give rise to cationic polymerization, we looked at the polymerization of isobutyl vinyl ether (IBVE) in a divided electrochemical cell with reticulated vitreous carbon (RVC) electrodes. Encouragingly, when a constant potential of 325 mV (vs Fc^+/Fc) was applied to a solution of IBVE, **1**, and tetraethylammonium perchlorate (Et_4NClO_4) in dichloromethane, cationic polymerization did occur (Table 2.1, entry 1). However, the polymers resulting from this direct electrolysis of the CTA

exhibited broad dispersities (\mathcal{D}) with bimodal molecular weight distributions (see supporting information, Figure 2.13).

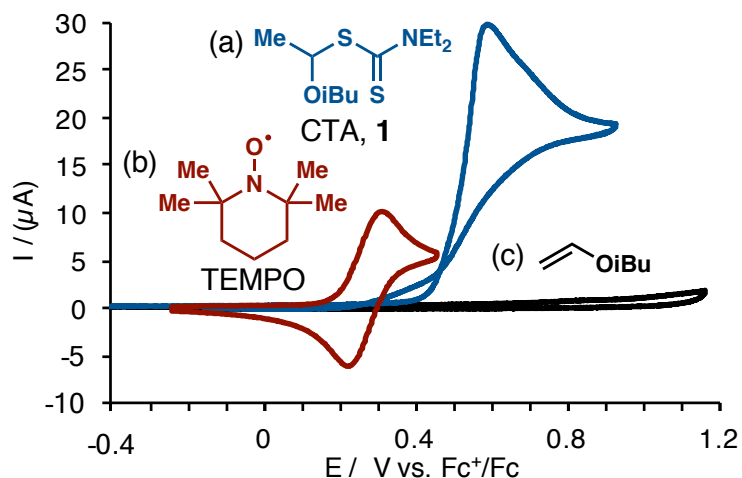
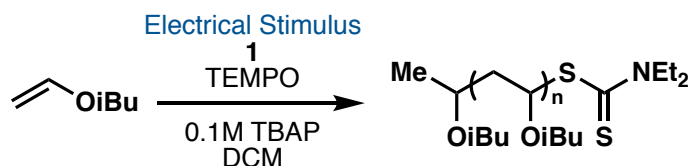


Figure 2.2. CV of (a) 1×10^{-3} M isobutoxy-*N,N*-diethyl dithiocarbamate, (b) 5×10^{-4} M (2,2,6,6-tetramethylpiperidin-1-yl)oxyl, and (c) 1×10^{-3} M isobutyl vinyl ether in 0.1 M tetrabutylammonium perchlorate in dichloromethane at 20 mVs^{-1} .

We reasoned that the observed uncontrolled polymerization could be attributed to polymer plating on the electrode as a result of the irreversible oxidation of the CTA.⁹ To circumvent this issue, we envisaged that the use of a mediator capable of reversible electron transfer at the electrode and homogenous oxidation of the CTA would provide controlled polymerization.¹³ Indeed, the addition of TEMPO (Figure 2.2b), which fit the criteria for the mediator, to the reaction mixture resulted in a 8.4 kg/mol polymer with a \mathcal{D} of 1.23 (Table 2.1, entry 2).¹⁴ Importantly, excellent agreement between theoretical and

Table 2.1: Development of IBVE polymerization mediated by the electrooxidation TEMPO.



Entry ^a	Stimuli	[M]:[1]: [TEMPO]	$M_{n,Theo}^b$ (kg/mol)	$M_{n,Exp}$ (kg/mol)	\bar{D}
1 ^c	325 mV	100:1:0	10.3	10.9	1.97
2 ^c	325 mV	100:1:1	8.3	8.4	1.23
3 ^c	325 mV	100:1:0.1	9.9	7.1	1.50
4 ^c	325 mV	100:1:50	9.9	6.6	1.39
5 ^c	325 mV	100:0:1	–	27.9	2.93
6	1 mA	100:2:1	5.0	6.8	1.07
7	1 mA	100:1.5:1.5	6.9	8.8	1.09
8	1 mA	100:1:1	10.4	10.1	1.15
9	0.1 mA	100:0.25:0.25	28.8	22.5	1.33
10 ^d	1 mA	100:1:1	9.5	8.1	1.45
11 ^e	1 mA	100:1:1	9.9	10.7	1.20

^a[IBVE] = 3.84 M (in DCM), V_{tot} = 5 mL, [Et₄NClO₄] = 0.1 M, RVC Anode, Ag Reference, RVC Cathode (Divided cell). ^b M_n (Theo) = [M]/[CTA] × MW_M × Conversion + MW_{CTA} . ^cPotential vs Fc⁺/Fc. ^dElectrolyte = [Et₄NPF₆] = 0.1 M. ^eElectrolyte = [Et₄NBF₄] = 0.1 M

experimental molar masses was observed, demonstrating that we have a controlled cationic polymerization that is electrochemically mediated. Approximately 1 equivalent of TEMPO with respect to CTA was found to be optimal for these polymerizations, with deviations to higher or lower concentrations leading to a loss in control over the molecular weight (Table 2.1, entries 2 vs 3-4). As a control experiment and in further support of our mechanistic hypothesis, elimination of the RAFT equilibrium by removal of the CTA led to uncontrolled polymerization (Table 2.1, entry 5).

Upon further investigation, we found that higher conversion of the monomer could be obtained under galvanostatic conditions, wherein the potential is allowed to drift in unison with $E_{1/2}$ of the TEMPO redox couple as the concentration of TEMPO⁺ increases.¹⁵ Delivering an anodic current (1 mA) resulted in controlled polymerizations that could be run to full conversion (Table 2.1, entries 6–9).¹⁶ Interestingly, switching the electrolyte to tetrabutylammonium hexafluorophosphate or tetrabutylammonium tetrafluoroborate resulted in slightly broader \bar{D} s (Table 2.1, entries 10,11).¹⁷

Under optimal galvanostatic conditions, monitoring the reaction conversion as a function of time revealed a short induction period followed by fast polymerization with full conversion being reached within 3 hours (Figure 2.3a). Additionally, M_n increased linearly and \bar{D} decreased with conversion, characteristic of a controlled chain-growth mechanism (Figure 2.3b).

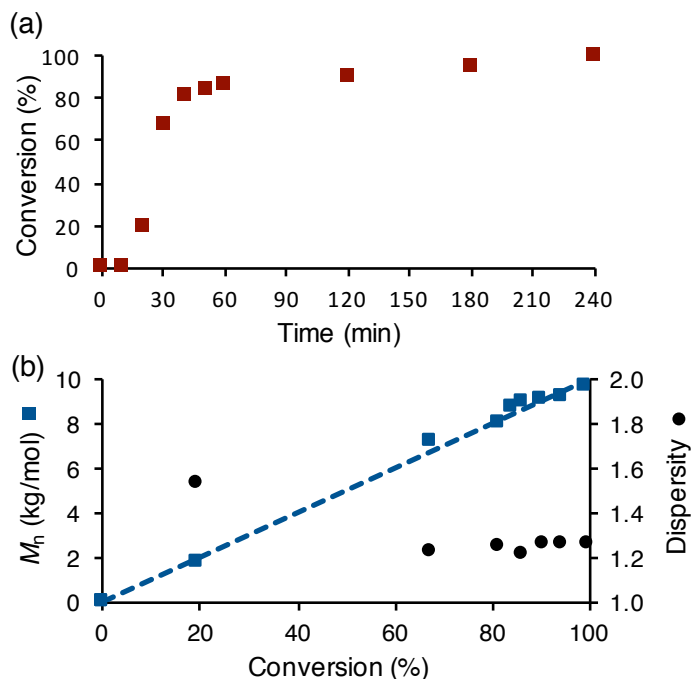


Figure 2.3. (a) Monitoring conversion isobutyl vinyl ether with time. (b) Exploring relationship between M_n and conversion.

To demonstrate temporal control over polymer chain growth, a reaction mixture of IBVE, CTA, and TEMPO was subjected to 1 mA anodic current for twenty minutes. Subsequently, the electrode was set to (-)875 mV vs Fc/Fc⁺ for 30 minutes; we reasoned that this potential should reduce the dithiocarbamate radical (or disulfide) to the corresponding anion, which would cap propagating oxocarbenium ions.¹⁸ Indeed, switching to a reducing potential stopped polymer chain growth with little to no background reaction observed. Reinitiation was then achieved by again applying the oxidizing current for fifteen minutes. This process was successfully repeated multiple times, with polymerization only occurring when an oxidizing current was applied (Figure 2.4). These data

demonstrated that we have excellent electrochemical control over polymer chain growth and the reactions can be reversibly initiated or terminated by switching the direction of current flow in the cell.

To explore the scope of our electrochemical polymerization protocol, we

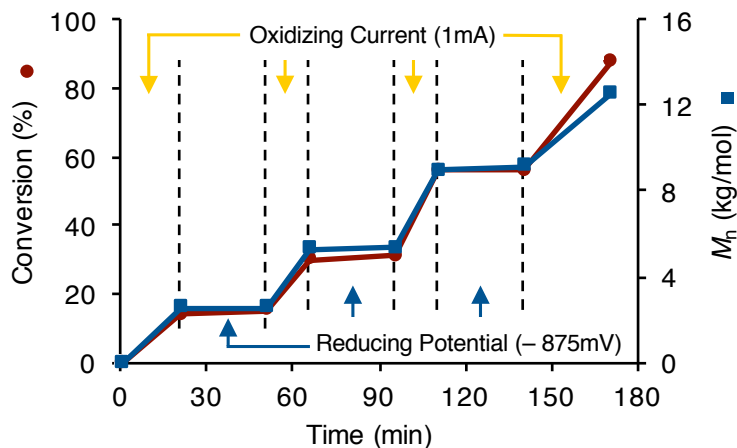


Figure 2.4. Temporal control of polymer chain growth with intermittent oxidizing current and reducing potential.

surveyed an array of vinyl ethers. *n*-Butyl vinyl ether (*n*BuVE), *n*-propyl vinyl ether (*n*PrVE), ethyl vinyl ether (EVE), and 2-chloroethyl vinyl ether (Cl-EVE) all underwent polymerization under the optimized galvanostatic conditions (Table 2.2). The resulting polymers showed good agreement between theoretical and experimental molecular weights, along with narrow \mathcal{D} s. Notably, 4-methoxystyrene was polymerized under slightly more demanding conditions (2 mA), constituting an improvement upon the photocontrolled polymerizations we previously reported, which did not promote polymerizations of styryl monomers.^{11a,19} Although the resulting polymer has slightly broader dispersities

when compared to the vinyl ethers, this preliminary finding highlights the versatility of this electrochemically mediated polymerization.

Table 2.2. Polymerization of vinyl ether and styryl monomers.

Entry ^a	Monomer	$M_{n, \text{Theo}}^b$ (kg/mol)	$M_{n, \text{Exp}}$ (kg/mol)	\bar{D}
1	<i>n</i> BuVE	9.9	9.7	1.32
2	<i>n</i> PrVE	10.2	8.1	1.11
3	EVE	10.4	9.7	1.14
4	Cl-EVE	10.3	11.3	1.12
5 ^c	<i>p</i> -OMe-Styrene	10.2	8.7	1.33

^a[M] = 42% in DCM v/v, $V_{\text{tot}} = 6$ mL, $[\text{Et}_4\text{NClO}_4] = 0.1$ M, RVC Anode, Ag Reference, RVC Cathode (Divided), Reaction time = 4 hr.. ^b M_n (Theo) = $[\text{M}]/[\text{CTA}] \times MW_{\text{M}} \times \text{Conversion} + MW_{\text{CTA}}$.
^cApplied current = 2 mA.

To further probe chain end fidelity delivered by this method we successfully chain extended a macroinitiator. A 5.1 kg/mol poly(EVE) was first synthesized under the optimized conditions, to which, IBVE was added to the anodic chamber and an oxidizing current was resumed. A clear shift to higher molar masses was observed to give a 8.0 kg/mol poly(EVE-*b*-IBVE) with narrow dispersity (Figure 2.5).

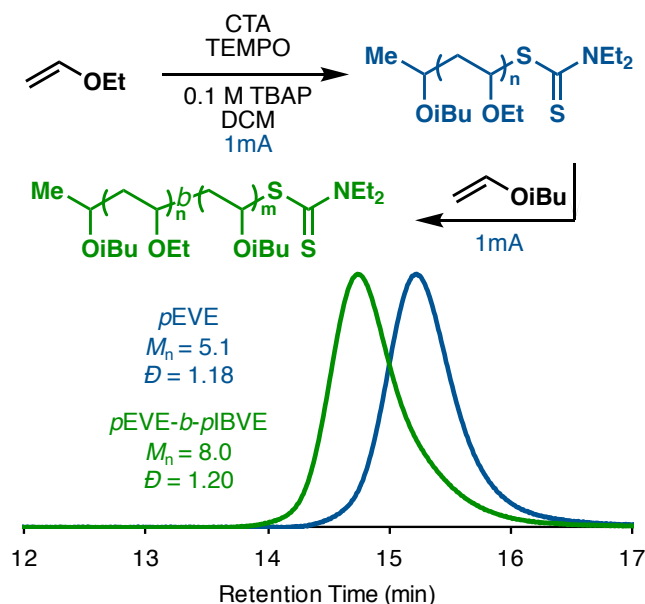


Figure 2.5. Synthesis and GPC traces of poly(ethyl vinyl ether) and poly(ethyl vinyl ether-*block*-isobutyl vinyl ether).

To further understand the role of TEMPO in these reactions, we found that when an oxidizing potential (325 mV vs Fc⁺/Fc) was applied to a solution of the CTA and TEMPO, tetraethylthiuram disulfide was observed as a result of

the dimerization of **II**, a byproduct of oxidatively cleaved CTA. Based on this result and our polymerization data above, we propose that the oxidized TEMPO cation undergoes an attack by the CTA to form a stabilized cationic intermediate **I** (Figure 2.6).²⁰ Fragmentation of the cation gives the dithiocarbamate radical **II**

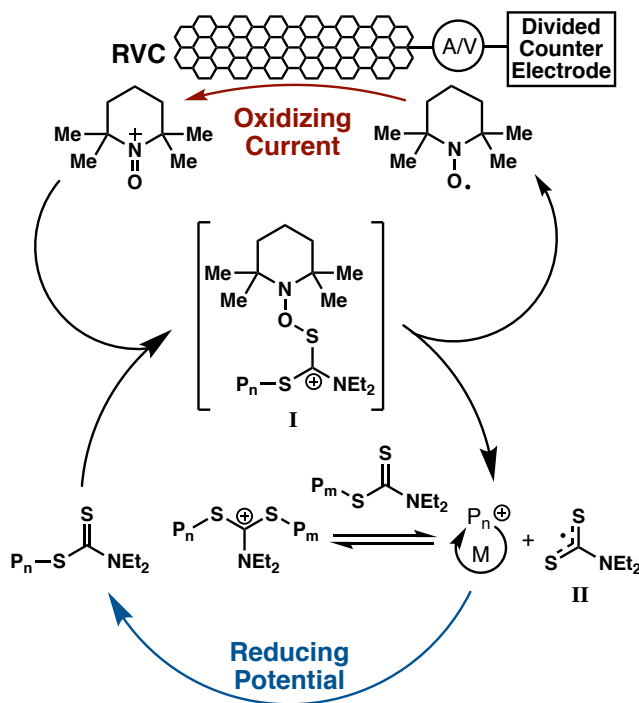


Figure 2.6. Proposed catalytic cycle of the TEMPO mediated polymerization of vinyl ethers.

and the oxocarbenium ion that participates in the RAFT process, as well as regenerates TEMPO; together, this two step process completes an innersphere electron transfer. We hypothesize that when the current in the electrochemical cell is reversed, dithiocarbamate radical **II** or its dimeric form gets reduced to

the anion and caps the propagating cation.¹⁷ This recapping step gives efficient electrochemical control over polymer chain growth.

2.4 Conclusion

In summary, we have developed an electrochemically mediated cationic polymerization, which offers excellent temporal control over polymer growth. A variety of poly(vinyl ethers) with narrow dispersities and predictable M_n values were obtained and the ability to polymerize less activated monomers was demonstrated. High chain end fidelity allows for the synthesis of block copolymers, while reversible electrochemical activation/deactivation of chain ends allows precise temporal control of chain growth. This new electrochemical handle for controlling cationic polymer growth should allow for the synthesis of complex polymer architectures, and provide a template for future electrochemically controlled polymerizations.

2.5 References

- (1) (a) Gregson, C. K. A.; Gibson, V. C.; Long, N. J.; Marshall, E. L.; Oxford, P. J.; White, A. J. P. *J. Am. Chem. Soc.* **2006**, *128*, 7410. (b) Broderick, E. M.; Guo, N.; Vogel, C. S.; Xu, C.; Sutter, J.; Miller, J. T.; Meyer, K.; Mehrkhodavandi, P.; Diasconescu, P. L.; *J. Am. Chem. Soc.* **2011**, *133*, 9278. (c) Broderick, E. M.; Guo, N.; Wu, T.; Vogel, C. S.; Xu, C.; Sutter, J.; Miller, J. T.; Meyer, K.; Cantat, T.; Diaconescu, P. L. *Chem. Commun.* **2011**, *47*, 9897. (d) Gregson, C. K. A.; Blackmore, I. J.; Gib-son, V. C.;

- Long, N. J.; Marshall, E. L.; White, A. J. P. *Dalton Trans.* **2006**, 3134. (e) Biernesser, A. B.; Li, B.; Byers, J. A. *J. Am. Chem. Soc.* **2013**, *135*, 15443. (f) Biernesser, A. B.; Delle Chiaie, K. R.; Curley, J. B.; Byers, J. A. *Angew. Chem., Int. Ed.* **2016**, *55*, 5251.
- (2) Chmielarz, P.; Fantin, M.; Park, S.; Isse, A. A.; Gennaro, A.; Magenau, A. J. D.; Sobkowiak, A.; Matyjaszewski, K.; *Prog. Polym. Sci.* **2017**, *69*, 47.
- (3) (a) Chen, M.; Zhong, M.; Johnson, J. A. *Chem. Rev.* **2016**, *116*, 10167. (b) Corrigan, N.; Shanmugam, S.; Xu, J.; Boyer, C. *Chem. Soc. Rev.* **2016**, *45*, 6165. (c) Dadashi-Silab, S.; Doran, S.; Yagci, Y. *Chem. Rev.* **2016**, *116*, 10212. (d) Trotta, J. T.; Fors, B. P. *Synlett* **2016**, *27*, 702. (e) McKenzie, T. G.; Fu, Q.; Uchiyama, M.; Satoh, K.; Xu, J.; Boyer, C.; Kamigaito, M.; Qiao, G. G. *Adv. Sci.* **2016**, *3*, 1500394.
- (4) Mohapatra, H.; Kleiman, M.; Esser-Kahn, A. P. *Nat. Chem.* **2017**, *9*, 135. (b) Wang, Z.; Pan, X.; Yan, J.; Dadashi-Silab, S.; Xie, G.; Zhang, J.; Wang, Z.; Xia, H.; Matyjaszewski, K. *ACS Macro Lett.* **2017**, *6*, 546. (c) McKenzie, T. G.; Colombo, E.; Fu, Q.; Ashokkumar, M.; Qiao, G. G. *Angew. Chem., Int. Ed.* **2017**, *56*, 12302. (d) Wang, Z.; Pan, X.; Li, L.; Fantin, M.; Yan, J.; Wang, Z.; Wang, Z.; Xia, H.; Matyjaszewski, K. *Macromolecules* **2017**, *50*, 7940.
- (5) Leibfarth, F. A.; Mattson, K. M.; Fors, B. P.; Collins, H. A.; Hawker, C. J. *Angew. Chem. Int. Ed.* **2013**, *52*, 199.

- (6) Yan, M.; Kawamata, Y.; Baran, P. S. *Chem. Rev.* **2017**, *117*, 13230.
- (7) (a) Magenau, A. J. D.; Strandwitz, N. C.; Gennaro, A.; Matyjaszewski, K. *Science* **2011**, *332*, 81. (b) Bortolamei, N.; Isse, A. A.; Magenau, A. J. D., Gennaro, A.; Matyjaszewski, K. *Angew. Chem. Int. Ed.* **2011**, *50*, 11391. (c) Fantin, M.; Isse, A. A.; Venzo, A.; Gennaro, A.; Matyjaszewski, K. *J. Am. Chem. Soc.* **2016**, *138*, 7216.
- (8) (a) Li, B.; Yu, B.; Huck, W. T. S.; Zhou, F.; Liu, W. *Angew. Chem., Int. Ed.* **2012**, *51*, 5092. (b) Shida, N.; Koizumi, Y.; Nishiyama, H.; Tomita, I.; Inagi, S. *Angew. Chem. Int. Ed.* **2015**, *54*, 3922. (c) Park, S.; Cho, H. Y.; Wegner, K. B.; Burdyska, J.; Magenau, A. J. D.; Paik, H.-J.; Jurga, S.; Matyjaszewski, K. *Macromolecules*, **2013**, *46*, 5856.
- (9) Rinsing the electrode after the reaction revealed bound polymer. For other examples of electrode passivation, see: Wang, Y.; Fantin, M.; Park, S.; Gottlieb, E.; Liye, F.; Matyjaszewski, K. *Macromolecules* **2017**, *50*, 7872.
- (10) Sang, W.; Xu, M.; Yan, Q. *ACS Macro Lett.* **2017**, *6*, 1337.
- (11) (a) Kottisch, V.; Michaudel, Q.; Fors, B. P. *J. Am. Chem. Soc.* **2016**, *138*, 15535. (b) Kottisch, V.; Michaudel, Q.; Fors, B. P. *J. Am. Chem. Soc.* **2017**, *139*, 10665. (c) Michaudel, Q.; Chauviré, T.; Kottisch, V.; Supej, M. J.; Stawiasz, K. J.; Shen, L.; Zipfel, W. R.; Abruña, H. D.; Freed, J. H.; Fors, B. P. *J. Am. Chem. Soc.* **2017**, *139*, 15530. (d) Michaudel, Q.; Kottisch, V.; Fors, B. P. *Angew. Chem., Int. Ed.* **2017**, *56*, 9670.

- (12) For references on cationic RAFT see: (a) Uchiyama, M.; Satoh, K.; Kamigaito, M. *Angew. Chem., Int. Ed.* **2015**, *54*, 1924. (b) Sugihara, S.; Konegawa, N.; Maeda, Y. *Macromolecules* **2015**, *48*, 5120. (c) Uchiyama, M.; Satoh, K.; Kamigaito, M. *Macromolecules* **2015**, *48*, 5533.
- (13) For a review on mediators in organic electrosynthesis see: Francke, R.; Little, R. D. *Chem. Soc. Rev.* **2014**, *43*, 2492.
- (14) (a) Hickey, D. P.; McCammant, M. S.; Giroud, F.; Sigman, M. S.; Minter, S. D. *J. Am. Chem. Soc.* **2014**, *136*, 15917. (b) Rafiee, M.; Miles, K. C.; Stahl, S. S. *J. Am. Chem. Soc.* **2015**, *137*, 14751.
- (15) This also circumvents the need for a reference electrode and allows for polymerization using a DC power source, greatly simplifying polymerization procedure (Figure S28), see: (a) Fu, N.; Sauer, G. S.; Saha, A.; Loo, A.; Sin, S. *Science* **2017**, *357*, 575. (b) Magenau, A. J. D.; Bortolamei, N.; Frick, E.; Park, S.; Gennaro, A.; Matyjaszewski, K. *Macromolecules* **2013**, *46*, 4346. (c) Park, S.; Chmielarz, P.; Gennaro, A.; Matyjaszewski, K. *Angew. Chem., Int. Ed.* **2015**, *54*, 2388. (d) Chmielarz, P.; Sobkowiak, A.; Matyjaszewski, K. *Polymer*, **2015**, *77*, 266.
- (16) Currents were selected so that initial voltage was near 325 mV(vs Fc⁺/Fc) and at lower loadings of **1** and TEMPO lower currents were necessary to achieve higher molar masses.

- (17) For an example of tetrafluoroborate reacting with an oxo-carbenium ion see: Suzuki, S.; Matsumodo, K.; Kawamura, K.; Suga, S.; Yoshida, J. *Org. Lett.* **2004**, *6*, 3755.
- (18) In the absence of any stimuli ($I=0$), polymerization rates are retarded with observable background reaction occurring. (a) Nichols, P. J.; Grant, M. W. *Aust. J. Chem.* **1982**, *35*, 2455.
- (19) For examples of photoinitiated cationic polymerizations of styryl monomers see: (a) Perkowski, A. J.; You, W.; Nicewicz, D. A. *J. Am. Chem. Soc.* **2015**, *137*, 7580. (b) Messina, M. S.; Axtell, J. C.; Wang, Y.; Chong, P.; Wixtrom, A. I.; Kirlikovali, K. O.; Upton, B. M.; Hunter, B. M.; Shafaat, O. S.; Khan, S. I.; Winkler, J. R.; Gray, H. B.; Alexandrova, A. N.; Maynard, H. D.; Spokoyny, A. M. *J. Am. Chem. Soc.* **2016**, *138*, 6952.
- (20) Alternatively, attack could also occur at the nitrogen, yielding the same intermediates after fragmentation. (a) Yoshida, E.; Nakamura, K.; Takata, T.; Endo, T. *J. Polym. Sci. A Polym. Chem.* **1993**, *31*, 1505. (b) Bailey, W. F.; Bobbitt, J. M.; Wiberg, K. B. *J. Org. Chem.* **2007**, *72*, 4504.

2. 6 Appendix

Experimental Information

General Reagent Information

Isobutyl vinyl ether (IBVE) (99%, TCI), ethyl vinyl ether (EVE) (99%, Sigma Aldrich), 2-chloroethyl vinyl ether (Cl-EVE) (97%, TCI), *n*-propyl vinyl

ether (*n*PrVE) (99%, Sigma Aldrich), and *n*-butyl vinyl ether (*n*BuVE) (98%, Sigma Aldrich) were dried over calcium hydride (CaH₂) (ACROS organics, 93% extra pure, 0–2 mm grain size) for 12 hours, distilled under nitrogen, and degassed by three freeze, pump, and thaw cycles. 4-methoxystyrene (97%, Sigma Aldrich) was dried over CaH₂ for 12 hours, distilled under vacuum, and degassed by free-pump-thaw three times. Carbon disulfide (99.9+%, Alfa Aesar), 2,2,6,6-tetramethylpiperidine 1-oxyl Free Radical (98%, TCI), tetrabutylammonium hexafluorophosphate (98%, TCI) and tetrabutylammonium tetrafluoroborate (98%, TCI) were used as received. Sodium *N,N*-diethylcarbamate trihydrate (98%, Alfa Aesar) was azeotropically dried with toluene. Tetrabutylammonium Perchlorate (98%, TCI) was purified by recrystallization from ethyl acetate three times and dried under reduced pressure at 60 °C for 12 hours. Ethyl Acetate and hexanes were purchased from Fischer Scientific. Dichloromethane (DCM) and diethylether (Et₂O) were purchased from J.T. Baker and were purified by vigorous purging with argon for 2 hours, followed by passing through two packed columns of neutral alumina under argon pressure. Ethanol (anhydrous, 200 proof) was purchased from Koptec. Alumina (1.0, 0.3, 0.05 μm pore size) was purchased from Extec. Reticulated vitreous carbon was purchased from ERG Aerospace. Microcloth PSA (polishing paper) and Abrasive Paper (600 grit) were purchased from Buehler.

General Analytical Information

All polymer samples were analyzed using a Tosoh EcoSec HLC 8320GPC system with two SuperHM-M columns in series at a flow rate of 0.350 mL/min with THF as the eluent. Number average molecular weights (M_n), weight-average molecular weights (M_w), and dispersities (\mathcal{D}) for all polymers (in Table 1 and 2) were determined by light scattering using a Wyatt miniDawn Treos multi-angle light scattering detector. The dn/dc values were calculated from light scattering in THF for poly(isobutyl vinyl ether), poly(ethyl vinyl ether), poly(2-chloroethyl vinyl ether), poly(*n*-propyl vinyl ether), poly(*n*-butyl vinyl ether) and block copolymers in THF. All reported GPC traces, as well as M_n 's and \mathcal{D} 's for chain extension experiments and ON/OFF experiments were acquired from refractive index chromatograms against TSKgel polystyrene standards.

Nuclear magnetic resonance (NMR) spectra were recorded on a Varian 400 MHz or a Bruker 500 MHz instrument. Electrolysis experiments were performed using a BASi EC Epsilon potentiostat, EG & G Princeton Applied Research potentiostat, or a DC power supply.

Cyclic Voltammetry Procedure

Cyclic voltammetric measurements were performed in a three-compartment glass cell with medium porosity glass frits separating the compartments. An Ag/Ag⁺ reference electrode and a Pt wire counter electrode

were used unless otherwise specified. All potentials are referenced to Fc/Fc⁺ which was acquired after all measurements (0.540 V vs Ag/Ag⁺). All 3-mm glassy carbon (GC) electrodes were purchased from CH Instruments. Prior to each experiment, electrodes were polished, sequentially, with 1.0 μm, 0.3 μm 0.05 μm Alumina in water on polishing paper. Following polishing, electrodes were sonicated in ethanol for 30 seconds and air dried.

General E-cell and Electrode Setup

Preparation of E-cell and electrode caps

Two chamber E-cells, separated by a fine frit and joined by a narrow passage above the volume of reaction contents were used for all experiments (Figure 2.7). Ground glass side arms (14/20) were used for addition of liquid reagents. Cell caps were constructed from teflon schlenk bomb screw on caps. Two (2 mm) holes were drilled with a drill press into the top of the cap. 2 mm (outer diameter) stainless steel rods were driven through the caps with a rubber mallet. 2mm (inner diameter) stainless steel tubes was fastened to the inner end of the stainless steel rods, to hold electrodes (Figure 2.7c).

Preparation of electrodes

Working (anode) and counter (cathode) electrodes were constructed by driving a 2mm pencil lead through a 50 mm X 50 mm X 100 mm portion of reticulated vitreous carbon (RVC) (Figure 2.7b). RVC is used as the working and counter, because of its high surface area and ease of use. The other end of the pencil lead was inserted into the stainless steel tube of the E-cell cap (Figure 2.7d). Pencil lead was cut to the desired length with a razor blade to maximize surface area in contact with the reaction, while allowing sufficient space for magnetic stirring. Silver wire (2 mm diameter) functioned as the pseudo-reference electrode. The silver wire was polished with fine grain (600 grit) sand paper and rinsed with dichloromethane between each experiment.

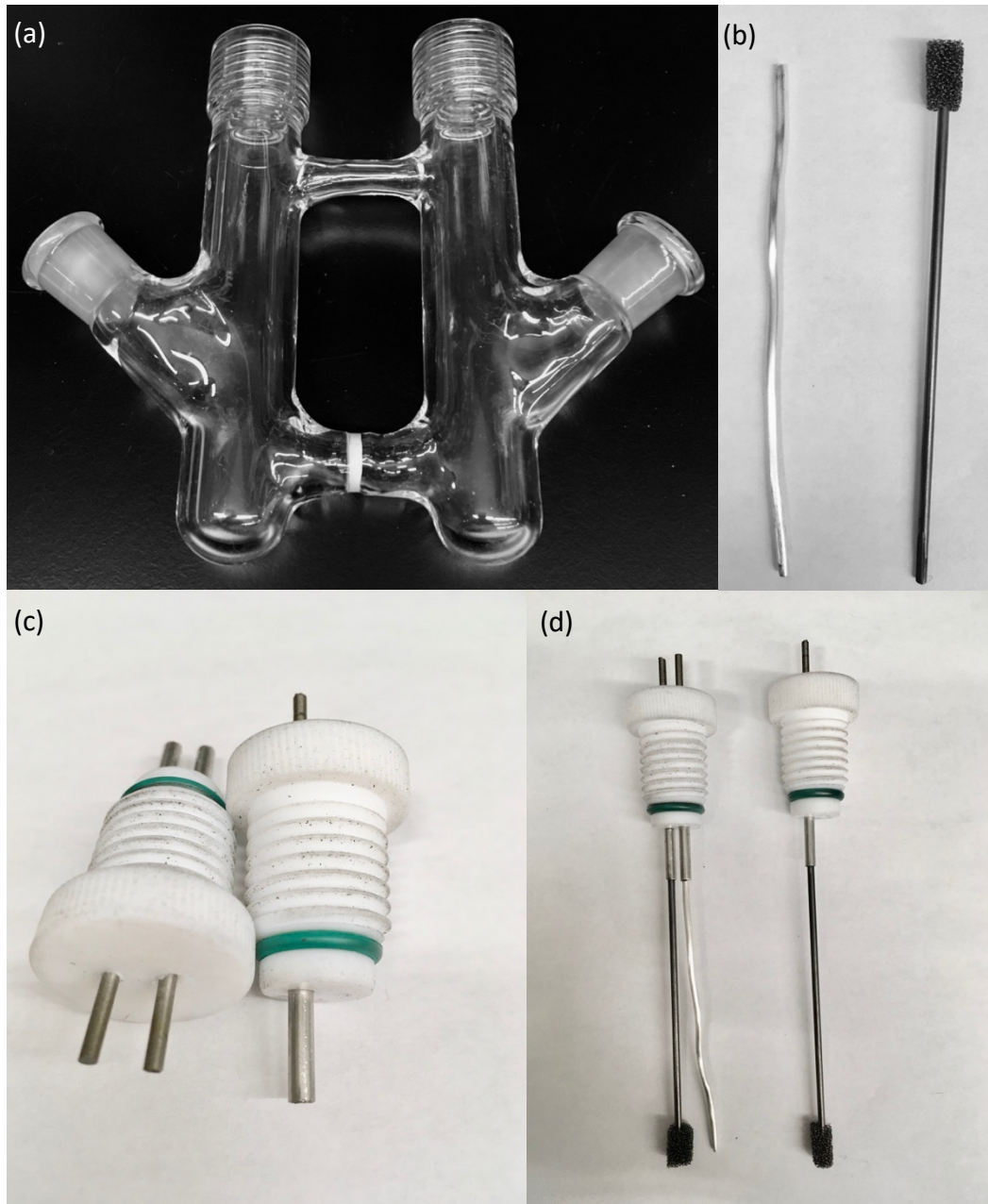
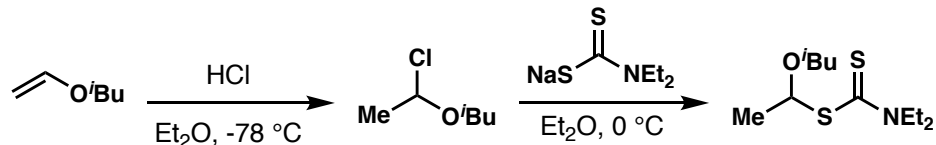


Figure 2.7. E-cell and electrode preparation

Experimental Procedures



Synthesis of S-1-isobutoxy N,N-diethyl dithiocarbamate¹

In a flame dried flask, a solution of HCl in Et₂O (10.3 mL, 2.0 M, 20.6 mmol, 1.2 equiv) was added dropwise to a solution of isobutyl vinyl ether (1.30 mL, 17.6 mmol, 1.0 equiv) in Et₂O (20 mL) over 10 minutes at -78 °C and stirred for 1.5 hours under nitrogen. This solution was added to a solution of sodium N,N-diethyl dithiocarbamate (4.01 g, 23.4 mmol, 1.3 equiv) in Et₂O (60 mL) over 30 min at 0 °C. The reaction proceeded for 1.5 hours at 0 °C followed by 1.5 hours at room temperature. Following, the reaction was diluted with Et₂O (60 mL) and washed with saturated aqueous sodium bicarbonate solution. The layers were separated and the aqueous phase was extracted with Et₂O two times. The combined organic phases were washed with brine before diluting with an equal part hexanes until the phase was cloudy. The organic phase was dried with sodium sulfate (until the yellow, organic phase was clear again), and concentrated in *vacuo*. The yellow oil was further purified by column chromatography (SiO₂, 5% ethyl acetate in hexanes) to yield a lighter yellow oil (2.42 g, 55% yield). ¹H NMR (CDCl₃, 500 MHz) δ 5.88 (q, J = 6.2 Hz, 1 H), 4.02 (q, J = 7.2 Hz, 2 H), 3.80 - 3.70 (m, 2 H), 3.46 (dd, J = 9.0, 6.6 Hz, 1 H), 3.34 (dd, J = 9.0, 6.6 Hz, 1 H), 1.91 - 1.78 (m, 1 H), 1.73 (d, J = 6.3 Hz, 3 H), 1.28

(dt, $J = 11.4, 7.2$ Hz, 6 H), 0.90 (d, $J = 6.7$ Hz, 6 H) ppm. ^{13}C NMR (CDCl_3 , 150 MHz) δ : 195.1, 91.7, 76.2, 48.9, 47.0, 28.5, 23.6, 19.5, 12.7, 11.8 ppm

Electropolymerization Reaction Setup

To an oven dried E-cell, a magnetic stir bar was added to both the anodic and cathodic chamber. An electrode cap, with the working and reference electrodes, was screwed onto the anodic chamber and the side arm was sealed with a rubber septa. A second electrode cap, with the counter electrode, was screwed onto the cathodic chamber and the system sealed with a second rubber septa (Figure 2.8). The rubber septa was pierced with a needle, evacuated, and backfilled with a positive of pressure of nitrogen was applied.



Figure 2.8. E-cell reaction setup

General Procedure for Electrochemically Mediated Polymerization of Isobutyl Vinyl Ether (Constant Potential) (Table 2.1, Entries 1–5)

The following procedure was preceded by Electropolymerization Reaction Setup (Figure 2.8). Once the E-cell cooled to room temperature, TEMPO (30.0 mg, 0.192 mmol, 1 equiv) was added to the anodic chamber and TBAP (171.0 mg, 0.5 mmol) was added to both the anodic and cathodic chamber through the side arms. A nitrogen atmosphere was established by evacuating and backfilling with nitrogen three times. A nitrogen filled balloon then replaced the positive nitrogen pressure supplied by the schlenk line. The anodic chamber was charged with isobutyl vinyl ether (2.50 mL, 19.2 mmol, 100 equiv), S-1-isobutoxy *N,N*-diethyl dithiocarbamate (CTA,1) (190 μ L, 1 M stock solution in DCM, 0.190 mmol, 1 equiv), and DCM (2.3 mL), via syringe. The cathodic chamber was charged with DCM (5.00 mL) Potentiostat leads were connected to the E-cell caps. Stirring commenced and an oxidizing potential (325 mV vs Fc^+/Fc) was applied for 6 hours. Following the desired reaction time, aliquots for NMR and GPC analysis were taken via a syringe ($M_{n,\text{Theo}} = 8.3$ kg/mol. $M_n = 8.4$ kg/mol, $\bar{D} = 1.23$).

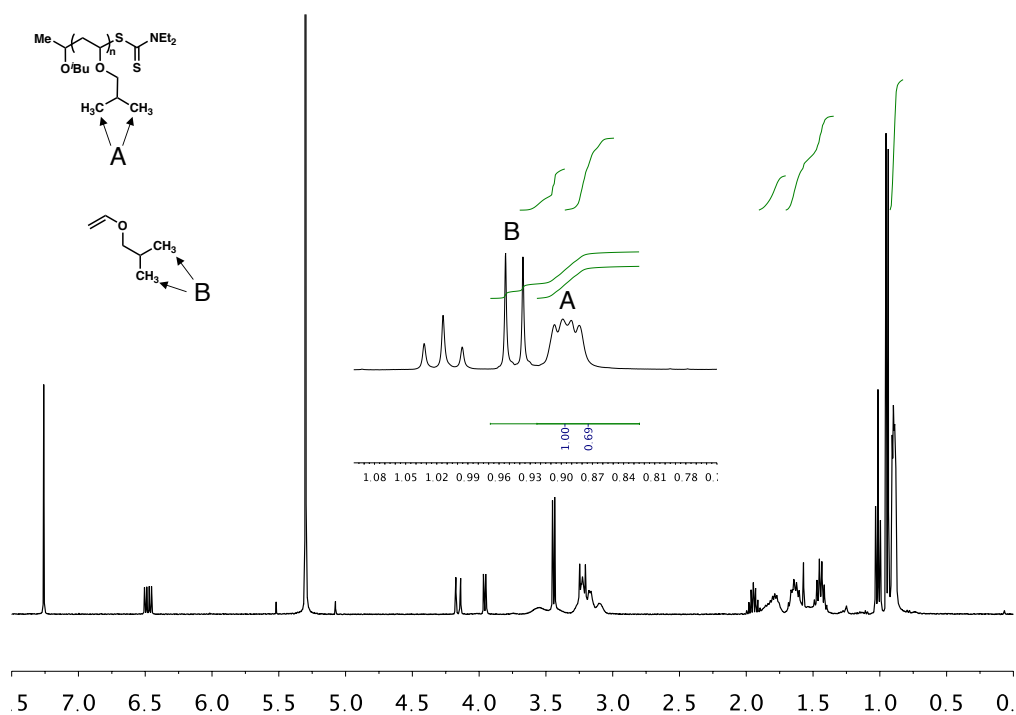


Figure 2.9. ¹H NMR of poly(isobutyl vinyl ether)

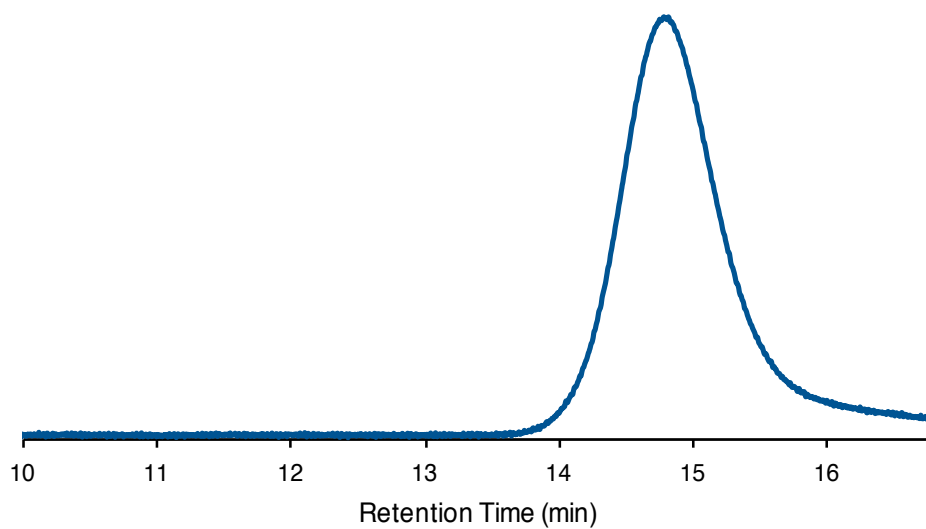


Figure 2.10. GPC trace of poly(isobutyl vinyl ether)

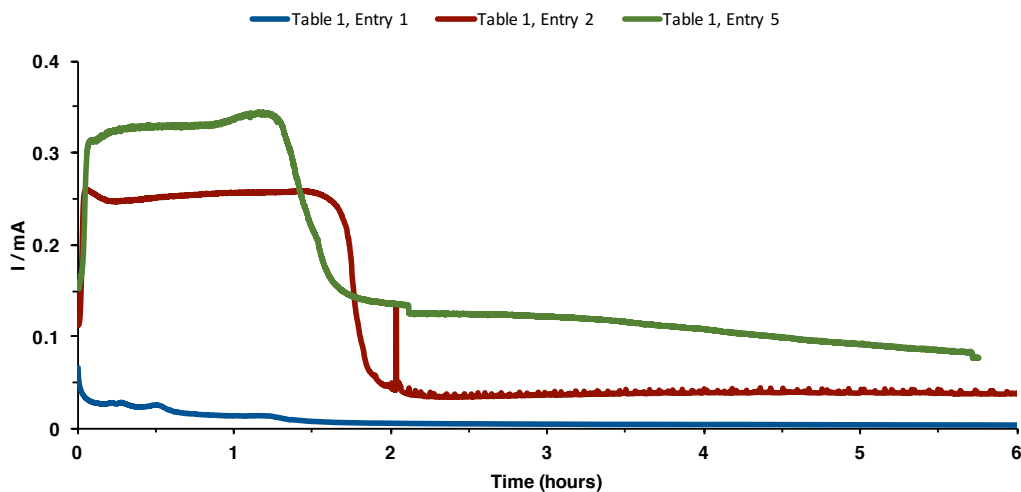


Figure 2.11. Current vs time profiles of potentiostatic polymerization (325 mV vs Ag wire) of isobutyl vinyl ether. Ratio of [IBVE]:[CTA]:[TEMPO] = 100:1:0 (table 2.1, entry 1), [IBVE]:[CTA]:[TEMPO] = 100:1:1 (table 2.1, entry 2), and [IBVE]:[CTA]:[TEMPO] = 100:0:1 (table 2.1, entry 5) in polymerizations.

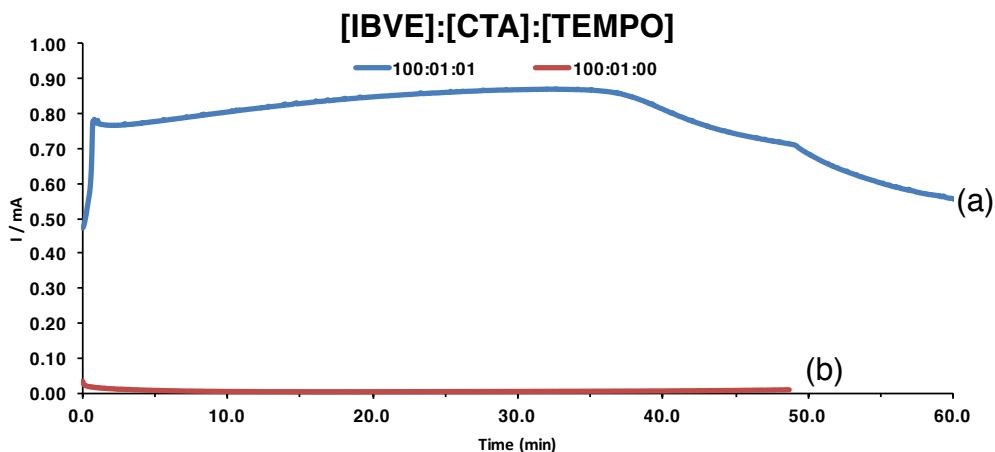


Figure 2.12. Current vs time profiles of potentiostatic polymerization (225 mV vs Ag wire) of isobutyl vinyl ether (a) [IBVE]:[CTA]:[TEMPO] = 100:1:1 resulting in 65% conversion ($M_n = 7.9$, $\bar{D} = 1.22$) and (b) [IBVE]:[CTA]:[TEMPO] = 100:1:0 resulting in no conversion of IBVE.

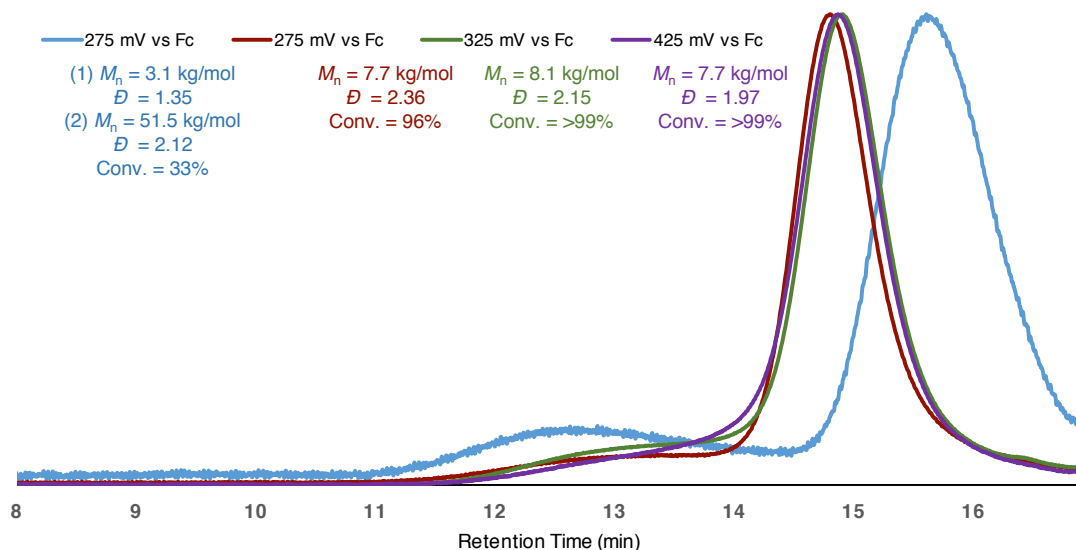


Figure 2.13. GPC traces of unmediated potentiostatic polymerizations of isobutyl vinyl ether. Overlay of distributions of polymerizations of IBVE with [IBVE]:[CTA]:[TEMPO] = 100:1:0 at varying potentials and conversions, showing broad and bimodal distributions.

Table 2.3. Unmediated polymerizations of isobutyl vinyl ether at varying potentials.

Entry	Applied Potential (mV) ^a	[M]:[1]:[TEMPO]	Conv. (%)	$M_{n, Theo}$ (kg/mol)	$M_{n, Exp}$ (kg/mol)	\bar{D}
1	275	100:01:00	96	9.9	7.7	2.36
2	325	100:1:0	>99	10.3	8.1	2.15
3	425	100:1:0	>99	10.3	7.7	1.97
4	625	100:1:0	>99	10.3	5.8	2.29

^aPotentials are referenced to Fc⁺/Fc.

General Procedure for Electrochemically Mediated Polymerization of Isobutyl Vinyl Ether (Constant Current) (Table 2.1, Entries 6-11)

The following procedure was preceded by Electropolymerization Reaction Setup (Figure 2.8). Once the E-cell cooled to room temperature, TEMPO (30.0 mg, 0.192 mmol, 0.5 equiv) was added to the anodic chamber and TBAP (171.0 mg, 0.5 mmol) was added to both the anodic and cathodic chamber through the side arms. A nitrogen atmosphere was established by evacuating and backfilling with nitrogen three times. A nitrogen filled balloon then replaced the positive nitrogen pressure supplied by the schlenk line. The anodic chamber was charged with isobutyl vinyl ether (2.50 mL, 19.2 mmol, 50 equiv), S-1-isobutoxy *N,N*-diethyl dithiocarbamate (CTA, **1**) (380 μ L, 1 M stock solution in DCM, 0.380 mmol, 1 equiv), and DCM (2.1 mL), via syringe. The cathodic chamber was charged with DCM (5.00 mL) Potentiostat leads were connected to the E-cell caps. Stirring commenced and an oxidizing current (1mA) was applied. Following the desired reaction time, aliquots for NMR and GPC analysis were taken via a syringe ($M_{n,Theo} = 5.0$ kg/mol, $M_{n,Exp} = 6.8$ kg/mol, $D = 1.07$).

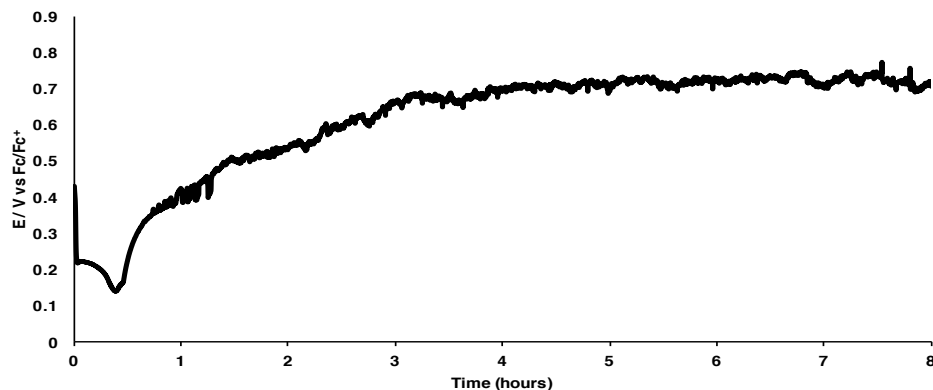


Figure 2.16. Potential vs time profile of galvanostatic (1mA) polymerization

Procedure for Electrochemically Mediated Polymerization of *n*-Butyl Vinyl Ether (Table 2.2, Entry 1)

The following procedure was preceded by Electropolymerization Reaction Setup (Figure 2.8). Once the E-cell cooled to room temperature, TEMPO (30.2 mg, 0.193 mmol, 1 equiv) was added to the anodic chamber and TBAP (171.0 mg, 0.5 mmol) was added to both the anodic and cathodic chamber through the side arms. A nitrogen atmosphere was established by evacuating and backfilling with nitrogen three times. A nitrogen filled balloon then replaced the positive nitrogen pressure supplied by the schlenk line. The anodic chamber was charged with *n*-butyl vinyl ether (2.50 mL, 19.3 mmol, 100 equiv), S-1-isobutoxy *N,N*-diethyl dithiocarbamate (CTA) (380 μ L, 0.5 M stock solution in DCM, 0.190 mmol, 1 equiv), and DCM (2.1 mL), via syringe. The cathodic chamber was charged with DCM (5.00 mL) Potentiostat leads were connected to the E-cell caps. Stirring commenced and an oxidizing current (1mA) was applied for 4 hours. Following the desired reaction time, aliquots for

NMR and GPC analysis were taken via a syringe ($M_{n, \text{Theo}} = 9.9 \text{ kg/mol}$, $M_{n, \text{Exp}} = 9.7 \text{ kg/mol}$, $D = 1.16$).

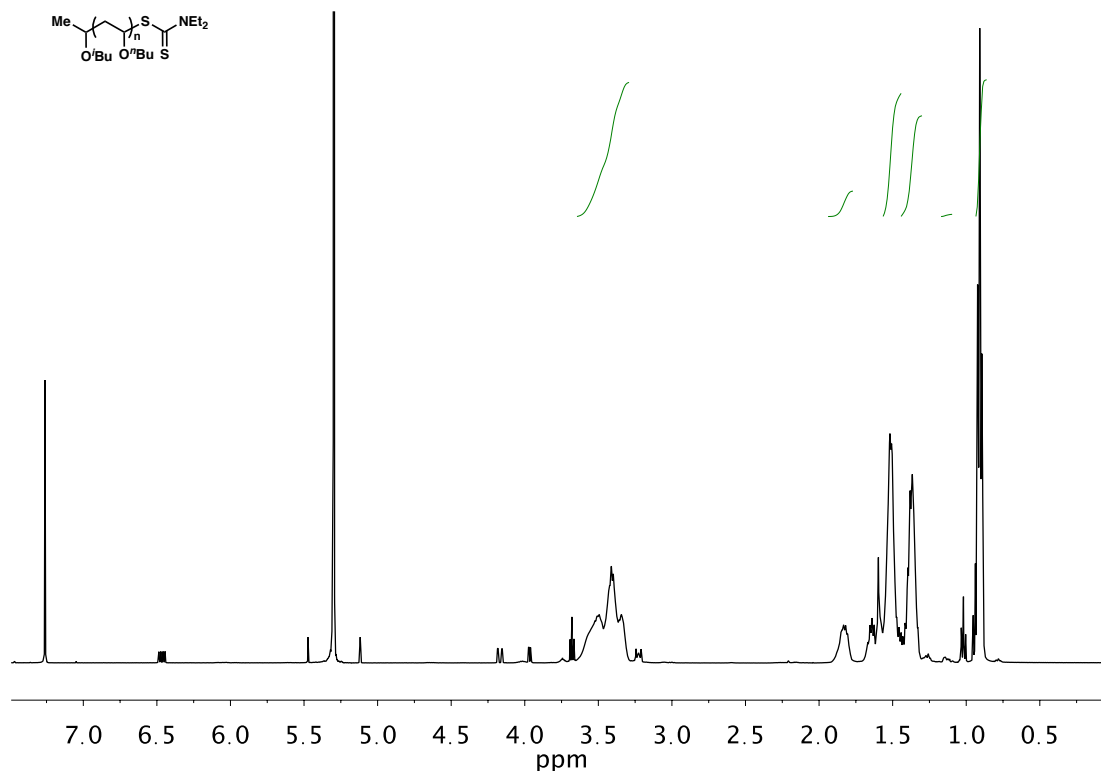


Figure 2.17. ^1H NMR of poly(n-butyl vinyl ether)

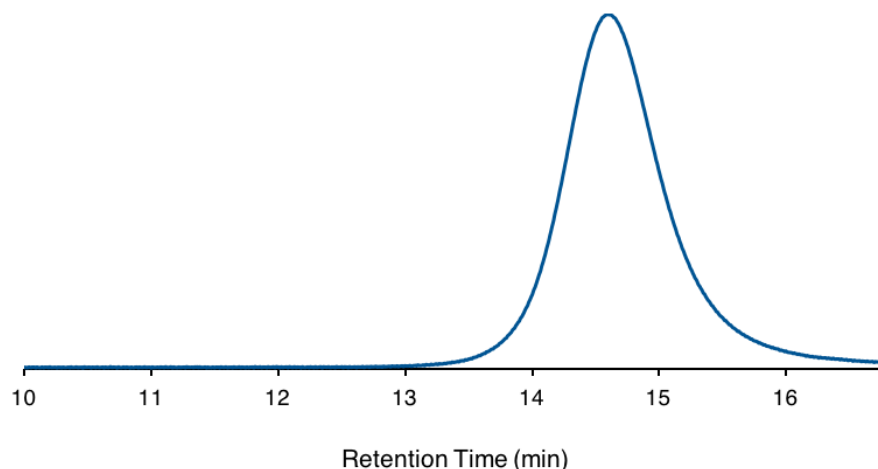


Figure 2.18. GPC trace of poly(*n*-butyl vinyl ether)

Procedure for Electrochemically Mediated Polymerization of *n*-Propyl Vinyl Ether (Table 2.2, Entry 2)

The following procedure was preceded by Electropolymerization Reaction Setup (Figure 2.8). Once the E-cell cooled to room temperature, TEMPO (29.7 mg, 0.190 mmol, 1 equiv) was added to the anodic chamber and TBAP (171.0 mg, 0.5 mmol) was added to both the anodic and cathodic chamber through the side arms. A nitrogen atmosphere was established by evacuating and backfilling with nitrogen three times. A nitrogen filled balloon then replaced the positive nitrogen pressure supplied by the schlenk line. The anodic chamber was charged with *n*-butyl vinyl ether (2.50 mL, 22.3 mmol, 117 equiv), S-1-isobutoxy *N,N*-diethyl dithiocarbamate (CTA, **1**) (380 μ L, 0.5 M stock

solution in DCM, 0.190 mmol, 1 equiv), and DCM (2.1 mL), via syringe. The cathodic chamber was charged with DCM (5.00 mL) Potentiostat leads were connected to the E-cell caps. Stirring commenced and an oxidizing current (1mA) was applied for 4 hours. Following the desired reaction time, aliquots for NMR and GPC analysis were taken via a syringe ($M_{n,Theo} = 10.2$ kg/mol, $M_{n,Exp} = 8.1$ kg/mol, $D = 1.11$).

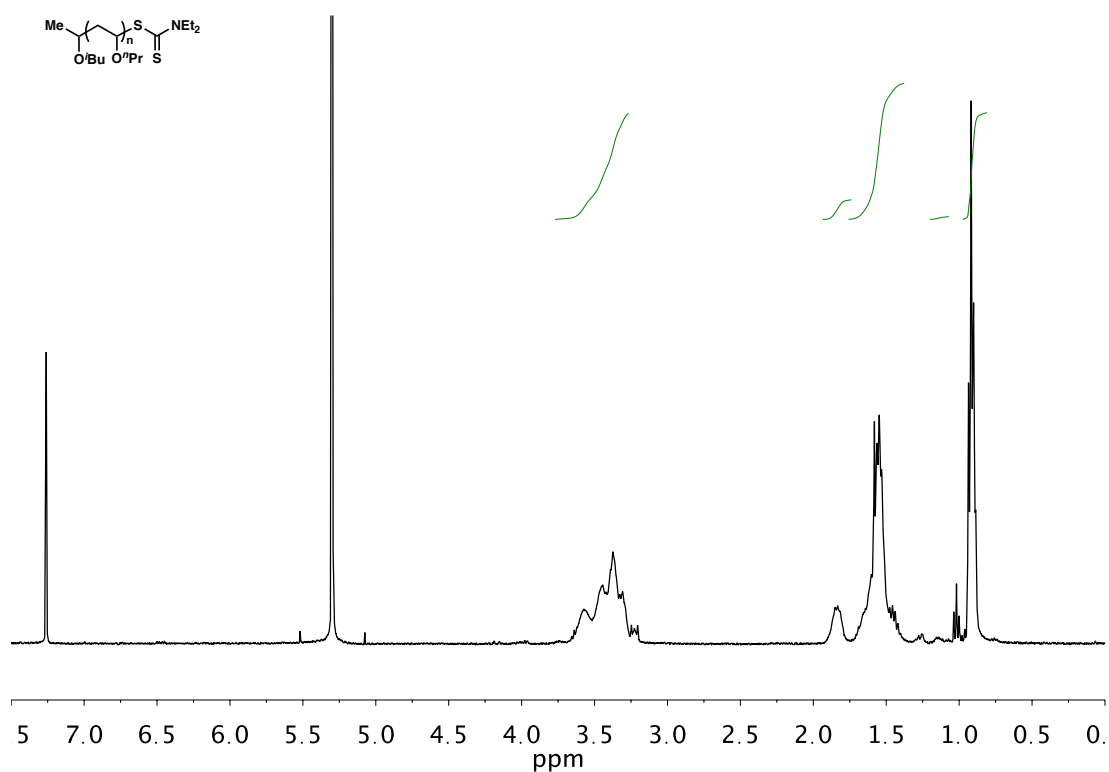


Figure 2.19. ^1H NMR of poly(*n*-propyl vinyl ether)

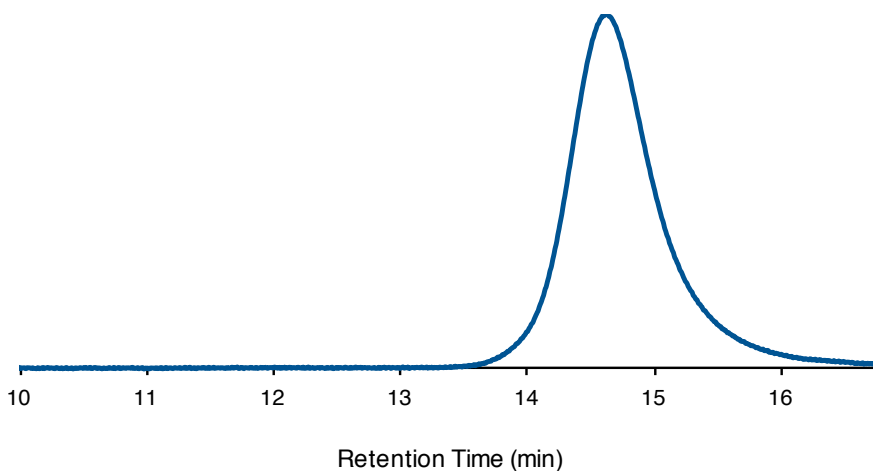


Figure 2.20. GPC trace of poly(*n*-propyl vinyl ether)

Procedure for Electrochemically Mediated Polymerization of Ethyl Vinyl Ether (Table 2.2, Entry 3)

The following procedure was preceded by Electropolymerization Reaction Setup (Figure 2.8). Once the E-cell cooled to room temperature, TEMPO (29.7 mg, 0.190 mmol, 1 equiv) was added to the anodic chamber and TBAP (205.1 mg, 0.6 mmol) was added to both the anodic and cathodic chamber through the side arms. A nitrogen atmosphere was established by evacuating and backfilling with nitrogen three times. A nitrogen filled balloon then replaced the positive nitrogen pressure supplied by the schlenk line. The anodic chamber was charged with ethyl vinyl ether (2.50 mL, 26.1 mmol, 137 equiv), S-1-isobutoxy *N,N*-diethyl dithiocarbamate (CTA, **1**) (190 μ L, 1.0 M stock solution in DCM, 0.190 mmol, 1 equiv), and DCM (3.3 mL), via syringe. The

cathodic chamber was charged with DCM (6.00 mL) Potentiostat leads were connected to the E-cell caps. Stirring commenced and an oxidizing current (1mA) was applied for 4 hours. Following the desired reaction time, aliquots for NMR and GPC analysis were taken via a syringe ($M_{n,Theo} = 10.4$ kg/mol, $M_{n,Exp} = 9.7$ kg/mol, $\bar{D} = 1.14$).

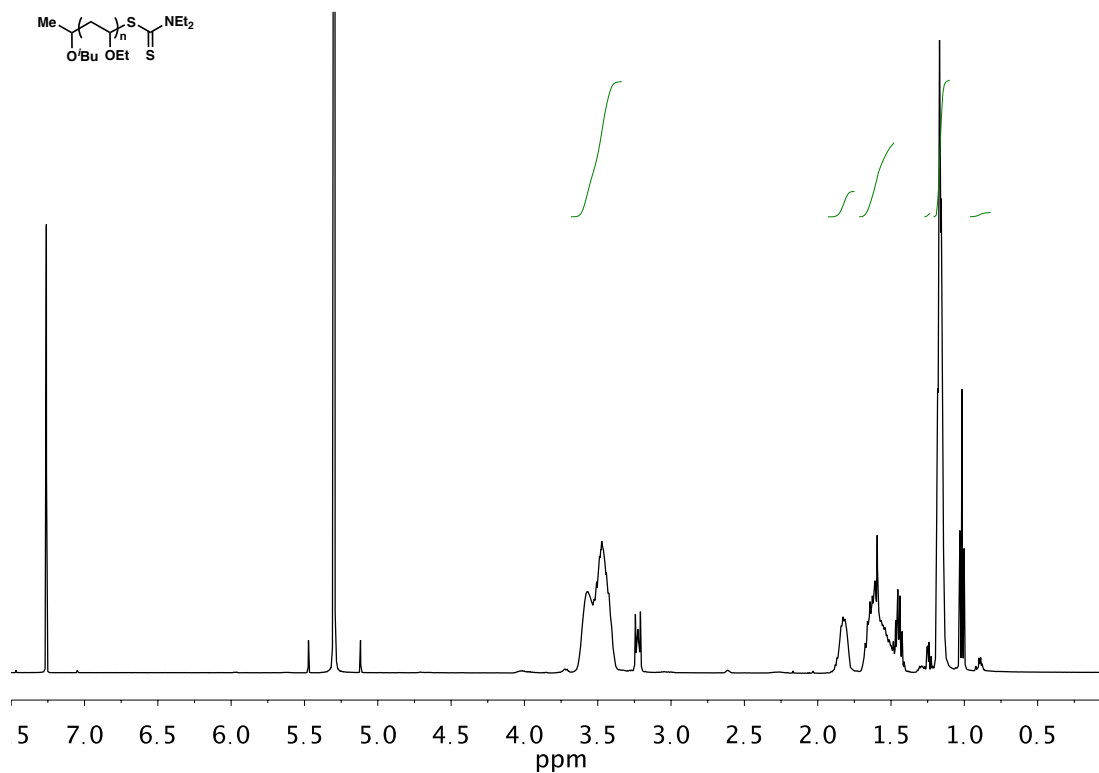


Figure 2.21. ^1H NMR of poly(ethyl vinyl ether)

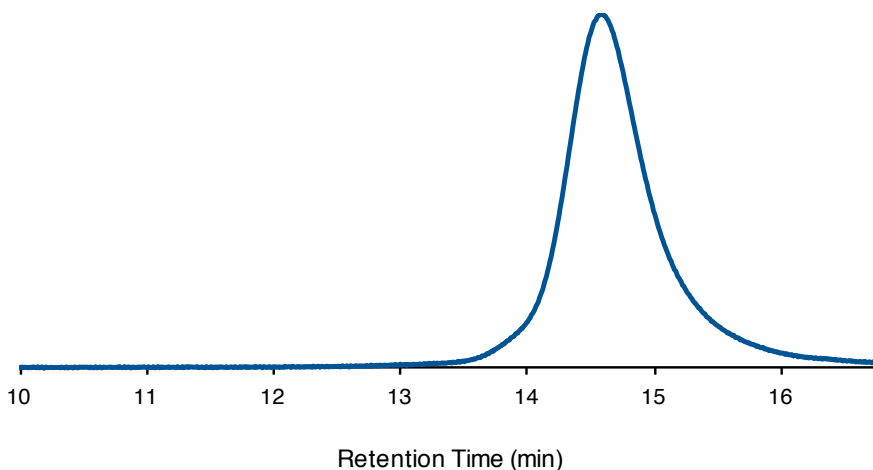


Figure 2.22. GPC trace of poly(ethyl vinyl ether)

Procedure for Electrochemically Mediated Polymerization of 2-Chloroethyl Vinyl Ether (Table 2.2, Entry 4)

The following procedure was preceded by Electropolymerization Reaction Setup (Figure 2.8). Once the E-cell cooled to room temperature, TEMPO (40.7 mg, 0.260 mmol, 1 equiv) was added to the anodic chamber and TBAP (205.1 mg, 0.6 mmol) was added to both the anodic and cathodic chamber through the side arms. A nitrogen atmosphere was established by evacuating and backfilling with nitrogen three times. A nitrogen filled balloon then replaced the positive nitrogen pressure supplied by the schlenk line. The anodic chamber was charged with 2-chloroethyl vinyl ether (2.50 mL, 24.6 mmol, 95 equiv), S-1-isobutoxy *N,N*-diethyl dithiocarbamate (CTA, **1**) (260 μ L, 1.0 M stock solution in DCM, 0.260 mmol, 1 equiv), and DCM (3.2 mL), via syringe. The cathodic chamber was charged with DCM (6.00 mL) Potentiostat

leads were connected to the E-cell caps. Stirring commenced and an oxidizing current (1mA) was applied for 4 hours. Following the desired reaction time, aliquots for NMR and GPC analysis were taken via a syringe ($M_{n,Theo} = 10.3$ kg/mol) $M_{n,Exp} = 11.3$ kg/mol, $D = 1.12$).

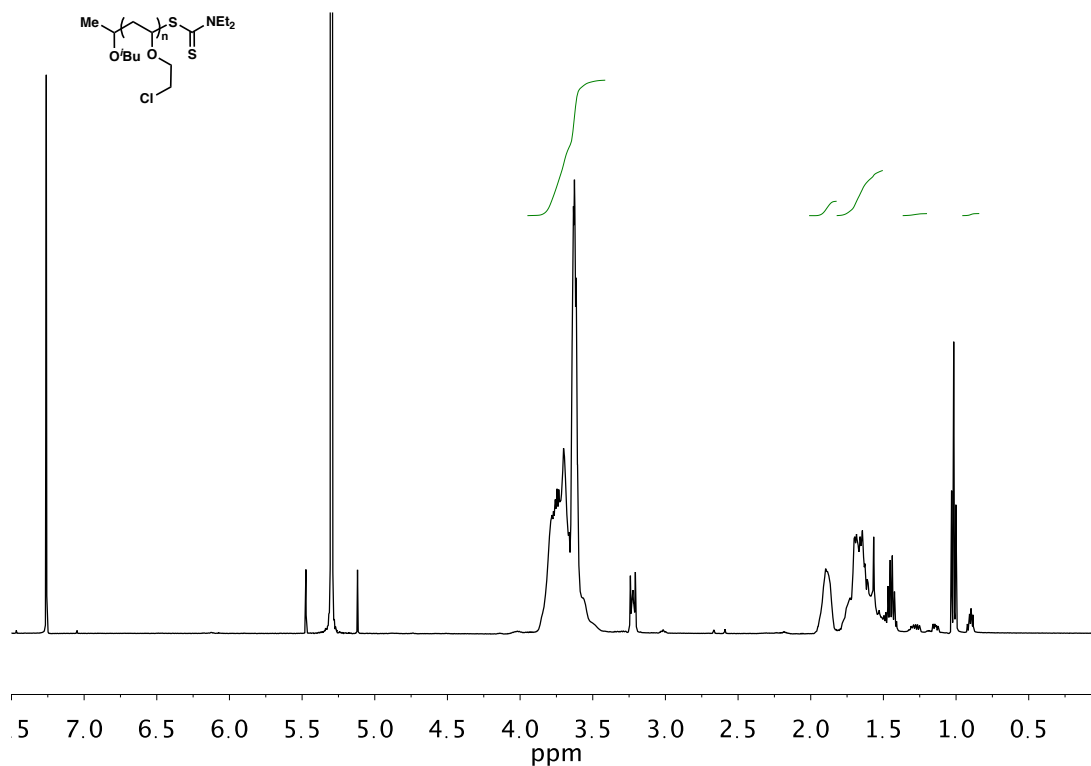


Figure 2.23. ^1H NMR of poly(2-chloroethyl vinyl ether)

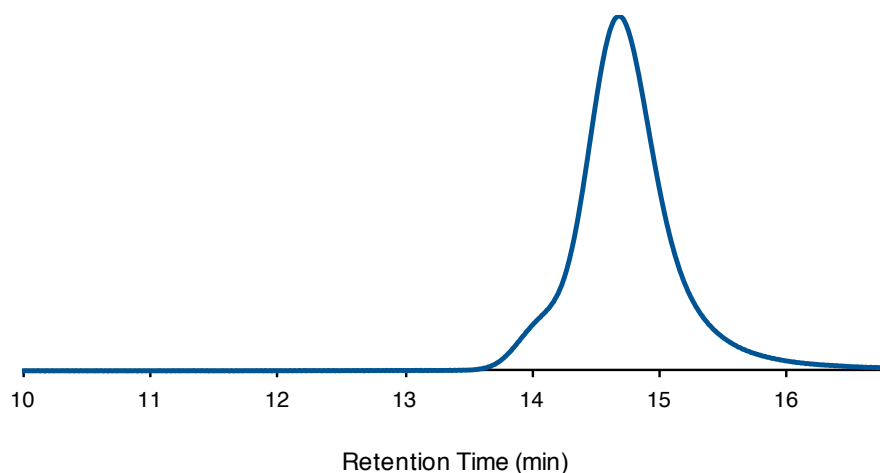


Figure 2.24. GPC trace of poly(2-chloroethyl vinyl ether)

Procedure for Electrochemically Mediated Polymerization of 4-Methoxystyrene (Table 2.2, Entry 5)

The following procedure was preceded by Electropolymerization Reaction Setup (Figure 2.8). Once the E-cell cooled to room temperature, TEMPO (39.1 mg, 0.250 mmol, 1 equiv) was added to the anodic chamber and TBAP (205.1 mg, 0.6 mmol) was added to both the anodic and cathodic chamber through the side arms. A nitrogen atmosphere was established by evacuating and backfilling with nitrogen three times. A nitrogen filled balloon then replaced the positive nitrogen pressure supplied by the schlenk line. The anodic chamber was charged with 4-methoxy-styrene (2.50 mL, 18.6 mmol, 74 equiv), S-1-isobutoxy *N,N*-diethyl dithiocarbamate (CTA, **1**) (250 μ L, 1.0 M stock solution in DCM, 0.250 mmol, 1 equiv), and DCM (3.2 mL), via syringe. The cathodic chamber was charged with DCM (6.00 mL) Potentiostat leads were

connected to the E-cell caps. Stirring commenced and an oxidizing current (2 mA) was applied for 10 hours. Following the desired reaction time, aliquots for NMR and GPC analysis were taken via a syringe ($M_{n, \text{Theo}} = 10.3 \text{ kg/mol}$, $M_{n, \text{Exp}} = 8.7 \text{ kg/mol}$, $D = 1.33$).

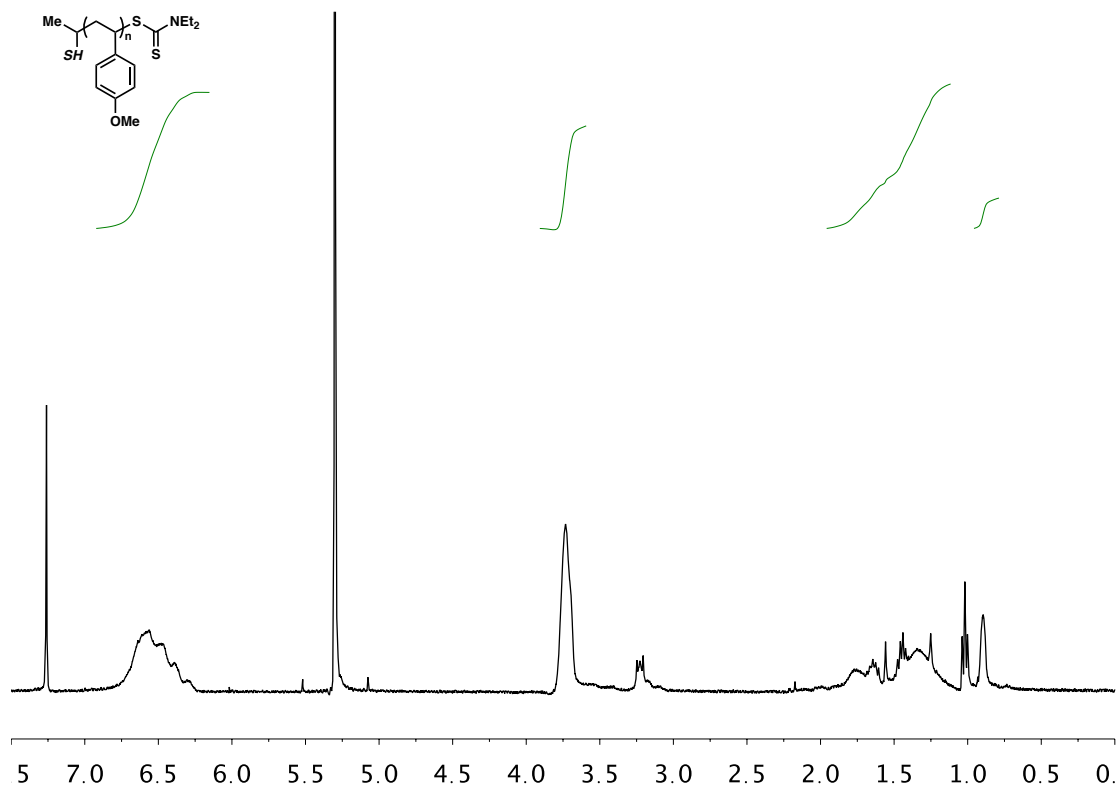


Figure 2.25. ^1H NMR of poly(4-methoxystyrene)

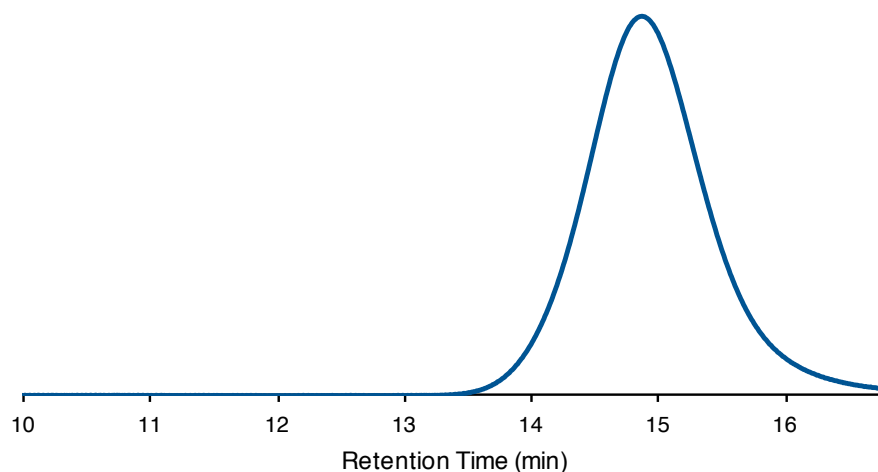


Figure 2.26. GPC trace of poly(4-methoxystyrene)

Procedure for Electrocontrolled Synthesis of Diblock Copolymer

The following procedure was preceded by Electropolymerization Reaction Setup (Figure 2.8). Once the E-cell cooled to room temperature, TEMPO (59.4 mg, 0.380 mmol, 1 equiv) was added to the anodic chamber and TBAP (205.1 mg, 0.6 mmol) was added to both the anodic and cathodic chamber through the side arms. A nitrogen atmosphere was established by evacuating and backfilling with nitrogen three times. A nitrogen filled balloon then replaced the positive nitrogen pressure supplied by the schlenk line. The anodic chamber was charged with ethyl vinyl ether (2.50 mL, 26.1 mmol, 69 equiv), S-1-isobutoxy *N,N*-diethyl dithiocarbamate (CTA, **1**) (380 μ L, 1.0 M stock solution in DCM, 0.380 mmol, 1 equiv), and DCM (3.1 mL), via syringe. The cathodic chamber was charged with DCM (6.00 mL) Potentiostat leads were connected to the E-cell caps. Stirring commenced and an oxidizing current

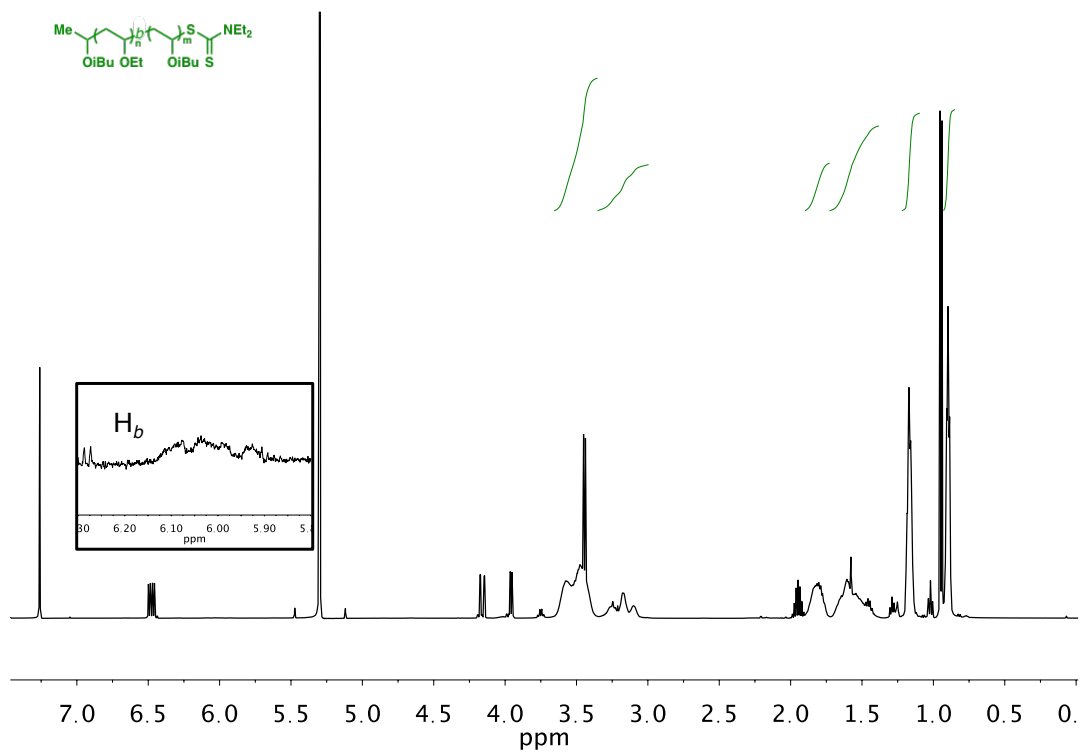


Figure 2.28. ^1H NMR of poly(ethyl vinyl ether-block-isobutyl vinyl ether)

Procedure for Electrocontrolled Initiation and Termination of the Polymerization of Isobutyl Vinyl Ether

RVC working and counter electrodes were dried in a vacuum oven for 4 hours at 200 °C before assembling E-cell

The following procedure was preceded by Electropolymerization Reaction Setup (Figure 2.8). Once the E-cell cooled to room temperature, TEMPO (29.7 mg, 0.19 mmol, 1 equiv) was added to the anodic chamber and TBAP (205.1 mg, 0.6 mmol) was added to both the anodic and cathodic chamber through the side arms. A nitrogen atmosphere was established by evacuating and backfilling with nitrogen three times. A nitrogen filled balloon then replaced the positive nitrogen pressure supplied by the schlenk line. The anodic chamber was charged with isobutyl vinyl ether (2.50 mL, 19.2 mmol, 100 equiv), S-1-isobutoxy *N,N*-diethyl dithiocarbamate (CTA, **1**) (190 μ L, 1.0 M stock solution in DCM, 0.190 mmol, 1 equiv), and DCM (3.3 mL), via syringe. The cathodic chamber was charged with DCM (6.00 mL) Potentiostat leads were connected to the E-cell caps. Stirring commenced and the following stimuli were applied, taking aliquots for NMR and GPC analysis at each time point:

Table 2.4. Applied Stimuli for ON/OFF Experiment

Time Period	Stimuli
0 → 20 min	1 mA
20 → 50min	– 875 mV vs Fc/Fc+
50 → 65 min	1 mA
65 → 95 min	– 875 mV vs Fc/Fc+
95 → 110 min	1 mA
110 → 140 min	– 875 mV vs Fc/Fc+
140 → 170 min	1 mA

Procedure for Kinetic Investigation of the Electrocontrolled Polymerization of Isobutyl Vinyl Ether

The following procedure was preceded by Electropolymerization Reaction Setup (Figure 2.8). Once the E-cell cooled to room temperature, TEMPO (29.7 mg, 0.19 mmol, 1 equiv) was added to the anodic chamber and TBAP (205.1 mg, 0.6 mmol) was added to both the anodic and cathodic chamber through the side arms. A nitrogen atmosphere was established by evacuating and backfilling with nitrogen three times. A nitrogen filled balloon then replaced the positive nitrogen pressure supplied by the schlenk line. The anodic chamber was charged with isobutyl vinyl ether (2.50 mL, 19.2 mmol, 100 equiv), S-1-isobutoxy *N,N*-diethyl dicarbamate (CTA, **1**) (190 μ L, 1.0 M stock solution in DCM, 0.190 mmol, 1 equiv), and DCM (3.3 mL), via syringe. The cathodic chamber was charged with DCM (6.00 mL) Potentiostat leads were connected to the E-cell caps. Stirring commenced and aliquots were taken at

10 min, 20 min, 30 min, 40 min, 50 min, 60 min, 120 min, 180 min, and 240 min with a syringe and analyzed by NMR and GPC.

General Procedure for Electrochemically Mediated Polymerization of Isobutyl Vinyl Ether by DC Power Supply

DC Power supplies generally cost less than \$100, greatly increasing the access and applicability of this method. They differ from potentiostats in that they can only have two leads, which can deliver a potential between working and counter or a direct current. For this reason a Ag wire reference was not included in the anodic electrode cap

The following procedure was preceded by Electropolymerization Reaction Setup (Figure 2.8). Once the E-cell cooled to room temperature, TEMPO (29.7 mg, 0.190 mmol, 1 equiv) was added to the anodic chamber and TBAP (205.1 mg, 0.6 mmol) was added to both the anodic and cathodic chamber through the side arms. A nitrogen atmosphere was established by evacuating and backfilling with nitrogen three times. A nitrogen filled balloon then replaced the positive nitrogen pressure supplied by the schlenk line. The anodic chamber was charged with isobutyl vinyl ether (2.50 mL, 19.2 mmol, 100 equiv), S-1-isobutoxy *N,N*-diethyl dithiocarbamate (CTA, **1**) (190 μ L, 1.0 M stock solution in DCM, 0.190 mmol, 1 equiv), and DCM (3.3 mL), via syringe. The cathodic chamber was charged with DCM (6.00 mL) The leads of the DC power supply were connected to the E-cell caps. Stirring commenced and an oxidizing

current (1mA) was applied for 4 hours. Then aliquots for NMR and GPC analysis were taken via a syringe ($M_{n, \text{Theo}} = 10.4 \text{ kg/mol}$, $M_n = 10.1 \text{ kg/mol}$, $D = 1.15$).

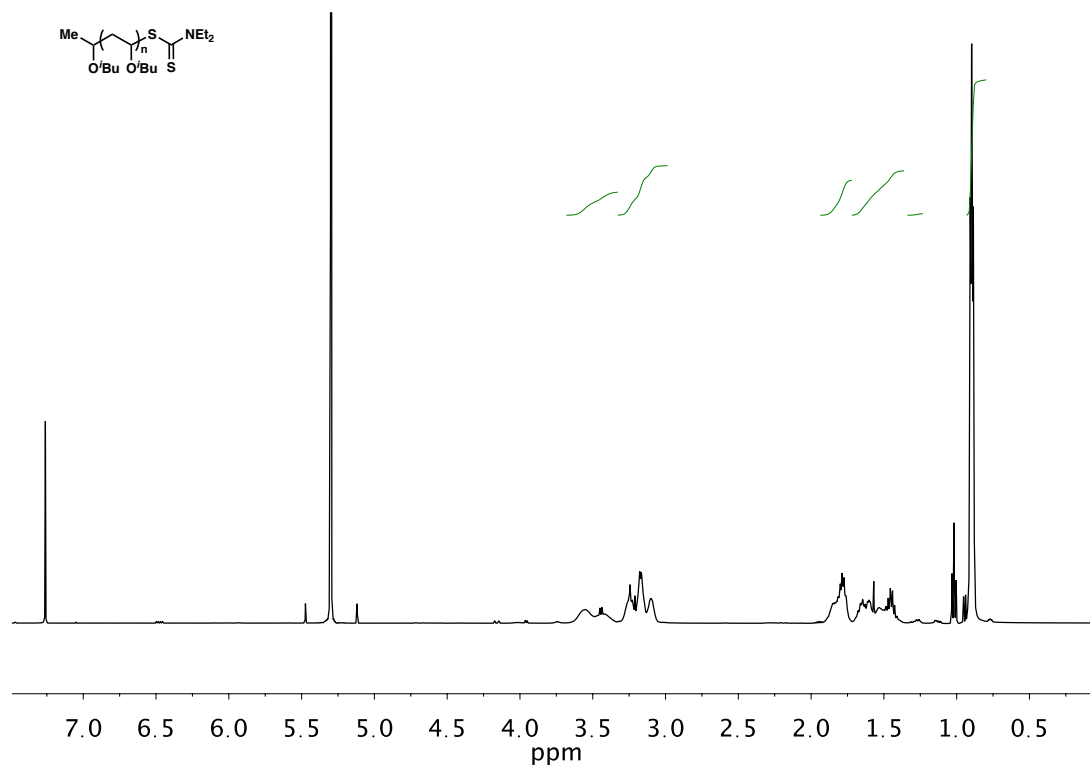


Figure 2.29. ^1H NMR of poly(isobutyl vinyl ether) (DC power supply)

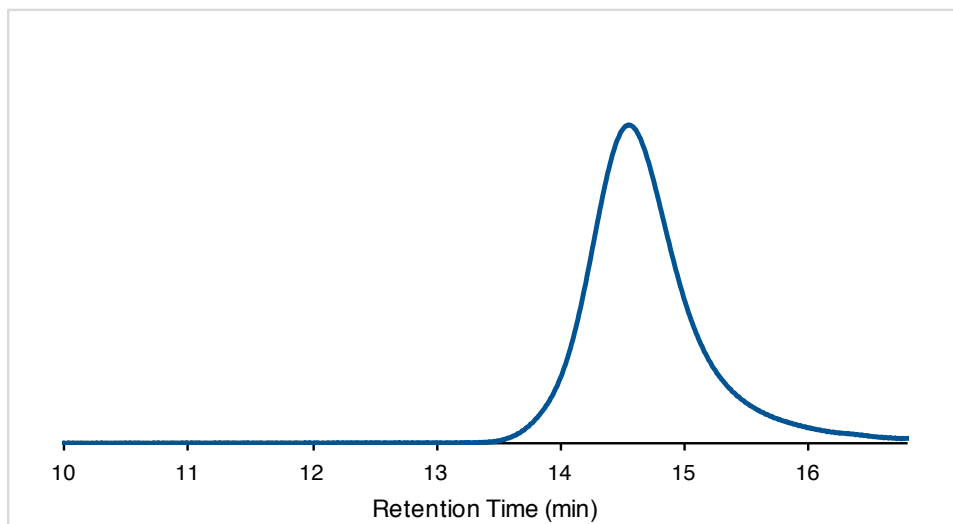


Figure 2.30. GPC trace of poly(isobutyl vinyl ether) (DC power supply)

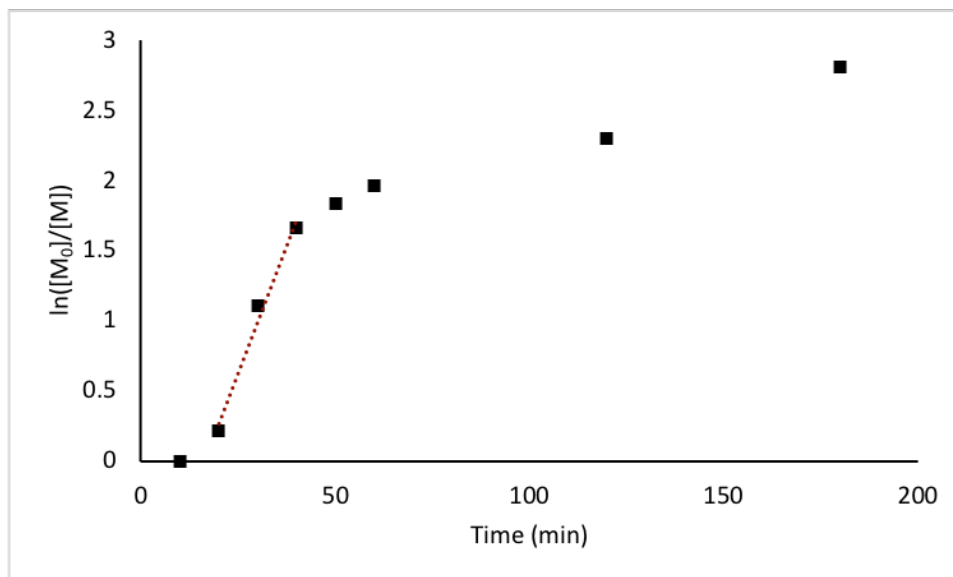


Figure 2.31. Kinetic Plot ($\ln([M_0]/[M])$ vs time)

Table 2.5. Conversions and Time of Reactions in Table 2.1

Entry ^a	Stimuli	[M]:[1]: [TEMPO]	Time (hr)	Conv. (%)	$M_{n,Theo}^b$ (kg/mol)	$M_{n,Exp}$ (kg/mol)	\bar{D}
1 ^c	325 mV	100:1:0	6	>99	10.3	10.9	1.97
2 ^c	325 mV	100:1:1	6	84	8.3	8.4	1.23
3 ^c	325 mV	100:1:0.1	6	>99	9.9	7.1	1.50
4 ^c	325 mV	100:1:50	6	>99	9.9	6.6	1.39
5 ^c	325 mV	100:0:1	6	67	–	27.9	2.93
6	1 mA	100:2:1	4	93	5.0	6.8	1.07
7	1 mA	100:1.5:1.5	4	>99	6.9	8.8	1.09
8	1 mA	100:1:1	4	>99	10.4	10.1	1.15
9	0.1 mA	100:0.25:0. 25	4	72	28.8	22.5	1.33
10 ^d	1 mA	100:1:1	4	92	9.5	7.9 (8.1)	1.45
11 ^e	1 mA	100:1:1	4	>99	9.9	10.7	1.20
12	325 mV	100:0:0	6	54	–	29.8	2.13

^a[IBVE] = 3.84 M (in DCM), V_{tot} = 5 mL, [Et₄NClO₄] = 0.1 M, RVC Anode, Ag Reference, RVC Cathode (Divided cell). ^bM_n (Theo) = [M]/[CTA] × MW_M × Conversion + MW_{CTA}. ^cPotential vs Fc⁺/Fc. ^dElectrolyte = [Et₄NPF₆] = 0.1 M. ^eElectrolyte = [Et₄NBF₄] = 0.1 M

Table 2.6. Conversion and Reaction Times in Table 2

Entry ^a	Monomer	Time (hr)	Conv. (%)	$M_{n,Theo}^b$ (kg/mol)	$M_{n,Exp}$ (kg/mol)	\bar{D}
1	<i>n</i> BuVE	4	96	9.9	9.7	1.32
2	<i>n</i> PrVE	4	>99	10.2	8.1	1.11
3	EVE	4	>99	10.4	9.7	1.14
4	Cl-EVE	4	>99	10.3	11.3	1.12
5 ^c	<i>p</i> -OMe- Styrene	10	>99	10.2	8.7	1.33

^a[M] = 42% in DCM v/v, V_{tot} = 6 mL, [Et₄NClO₄] = 0.1 M, RVC Anode, Ag Reference, RVC Cathode (Divided), Reaction time = 4 hr. ^bM_n (Theo) = [M]/[CTA] × MW_M × Conversion + MW_{CTA}. ^cApplied current = 2 mA.

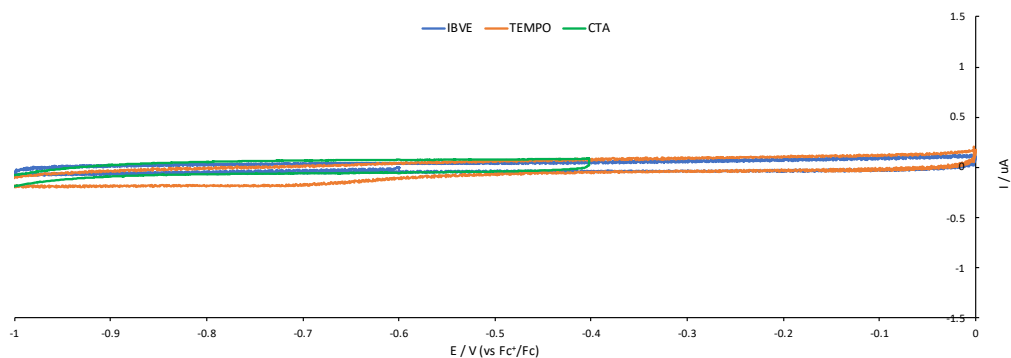
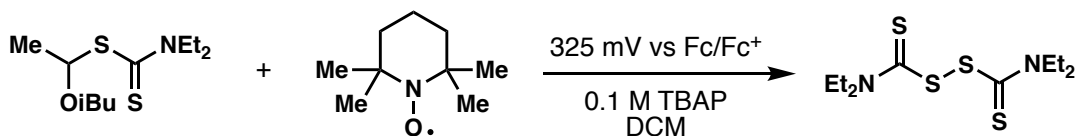


Figure 2.32. Reductive CVs of IBVE, CTA, TEMPO

Generation of Tetraethylthiuram Disulfide Through the Electrocatalytic Oxidation of CTA by TEMPO



The following procedure was preceded by Electropolymerization Reaction Setup (Figure 2.8). Once the E-cell cooled to room temperature, TEMPO (78.2 mg, 0.500 mmol, 1 equiv) was added to the anodic chamber and TBAP (205.1 mg, 0.6 mmol) was added to both the anodic and cathodic chamber through the side arms. A nitrogen atmosphere was established by evacuating and backfilling with nitrogen three times. A nitrogen filled balloon then replaced the positive nitrogen pressure supplied by the schlenk line. The anodic chamber was charged with isobutyl vinyl ether S-1-isobutoxy *N,N*-diethyl dithiocarbamate (CTA, **1**) (0.50 mL, 1.0 M stock solution in DCM, 0.500 mmol, 1 equiv), and DCM (5.5 mL), via syringe. The cathodic chamber was charged

with DCM (6.00 mL) The leads of the DC power supply were connected to the E-cell caps. Stirring commenced and an oxidizing potential (325 mV vs Fc/Fc⁺) was applied for 3 hours. Reaction contents of anodic chamber was passed through a silica plug with ethyl acetate to remove electrolyte. Eluent was collected and concentrated under vacuo and purification by preparative TLC (15 % ethyl acetate in hexanes) afforded tetraethylthiuram disulfide (analyzed by ¹H NMR spectroscopy, which was in agreement with data reported in the literature).²

References:

- (1) Uchiyama, M.; Satoh, K.; Kamigaito, M. *Angew. Chem. Int. Ed.* **2015**, *54*, 1924.
- (2) Michaudel, Q.; Chauviré, T.; Kottisch, V.; Supej, M. J.; Stawiasz, K. J.; Shen, L.; Zipfel, W. R.; Abruña, H. D.; Freed, J. H.; Fors, B. P. *J. Am. Chem. Soc.* **2017**, *139*, 15530.

CHAPTER 3
ON DEMAND SWITCHING OF POLYMERIZATION MECHANISM AND
MONOMER SELECTIVITY WITH ORTHOGONAL STIMULI

3.1 Abstract

The development of next-generation materials is coupled with the ability to predictably and precisely synthesize polymers with well-defined structures and architectures. In this regard, the discovery of synthetic strategies that allow on demand control over monomer connectivity during polymerization would provide access to complex structures in a modular fashion and remains a grand challenge in polymer chemistry. In this manuscript, we report a method where monomer selectivity is controlled during the polymerization by the application of two orthogonal stimuli. Specifically, we developed a cationic polymerization where polymer chain growth is controlled by a chemical stimulus and paired it with a compatible photocontrolled radical polymerization. By alternating the application of the chemical and photochemical stimuli the incorporation of vinyl ethers and acrylates could be dictated by switching between cationic and radical polymerization mechanisms, respectively. This enables the synthesis of multiblock copolymers where each block length is governed by the amount of time a stimulus is applied and the quantity of blocks is determined by the number of times the two stimuli are toggled. This new method allows on demand control

over polymer structure with external influences and highlights the potential for using stimuli-controlled polymerizations to access novel materials.

3.2 Introduction

Macromolecular properties are inherently influenced by polymer molar mass, monomer sequence, and architecture, as evidenced by the diversity of functions observed among biomacromolecules derived from a limited library of molecular building blocks. Therefore, the discovery of synthetic techniques that give increased control over monomer connectivity and structure in a polymer will broaden the range of applications of these materials. Chemists have made significant progress in making well-defined materials with the development of “living” polymerizations that enable the formation of macromolecules with predictable molar masses (M_n) and narrow molar mass distributions (dispersity, D) with high chain end fidelity capable of post polymerization modification.^{1,2} Even greater control over polymerization processes has recently been achieved through regulation of chain growth with various external stimuli^{3,4} (*i.e.*, thermal,^{5–7} chemical,^{8–13} mechanochemical,^{14–17} electrochemical,^{18,19} and photochemical^{20–45}). However, the ability to precisely control monomer connectivity during a polymerization remains a grand challenge.

Temporal control of polymer chain growth in externally regulated polymerizations provides an excellent opportunity to precisely control macromolecular structure and function. To exploit this unique level of control,

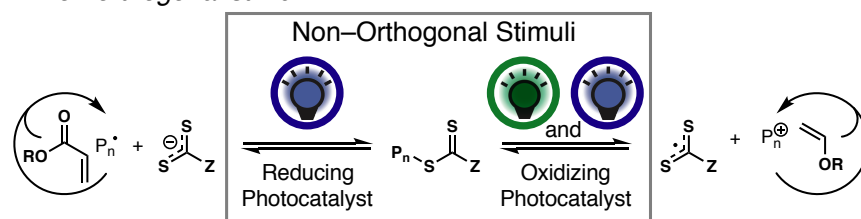
we envisioned a system where monomer selectivity at a given polymer chain end could be switched on demand with two different stimuli.^{46,47} This strategy would enable the one pot synthesis of polymers where the monomer connectivity would be precisely dictated by external influences and would be a step closer to nature's ability to perfectly control polymer sequence.

To achieve this goal, we were inspired by systems developed by Kamigaito and co-workers where both radical and cationic polymerization processes are active in a single reaction, allowing blocks of two monomers that react via different mechanisms to be randomly incorporated into the same polymer chain.⁴⁸⁻⁵² We reasoned that temporal control over the cationic and radical mechanisms via two stimuli would allow on demand switching of polymerization mechanism *in situ* and lead to precise control over the block structure of the final polymer.

Taking a step toward this challenge, our group recently developed a two-photocatalyst system that took advantage of photocontrolled cationic and radical reversible addition-fragmentation chain transfer (RAFT) polymerizations (Figure 3.1.a).^{53,54} Irradiating our system with green light led to promotion of the cationic polymerization of isobutyl vinyl ether (IBVE) through selective excitation of an oxidizing photocatalyst.^{55,56} Alternatively, irradiation with blue light excited both the reducing and oxidizing photocatalysts in solution leading to simultaneous radical polymerization of methyl acrylate (MA) and cationic polymerization of IBVE (Figure 3.1.a). Although this two photocatalyst system

demonstrated that the polymerization mechanism could be changed *in situ*, selective promotion of the radical mechanism was not possible due to the overlap of the absorption spectra of the two catalysts. In order to overcome this limitation, polymerization processes where chain growth is regulated by two orthogonal and compatible stimuli is necessary to allow selective promotion of either the radical or cationic pathways (Figure 3.1.b).

a) Previous work: Interconversion of polymerization mechanism via non-orthogonal stimuli



b) This work: External control of polymerization mechanism via orthogonal stimuli

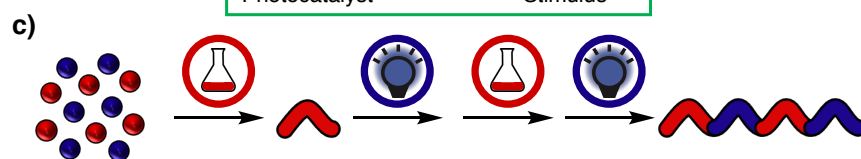
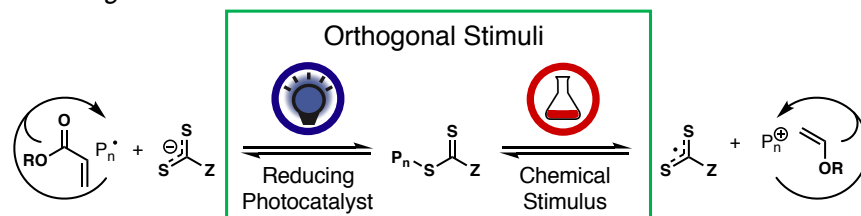


Figure 3.1. (a) Interconversion of polymerization mechanisms via non-orthogonal photoirradiation of two photocatalysts with blue and green light. (b) Generation of cations and radicals at polymer chain ends via two orthogonal stimuli. (c) The synthesis of tetrablock vinyl ether-*b*-methyl acrylate copolymers via a chemical-photochemical gated mechanistic switch.

Herein, we report the development of a new chemically controlled cationic polymerization of vinyl ether monomers. Combining this cationic polymerization with a photocontrolled radical process enables completely orthogonal switching of polymerization mechanism at a single chain end *in situ*. This increased level of control is successfully applied to the one-pot synthesis of multiblock copolymers of IBVE and MA, without the need of subsequent polymer isolation, purification, or chain-end modification (Figure 3.1.c).

3.3 Results and Discussion

To gain precise control over polymerization mechanism *in situ*, we set out to develop a cationic polymerization regulated by a stimulus orthogonal and compatible with the photocontrolled radical polymerization process. In recent years, chemists have investigated a number of stimuli compatible with light to induce polymerization, including mechanical force, electricity, redox events triggered by chemical additives, and temperature. Among those, we opted for a chemical stimulus that could be used to initiate and reversibly terminate the propagating cation. We hypothesized that the cationic polymerization could be initiated with a mild single electron oxidant (Figure 3.2.a).

Specifically, we reasoned that the addition of ferrocenium salts (FcX) should selectively oxidize the chain transfer agents (CTA) **1a** or **1b** and, consequently, shuttle a predictable amount of an oxocarbenium ion into the RAFT mechanism (Figure 3.2.b).⁵⁷ Importantly, temporal control over chain

growth could be achieved through the addition of a dithiocarbamate anion, **2**, to recap propagating cations as well as reduce any remaining ferrocenium to ferrocene, completely halting the polymerization (Figure 3.2.c). This process would provide a cationic polymerization that could be reversibly activated/deactivated through the addition of two chemical species. Moreover, the rate of polymerization could be dictated by the concentration of FcX added.

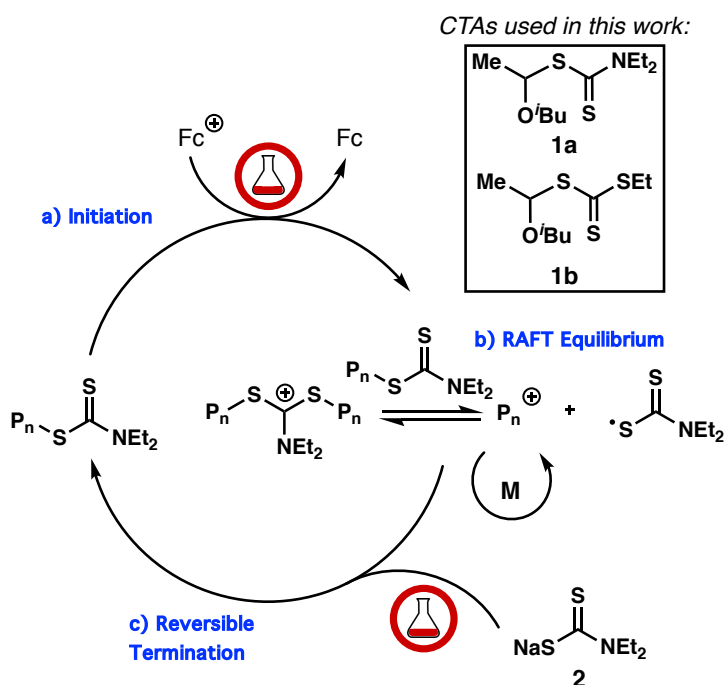


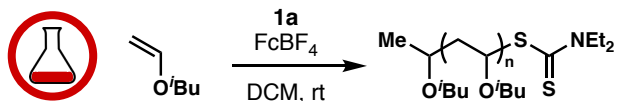
Figure 3.2. Proposed mechanism including (a) initiation, (b) reversible addition-fragmentation chain transfer (RAFT) equilibrium and (c) termination of the chemically (red flask) gated cationic polymerization of vinyl ether monomers (M = monomer).

To test our hypothesis, we examined the use of ferrocenium tetrafluoroborate (FcBF_4) to initiate the cationic polymerization of vinyl ethers. Treating a solution of IBVE and **1a** with FcBF_4 in dichloromethane (DCM) gave a 10.3 kg/mol polymer with a narrow \mathcal{D} of 1.11 (Table 3.1, entry 1). Importantly, the experimental molar mass aligned well with the theoretical value, demonstrating that this system has excellent initiator efficiency. Control experiments demonstrated that performing the reaction in the absence of FcBF_4 gave no polymerization (Table 3.1, entry 2), while removal of **1a** gave a broad dispersity, high molecular weight polymer (Table 3.1, entry 3). At higher loadings of FcBF_4 (5 mol% relative to IBVE), experimental M_n 's deviated from theoretical values (Table 3.1, entry 4), through promotion of uncontrolled polymerization pathways like those observed in the absence of **1a**. Additionally, at very low concentrations of FcBF_4 (0.0025 mol%), no conversion of monomer is observed (Table 3.1, entry 5), unless the more active CTA **1b** is used (Table 3.1, entry 6).

Interestingly, initiating the polymerization with FcBF_4 proved to be effective at synthesizing high molecular weight poly(IBVE) up to 65 kg/mol with narrow \mathcal{D} values (Table 3.1, entry 7–11). This is a significant advantage over our previously reported photocontrolled cationic polymerizations where we observed a loss in control when targeting molar masses above 20 kg/mol. We attribute this increased efficiency to the lower oxidation potential of ferrocene (Fc) relative to **1a**, creating milder polymerization conditions that limit the

generation of new chains via direct oxidation of IBVE, a previously observed undesired pathway.⁵⁵ Under the reported reaction conditions, high degrees of polymerization were achieved within three hours. Additionally, these conditions

Table 3.1. Reaction optimization



Entry ^a	[IBVE]:[CTA]: [Fc ⁺]	Conv. (%)	$M_{n, \text{Theo}}$ ^b (kg/mol)	$M_{n, \text{Exp}}$ ^c (kg/mol)	\bar{D}
1	100:1:0.01	> 99	10.2	10.3	1.11
2	100:1:0	0	0	0	0
3	100:0:0.01	89	–	243	2.35
4	100:1:5.0	>99	10.2	14.7	1.14
5	100:1:0.0025	0	0	0	0
6 ^d	100:1:0.0025	> 99	10.2	11.1	1.45
7	100:1:1.0	> 99	10.2	10.6	1.10
8	200:1:0.01	> 99	20.2	19.0	1.11
9	400:1:0.02	> 99	40.2	35.1	1.16
10	600:1:0.04	> 99	60.5	54.6	1.28
11	800:1:0.04	> 99	80.5	65.3	1.24
12 ^e	100:1:0.01	> 99	10.2	10.1	1.25

^a[IBVE] = 3.1 M (in DCM), Reaction Volume = 0.65 mL. ^b $M_{n, \text{Theo}}$
 $M_{n, \text{Theo}} = [\text{M}]/[\text{CTA}] \times \text{MW}_{\text{Monomer}} \times \text{Conversion} + \text{MW}_{\text{CTA}}$. ^c $M_{n, \text{Exp}}$
determined by gel permeation chromatography with a multi-angle light scattering detector. ^dCTA = **1b**. ^eOpen to air.

provide a polymerization robust enough to proceed under ambient atmosphere while maintaining low \bar{D} and excellent control over the final polymer M_n (Table 3.1, entry 12).⁵⁸ This result demonstrates the practicality of the polymerization and avoids the requirement of advanced air and water free techniques.

Importantly, the new FcBF₄-initiated process delivered effective cationic polymerization of a range of vinyl ether monomers that had varied steric and electronic characteristics, along with *para*-methoxystyrene. In each case, excellent agreement between theoretical and experimental *M_n*'s were observed while maintaining narrow *D* values (Figure 3.3).

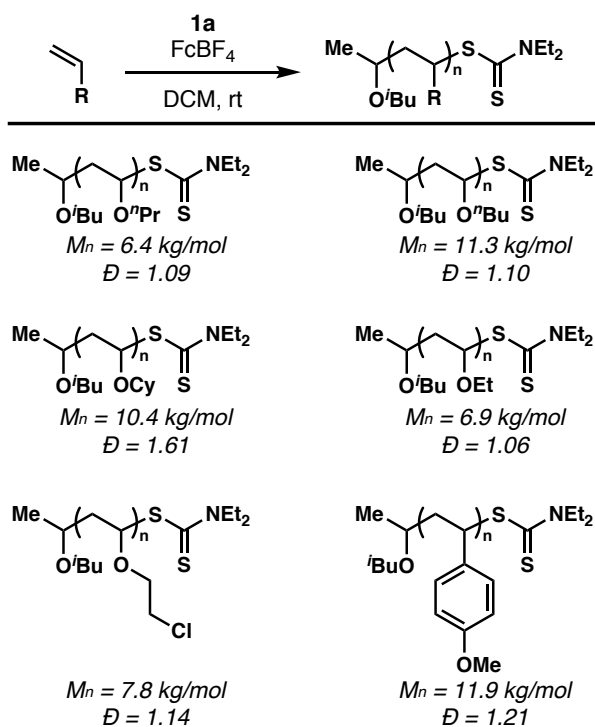


Figure 3.3. Substrate scope of vinyl monomers that can be polymerized via ferrocenium-mediated cationic RAFT polymerization.

To grow multiblock copolymers employing this method excellent chain end fidelity is essential. To demonstrate that active chain-ends are maintained

in these polymerizations, we synthesized a poly(IBVE) macroinitiator under our standard conditions and then chain-extended it with ethyl vinyl ether (EVE) to give a well-defined poly(IBVE-*b*-EVE) diblock copolymer (See Supporting Information: Figures 3.19–3.21). Importantly, we observed a clear shift in the size exclusion chromatography trace to higher molar mass with no tailing, demonstrating that the dithiocarbamate chain ends are intact after the polymerization.

Thus far, we have shown that ferrocenium is an effective mediator of the cationic polymerization vinyl ethers. However, the ability to temporally control chain growth on demand is required to pair this system with a photocontrolled radical polymerization and enable switching of polymerization mechanism. We hypothesized that the chemically controlled polymerization could be reversibly terminated through the addition of one equivalent of the dithiocarbamate anion **2** relative to the amount of FcBF₄ added to initiate polymerization (Figure 3.2.c). Theoretically, the anion should cap propagating cations to generate a dormant chain end, while reducing unreacted Fc⁺ to Fc, preventing the generation of new propagating cations. To test this hypothesis, polymerization of IBVE was initiated through the addition of FcBF₄ under our standard conditions (Figure 3.4). After 25 minutes, **2** was added and conversion of the monomer immediately halted. Importantly, the subsequent addition of FcBF₄ once again initiated the cationic polymerization. This process was repeated multiple times,

demonstrating excellent temporal control over the polymerization with a chemical stimulus.

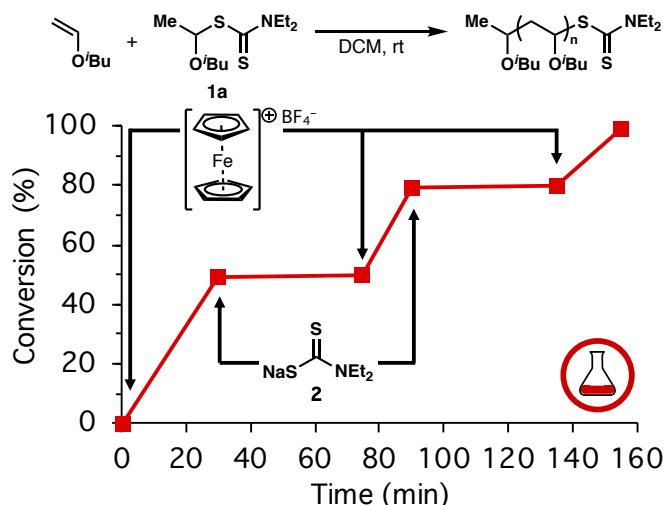


Figure 3.4. Temporal control over polymer initiation and reversible termination via the addition of FcBF_4 and **2**, respectively.

Significantly, our new chemically-regulated cationic polymerization method is orthogonal to visible light and should be compatible with the radical photoinduced electron transfer (PET)-RAFT polymerizations employing $\text{Ir}(\text{ppy})_3$ as the photocatalyst. Therefore, combining these two polymerizations in one pot should enable switching of polymerization mechanisms through modulation of the two stimuli, although consideration must be given to the mechanism of switching. We have previously demonstrated efficient initiation of the radical polymerization of MA from a poly(IBVE) macroinitiator due to the favourable formation of an α -oxy radical, which will enable efficient chain extension of MA from poly(IBVE). Conversely, initiation of the polymerization of IBVE from the

poly(MA) chain end could be problematic because it requires the formation of a high energy γ -acyl cation. However, we proposed that we could circumvent this issue by taking advantage of the small amounts of incorporation of IBVE during the radical copolymerization with MA. As previously shown by Kamigaito, the majority of dormant chain ends are thioacetals derived from vinyl ether monomers due to the radical RAFT fragmentation kinetics.⁵⁹ These thioacetals are effective at generating a cation and can promote vinyl ether homopolymerization.

Indeed, when exposing **1b**, equimolar amounts of MA and IBVE, and 0.02 mol% Ir(ppy)₃ to blue light, poly(MA) is synthesized with 20–30% incorporation of IBVE (Figure 3.5.a). Chain-end analysis by ¹H NMR of the final polymer revealed the presence of greater than 90% thioacetal chain ends (Figure 3.5.b). Gratifyingly, upon removal of blue light irradiation and addition of FcBF₄ to the crude reaction mixture, the polymer was successfully chain extended via cationic polymerization to give a well-defined poly(MA-*b*-IBVE) block polymer (Figure 3.5.a). This result demonstrates successful switching from radical to cationic polymerization *in situ* through modulation of the external stimuli, which is a key requirement for the controlled synthesis of multiblock copolymers. This approach represents a significant advance over our previously reported photocontrolled switching method, due to the orthogonal stimuli that enables us to selectively invoke the radical mechanism.

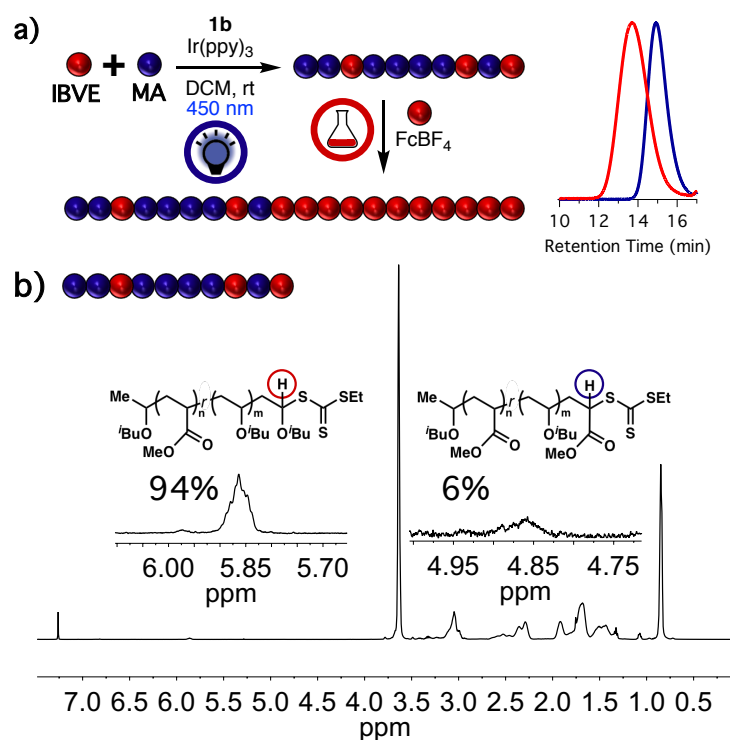


Figure 3.5. (a) A random copolymer of MA and IBVE can act as a macroinitiator for poly(MA-*b*-IBVE). (b) ¹H NMR chain-end analysis of the random copolymer revealed > 90% thioacetal chain ends.

With the ability to switch polymerization mechanism on demand, we set out to explore the range of copolymer sequences that can be targeted through modulation of the order of applied stimuli. Figure 3.6.a shows the monomer conversion over time for the synthesis of poly(MA-*b*-IBVE) diblock copolymer, where we first promoted the radical polymerization with light followed by the chemically controlled cationic polymerization. This can be extended to triblock copolymers under the same conditions by adding an additional switching event. After the first mechanistic switch from radical to cationic polymerization to

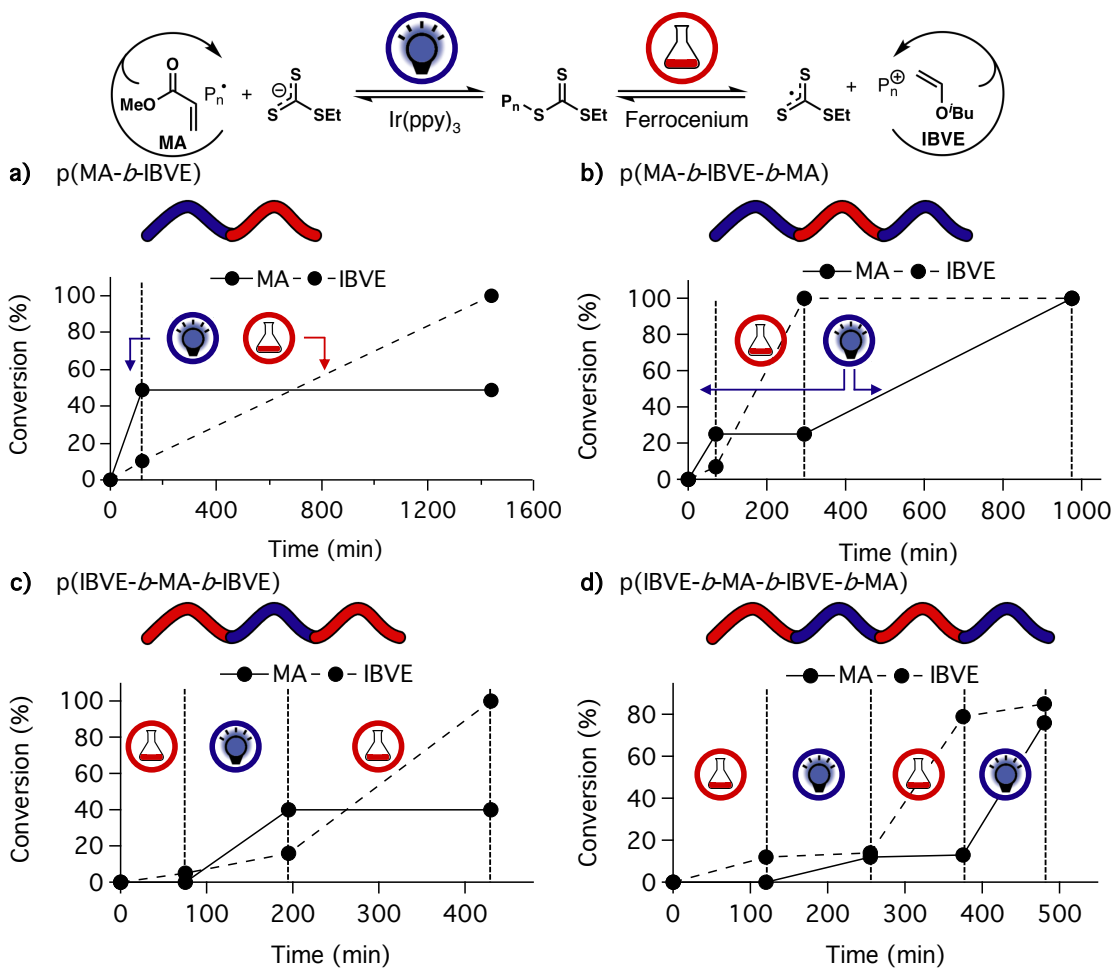


Figure 3.6. Conversion of MA (solid line) and IBVE (dashed line) over time upon applying chemically controlled cationic and photochemically controlled radical polymerization. (a) Conversion plot for poly(MA-*b*-IBVE). (b) Conversion plot for poly(MA-*b*-IBVE-*b*-MA). (c) Conversion plot for poly(IBVE-*b*-MA-*b*-IBVE). (d) Conversion plot for poly(IBVE-*b*-MA-*b*-IBVE-*b*-MA).

generate poly(MA-*b*-IBVE), vinyl ether polymerization can be successfully halted by the addition of **2**. Subsequent re-exposure to blue light initiates radical polymerization of MA resulting in poly(MA-*b*-IBVE-*b*-MA) triblock with predictable molar mass and narrow dispersity (Figure 3.6.b).

Interestingly, from the same solution conditions the inverse triblock copolymer can be synthesized by simply altering the sequence of the two applied stimuli. Specifically, initiating polymerization of IBVE, in the presence of MA and Ir(ppy)₃, by treatment with FcBF₄ in the absence of blue light (Figure 3.6.c), we observed solely conversion of IBVE over the first hour. Addition of **2** resulted in termination of the cationic polymerization, followed by irradiation with blue light for two hours to promote radical polymerization of the acrylate. Turning the light off and treating the reaction with 0.05 mol% FcBF₄ resulted in a clean mechanistic switch from radical polymerization of MA to the cationic polymerization of vinyl ethers, generating a well-defined poly(IBVE-*b*-MA-*b*-IBVE) triblock. This can be taken a step further, generating a poly(IBVE-*b*-MA-*b*-IBVE-*b*-MA) tetrablock copolymer (Figure 3.6.d) by adding one additional switching event to the last triblock copolymer. It is worth noting that the length of each block can be controlled by the length of time the stimulus is applied and the number of blocks can be dictated by the number of times the stimuli are toggled. These data clearly show that pairing orthogonal stimuli to control polymerization mechanism and monomer selectivity is a powerful approach toward the synthesis of advanced polymeric structures.

3.4 Conclusion

In conclusion, we have developed a system that enables switching of polymerization mechanism and monomer selectivity in situ with two external

stimuli. The identification of a cationic polymerization controlled by a chemical stimulus that was both orthogonal and compatible with the photocontrolled radical polymerization was key to achieving efficient switching. We demonstrated that ferrocenium salts were highly efficient initiators for the cationic RAFT polymerization of vinyl ethers and showed that reversible termination could be achieved through the addition of a dithiocarbamate anion. By pairing this new chemically-controlled cationic polymerization with a photocontrolled RAFT polymerization, we were able to selectively and reversibly promote the polymerization of vinyl ethers or acrylates. Under identical solution conditions, this enabled the synthesis of an array of well-defined multiblock copolymers where the final structure was dictated by the two stimuli; the length of each block was controlled by the amount of time the stimulus was applied and the number of blocks was governed by the alternating application of the two stimuli. These results demonstrate the power of combining controlled polymerization processes that are regulated by different external stimuli and lays the groundwork for developing systems where polymer sequence, structure, and architecture are controlled on demand via external influences.

3.5 References

- (1) Szwarc, M. *Nature* **1956**, *178*, 1168.
- (2) Lunn, David, J.; Discekici, Emre, H.; de Alaniz, J. R.; Guntekunst, W. R.; Hawker, C. J. *J. Polym. Sci., Part A: Polym. Chem.* **2017**, *55*, 2903.

- (3) Leibfarth, F. A.; Mattson, K. M.; Fors, B. P.; Collins, H. A.; Hawker, C. J. *Angew. Chem. Int. Ed.* **2013**, *52*, 199.
- (4) Teator, A. J.; Lastovickova, D. N.; Bielawski, C. W. *Chem. Rev.* **2016**, *116*, 1969.
- (5) Yağci, Y.; Reetz, I. *Prog. Polym. Sci.* **1998**, *23*, 1485.
- (6) Naumann, S.; Buchmeiser, M. R. *Catal. Sci. Technol.* **2014**, *4*, 2466.
- (7) Naumann, S.; Buchmeiser, M. R. *Macromol. Rapid Comm.* **2014**, *35*, 682.
- (8) Gregson, C. K. A.; Gibson, V. C.; Long, N. J.; Marshall, E. L.; Oxford, P. J.; White, A. J. P. *J. Am. Chem. Soc.* **2006**, *128*, 7410.
- (9) A. Gregson, C. K.; J. Blackmore, I.; C. Gibson, V.; J. Long, N.; L. Marshall, E.; P. White, A. J. *Dalton Trans.* **2006**, *0*, 3134.
- (10) Broderick, E. M.; Guo, N.; Vogel, C. S.; Xu, C.; Sutter, J.; Miller, J. T.; Meyer, K.; Mehrkhodavandi, P.; Diaconescu, P. L. *J. Am. Chem. Soc.* **2011**, *133*, 9278.
- (11) Broderick, E. M.; Guo, N.; Wu, T.; Vogel, C. S.; Xu, C.; Sutter, J.; Miller, J. T.; Meyer, K.; Cantat, T.; Diaconescu, P. L. *Chem. Commun.* **2011**, *47*, 9897.
- (12) Wang, X.; Thevenon, A.; Brosmer, J. L.; Yu, I.; Khan, S. I.; Mehrkhodavandi, P.; Diaconescu, P. L. *J. Am. Chem. Soc.* **2014**, *136*, 11264.

- (13) Biernesser, A. B.; Li, B.; Byers, J. A. *J. Am. Chem. Soc.* **2013**, *135*, 16553.
- (14) Mohapatra, H.; Kleiman, M.; Esser-Kahn, A. P. *Nat. Chem.* **2017**, *9*, 135.
- (15) Wang, Z.; Pan, X.; Li, L.; Fantin, M.; Yan, J.; Wang, Z.; Wang, Z.; Xia, H.; Matyjaszewski, K. *Macromolecules* **2017**, *50*, 7940.
- (16) McKenzie, T. G.; Colombo, E.; Fu, Q.; Ashokkumar, M.; Qiao, G. G. *Angew. Chem. Int. Ed.* **2017**, *56*, 12302.
- (17) Wang, Z.; Pan, X.; Yan, J.; Dadashi-Silab, S.; Xie, G.; Zhang, J.; Wang, Z.; Xia, H.; Matyjaszewski, K. *ACS Macro Lett.* **2017**, *6*, 546.
- (18) Chmielarz, P.; Fantin, M.; Park, S.; Isse, A. A.; Gennaro, A.; Magenau, A. J. D.; Sobkowiak, A.; Matyjaszewski, K. *Prog. Polym. Sci.* **2017**, *69*, 47.
- (19) Peterson, B. M.; Lin, S.; Fors, B. P. *J. Am. Chem. Soc.* **2018**, *140*, 2076.
- (20) Murata, K.; Saito, K.; Kikuchi, S.; Akita, M.; Inagaki, A. *Chem. Commun.* **2015**, *51*, 5717.
- (21) Chen, M.; Zhong, M.; Johnson, J. A. *Chem. Rev.* **2016**, *116*, 10167.
- (22) Corrigan, N.; Shanmugam, S.; Xu, J.; Boyer, C. *Chem. Soc. Rev.* **2016**, *45*, 6165.
- (23) Ciftci, M.; Yoshikawa, Y.; Yagci, Y. *Angew. Chem. Int. Ed.* **2017**, *56*, 519.
- (24) Kutahaya, C.; Schmitz, C.; Strehmel, V.; Yagci, Y.; Strehmel, B. *Angew. Chem. Int. Ed.* **2018**, *57*, 7898.
- (25) Dadashi-Silab, S.; Doran, S.; Yagci, Y. *Chem. Rev.* **2016**, *116*, 10212.

- (26) Trotta, J. T.; Fors, B. P. Organic Catalysts for Photocontrolled Polymerizations. *Synlett* **2016**, 27, 702.
- (27) McKenzie, T. G.; Fu, Q.; Uchiyama, M.; Satoh, K.; Xu, J.; Boyer, C.; Kamigaito, M.; Qiao, G. G. *Adv. Sci.* **2016**, 3, 1500394.
- (28) Fors, B. P.; Hawker, C. J. *Angew. Chem. Int. Ed.* **2012**, 51, 8850.
- (29) Konkolewicz, D.; Schröder, K.; Buback, J.; Bernhard, S.; Matyjaszewski, K. *ACS Macro Lett.* **2012**, 1, 1219.
- (30) Anastasaki, A.; Nikolaou, V.; Zhang, Q.; Burns, J.; Samanta, S. R.; Waldron, C.; Haddleton, A. J.; McHale, R.; Fox, D.; Percec, V.; et al. *J. Am. Chem. Soc.* **2014**, 136, 1141.
- (31) Treat, N. J.; Sprafke, H.; Kramer, J. W.; Clark, P. G.; Barton, B. E.; Read de Alaniz, J.; Fors, B. P.; Hawker, C. J. *J. Am. Chem. Soc.* **2014**, 136, 16096.
- (32) Pan, X.; Malhotra, N.; Simakova, A.; Wang, Z.; Konkolewicz, D.; Matyjaszewski, K. *J. Am. Chem. Soc.* **2015**, 137, 15430.
- (33) Jones, G. R.; Whitfield, R.; Anastasaki, A.; Haddleton, D. M. *J. Am. Chem. Soc.* **2016**, 138, 7346.
- (34) Theriot, J. C.; Lim, C.-H.; Yang, H.; Ryan, M. D.; Musgrave, C. B.; Miyake, G. M. *Science* **2016**, 352, 1082.
- (35) Pearson, R. M.; Lim, C.-H.; McCarthy, B. G.; Musgrave, C. B.; Miyake, G. M. *J. Am. Chem. Soc.* **2016**, 138, 11399.

- (36) Ramsey, B. L.; Pearson, R. M.; Beck, L. R.; Miyake, G. M. *Macromolecules* **2017**, *50*, 2668.
- (37) Koumura, K.; Satoh, K.; Kamigaito, M. *Macromolecules* **2008**, *41*, 7359.
- (38) Xu, J.; Jung, K.; Atme, A.; Shanmugam, S.; Boyer, C. *J. Am. Chem. Soc.* **2014**, *136*, 5508.
- (39) Shanmugam, S.; Xu, J.; Boyer, C. *J. Am. Chem. Soc.* **2015**, *137*, 9174.
- (40) Shanmugam, S.; Xu, J.; Boyer, C. *Chem. Sci.* **2015**, *6*, 1341.
- (41) Shanmugam, S.; Xu, J.; Boyer, C. *Angew. Chem. Int. Ed.* **2016**, *55*, 1036.
- (42) Xu, J.; Shanmugam, S.; Fu, C.; Aguey-Zinsou, K.-F.; Boyer, C. *J. Am. Chem. Soc.* **2016**, *138*, 3094.
- (43) Shanmugam, S.; Boyer, C. *J. Am. Chem. Soc.* **2015**, *137*, 9988.
- (44) Chen, M.; MacLeod, M. J.; Johnson, J. A. *ACS Macro Lett.* **2015**, *4*, 566.
- (45) Theriot, J. C.; Miyake, G. M.; Boyer, A. C. *ACS Macro Lett.* **2018**, *7*, 662.
- (46) Qi, M.; Dong, Q.; Wang, D.; Byers, J. A. *J. Am. Chem. Soc.* **2018**, *140*, 5686.
- (47) Kikuchi, S.; Saito, K.; Akita, M.; Inagaki, A. *Organometallics* **2018**, *37*, 359.
- (48) Guerre, M.; Uchiyama, M.; Lopez, G.; Améduri, B.; Satoh, K.; Kamigaito, M.; Ladmiral, V. *Polym. Chem.* **2018**, *9*, 352.
- (49) Satoh, K.; Hashimoto, H.; Kumagai, S.; Aoshima, H.; Uchiyama, M.; Ishibashi, R.; Fujiki, Y.; Kamigaito, M. *Polym. Chem.* **2017**, *8*, 5002.

- (50) Guerre, M.; Uchiyama, M.; Folgado, E.; Semsarilar, M.; Améduri, B.; Satoh, K.; Kamigaito, M.; Ladmiral, V. *ACS Macro Lett.* **2017**, *6*, 393.
- (51) Uchiyama, M.; Satoh, K.; Kamigaito, M. *Angew. Chem. Int. Ed.* **2015**, *54*, 1924.
- (52) Aoshima, H.; Uchiyama, M.; Satoh, K.; Kamigaito, M. *Angew. Chem. Int. Ed.* **2014**, *53*, 10932.
- (53) Kottisch, V.; Michaudel, Q.; Fors, B. P. *J. Am. Chem. Soc.* **2017**, *139*, 10665.
- (54) Previous work employing two wavelengths of light to promote PET-RAFT and ROP polymerization mechanisms from two different chain ends can be found in: Fu, C.; Xu, J.; Boyer, C. *Chem. Commun.* **2016**, *52*, 7126.
- (55) Kottisch, V.; Michaudel, Q.; Fors, B. P. *J. Am. Chem. Soc.* **2016**, *138*, 15535.
- (56) Michaudel, Q.; Chauviré, T.; Kottisch, V.; Supej, M. J.; Stawiasz, K. J.; Shen, L.; Zipfel, W. R.; Abruña, H. D.; Freed, J. H.; Fors, B. P. *J. Am. Chem. Soc.* **2017**, *139*, 15530.
- (57) CTAs **1a** and **1b** were selected due to the control provided in cationic polymerizations and their potential to function in radical polymerizations: See reference 49.
- (58) Yeow, J.; Chapman, R.; Gormley, A. J.; Boyer, C. *Chem. Soc. Rev.*, **2018**, *47*, 4357.

- (59) Kumagai, S.; Nagai, K.; Satoh, K.; Kamigaito, M. *Macromolecules* **2010**, *43*, 7523.

3.6 Appendix

General Reagent Information

Isobutyl vinyl ether (IBVE) (99%, TCI), ethyl vinyl ether (EVE) (99%, Sigma Aldrich), 2-chloroethyl vinyl ether (Cl-EVE) (97%, TCI), *n*-propyl vinyl ether (*n*PrVE) (99%, Sigma Aldrich), and *n*-butyl vinyl ether (*n*BuVE) (98%, Sigma Aldrich), cyclohexyl vinyl ether (CyVE) (98%, Sigma Aldrich) and methyl acrylate (MA) (>99%, TCI) were dried over calcium hydride (CaH₂) (ACROS organics, 93% extra pure, 0–2 mm grain size) for 12 hours, distilled under nitrogen, and degassed by three freeze-pump-thaw cycles. 4-Methoxystyrene (97%, Sigma Aldrich) was dried over CaH₂ for 12 hours, distilled under vacuum, and degassed by three freeze-pump-thaw cycles. Sodium *N,N*-diethyldithiocarbamate trihydrate (**2**) (98%, Alfa Aesar) was azeotropically dried with toluene. Ethanethiol (97%, Alfa Aesar) and carbon disulfide (99.9+%, Alfa Aesar) were distilled before use. Ferrocenium tetrafluoroborate (FcBF₄) (97%, Sigma Aldrich), HCl in Et₂O (2.0 M, Sigma Aldrich), Tris[2-phenylpyridinatoC₂,N]iridium(III) (Ir(ppy)₃) (Ark Pharm) and sodium hydride (60%, dispersion in mineral oil, Sigma Aldrich) were used as received. Dichloromethane (DCM), acetonitrile (MeCN), and diethylether (Et₂O) were purchased from J.T. Baker and were purified by vigorous purging with argon for

2 hours, followed by passing through two packed columns of neutral alumina under argon pressure. Hexanes and ethyl acetate were purchased from Fischer Scientific and used as received. Ethanol (anhydrous, 200 proof) was purchased from Koptec. Alumina (1.0, 0.3, 0.05 μm pore size) was purchased from Extec. S-1-isobutoxyethyl *N,N*-diethyl dithiocarbamate (**1a**)¹ and S-1-isobutoxyethyl S'-ethyl trithiocarbonate (**1b**)¹ were synthesized according to literature procedures.

General Analytical Information

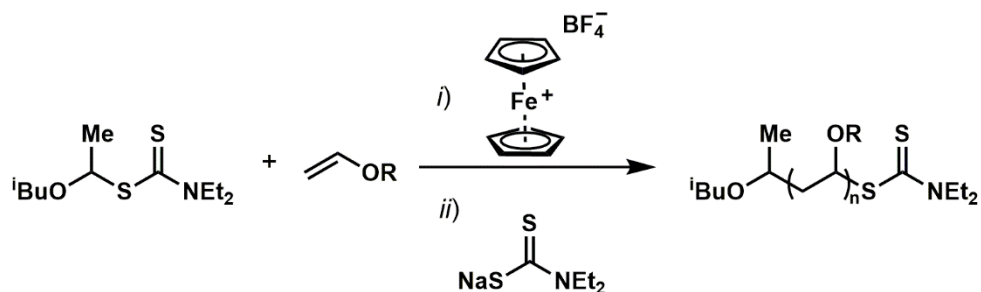
All polymer samples were analyzed using a Tosoh EcoSec HLC 8320GPC system with two SuperHM-M columns in series at a flow rate of 0.350 mL/min. THF was used as the eluent and all number-average molecular weights (M_n), weight-average molecular weights (M_w), and dispersities (\mathcal{D}) were determined by light scattering using a Wyatt miniDawn Treos multi-angle light scattering detector. Nuclear magnetic resonance (NMR) spectra were recorded on a Varian 400 MHz, a Varian 600 MHz, or a Bruker 500 MHz instrument.

Safety Statement

No unexpected or unusually high safety hazards were encountered.

Experimental Procedures

General Procedure for Chemically Controlled Polymerization



In a nitrogen filled glove box, an oven-dried one-dram vial was equipped with a stir bar and charged with IBVE (0.13 mL, 1.00 mmol, 100 equiv), 0.02 mL of a stock solution of **1a** in DCM (0.5 M, 0.01 mmol, 1 equiv), 0.13 mL of DCM, and then 0.05 mL of a stock solution of FcBF_4 in DCM (2.0 mM, 0.1 μmol , 0.01 mol % relative to IBVE). The vial was sealed with a cap equipped with a Teflon septum under an atmosphere of nitrogen and left to stir. After the desired reaction time (2–3 hours), the reaction was quenched by addition of 0.05 mL of a stock solution of sodium *N,N*-diethyl dithiocarbamate in MeCN (0.03 M, 0.15 mmol) and aliquots were taken for GPC and ^1H NMR.

Table 3.2. Breadth of Polymerizable Monomers

Monomer ^a	Conv. (%)	<i>M_n</i> , Theo (kg/mol)	<i>M_n</i> , Exp (kg/mol)	<i>D</i>
<i>n</i> BuVE	> 99	9.9	11.3	1.10
<i>n</i> PrVE	> 99	8.7	6.4	1.09
EVE	> 99	7.4	6.9	1.06
Cl-EVE ^b	93	10	7.8	1.14
CyVE ^c	> 99	12.7	10.4	1.61
<i>p</i> -OMe-Styrene ^c	96	13.3	11.9	1.21

^aStandard Reaction Conditions: Vinyl Monomer (100 equiv), **1a** (0.01 equiv), and FcBF₄ (0.01 mol%) at room temperature in dichloromethane. ^bUsing 0.04 mol% FcBF₄. ^cUsing 0.10 mol% FcBF₄.

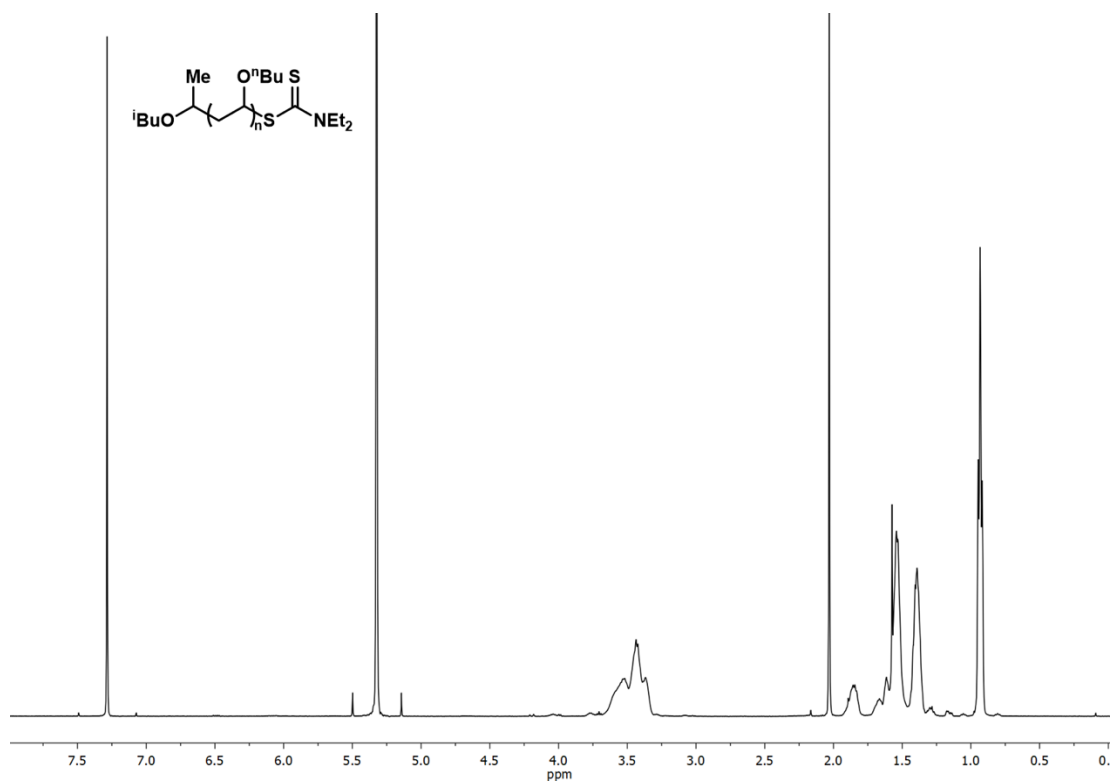


Figure 3.7. ^1H NMR of poly(*n*-butyl vinyl ether) $M_n = 11.3$ kg/mol, $\text{Đ} = 1.10$ (Table 3.2, entry 1).

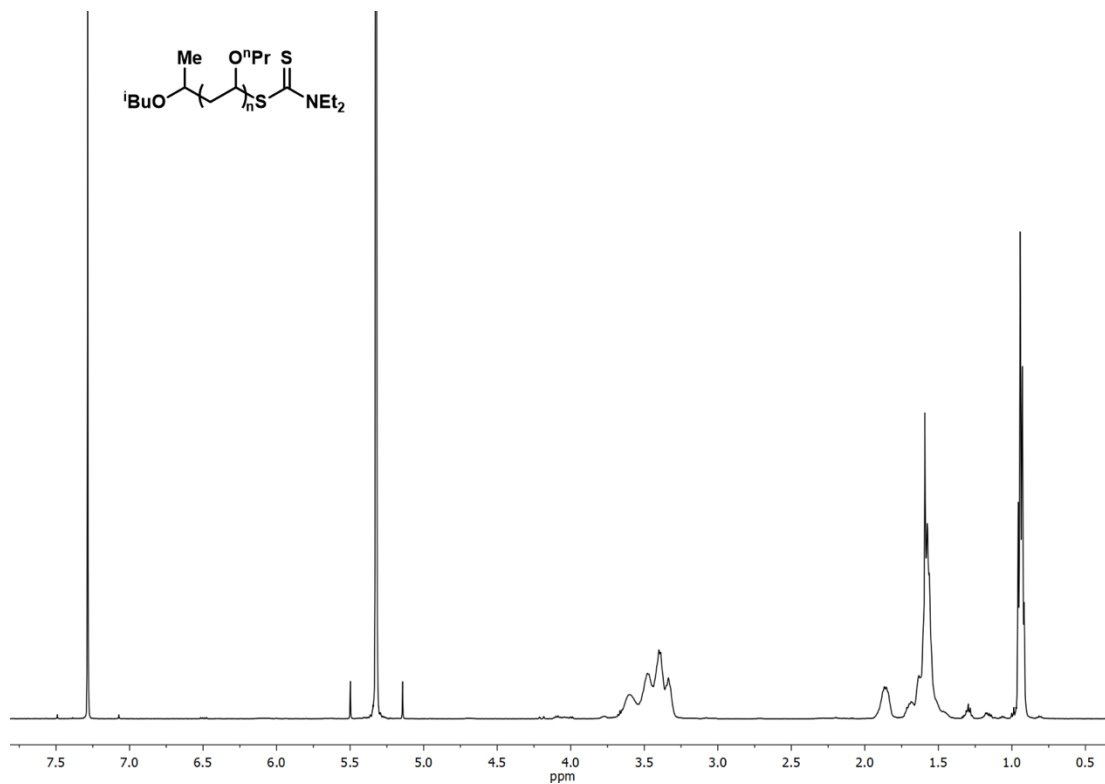


Figure 3.8. ¹H NMR of poly(*n*-propyl vinyl ether) M_n = 6.4 kg/mol, Đ = 1.09 (Table 3.2, entry 2).

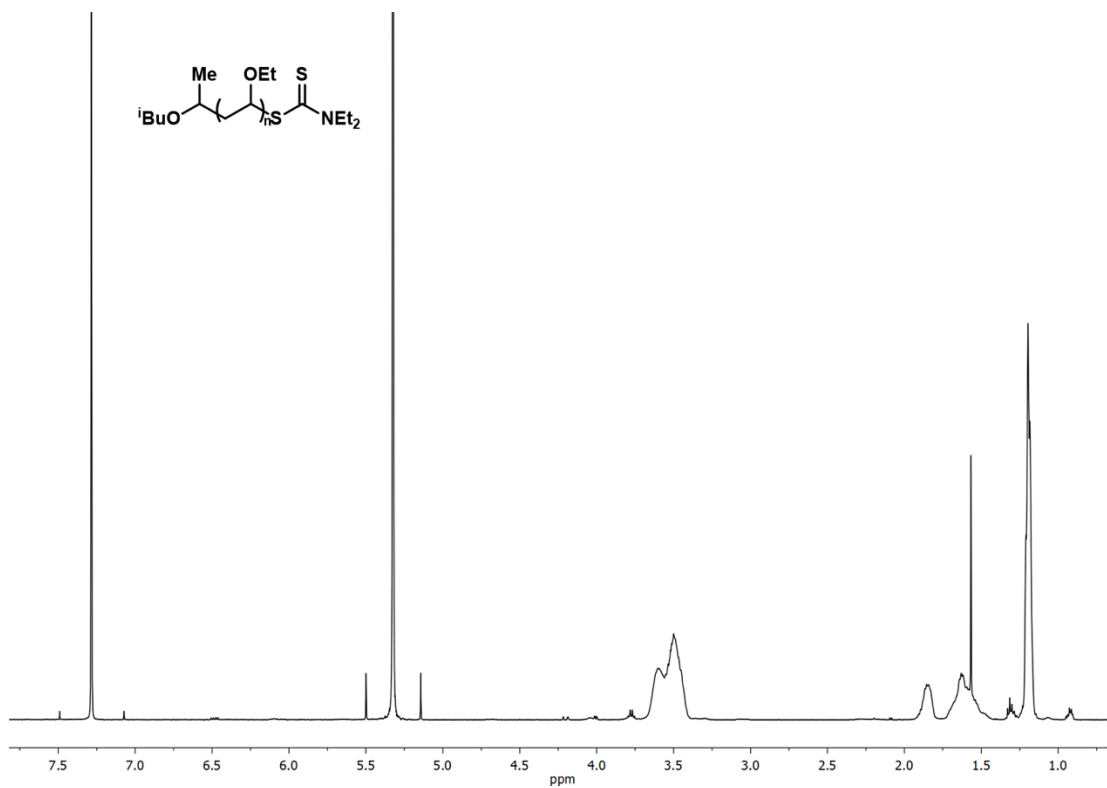


Figure 3.9. ¹H NMR of poly(ethyl vinyl ether) M_n = 6.9 kg/mol, Đ = 1.06 (Table 3.2, entry 3).

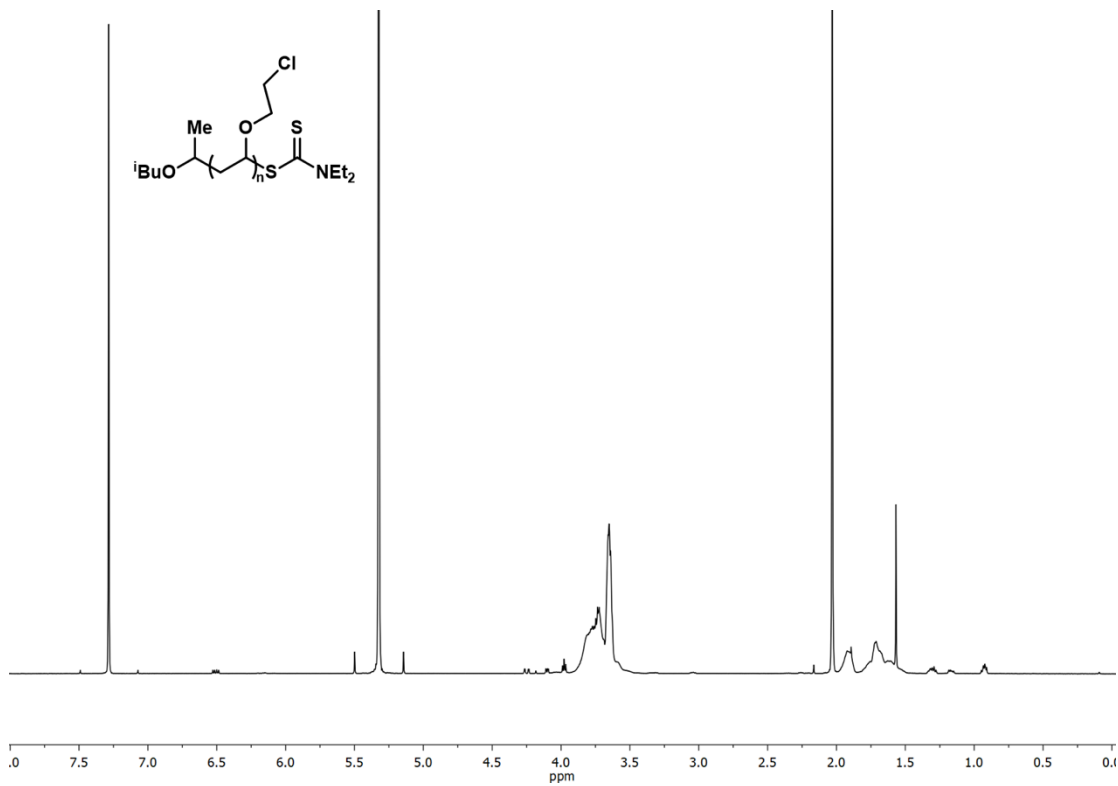


Figure 3.10. ^1H NMR of poly(2-chloroethyl vinyl ether) $M_n = 7.8$ kg/mol, $\bar{D} = 1.14$ (Table 3.2, entry 4).

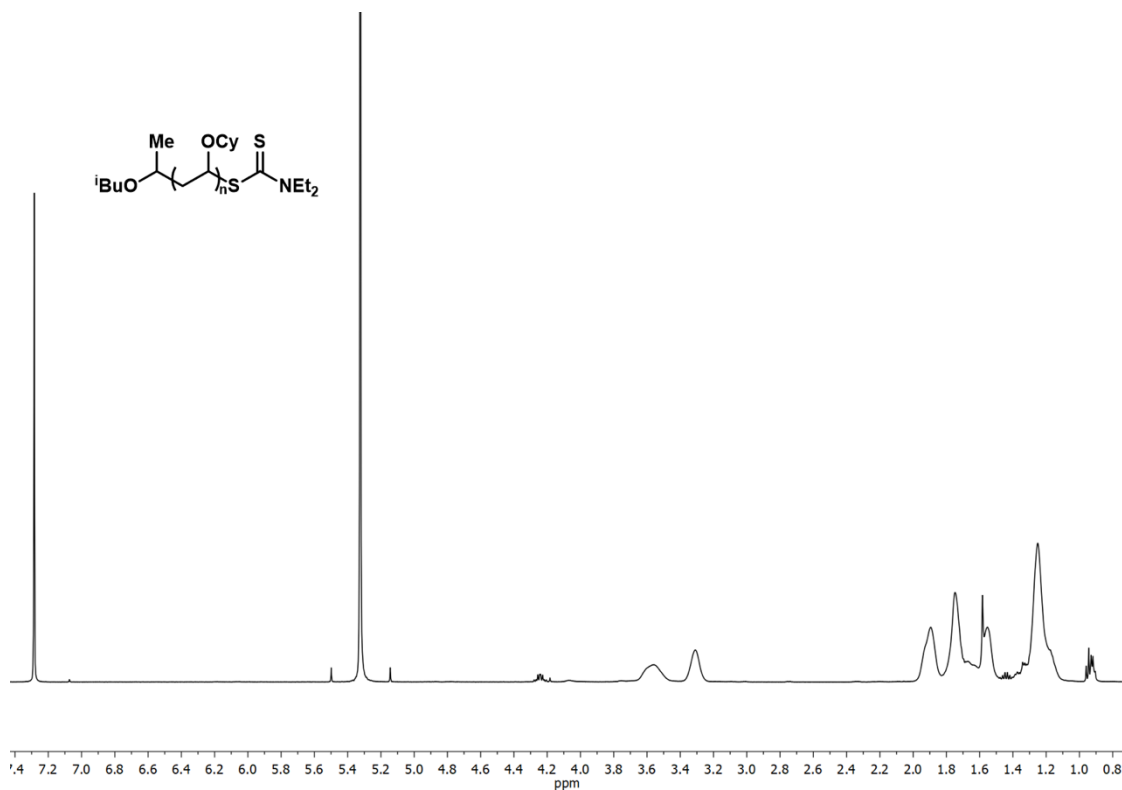


Figure 3.11. ^1H NMR of poly(cyclohexyl vinyl ether) $M_n = 10.4$ kg/mol, $\bar{D} = 1.61$ (Table 3.2, entry 5).

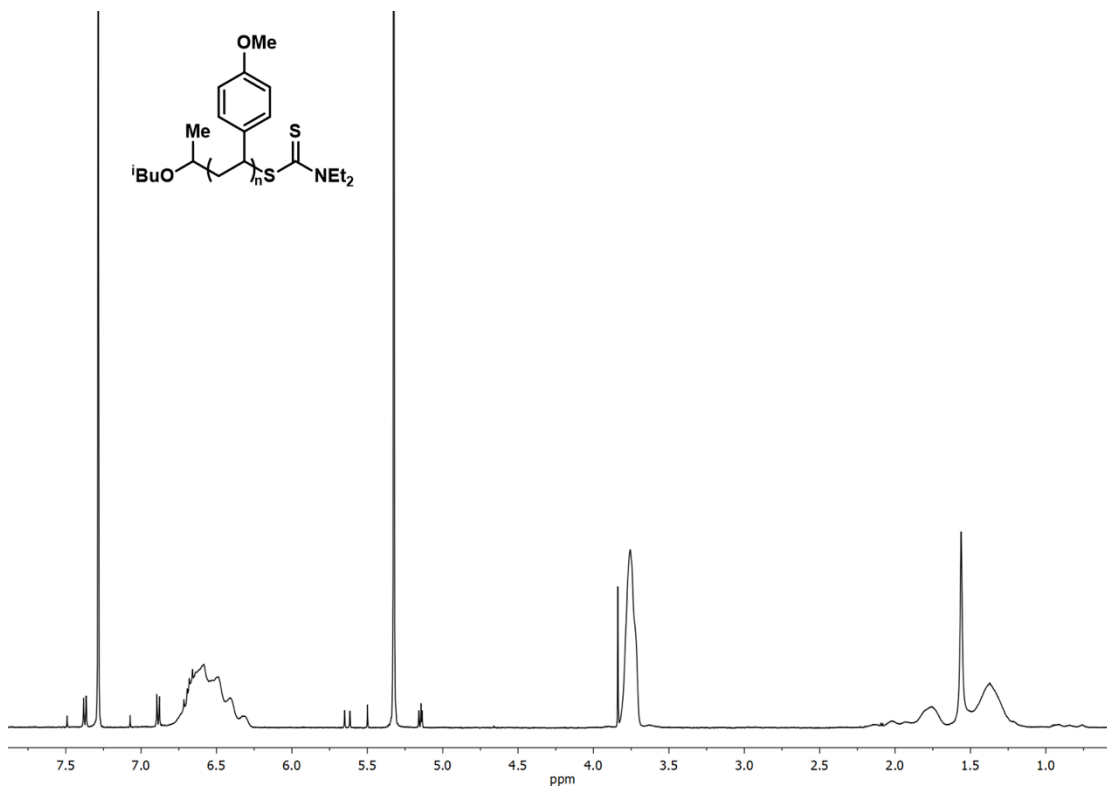
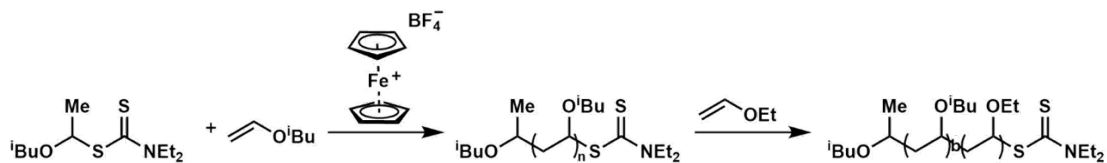


Figure 3.12. ¹H NMR of poly(*p*-OMe-Styrene) Mn = 11.9 kg/mol, Đ = 1.21 (Table 3.2, entry 6).

Procedure for Chemical Synthesis of Diblock Copolymer



In a nitrogen filled glove box, an oven-dried one-dram vial was equipped with a stir bar and charged with IBVE (0.26 mL, 2.00 mmol, 100 equiv), 0.04 mL of a stock solution of **1a** in DCM (0.5 M, 0.01 mmol, 1 equiv), 0.25 mL of DCM, and then 0.10 mL of a stock solution of FcBF₄ in DCM (2.0 mM, 0.2 μmol, 0.01 mol % relative to IBVE). The vial was sealed with a cap equipped with a Teflon septum under an atmosphere of nitrogen and left to stir. The reaction was run to full conversion (5 hours) and an aliquot was taken and quenched by addition of sodium *N,N*-diethyl dithiocarbamate for GPC ($M_n = 8.5$ kg/mol, $\mathcal{D} = 1.14$) and ¹H NMR analysis prior to the addition of EVE (0.20 mL, 2.00 mmol, 100 equiv). After reaching full conversion (16 hours), the reaction was quenched by addition of sodium *N,N*-diethyl dithiocarbamate and aliquots were taken for GPC and ¹H NMR. $M_n(\text{GPC}) = 13.4$ kg/mol, $\mathcal{D} = 1.09$.

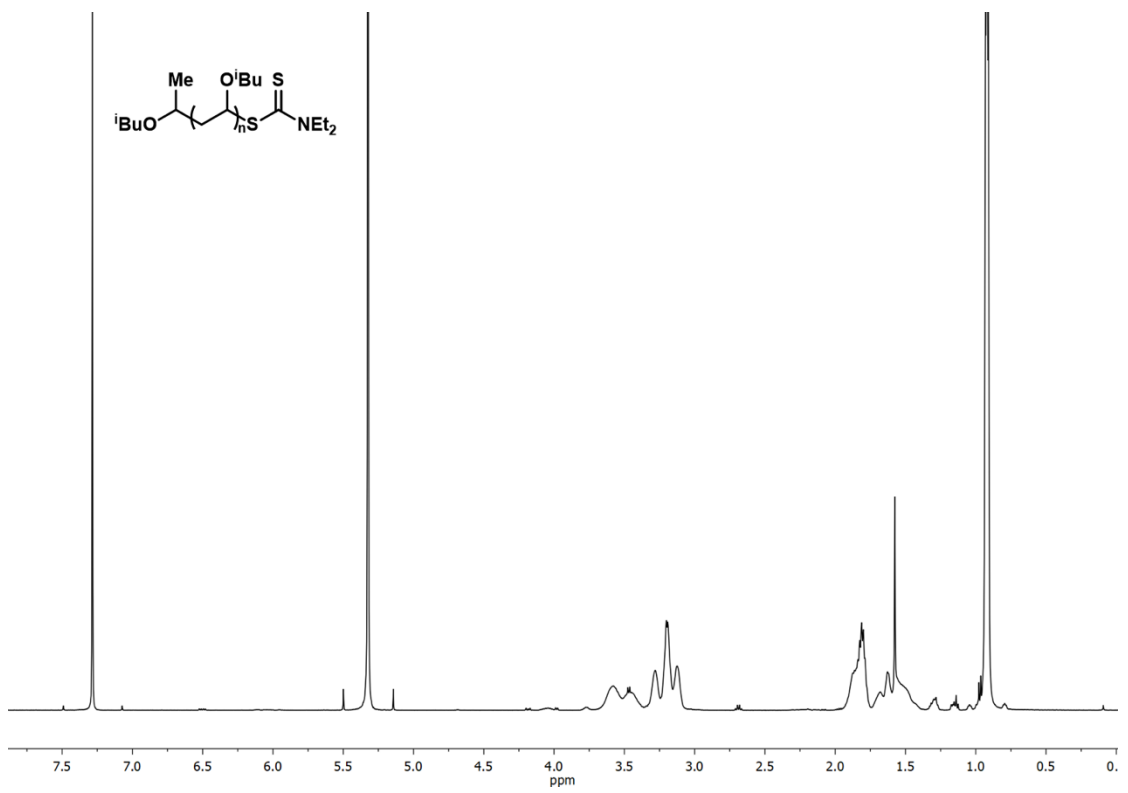


Figure 3.13. ¹H NMR of poly(isobutyl vinyl ether) Mn = 8.5 kg/mol, Đ = 1.14.

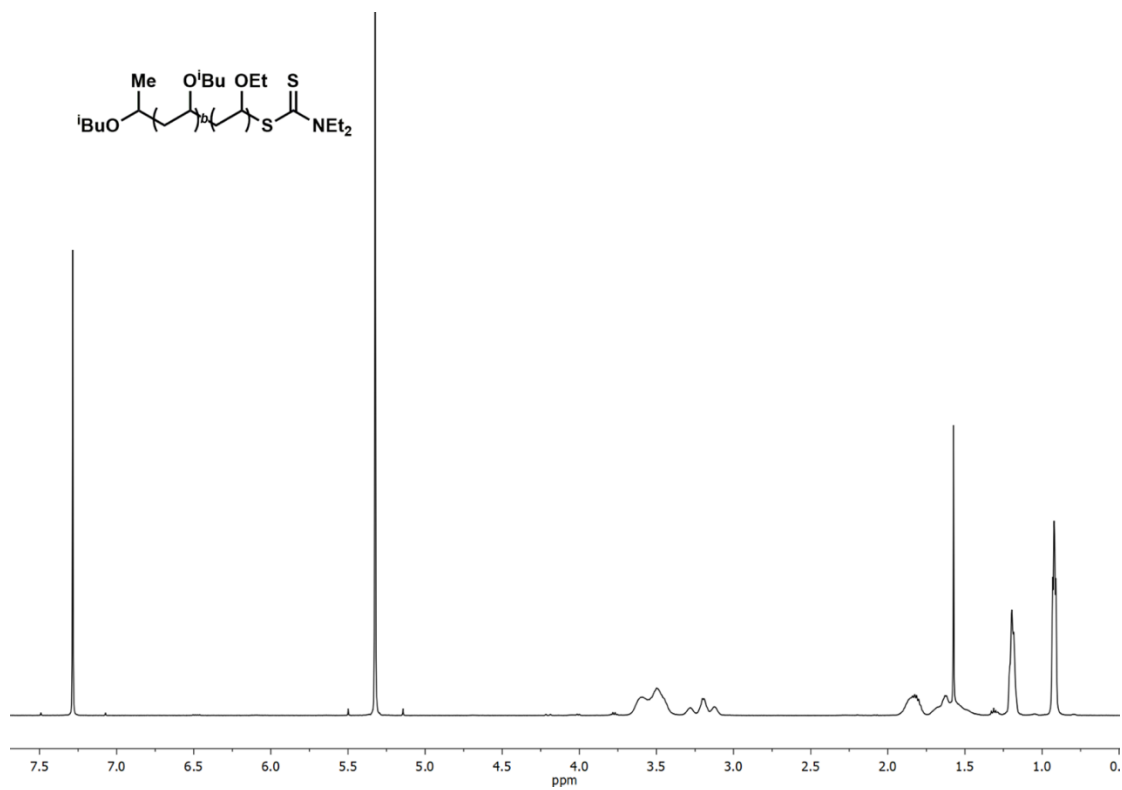


Figure 3.14. ^1H NMR of poly(isobutyl vinyl ether-*block*-ethyl vinyl ether) $M_n = 13.4$ kg/mol, $\text{Đ} = 1.09$.

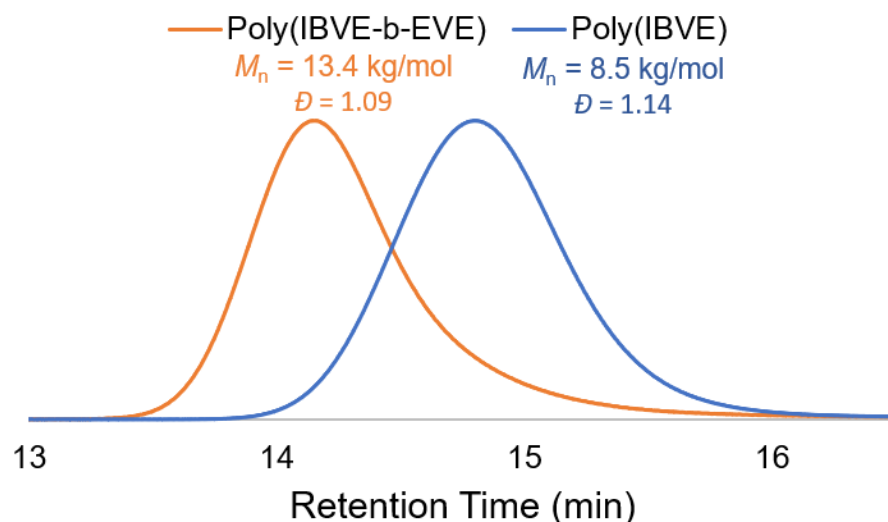


Figure 3.15. GPC traces of poly(isobutyl vinyl ether) and poly(isobutyl vinyl ether-*block*-ethyl vinyl ether)

Procedure for Chemical Initiation and Termination of the Polymerization of Isobutyl Vinyl Ether

In a nitrogen filled glove box, an oven-dried one-dram vial was equipped with a stir bar and charged with IBVE (0.260 mL, 2.00 mmol, 100 equiv), **1a** (0.040 mL of a 0.55 mM solution in DCM, 0.022 mmol, 1 equiv), FcBF₄ (0.100 mL, 2 μmol, 0.01 equiv), and 0.25 mL DCM. The vial was sealed with a cap equipped with a Teflon septum under an atmosphere of nitrogen. After 30 min (total time = 30 min), sodium *N,N*-diethyl dithiocarbamate (0.040 mL of a 5.8 mM solution in 1:1 DCM: MeCN, 2 μmol, 0.01 equiv) was added to terminate the polymerization. After a 45 min “off” period (total time = 75 min), FcBF₄ (0.04 mL of a 7.3 mM solution in DCM, 2 μmol, 0.01 equiv) was added to reinitiate polymerization. After a 15 min “on” period (total time = 90 min), sodium *N,N*-

diethyl dithiocarbamate (0.040 mL of a 5.8 mM solution in 1:1 DCM: MeCN, 2 μ mol, .01 equiv) was added to the reaction. After a 45 min “off” period (total time = 135 min), FcBF₄ (0.04 mL of a 7.3 mM solution in DCM, 2 μ mol, 0.01 equiv) was added to reinitiate polymerization. Aliquots were taken after each addition of FcBF₄ and *N,N*-diethyl dithiocarbamate and the end of reaction (time = 155 min) for ¹H NMR and GPC analysis.

Procedure for Diblock Copolymer Synthesis of Methyl Acrylate and Isobutyl Vinyl Ether (p(MA-*b*-IBVE), Figure 3.5a and 3.6a)

In a nitrogen filled glove box, an oven-dried one-dram vial was equipped with a stir bar and charged with IBVE (0.26 mL, 2.00 mmol, 100 equiv), MA (0.18 mL, 2.00 mmol, 100 equiv), 0.13 mL of a stock solution of Ir(ppy)₃ in DCM (3 mM, 0.40 μ mol, 0.02 mol% relative to MA), and 0.02 mL of a stock solution of **1b** in DCM (1 M, 0.02 mmol, 1 equiv). The vial was sealed with a cap equipped with a Teflon septum under an atmosphere of nitrogen, placed next to blue KESSIL lamps (~460 nm) outside of the glove box, and stirred while cooling by blowing compressed air over the reaction vial. After 2 hours of reaction time, the vial was transferred back into the glove box. Under inert atmosphere, an aliquot for ¹H NMR and GPC analysis was taken prior to the addition of additional IBVE (0.13 mL, 1.00 mmol, 50 equiv) and 0.045 mL of a stock solution of FcBF₄ in DCM (22 mM, 1 μ mol, 0.033 mol% relative to IBVE). The reaction was quenched with **2** after 24 hours. The solvent was removed under *vacuo* to yield the pure

polymer. GPC traces of the polymers before and after chain extension are shown in Figure 3.5a.

Chain Extension from poly(Methyl Acrylate) Synthesized in the Absence of IBVE (Figure 3.5a)

In a nitrogen filled glove box, an oven-dried one-dram vial was equipped with a stir bar and charged with MA (0.18 mL, 2.00 mmol, 100 equiv), 0.13 mL of a stock solution of Ir(ppy)₃ in DCM (3 mM, 0.40 μmol, 0.02 mol% relative to MA), and 0.02 mL of a stock solution of **1b** in DCM (1 M, 0.02 mmol, 1 equiv). The vial was sealed with a cap equipped with a Teflon septum under an atmosphere of nitrogen, placed next to blue KESSIL lamps (~460 nm) outside of the glove box, and stirred while cooling by blowing compressed air over the reaction vial. After 2 hours of reaction time, the vial was transferred back into the glove box. Under inert atmosphere, an aliquot for ¹H NMR and GPC analysis was taken prior to the addition of IBVE (0.26 mL, 2.00 mmol, 100 equiv) and 0.045 mL of a stock solution of FcBF₄ in DCM (22 mM, 1 μmol, 0.05 mol% relative to IBVE). The reaction was quenched with **2** after 24 hours. The solvent was removed under *vacuo* to yield pMA and PIBVE resulting from uncontrolled cationic polymerization. GPC traces of the first aliquot and final polymer are displayed in Figure 3.16.

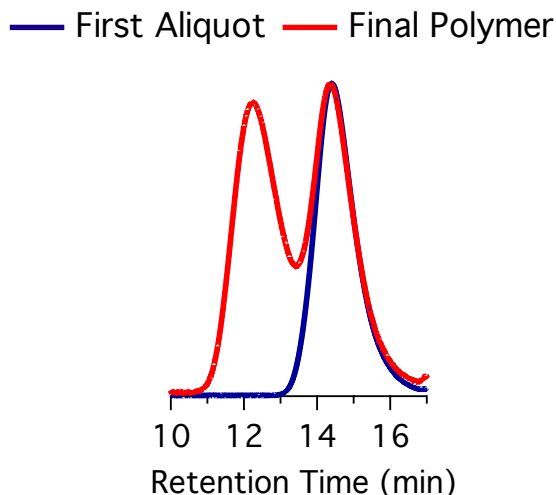


Figure 3.16. GPC Traces of Chain Extension from p(MA) Synthesized in the absence of IBVE: GPC trace of the first aliquot (poly(methyl acrylate)) and final polymer (homopolymers of poly(methyl acrylate) and poly(isobutyl vinyl ether)) demonstrate that chain extension does not occur when methyl acrylate block is synthesized in the absence of a vinyl ether.

Procedure for Triblock Copolymer Synthesis of Methyl Acrylate and Isobutyl Vinyl Ether (p(MA-*b*-IBVE-*b*-MA), Figure 3.6b)

In a nitrogen filled glove box, an oven-dried one-dram vial was equipped with a stir bar and charged with IBVE (0.26 mL, 2.00 mmol, 100 equiv), MA (0.18 mL, 2.00 mmol, 100 equiv), 0.13 mL of a stock solution of Ir(ppy)₃ in DCM (3 mM, 0.40 μmol, 0.02 mol% relative to MA), and 0.02 mL of a stock solution of **1b** in DCM (1 M, 0.02 mmol, 1 equiv). The vial was sealed with a cap equipped with a Teflon septum under an atmosphere of nitrogen, placed next to blue KESSIL lamps (~460 nm) outside of the glove box, and stirred while cooling by blowing compressed air over the reaction vial. After 1 hour of reaction time, the

vial was transferred back into the glove box. Under inert atmosphere, an aliquot for ^1H NMR and GPC analysis was taken prior to the addition of 0.045 mL of a stock solution of FcBF_4 in DCM (22 mM, 1 μmol , 0.05 mol% relative to IBVE). The reaction was stirred at room temperature for 2 hours, followed by the addition of **2** (1 μmol) to halt the cationic polymerization. Under inert atmosphere, aliquots for NMR and GPC analysis were taken at designated time points prior to a change in stimuli. The reaction was stopped after 11 hours of blue light irradiation. The solvent was removed in *vacuo* to yield the final polymer. GPC traces of the polymer are shown in Figure 3.17. ($M_{n,\text{Theo}}$ (kg/mol) = 18.9, $M_{n,\text{Exp}}$ (kg/mol) = 15.7, $D = 1.68$)

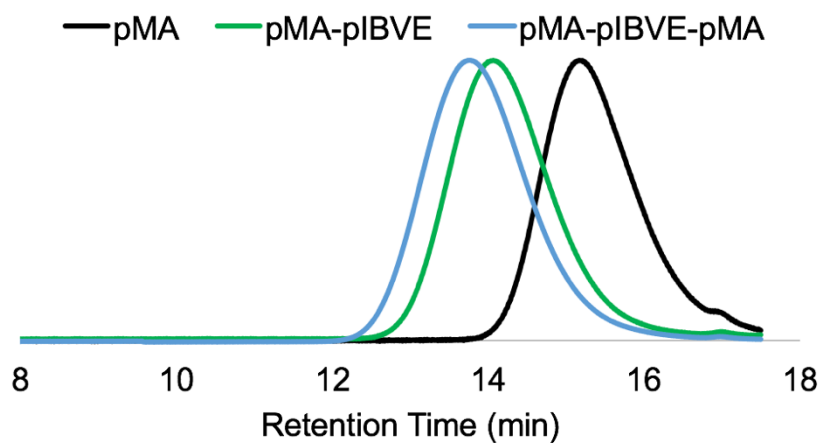


Figure 3.17. GPC traces of p(MA-*b*-IBVE-*b*-MA) (Figure 3.6b)

Procedure for Triblock Copolymer Synthesis of Methyl Acrylate and Isobutyl Vinyl Ether (p(IBVE-*b*-MA-*b*-IBVE), Figure 3.6c)

In a nitrogen filled glove box, an oven-dried one-dram vial was equipped with a stir bar and charged with IBVE (0.26 mL, 2.00 mmol, 100 equiv), MA (0.18 mL, 2.00 mmol, 100 equiv), 0.13 mL of a stock solution of Ir(ppy)₃ in DCM (3 mM, 0.40 μmol, 0.02 mol% relative to MA), .07 mL of a stock solution of FcBF₄ in DCM (4 mM, 0.50 μmol, 0.025 mol% relative to IBVE) and 0.02 mL of a stock solution of **1b** in DCM (1 M, 0.02 mmol, 1 equiv). The vial was sealed with a cap equipped with a Teflon septum under an atmosphere of nitrogen and stirred at room temperature for 1 hour before the addition of **2** (0.4 μmol). The vial was irradiated with blue KESSIL lamps (~460 nm) outside of the glove box, and stirred while cooling by blowing compressed air over the reaction vial. After 2 hours of irradiation, the vial was transferred back into the glove box. The addition of 0.03 mL of a stock solution of FcBF₄ in DCM (22 mM, 0.67 μmol, 0.033 mol% relative to IBVE) reinitiated cationic polymerization. Under inert atmosphere, aliquots for NMR and GPC analysis were taken at designated time points prior to a change in stimulus. The reaction was quenched with **2** after 8 hours. The solvent was removed in *vacuo* to yield the pure polymer. GPC traces of the polymer are shown in Figure 3.18. ($M_{n,Theo}$ (kg/mol) = 13.6, $M_{n,Exp}$ (kg/mol) = 10.6, $D = 1.20$)

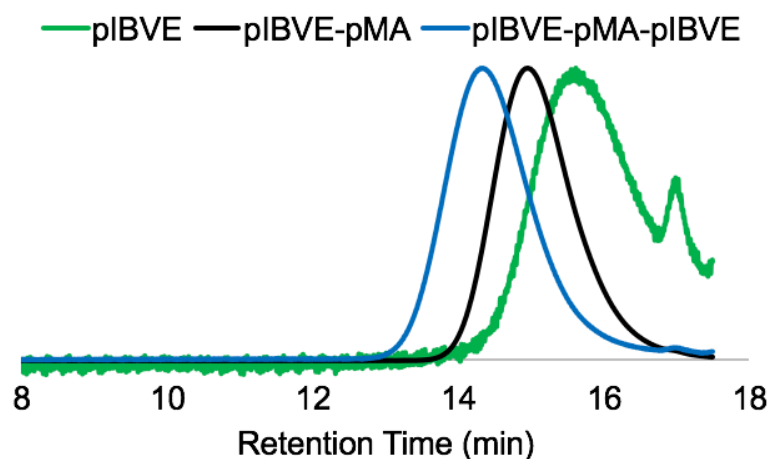


Figure 3.18. GPC traces of p(IBVE-*b*-MA-*b*-IBVE) (Figure 3.6c)

Procedure for Tetrablock Copolymer Synthesis of Methyl Acrylate and Isobutyl Viny Ether (p(IBVE-*b*-MA-*b*-IBVE-*b*-MA), Figure 3.6d)

In a nitrogen filled glove box, an oven-dried one-dram vial was equipped with a stir bar and charged with IBVE (0.26 mL, 2.00 mmol, 100 equiv), MA (0.18 mL, 2.00 mmol, 100 equiv), 0.13 mL of a stock solution of Ir(ppy)₃ in DCM (3 mM, 0.40 μmol, 0.02 mol% relative to MA), 0.07 mL of a stock solution of FcBF₄ in DCM (4 mM, 0.50 μmol, 0.025 mol% relative to IBVE) and 0.02 mL of a stock solution of **1b** in DCM (1 M, 0.02 mmol, 1 equiv). The vial was sealed with a cap equipped with a Teflon septum under an atmosphere of nitrogen and stirred at room temperature for 2 hours before the addition of **2** (0.4 μmol). The vial was then placed next to blue KESSIL lamps (~460 nm) outside of the glove box, and stirred while cooling by blowing compressed air over the reaction vial. After 2 hours of irradiation, the vial was transferred back into the glove box. The

addition of 0.045 mL of a stock solution of FcBF_4 in DCM (22 mM, 1 μmol , 0.05 mol% relative to IBVE) reinitiated cationic polymerization. The reaction was stirred for 2 hours at room temperature before the addition of **2** (1 μmol) halted the cationic polymerization. The vial was then re-exposed to blue light. Under inert atmosphere, aliquots for NMR and GPC analysis were taken at designated time points prior to a change in stimuli. The reaction was stopped after 2 hours of irradiation. The solvent was removed *in vacuo* to yield the pure polymer. GPC traces of the polymer are shown in Figure 3.19. ($M_{n,\text{Theo}}$ (kg/mol) = 15.1, $M_{n,\text{Exp}}$ (kg/mol) = 18.2, $D = 1.41$)

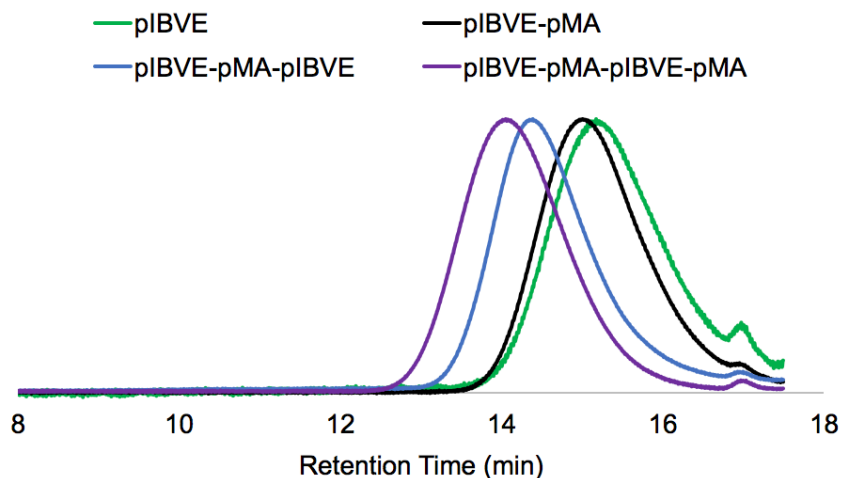
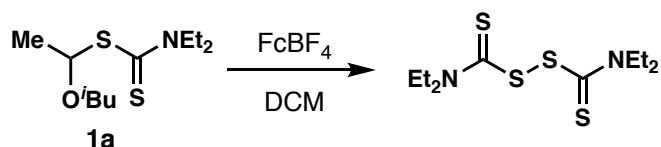


Figure 3.19. GPC traces of p(IBVE-*b*-MA-*b*-IBVE-*b*-MA) (Figure 3.6d)

Generation of Tetraethylthiuram Disulfide Through the Oxidation of CTA by Ferrocenium Tetrafluoroborate



In a nitrogen-filled glove box, an oven-dried one-dram vial was equipped with a stir bar and charged with FcBF₄ (273mg, 1.00 mmol, 5 equiv) and CTA **1a** (0.4 mL (0.5 M in DCM), 0.2 mmol, 1 equiv). After 2 hours, the reaction was passed through a silica plug with ethyl acetate. Tetraethylthiuram disulfide was observed in the ¹H NMR of the filtrate.²

Radical Copolymerization of Methyl Acrylate and Isobutyl Vinyl Ether with Different Feed Ratios

In a nitrogen filled glove box, an oven-dried one-dram vial was equipped with a stir bar and charged with IBVE, MA, 0.13 mL of a stock solution of Ir(ppy)₃ in DCM (3 mM, 0.40 μmol, 0.02 mol% relative to monomers), and 0.02 mL of a stock solution of **1b** in DCM (1 M, 0.02 mmol, 1 equiv). The ratio of MA to IBVE was varied as shown in Table S2, while maintaining the total amount of monomers at 2 mmol. The vial was sealed with a cap equipped with a Teflon septum under an atmosphere of nitrogen, placed next to blue KESSIL lamps (~460 nm) outside of the glove box, and stirred while cooling by blowing compressed air over the reaction vial. Aliquots for GPC and NMR were taken after the reaction time of 13 hours. The solvent was removed *in vacuo* to yield

the pure polymers. The amount of thioacetal chain end was determined by ^1H NMR.

Table 3.3. Amount of Thioacetal Chain End in Copolymers of Methyl Acrylate and Isobutyl Vinyl Ether.

Entry	MA : IBVE (feed ratio)	MA : IBVE (polymer comp.)	M_n (kg/mol)	\bar{D}	Thioacetal Chain End (%)
1	2:1	4:1	9.6	1.39	>95
2	10:1	14:1	11.0	1.58	>95
3	1:2	2:1	6.8	1.26	>95

Appendix References

- (1) Kottisch, V.; Michaudel, Q.; Fors, B. P. *J. Am. Chem. Soc.* **2016**, *138*, 15535–15538.
- (2) Michaudel, Q.; Chauviré, T.; Kottisch, V.; Supej, M. J.; Stawiasz, K. J.; Shen, L.; Zipfel, W. R.; Abruña, H. D.; Freed, J. H.; Fors, B. P. *J. Am. Chem. Soc.* **2017**, *139*, 15530.
- (3) Peterson, B. M.; Lin, S.; Fors, B. P. *J. Am. Chem. Soc.* **2018**, *140*, 2076.

CHAPTER 4

DUAL STIMULI SWITCHING: INTERCONVERTING CATIONIC AND RADICAL POLYMERIZATIONS WITH ELECTRICITY AND LIGHT

4.1 Abstract

Increasing demand for advanced materials that are essential to emerging technologies calls for synthetic methods which can easily generate polymers with complex structures. Multiblock copolymers display a range of material properties depending on the length and number of polymer blocks. Currently, there remains a lack of polymerization processes that can easily synthesize these multiblock structures. Herein, we report the in situ synthesis of multiblock copolymers by controlling the incorporation of vinyl ether and acrylate monomers with electrochemical and photochemical stimuli, respectively. To achieve this, we developed a cationic polymerization where polymer chain growth is controlled through the reversible electrochemical oxidation of the polymer chain end and coupled this with a compatible photocontrolled radical polymerization. This process was used to generate higher-order multiblock copolymers wherein the number of blocks and the length of each segment is controlled on demand by the two stimuli. This method, which lends itself toward automation, will aid in accelerating the rate at which next generation materials are discovered.

4.2 Introduction

Polymer properties are determined not only by the structures of the parent monomers but also by the final macromolecular structure. There have been numerous studies of block copolymers showing that the composition, length, and total number of blocks can be used to tune the final material function.¹⁻⁴ On this basis, there is a demand to develop methods to synthesize block copolymers with precise structural complexity to identify materials for next generation applications. To accelerate this discovery process, we envisaged an automated system where one could input any desired multiblock copolymer structure and automatically synthesize it from a single solution of reagents. This type of system would enable the facile formation of a library of block polymers with control over the number of blocks, as well as the length of each individual block in the material. To achieve this, we need a method where the selectivity for monomer incorporation could be controlled and switched during the polymerization to give the desired structure.

Externally regulated polymerizations (*e.g.*, thermal,⁵⁻⁷ chemical,⁸⁻¹³ mechanochemical,¹⁴⁻¹⁷ electrochemical,¹⁸⁻²² and photochemical²³⁻³³) offer an opportunity to control monomer selectivity at a growing polymer chain end.³⁴ Taking advantage of this strategy, the Byers^{11,21} and Diaconescu^{12,13} groups have independently developed chemically and electrochemically controlled ring opening polymerizations (ROP) that allow switching between incorporation of lactones and epoxides. Utilizing a combination of thermal and photochemical

stimuli, You and coworkers³⁵ developed a polymerization wherein ROP of thiiranes could be interconverted with radical reversible addition-fragmentation chain transfer (RAFT) polymerization of acrylamides.

In a unique approach to control monomer selectivity, our group has developed methods that enable the stimuli controlled oxidation or reduction of a polymer chain end. This allowed us to switch between a cationic and radical RAFT polymerization mechanism, leading to the selective polymerization of vinyl ethers or acrylates, respectively. In the first system, we used both an oxidizing and reducing photocatalyst to control each polymerization. Irradiation with green light selectively promoted a cationic polymerization. However, irradiation with blue light excited both photocatalysts and led to initiation of both polymerization mechanisms simultaneously. Although this system demonstrated that polymerization mechanism could be switched by changing the stimulus, it did not give control over the synthesis of well-defined multiblock copolymers. To have deterministic control over the final structure, we needed orthogonal stimuli that allowed each polymerization to be independently promoted. To this end, we designed a second system where we coupled a photocontrolled radical polymerization of acrylates with a chemically controlled cationic polymerization of vinyl ethers.³⁶ This allowed for the synthesis of well-defined multiblock copolymers. However, this approach relied on the manual addition of exogenous oxidizing and reducing agents for the chemically controlled cationic polymerization, which can introduce impurities to the system

and cause termination events. In order to automate this system and enable the facile synthesis of structurally precise block polymers, two completely external and orthogonal stimuli are necessary to dictate polymerization mechanism.

We hypothesized that combining a photocontrolled radical polymerization with an electrochemically controlled cationic polymerization would allow switching between acrylates and vinyl ethers without having to manipulate reagents (Figure 4.1). This would be ideal for an automated system where the final polymer structure could be dictated by the order and total amount of time that current and light were applied to the system. Previously, we developed an electrochemically controlled cationic polymerization of vinyl

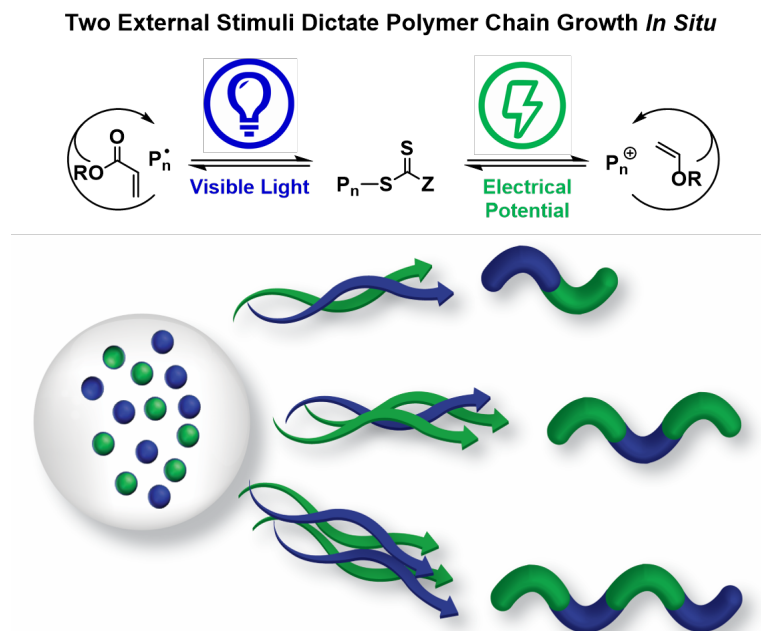


Figure 4.1. Dictating polymer structure by switching between photochemically controlled radical and electrochemically controlled cationic polymerizations

ethers mediated by 2,2,6,6-tetramethyl-1-piperidinyloxy (TEMPO).¹⁸ Unfortunately, this method would inhibit a photocontrolled radical process as the aminoxyl radical mediator, TEMPO, would couple with the propagating radical chain end and terminate the polymerization of acrylates. To address this challenge, in this manuscript we developed an electrochemically controlled cationic polymerization of vinyl ethers that uses a mediator which is compatible with a radical polymerization of acrylates and demonstrate that we can efficiently switch monomer selectivity with electrochemistry and light.

4.3. Results and Discussion

Development of a Ferrocene Mediated Electrochemically Controlled Cationic Polymerization

Previously, we demonstrated that ferrocenium salts (FcX) could oxidize dithiocarbonyl chain transfer agents (CTAs) to promote cationic RAFT polymerizations.³⁶ Therefore, we posited that ferrocene (Fc) would be an efficient electrochemical mediator for the cationic polymerization and would be compatible with the photocontrolled radical polymerization of acrylates. Specifically, electrochemical oxidation of Fc to ferrocenium would oxidize the dithiocarbonyl CTA and initiate cationic polymerization (Figure 4.2). Reversal of the current in the electrochemical cell will reduce the dithiocarbonyl disulfide to the anion, thereby leading to reversible termination of the growing polymer chain. Importantly this will allow chain growth to be turned on and off by the

direction of current in the cell and the rate of the polymerization to be controlled by the current density applied, providing temporal control.

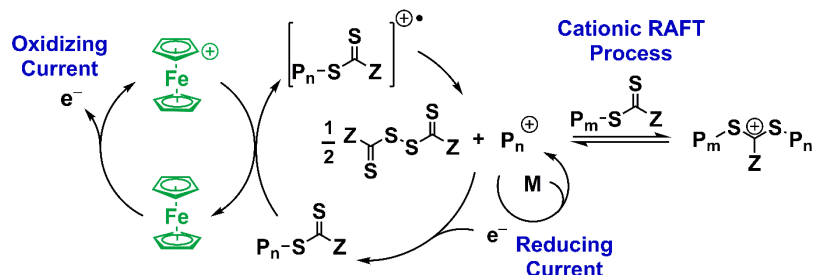


Figure 4.2. Proposed mechanism of electrochemically controlled cationic polymerization mediated by ferrocene (M = monomer).

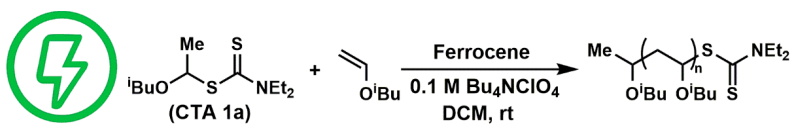
To test our hypothesis, we investigated the polymerization of isobutyl vinyl ether (IBVE) in a divided electrochemical cell using reticulated vitreous carbon (RVC) electrodes. Applying a constant potential to a solution of IBVE, CTA (**1a**), Fc, and tetrabutylammonium perchlorate (Bu₄NClO₄) in dichloromethane (DCM) initiated polymerization of IBVE. The resulting polymer displayed excellent agreement between theoretical and experimental number average molar masses (M_n s) and a low dispersity (D) value, demonstrating a controlled cationic polymerization (Table 4.1, entry 1). Removal of CTA from the reaction solution results in an uncontrolled polymerization (Table 4.1, entry 2). Additionally, in the absence of Fc no polymerization is observed, demonstrating that a redox mediator is required to promote the reaction under these mild oxidizing conditions (Table 4.1, entry 3).

By varying the monomer-to-CTA ratio, a range of M_n s were targeted while simultaneously retaining good agreement between experimental and theoretical molecular weights and low \bar{D} s (Table 4.1, entries 4-7). Greater control of the polymerization is achieved by applying a constant current instead of a constant potential, thus substantially decreasing \bar{D} (Table 4.1, entry 5). Furthermore, changing the electrolyte counterion to either tetrafluoroborate or hexafluorophosphate results in polymers with similarly low \bar{D} values (Table 4.1, entries 8-9).

The polymerization kinetics were monitored over the course of the reaction by gel permeation chromatography (GPC) and ^1H NMR. After applying 1.5 mA of anodic current over a 15 minute period, a linear relationship between conversion and M_n is observed, indicative of a chain growth polymerization (Figure 4.3a). Importantly, the applied current density dictates polymerization rate as the concentration of propagating cationic chain ends is directly proportional to ferrocenium concentration (see Chapter 4.6 Appendix, Figure 4.7).^{37,38} This feature of the polymerization gives an additional layer of control when attempting to iteratively synthesize blocks of varying size. Additionally, it was observed that the rate of ferrocenium generation has little effect on the control over the cationic RAFT polymerization, producing poly(IBVE) with low \bar{D} and good agreement with the theoretical molecular weight (Table 4.2). This indicates that generating active mediator more quickly at higher current

densities does not lead to a loss in control over the polymerization, while affording us the ability to alter the rate of reaction.

Table 4.1. Living Characteristics of Ferrocene Mediated Electrochemically Controlled Cationic Polymerization



Entry ^a	[M]:[CTA]:[Fc]	$M_{n,d}$ (kg/mol)	$M_{n,Exp}$	\bar{D}
1 ^c	100:1:1	10.4	10.2	1.21
2 ^c	100:0:1	—	46.1	2.25
3 ^c	100:1:0	—	—	—
4 ^d	50:1:0.2	5.2	4.7	1.32
5 ^d	100:1:0.2	10.4	10.6	1.13
6 ^d	150:1:0.2	16.1	14.5	1.04
7 ^d	200:1:0.2	20.4	20.9	1.14
8 ^e	100:1:0.2	10.4	12.9	1.13
9 ^f	100:1:0.2	10.4	11.6	1.18

^a [IBVE] = 3.2 M (in DCM), V_{tot} = 6 mL, [Bu₄NClO₄] = 0.1 M, RVC or Steel Anode, RVC or Steel Cathode (Divided cell).

^b $M_{n,Thero} = [M]/[CTA] \times MW_M \times Conversion + MW_{CTA}$.

^c Applied 440 mV vs. Ag Reference.

^d Applied 1 mA of current.

^e [Bu₄NPF₆] = 0.1 M.

^f [Bu₄NBF₄] = 0.1 M.

Gaining Temporal Control

In order to switch polymerization mechanism *in situ*, we must be able to reversibly terminate the cationic polymerization. We posited that applying a cathodic current will reduce the disulfide to the dithiocarbonyl anion which will cap the propagating polymer chain ends and reversibly terminate the

polymerization. To test this hypothesis, polymerization was initiated by applying +0.5 mA of current over 15 minutes to a solution of IBVE, Fc, CTA (**1a**), and Bu₄NClO₄ in DCM after which current application was halted. After 30 minutes of polymerization, -0.5 mA of current was applied to reversibly terminate the reaction. Following a 60 minute “off” period, the polymerization could be reinitiated by subjecting the reaction to anodic current—this overall process was repeated two times, demonstrating good temporal control over the polymerization (Figure 4.3b). Notably, in the third “on” period twice the current was passed, yielding an increased rate of polymerization; this result demonstrates the ease of controlling the polymerization rate through modulation of current density. Additionally, this new electrochemical polymerization can be applied to a large range of vinyl ether monomers of varying steric and electronic parameters, as well as *para*-methoxystyrene. In each case, polymers with low *D* values and excellent agreement between theoretical and experimental *M_n*s were obtained (Table 4.3).

The temporal control over this electrochemically controlled cationic polymerization validates this method as a good candidate to be paired with a photochemically controlled radical polymerization for *in situ* synthesis of multiblock copolymers. Drawing from previous experience, we chose Ir(ppy)₃ as the photocatalyst to mediate the radical polymerization of methyl acrylate (MA).^{31,36,39} It is important to note that successful switching requires that

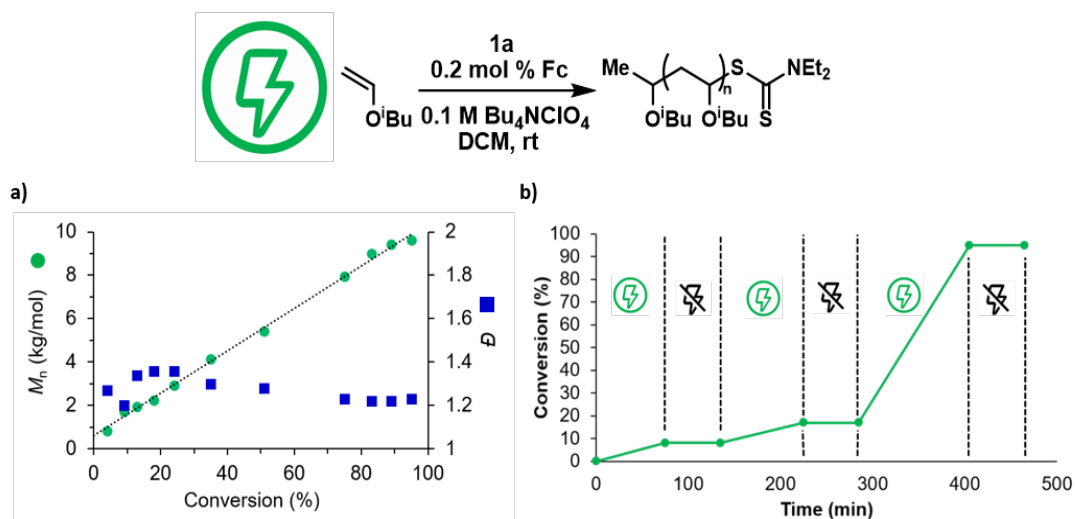


Figure 4.3. (a) Relationship between M_n and conversion for the electrochemical polymerization of vinyl ethers. (b) Temporal control over polymer chain growth through application of oxidizing and reducing potentials. [IBVE] = 3.2 M (in DCM), V_{tot} = 6 mL, [Bu₄NClO₄] = 0.1 M, Steel Anode, Steel Cathode (Divided cell).

temporal control of each polymerization be retained when all reagents for both polymerizations are combined.

To demonstrate that the electrochemically mediated cationic polymerization is unaffected by the presence of Ir(ppy)₃ and MA, +0.5 mA of current was applied over 10 minutes to a solution containing Fc, Ir(ppy)₃, IBVE, MA, CTA (**1b**), and Bu₄NClO₄ in DCM. We observed efficient polymerization of IBVE, producing a polymer with a M_n of 8.8 kg/mol and a low dispersity of 1.15. Importantly, the experimental M_n aligned well with the theoretical molar mass, and the polymerization can be turned on and off by simply changing the direction of current. Unfortunately, upon irradiation of an identical reaction solution with 456 nm blue LEDs, we observed no conversion of MA over 6 hours. For

comparison, the radical polymerization of MA reached 88% conversion after the same time period in the absence of ferrocene and electrolyte (Table 4.4). We hypothesized that Fc was quenching the excited state of Ir(ppy)₃, as it is known to be a triplet quencher.⁴⁰ Indeed, mM concentrations of Fc showed strong quenching of the Ir(ppy)₃ photoluminescence (Figure 4.4). This observation illustrates that the Fc is inhibiting the photochemical radical polymerization. Importantly, by substantially lowering the concentration of Fc in solution, the reaction rate of the radical polymerization could be recovered while also retaining good temporal control over both the photochemical and electrochemical polymerizations (Figure 4.16, 4.20). These results demonstrate that both the cationic and radical polymerizations are compatible with one another, which provides the opportunity to switch between polymerization mechanisms at will.

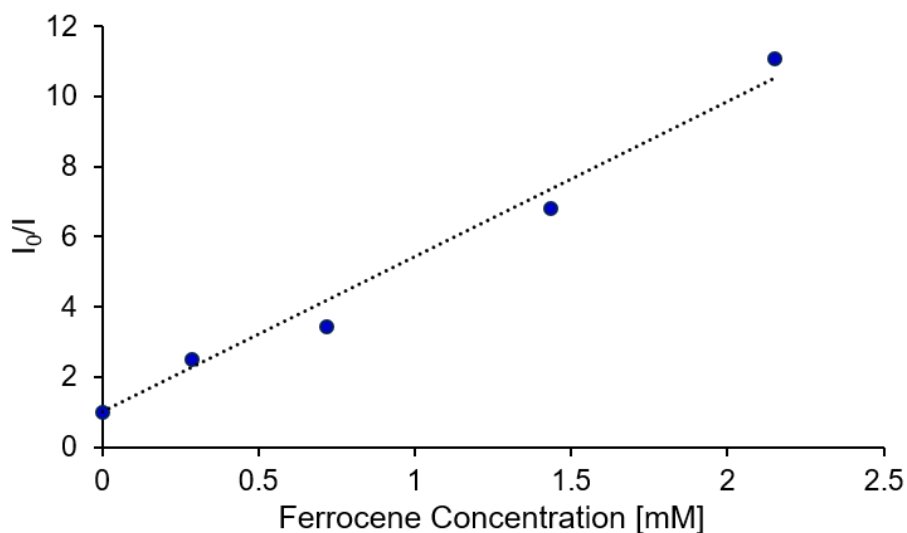


Figure 4.4. Stern-Volmer plot for the fluorescence quenching of Ir(ppy)₃ by ferrocene ($\lambda_{\text{ex}} = 455 \text{ nm}$).

Stimuli Switching Facilitates Multiblock Polymers

With orthogonal and compatible polymerization processes in hand, we set out to make multiblock copolymers. Upon applying +0.5 mA of current to MA, IBVE, Ir(ppy)₃, Fc, and Bu₄NClO₄ in DCM, IBVE is exclusively polymerized. Following the application of -0.5 mA of current to reversibly terminate the cationic polymerization, the solution was subjected to blue light irradiation affording a well-defined poly(IBVE-*b*-MA) block polymer (Figure 4.5a). Importantly, from the same solution conditions, the inverse diblock polymer can be synthesized by simply changing the order of the two applied stimuli (Figure 4.23, 4.24). Of note, we have previously demonstrated that we can polymerize IBVE from a poly(MA) macroinitiator; the incorporation of a small amount of IBVE during the radical polymerization results in thioacetal chain ends, which enables efficient initiation of the cationic process.^{36,41}

We sought to explore the range of copolymer sequences that we could generate by alternating the order of applied stimuli. To synthesize a poly(IBVE-*b*-MA-*b*-IBVE) triblock copolymer, we first applied anodic current to promote the cationic polymerization of IBVE. The polymerization was then reversibly terminated by the application of cathodic current, which is followed by an off period in the absence of stimuli that illustrates the stability of the system. We then irradiated the solution with blue light to promote the radical polymerization of methyl acrylate, wherein a small amount of isobutyl vinyl ether is

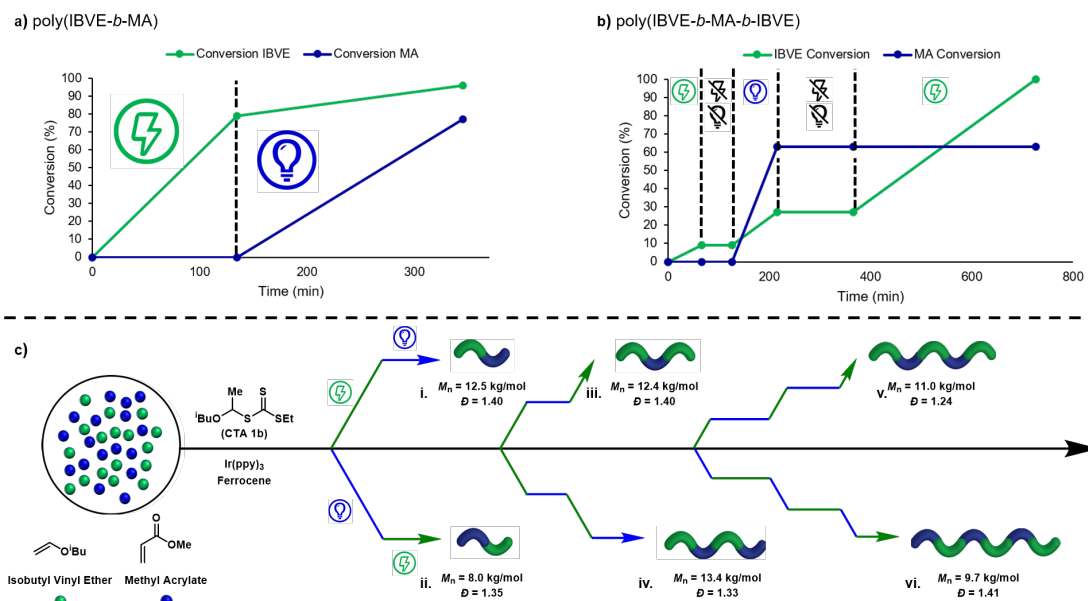


Figure 4.5. Conversion of IBVE (green line) and MA (blue line) for dual stimuli switching using alternating application of photochemical or electrochemical stimuli to synthesize (a) poly(IBVE-*b*-MA) and (b) poly(IBVE-*b*-MA-*b*-IBVE). (c) Range of accessible multiblock copolymers synthesized via electro-photo-switchable RAFT polymerization: i. poly(IBVE-*b*-MA), ii. poly(MA-*b*-IBVE), iii. poly(IBVE-*b*-MA-*b*-IBVE), iv. poly(IBVE-*b*-MA-*b*-IBVE-*b*-MA), v. poly(IBVE-*b*-MA-*b*-IBVE-*b*-MA-*b*-IBVE), and vi. poly(MA-*b*-IBVE-*b*-MA-*b*-IBVE-*b*-MA-*b*-IBVE).

incorporated, followed by another off period upon the removal of light. Subsequent application of electrical current generated the terminal IBVE block (Figure 4.5b). This triblock copolymer synthesis with two alternating off periods, demonstrates the excellent temporal control and chain-end fidelity of the dual stimuli system. This methodology can be taken a step further to generate tetrablock copolymers by simply adding an additional switching event (Figure 4.27, 4.28). Interestingly, while our past methodology was able to achieve the synthesis of tetrablock copolymers, the need for successive addition of

exogenous ferrocenium greatly limited the number of switching events that could take place due to increased termination events and inhibition of the photochemical radical polymerization by ferrocene quenching.³⁶ In this electro-photo-switchable system we can maintain low concentrations of ferrocene and negate the need for any exogenous reagents facilitating enhanced control over the process. This novel polymerization methodology enables the synthesis of penta- and hexablock copolymers composed of methyl acrylate and isobutyl vinyl ether, which were previously inaccessible by any previous methodologies (Figure 4.5c). Significantly, the size of each block can be controlled by the length of application and intensity (*i.e.*, current density or light intensity) of each stimulus, while the number of blocks is dictated by the number of times the two stimuli are switched. The control offered by this method paves the way toward generating libraries of block polymer structures through automated switching of the applied stimuli.

4.4 Conclusion

In conclusion, we have developed a system that enables switching of polymerization mechanisms, and thereby monomer selectivity *in situ* using two external stimuli, visible light and electrical potential. To achieve this goal, we designed an electrochemical cationic polymerization mediated by ferrocene. Pairing this electrochemical cationic polymerization with a photochemical radical polymerization enabled us to successfully switch polymerization

mechanism *in situ*. A variety of well-defined multiblock copolymers were synthesized where the final structure was dictated by the order and duration of the applied stimuli. This new switchable polymerization demonstrates the power of pairing two orthogonal, external stimuli and will facilitate the synthesis of advanced polymer structures in a one-pot process; thus, accelerating the discovery of next-generation materials.

4.5 References

- (1) Lutz, J. -F. *Polym. Chem.* **2010**, *1*, 55.
- (2) Lutz, J.-F.; Ouchi, M.; Liu, D. R.; Sawamoto, M. *Science*. **2013**, *341*, 1238149.
- (3) Bates, F. S.; Hillmyer, M. A.; Lodge, T. P.; Bates, C. M.; Delaney, K. T.; Fredrickson, G. H. *Science* **2012**, *336*, 434.
- (4) Corrigan, N.; Ciftci, M.; Jung, K.; Boyer, C. *Angew. Chem. Int. Ed.* **2019**, 10.1002/anie.201912001.
- (5) Reetz, I. V. O.; Yagci, Y. *Prog. Polym. Sci.* **1998**, *23*, 1485.
- (6) Naumann, S.; Buchmeiser, M. R. *Catal. Sci. Technol.* **2014**, *4*, 2466.
- (7) Naumann, S.; Buchmeiser, M. R. *Macromol. Rapid Commun.* **2014**, *35*, 682.
- (8) Gregson, C. K. A.; Blackmore, I. J.; Gibson, V. C.; Long, N. J.; Marshall, E. L.; White, A. J. P. *Dalton Trans.* **2006**, 3134.

- (9) Gregson, C. K. A.; Gibson, V. C.; Long, N. J.; Marshall, E. L.; Oxford, P. J.; White, A. J. P. *J. Am. Chem. Soc.* **2006**, *128*, 7410.
- (10) Broderick, E. M.; Guo, N.; Vogel, C. S.; Xu, C.; Sutter, J.; Miller, J. T.; Meyer, K.; Mehrkhodavandi, P.; Diaconescu, P. L. *J. Am. Chem. Soc.* **2011**, *133*, 9278.
- (11) Biernesser, A. B.; Delle Chiaie, K. R.; Curley, J. B.; Byers, J. A. *Angew. Chem. Int. Ed.* **2016**, *55*, 5251.
- (12) Wang, X.; Thevenon, A.; Brosmer, J. L.; Yu, I.; Khan, S. I.; Mehrkhodavandi, P.; Diaconescu, P. L. *J. Am. Chem. Soc.* **2014**, *136*, 11264.
- (13) Broderick, E. M.; Guo, N.; Wu, T.; Vogel, C. S.; Xu, C.; Sutter, J.; Miller, J. T.; Meyer, K.; Cantat, T.; Diaconescu, P. L. *Chem. Commun.* **2011**, *47*, 9897.
- (14) Mohapatra, H.; Kleiman, M.; Esser-Kahn, A. P. *Nat. Chem.* **2017**, *9*, 135.
- (15) McKenzie, T. G.; Colombo, E.; Fu, Q.; Ashokkumar, M.; Qiao, G. G. *Angew. Chem. Int. Ed.* **2017**, *56*, 12302.
- (16) Wang, Z.; Pan, X.; Li, L.; Fantin, M.; Yan, J.; Wang, Z.; Wang, Z.; Xia, H.; Matyjaszewski, K. *Macromolecules.* **2017**, *50*, 7940.
- (17) Wang, Z.; Pan, X.; Yan, J.; Dadashi-Silab, S.; Xie, G.; Zhang, J.; Wang, Z.; Xia, H.; Matyjaszewski, K. *ACS Macro Lett.* **2017**, *6*, 546.
- (18) Peterson, B. M.; Lin, S.; Fors, B. P. *J. Am. Chem. Soc.* **2018**, *140*, 2076.

- (19) Chmielarz, P.; Fantin, M.; Park, S.; Isse, A. A.; Gennaro, A.; Magenau, A. J. D.; Sobkowiak, A.; Matyjaszewski, K. *Prog. Polym. Sci.* **2017**, *69*, 47.
- (20) Wang, Y.; Fantin, M.; Matyjaszewski, K. *J. Polym. Sci. A Polym. Chem.* **2019**, *57*, 376.
- (21) Qi, M.; Dong, Q.; Wang, D.; Byers, J. A. *J. Am. Chem. Soc.* **2018**, *140*, 5686.
- (22) Zhu, J.; Hao, X.; Yan, Q. *Sci. China Chem.* **2019**, *62*, 1023.
- (23) Corrigan, N.; Shanmugam, S.; Xu, J.; Boyer, C. *Chem. Soc. Rev.* **2016** *36*, 6165.
- (24) Mckenzie, T. G.; Fu, Q.; Uchiyama, M.; Satoh, K.; Xu, J.; Boyer, C.; Kamigaito, M.; Qiao, G. G. *Adv. Sci.* **2016**, *3*, 1500394.
- (25) Shanmugam, S.; Boyer, C. *J. Am. Chem. Soc.* **2015**, *137*, 9988.
- (26) Dadashi-Silab, S.; Doran, S.; Yagci, Y. *Chem. Rev.* **2016**, *116*, 10212.
- (27) Chen, M.; Zhong, M.; Johnson, J. A. *Chem. Rev.* **2016**, *116*, 10167.
- (28) Trotta, J. T.; Fors, B. P. *Synlett.* **2016**, *27*, 702.
- (29) Murata, K.; Saito, K.; Kikuchi, S.; Akita, M.; Inagaki, A. *Chem. Commun.* **2015**, *51*, 5717.
- (30) Theriot, J. C.; Lim, C.; Yang, H.; Ryan, M. D.; Musgrave, C. B.; Miyake, G. M. *Science* **2016**, *352*, 1082.
- (31) Xu, J.; Jung, K.; Atme, A.; Shanmugam, S.; Boyer, C. *J. Am. Chem. Soc.* **2014**, *136*, 5508.

- (32) Satoh, K.; Sun, Z.; Uchiyama, M.; Kamigaito, M.; Xu, J.; Boyer, C. *Polym. J.* **2020**, *52*, 65.
- (33) Fu, C.; Xu, J.; Boyer, C. *Chem. Commun.* **2016**, *52*, 7126.
- (34) Leibfarth, F. A.; Mattson, K. M.; Fors, B. P.; Collins, H. A.; Hawker, C. J. *Angew. Chem. Int. Ed.* **2013**, *52*, 199.
- (35) Zhang, Z., Zeng, T., Xia, L., Hong, C., Wu, D., and You, Y. *Nat. Commun.* **2018**, *9*, 2577.
- (36) Peterson, B. M.; Kottisch, V.; Supej, M. J.; Fors, B. P. *ACS Cent. Sci.* **2018**, *4*, 1228.
- (37) The amount of ferrocenium generated can be estimated by the total amount of charge passed under galvanostatic conditions.
- (38) An induction period is observed which corresponds to the amount of time it takes to generate sufficient ferrocenium to initiate polymerization.
- (39) Phommalyasack-Lovan, J.; Chu, Y.; Boyer, C.; Xu, J. *Chem. Commun.* **2018**, *54*, 6591.
- (40) Farmilo, A.; Wilkinson, F. *Chem. Phys. Lett.* **1975**, *34*, 575.
- (41) Aoshima, H.; Uchiyama, M.; Satoh, K.; Kamigaito, M. *Angew. Chem. Int. Ed.* **2014**, *53*, 10932.

4.6 Appendix

Experimental Information

General Reagent Information

Isobutyl vinyl ether (IBVE) (99%, TCI), ethyl vinyl ether (EVE) (99%, Sigma Aldrich), 2-chloroethyl vinyl ether (Cl-EVE) (97%, TCI), *n*-propyl vinyl ether (nPrVE) (99%, Sigma Aldrich), *n*-butyl vinyl ether (nBuVE) (98%, Sigma Aldrich), cyclohexyl vinyl ether (CyVE) (98%, Sigma Aldrich), 2,3-dihydrofuran (99%, Sigma Aldrich), and methyl acrylate (MA) (99%, Sigma Aldrich) were dried over calcium hydride (CaH₂) (ACROS organics, 93% extra pure, 0–2 mm grain size) for 12 h, distilled under nitrogen, and degassed by three freeze-pump-thaw cycles. 4-Methoxystyrene (97%, Sigma Aldrich) was dried over calcium hydride (CaH₂) (ACROS organics, 93% extra pure, 0–2 mm grain size) for 12 h, distilled under vacuum, and degassed by three freeze-pump-thaw cycles. Sodium *N,N*-diethyldithiocarbamate trihydrate (**2**) (98%, Alfa Aesar) was azeotropically dried with toluene. Ethanethiol (97%, Alfa Aesar) and carbon disulfide (99.9+%, Alfa Aesar) were distilled before use. Tetrabutylammonium hexafluorophosphate (Bu₄NPF₆) (98%, TCI), tetrabutylammonium tetrafluoroborate (Bu₄NBF₄) (98%, TCI), HCl in Et₂O (2.0 M, Sigma Aldrich), Tris[2-phenylpyridinatoC²,N]iridium(III) (Ir(ppy)₃) (Strem, 95%), and sodium hydride (60%, dispersion in mineral oil, Sigma Aldrich) were used as received. Ferrocene (98%, TCI) was purified by sublimation prior to use. Tetrabutylammonium perchlorate (Bu₄NClO₄) (98%, TCI) was purified by recrystallization from ethyl acetate three times, and dried *in vacuo* in the presence of P₂O₅. Dichloromethane (DCM), acetonitrile (MeCN), and diethyl ether (Et₂O) were purchased from J.T. Baker and were purified by vigorous

purging with argon for 2 h, followed by passing through two packed columns of neutral alumina under argon pressure. Hexanes and ethyl acetate were purchased from Fischer Scientific and used as received. Ethanol (anhydrous, 200 proof) was purchased from Koptec. Alumina (1.0, 0.3, 0.05 μm pore size) was purchased from Extec. Reticulated vitreous carbon was purchased from ERG Aerospace. Microcloth PSA (polishing paper) and Abrasive Paper (600 grit) were purchased from Buehler. Stainless steel wire was purchased from McMasterCarr. S-1-isobutoxyethyl *N,N*-diethyl dithiocarbamate (**1a**)¹ and S-1-isobutoxyethyl *S'*-ethyl trithiocarbonate (**1b**)¹ were synthesized according to literature procedures.

General Analytical Information

All polymer samples were analyzed using a Tosoh EcoSec HLC 8320 GPC system with two SuperHM-M columns in series at a flow rate of 0.350 mL/min. THF was used as the eluent and all number-average molecular weights (M_n), weight-average molecular weights (M_w), and dispersities (\mathcal{D}) were determined by light scattering using a Wyatt miniDawn Treos multi-angle light scattering detector. The dn/dc values were calculated from light scattering in tetrahydrofuran (THF) for poly(ethyl vinyl ether), poly(2-chloroethyl vinyl ether), poly(*n*-propyl vinyl ether), poly(*n*-butyl vinyl ether), and block copolymers. Nuclear magnetic resonance (NMR) spectra were recorded on a Varian 400 MHz, a Varian 600 MHz, or a Bruker 500 MHz instrument. Varian Cary Eclipse Fluorescence Spectrophotometer was used for the quenching studies.

Electrolysis experiments were performed using a BASi EC Epsilon potentiostat or a DC power supply.

General Electrochemical Cell and Electrode Setup

Preparation of electrochemical cell and caps

Two-chambered electrochemical cells, separated by a fine frit and joined by a narrow passage above the volume of the reaction contents, were used for all experiments (Figure 4.6.a-d). Ground glass joints (14/20) sealed with septa were used for addition of liquid reagents. Cell caps were constructed from Teflon schlenk bomb screw on caps. Two (2mm) holes were drilled with a drill press into the top of the cap. A 2 mm stainless steel rod was driven through the cap and 2 mm (inner diameter) stainless steel tube was fastened to the inner end of the stainless steel rods to hold the electrodes.

Preparation of reticulated vitreous carbon (RVC) electrodes

The RVC electrodes were constructed by driving a 2 mm pencil lead through a 50 mm x 50 mm x 100 mm section of RVC (Figure 4.6.e). For use in the electrochemical cell, the other end of the pencil lead was inserted into the stainless steel tube of the electrochemical cell caps (Figure 4.6.b and 4.6.c). The pencil lead was cut to the desired length with a razor blade to maximize electrode surface area in contact with the reaction while allowing for space for magnetic stirring.

Preparation of stainless steel wire electrodes

Stainless steel electrodes were constructed by tightly wrapping ~50 cm of 0.5 mm diameter steel wire around a 2 mm diameter rod (Figure 4.6.f). The wires were wrapped until the coil reached approximately 3 cm in length leaving an additional 15 cm of wire for connecting to the DC power source (Figure 4.6.a and 4.6.d). For use in the electrochemical cell, the wires were pierced through 14/20 septa sealing the side arms of the electrochemical cell and connected directly to the DC power source.

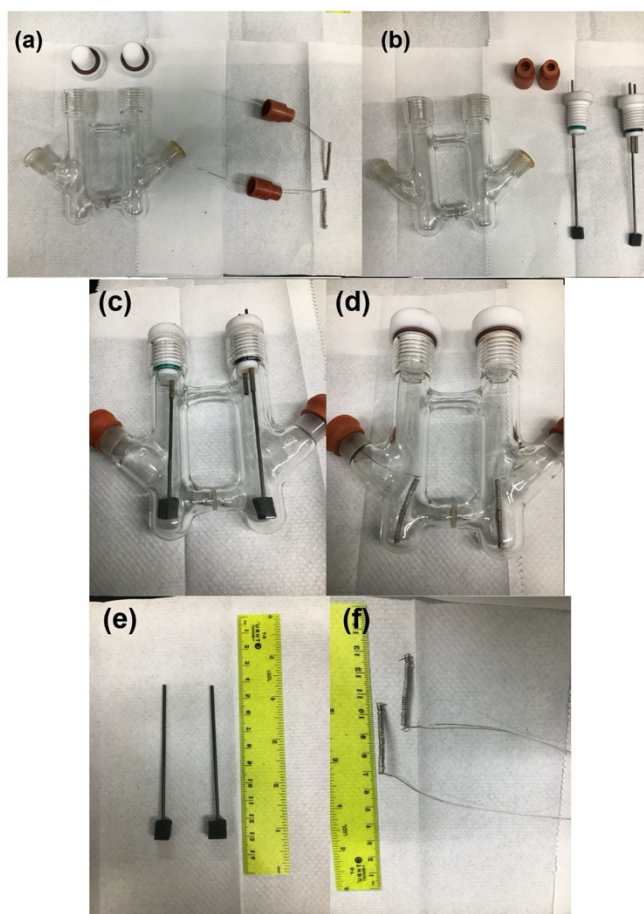
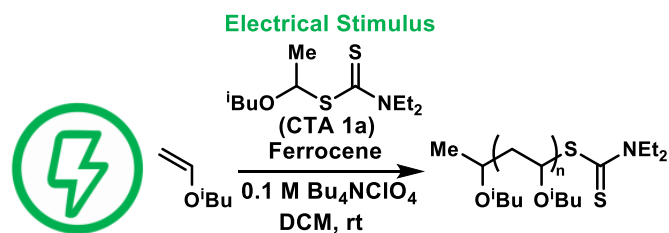


Figure 4.6. Electrochemical cell and electrode preparation

to stir for 3 h. Aliquots taken by syringe under a blanket of N₂ and were then analyzed by NMR and GPC.

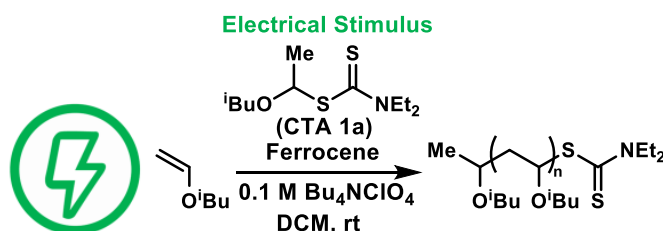
General Procedure for Ferrocene Mediated Electrochemically Controlled Cationic Polymerization (Constant Potential)



To an oven dried electrochemical cell, a magnetic stir bar was added to both the working and counter compartment. The cell was equipped with a reticulated vitreous carbon (RVC) anode, RVC cathode, a Ag wire quasi-reference electrode in the working compartment, and then sealed with the cell caps and rubber septa. The electrochemical cell was then evacuated and backfilled with positive pressure of nitrogen. Once the electrochemical cell had cooled to room temperature, ferrocene (7.1 mg, 0.038 mmol, 0.2 mol% relative to IBVE) was added to the working compartment and Bu₄NClO₄ (205 mg, 0.60 mmol) was added to both the working and counter compartments. The cell was then evacuated and backfilled with positive pressure of nitrogen three times. Then the working compartment was charged with isobutyl vinyl ether (2.5 mL, 19.2 mmol, 100 equiv), 0.38 mL of a stock solution of **1a** in DCM (0.5 M, 0.19 mmol, 1 equiv), and 3.0 mL of DCM. The counter compartment was charged with 6.0 mL of DCM. Potentiostat leads were connected to the electrodes.

Stirring began and an oxidizing potential of 440 mV vs. Ag was applied for 1 h, and the reaction was left to stir for 12 h. Aliquots were taken by syringe under a blanket of N₂ and were then analyzed by NMR and GPC.

General Procedure for Determining the Impact that Current Density has on Ferrocene Mediated Electrochemically Controlled Cationic Polymerization



To an oven dried electrochemical cell, a magnetic stir bar was added to both the working and counter compartment. The cell was equipped with a reticulated vitreous carbon (RVC) anode and RVC cathode and then sealed with the cell caps and rubber septa. The electrochemical cell was then evacuated and backfilled with positive pressure of nitrogen. Once the electrochemical cell had cooled to room temperature, ferrocene (7.1 mg, 0.038 mmol, 0.2 mol% relative to IBVE) was added to the working compartment and Bu₄NClO₄ (205 mg, 0.60 mmol) was added to both the working and counter compartments. The cell was then evacuated and backfilled with positive pressure of nitrogen three times. Then the working compartment was charged with isobutyl vinyl ether (2.5 mL, 19.2 mmol, 100 equiv), 0.38 mL of a stock solution of **1a** in DCM (0.5 M,

0.19 mmol, 1 equiv), and 3.0 mL of DCM. The counter compartment was charged with 6.0 mL of DCM. The leads of the DC power supply were connected to the electrodes. Stirring began, a variable amount of anodic current was applied to generate the desired concentration of ferrocenium, and the reaction was left to stir. Aliquots were taken by syringe under a blanket of N₂ and were then analyzed by NMR and GPC.

Table 4.2. Effect of applied current density on cationic polymerization control

Applied Stimuli ^a	Fc ⁺ Generated (μmol) ^b	M _n , Theo (kg/mol) ^c	M _n , Exp (kg/mol)	Đ
1.0 mA	19.2	10.4	10.8	1.09
1.0 mA	9.6	10.4	10.6	1.13
1.0 mA	1.9	10.4	11.7	1.07
1.0 mA	0.19	—	—	—
2.0 mA	9.6	10.4	9.9	1.18
0.5 mA	9.6	10.4	10.0	1.13
0.1 mA	9.6	10.1	9.9	1.14

^a [IBVE] = 3.2 M (in DCM), V_{tot} = 6 mL, [M]:[CTA]:[Fc] : 100:1:0.2, [Bu₄NClO₄] = 0.1 M, RVC Anode, RVC Cathode. ^b(Fc⁺ generated) = (I/(F*t), where I = current, F = Faraday's Constant, and t = time in sec.

^c M_{n, Thero} = [M]/[CTA] X MW_M X Conversion + MW_{CTA}.

Procedure for Determining the Effects of Current Density on the Rate of Electrochemically Controlled Cationic Polymerization.

To an oven dried electrochemical cell, a magnetic stir bar was added to both the working and counter compartment. The cell was equipped with a stainless steel wire anode and stainless steel wire cathode and then sealed with the cell caps and rubber septa. The electrochemical cell was then evacuated

and backfilled with positive pressure of nitrogen. Once the electrochemical cell had cooled to room temperature, ferrocene (7.1 mg, 0.038 mmol, 0.20 mol% relative to IBVE) was added to the working compartment and Bu_4NClO_4 (205 mg, 0.60 mmol) was added to both the working and counter compartments. The cell was then evacuated and backfilled with positive pressure of nitrogen three times. Then the working compartment was charged with isobutyl vinyl ether (2.5 mL, 19.2 mmol, 100 equiv), 0.38 mL of a stock solution of **1a** in DCM (0.5 M, 0.19 mmol, 1 equiv), and 3.0 mL of DCM. The counter compartment was charged with 6.0 mL of DCM. The leads of the DC power supply were connected to the electrodes. Stirring began and an anodic current was applied for 20 min, and the reaction was left to stir. Aliquots were taken by syringe under a blanket of N_2 and were then analyzed by NMR and GPC.

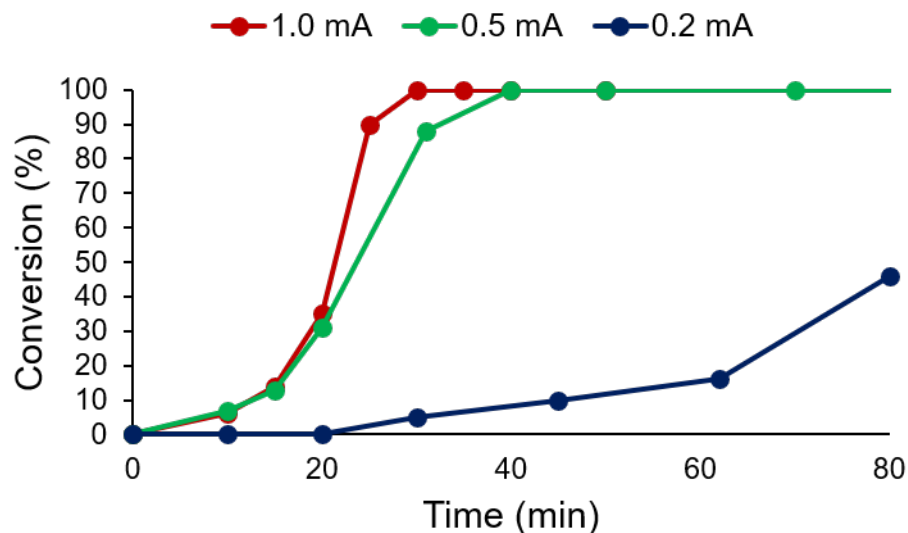


Figure 4.7. Effect of current density on rate of electrochemical cationic polymerization.²

Table 4.3. Monomers Polymerized through Ferrocene Mediated Electrochemically Controlled Cationic Polymerization

Monomer ^a	Conv. (%)	$M_{n,Theo}$ (kg/mol)	$M_{n,Exp}$ (kg/mol)	\bar{D}
<i>n</i> BuVE	>99%	10.3	7.7	1.35
<i>n</i> PrVE ^b	>99%	9.0	6.2	1.31
EVE	97%	7.4	8.2	1.11
Cl-EVE ^b	>99%	10.6	6.0	1.30
CyVE ^c	>99%	12.8	10.0	1.64
<i>p</i> -OMe-Styrene ^d	43%	6.0	4.2	1.41
Dihydrofuran	>99%	7.5	6.9	1.46

^a Standard Reaction Conditions: Vinyl monomer (100 equiv, 3.2 M), **1b** (0.19 mmol, 1 equiv), [Bu₄NClO₄] = 0.1 M, ferrocene (0.0038 mmol, 0.02 mol% relative to IBVE), and stainless steel anode and cathode in DCM. ^b Using 0.038 mmol ferrocene (0.2 mol% relative to IBVE). ^c Using 0.076 mmol ferrocene (0.4 mol% relative to IBVE). ^d Vinyl monomer (100 equiv, 1.6 M), **1b** (0.19 mmol, 1 equiv), [Bu₄NBF₄] = 0.1 M, ferrocene (0.038 mmol, 0.2 mol% relative to IBVE).

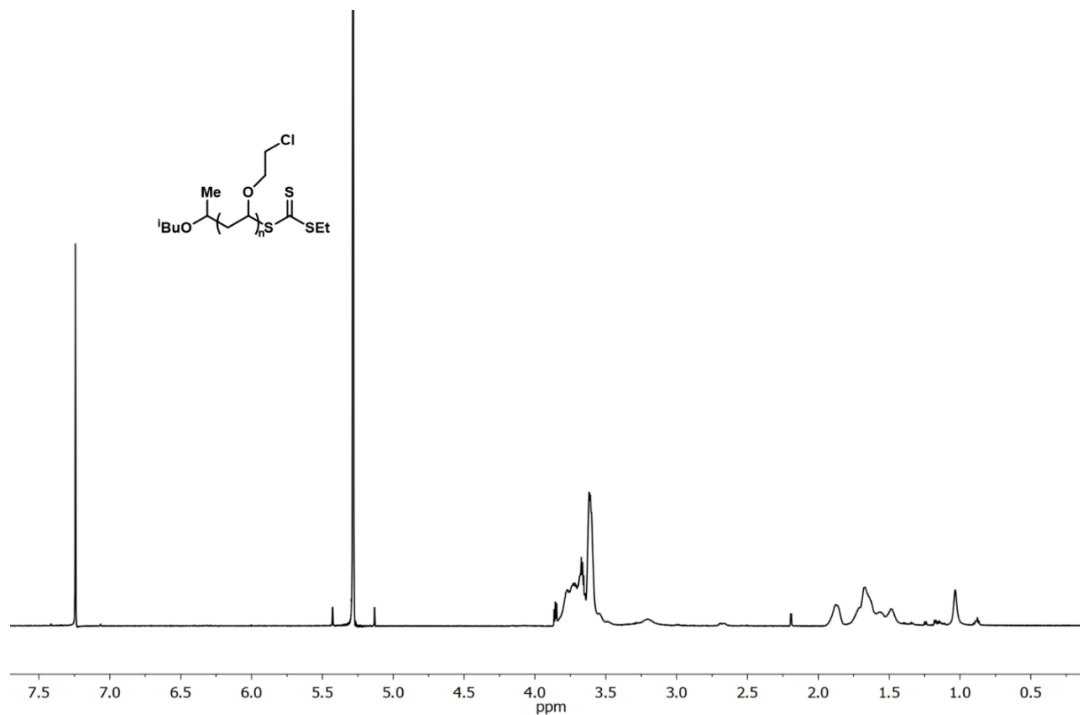


Figure 4.11.a. ¹H NMR of poly(2-chloroethyl vinyl ether), $M_n = 6.0$ kg/mol, $\bar{D} = 1.30$ (Table 4.2, entry 4).

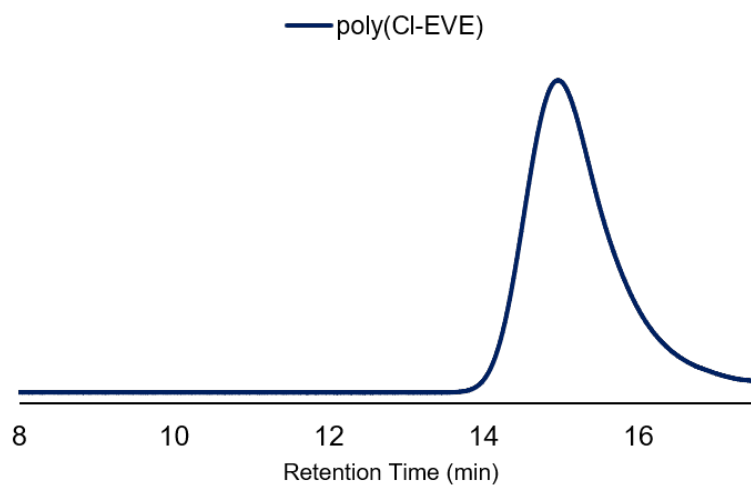


Figure 4.11.b. GPC trace of poly(2-chloroethyl vinyl ether)

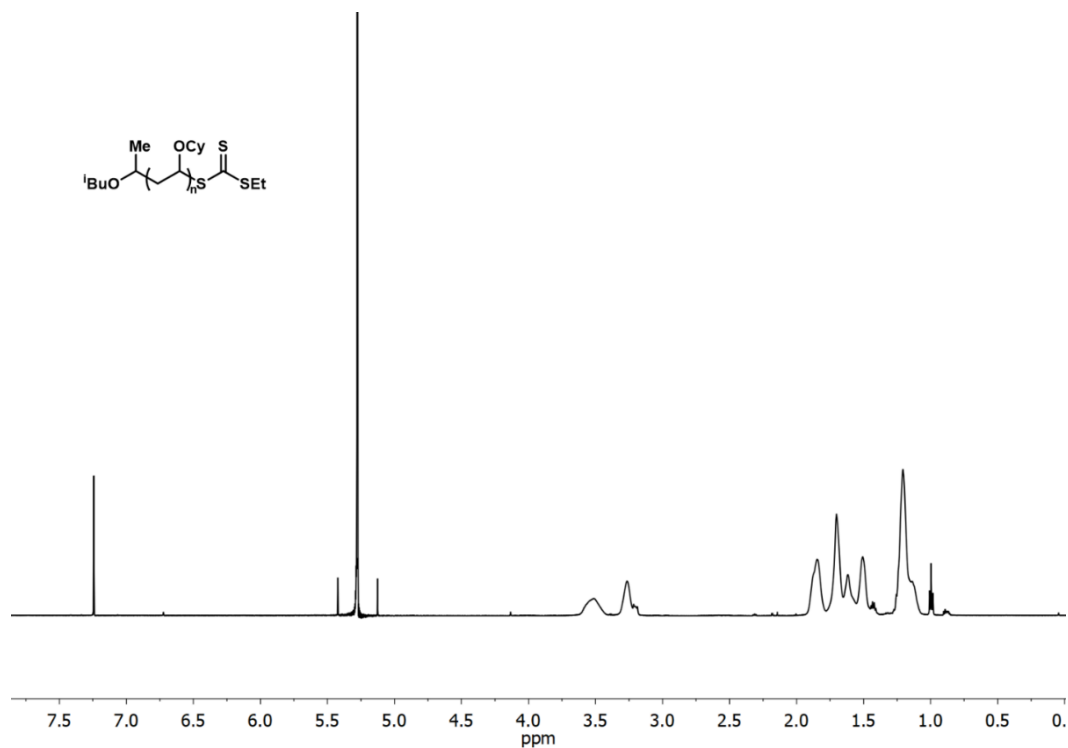


Figure 4.12.a. $^1\text{H NMR}$ of poly(cyclohexyl vinyl ether), $M_n = 10.0 \text{ kg/mol}$, $\bar{D} = 1.64$ (Table 4.2, entry 5).

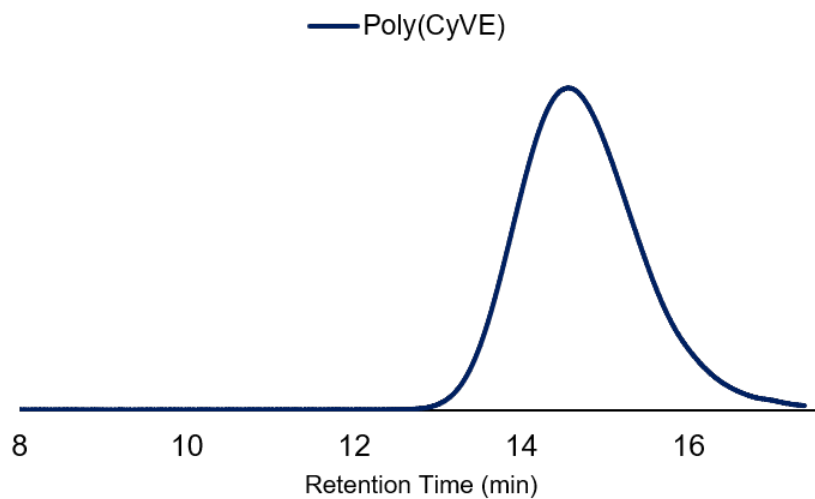


Figure 4.12.b. GPC trace of poly(cyclohexyl vinyl ether)

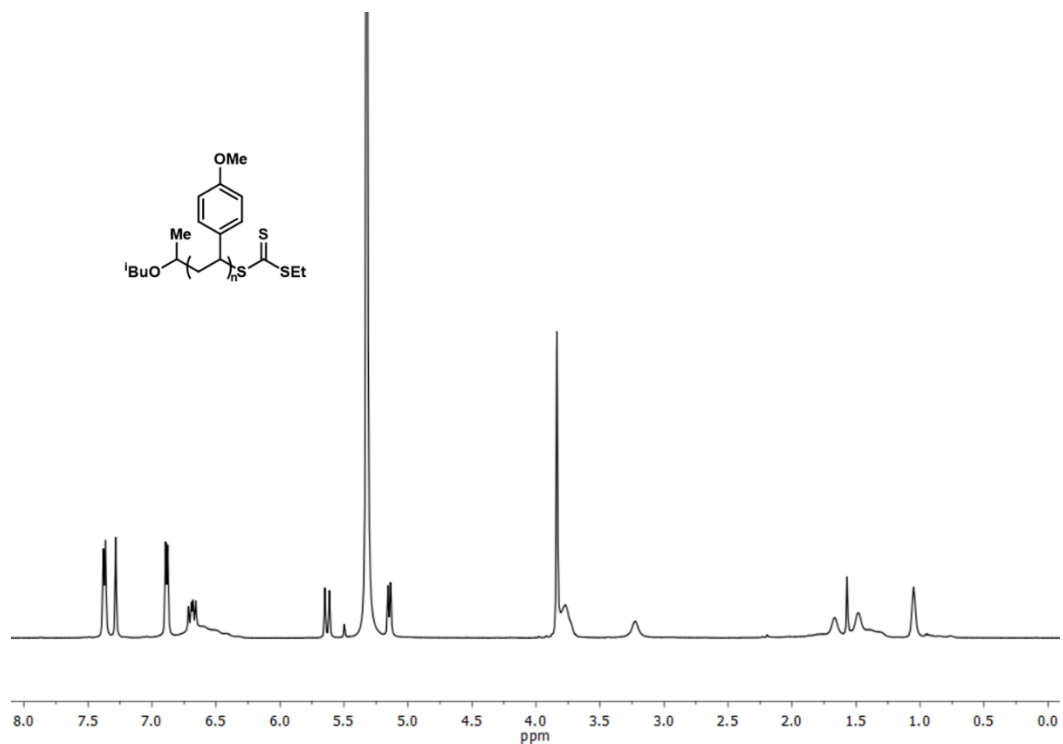


Figure 4.13.a. ¹H NMR of poly(*p*-OMe-Styrene), $M_n = 4.2$ kg/mol, $\bar{D} = 1.41$ (Table 4.2, entry 6).

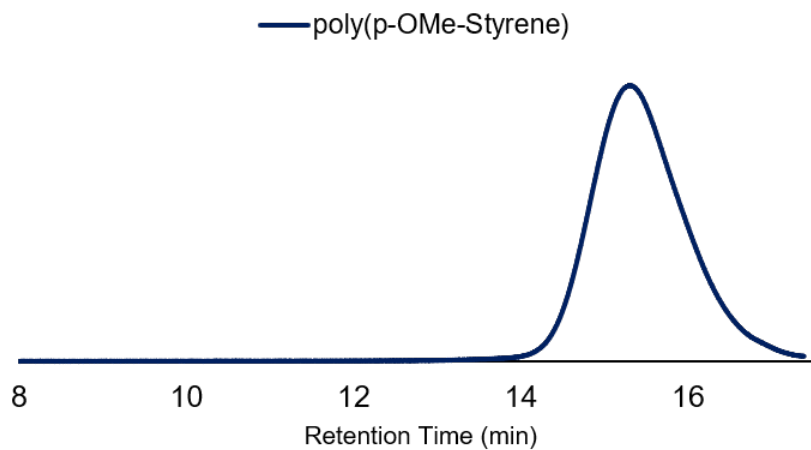


Figure 4.13.b. GPC trace of poly(*p*-OMe-Styrene)

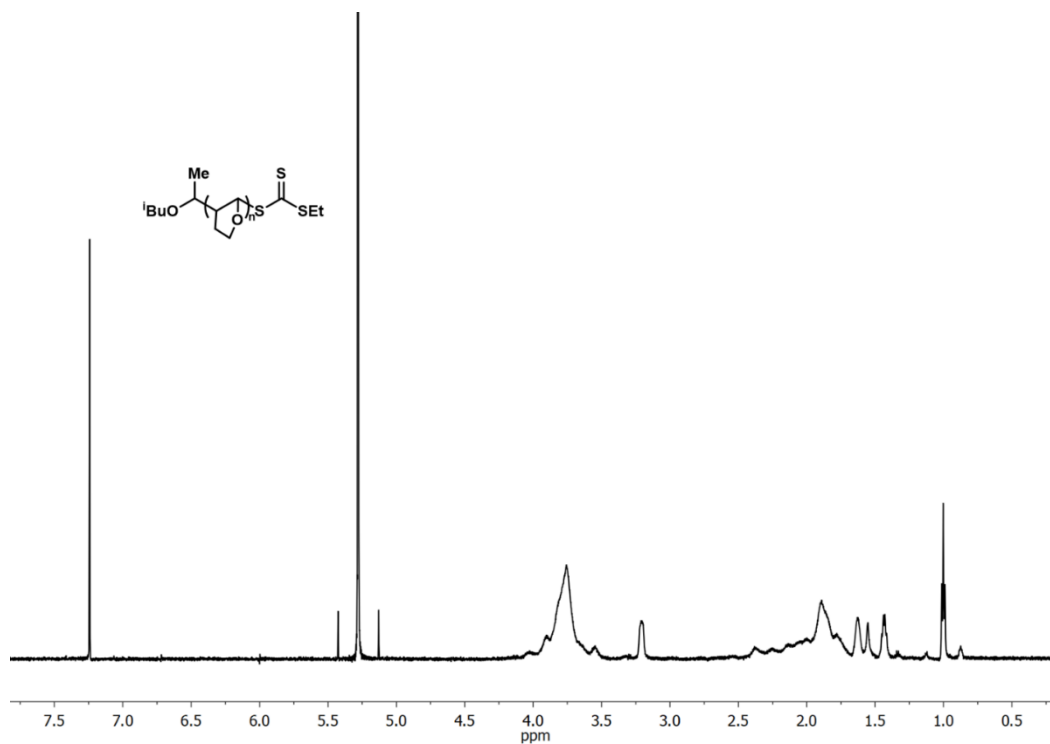


Figure 4.14.a. ^1H NMR of poly(2,3-dihydrofuran), $M_n = 6.9$ kg/mol, $\bar{D} = 1.46$, (Table 4.2, entry 7)

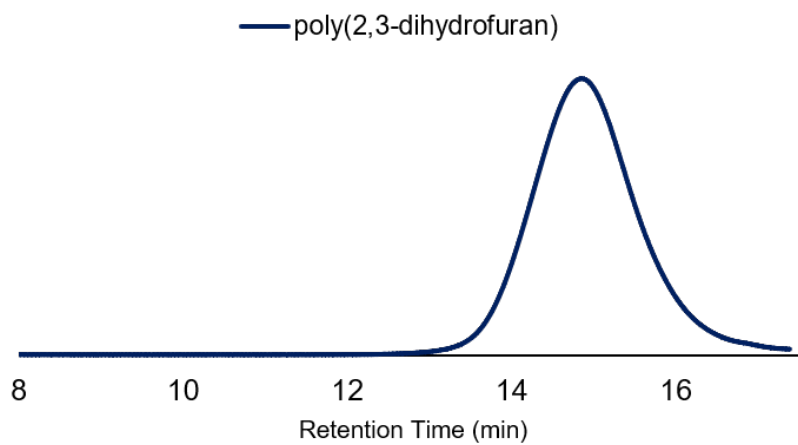
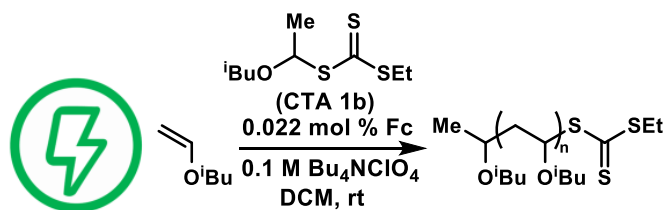


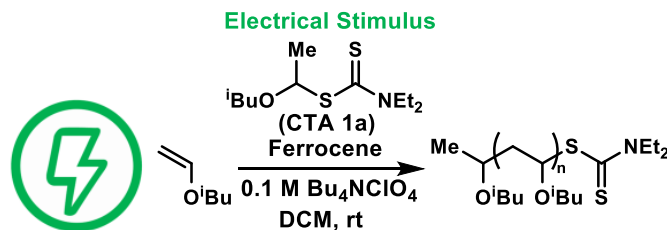
Figure 4.14.b. GPC trace of poly(2,3-dihydrofuran)

Procedure for Testing Oxygen Tolerance of Ferrocene Mediated Electrochemically Controlled Cationic Polymerization



To an oven dried electrochemical cell, a magnetic stir bar was added to both the working and counter compartment. The cell was equipped with a stainless steel wire anode and stainless steel wire cathode and then sealed with the cell caps and rubber septa. The electrochemical cell was then left under an ambient atmosphere. Once the electrochemical cell had cooled to room temperature, 0.050 mL of a stock solution of ferrocene in DCM (0.084 M, 0.78 mg, 0.0042 mmol, 0.022 mol% relative to IBVE) was added to the working compartment and Bu_4NClO_4 (205 mg, 0.60 mmol) was added to both the working and counter compartments. The working compartment was then charged with isobutyl vinyl ether (2.5 mL, 19.2 mmol, 100 equiv), 0.38 mL of a stock solution of **1b** in DCM (0.5 M, 0.19 mmol, 1 equiv), and 3.0 mL of DCM. The counter compartment was charged with 6.0 mL of DCM. The leads of the DC power supply were connected to the electrodes. Stirring began and an anodic current (0.5 mA) was applied for 5 min, and the reaction was left to stir open to air for 18 h. Aliquots taken by syringe were then analyzed by NMR and GPC. ($M_{n,\text{Theo}} = 10.4$ kg/mol, $M_{n,\text{Exp}} = 9.1$, $D = 1.38$).

Procedure for Reversibly Initiating and Terminating Electrochemically Controlled Cationic Polymerization



To an oven dried electrochemical cell, a magnetic stir bar was added to both the working and counter compartment. The cell was equipped with a stainless steel wire anode and stainless steel wire cathode and then sealed with the cell caps and rubber septa. The electrochemical cell was then evacuated and backfilled with positive pressure of nitrogen. Once the electrochemical cell had cooled to room temperature, ferrocene (7.1 mg, 0.038 mmol, 0.20 mol% relative to IBVE) was added to the working compartment and Bu₄NClO₄ (205 mg, 0.60 mmol) was added to both the working and counter compartments. The cell was then evacuated and backfilled with positive pressure of nitrogen three times. The working compartment was then charged with isobutyl vinyl ether (2.5 mL, 19.2 mmol, 100 equiv), 0.38 mL of a stock solution of **1a** in DCM (0.5 M, 0.19 mmol, 1 equiv), and 3.0 mL of DCM. The counter compartment was charged with 6.0 mL of DCM. The leads of the DC power supply were connected to the electrodes. Polymerization was initiated by applying an anodic current of 0.5 mA for 15 min followed by a reaction period of 30 min; this polymerization was then reversibly terminated by applying a cathodic current of -0.5 mA for 30

min. After a 1 h off period, the polymerization was reinitiated by applying an anodic current of 0.5 mA for 15 min, a 45 min reaction period, and then reversibly terminating the polymerization by applying a cathodic current of -0.5 mA for 30 min. After a 1 h off period, 0.5 mA of anodic current was applied for 30 min and the reaction was left to react for 30 min before being reversibly terminated by application of -0.5 mA of a cathodic current for 1 h; this was then followed with an additional 1 h off period. Aliquots for NMR and GPC analysis were taken under inert atmosphere.

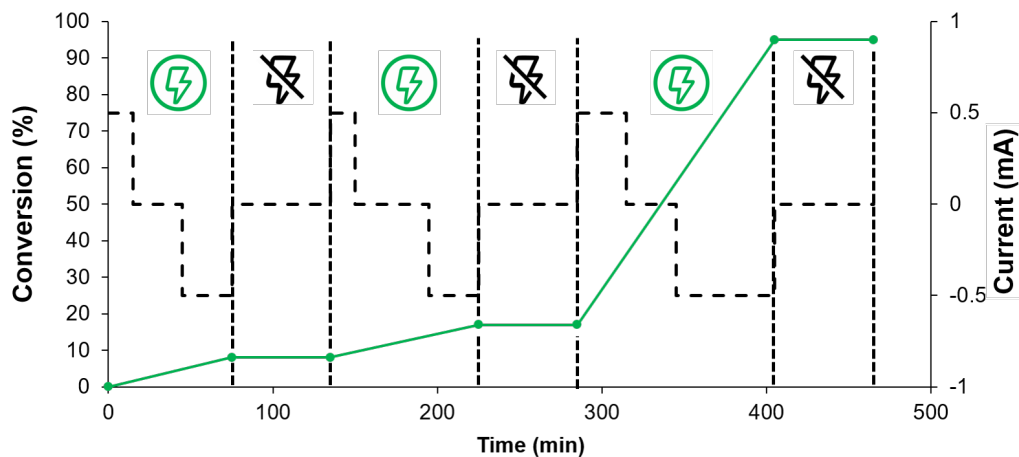
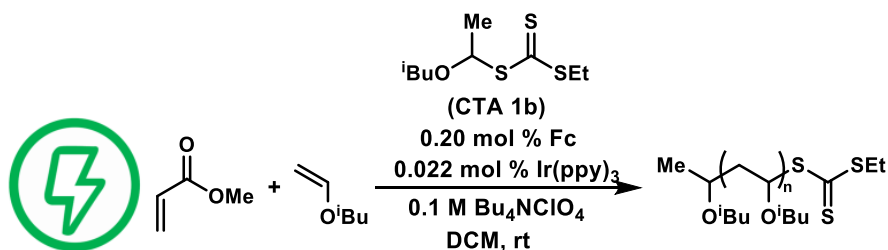


Figure 4.15. Electrochemical On/Off experiment for the cationic polymerization of isobutyl vinyl ether showing the conversion of isobutyl vinyl ether (green line) and applied current (black dashed line).

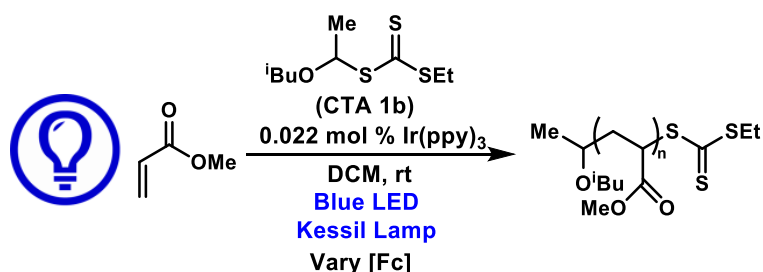
Initial Procedure for Ferrocene Mediated Electrochemically Controlled Cationic Polymerization in Presence of Radical Monomer and Photocatalyst



To an oven dried electrochemical cell, a magnetic stir bar was added to both the working and counter compartment. The cell was equipped with a stainless steel wire anode and stainless steel wire cathode and then sealed with the cell caps and rubber septa. The electrochemical cell was then evacuated and backfilled with positive pressure of nitrogen. Once the electrochemical cell had cooled to room temperature, ferrocene (7.1 mg, 0.038 mmol, 0.20 mol% relative to IBVE) was added to the working compartment and Bu_4NClO_4 (205 mg, 0.60 mmol) was added to both the working and counter compartments. The cell was then evacuated and backfilled with positive pressure of nitrogen three times. The working compartment was then charged with isobutyl vinyl ether (2.5 mL, 19.2 mmol, 100 equiv), methyl acrylate (1.7 mL, 19.0 mmol, 100 equiv), 1.0 mL of a stock solution of Ir(ppy)_3 in DCM (4.58 mM, 0.042 mmol, 0.022 mol% relative to MA), 0.38 mL of a stock solution of **1b** in DCM (0.5 M, 0.19 mmol, 1 equiv), and 0.4 mL of DCM. The counter compartment was charged with 6.0 mL

of DCM. The leads of the DC power supply were connected to the electrodes. Stirring began and an anodic current (0.5 mA) was applied for 10 min, and the reaction was left to stir for 8 h. Aliquots taken by syringe were then analyzed by NMR and GPC. ($M_{n, \text{Theo}} = 10.4 \text{ kg/mol}$, $M_{n, \text{Exp}} = 8.8$, $D = 1.15$).

Optimization of the Photocontrolled Radical Polymerization of Acrylates in Presence of Ferrocene



To an oven dried two-dram vial, a magnetic stir bar was added and the vial was charged with methyl acrylate (1.7 mL, 19.0 mmol, 100 equiv), 1.0 mL of a stock solution of Ir(ppy)_3 in DCM (4.58 mM, 0.042 mmol, 0.022 mol% relative to MA), 0.38 mL of a stock solution of **1b** in DCM (0.5 M, 0.19 mmol, 1 equiv), a variable amount of ferrocene, and 3.0 mL of DCM. The vial was then sealed with a septum cap under an atmosphere of nitrogen, irradiated with a blue LED Kessil Lamp, and stirred while cooling by blowing compressed air over the vial. Aliquots were taken periodically under an inert atmosphere (Figure 4.16) and then analyzed by NMR and GPC (Table 4.4).

Table 4.4. Effect of ferrocene concentration on photocontrolled radical polymerization of methyl acrylate

Entry	[Fc] (mM)	Conversion MA	$M_{n,Theo}$ (kg/mol)	$M_{n,Exp}$ (kg/mol)	\bar{D}
1	0	88%	8.5	10.3	1.36
2	0.7	59%	5.7	7.4	1.41
3	7.0	0%	—	—	—

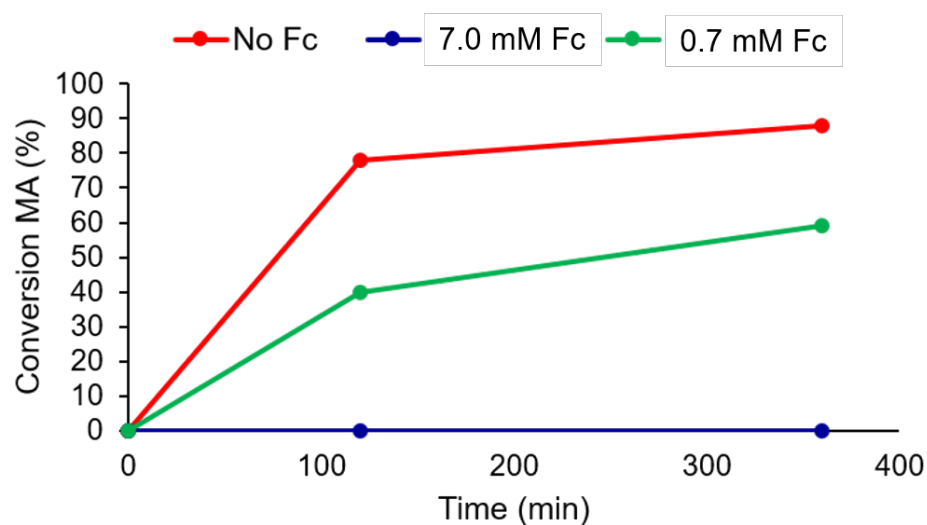


Figure 4.16. Effect of ferrocene concentration on photocontrolled radical polymerization of methyl acrylate.

Procedure for Photoluminescence Quenching Studies

A Varian Cary Eclipse Fluorescence Spectrophotometer was used for the quenching studies. The solutions of $\text{Ir}(\text{ppy})_3$ were excited at 456 nm and the fluorescence spectra were recorded between 460 and 800 nm. The emission of a 0.15 mM solution of $\text{Ir}(\text{ppy})_3$ in DCM was measured at varying concentrations

of Ferrocene (0 – 2.15 mM). As shown in Figure 4.17 concentration dependent fluorescence quenching was observed.

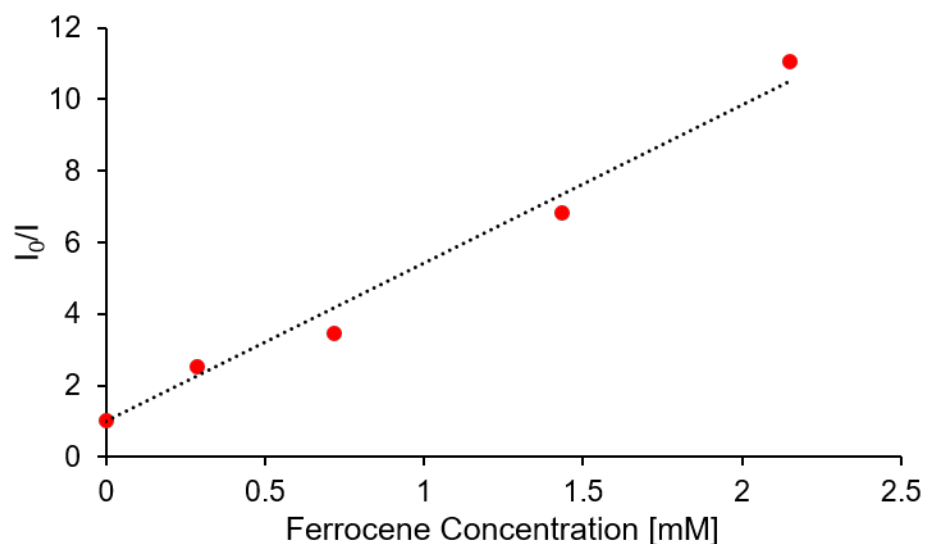


Figure 4.17. Stern-Volmer plot for the fluorescence quenching of $\text{Ir}(\text{ppy})_3$ by ferrocene

Procedure for Temporal Control Over Electrochemical Cationic Polymerization under Optimized Switchable Polymerization Conditions

To an oven dried electrochemical cell, a magnetic stir bar was added to both the working and counter compartment. The cell was equipped with a stainless steel wire anode and stainless steel wire cathode and then sealed with the cell caps and rubber septa (Figure 4.19.a and 4.19.b). The electrochemical cell was then evacuated and backfilled with positive pressure of nitrogen. Once

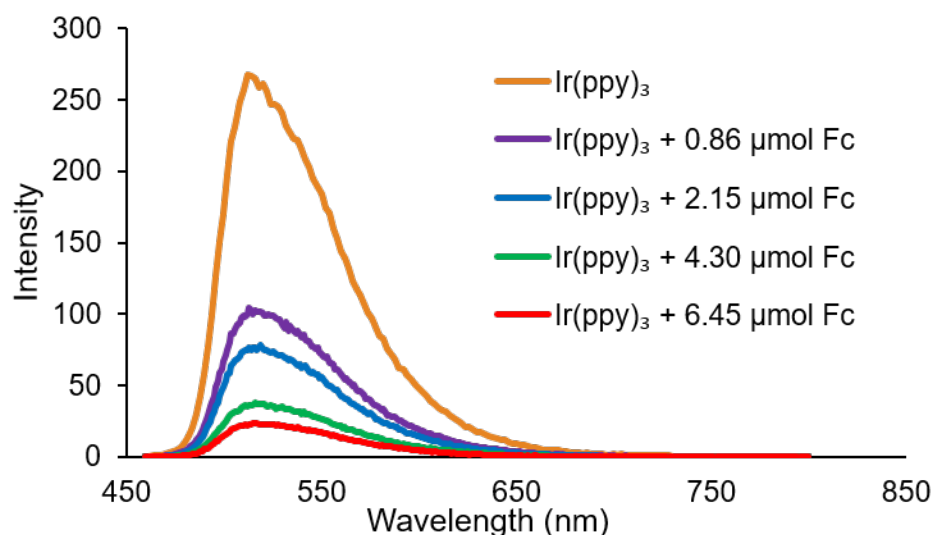


Figure 4.18. Fluorescence Quenching of Ir(ppy)_3 by ferrocene.

the electrochemical cell had cooled to room temperature, 0.050 mL of a stock solution of ferrocene in DCM (0.084 M, 0.78 mg, 0.0042 mmol, 0.022 mol% relative to IBVE) was added to the working compartment and Bu_4NClO_4 (205 mg, 0.60 mmol) was added to both the working and counter compartments. The cell was then evacuated and backfilled with positive pressure of nitrogen three times. The working compartment was then charged with isobutyl vinyl ether (2.5 mL, 19.2 mmol, 100 equiv), methyl acrylate (1.7 mL, 19.0 mmol, 100 equiv), 1.0 mL of a stock solution of Ir(ppy)_3 in DCM (4.58 mM, 0.042 mmol, 0.022 mol% relative to MA), 0.38 mL of a stock solution of **1b** in DCM (0.5 M, 0.19 mmol, 1 equiv), and 0.4 mL of DCM. The counter compartment was charged with 6.0 mL of DCM. The leads of the DC power supply were connected to the electrodes, and a blue LED kessil lamp was situated 3 cm away from the working

compartment. Polymerization was initiated by applying an anodic current of 0.4 mA for 6 min followed by a reaction period of 30 min; this polymerization was then reversibly terminated by applying a cathodic current of -0.4 mA for 12 min. After an off period of 1 h, the reaction was reinitiated through application of anodic current for 6 min, a 10 min reaction period, and then reversibly terminating the polymerization by applying a cathodic current of 0.4 mA for 12 min. After a 3 h off period, 0.4 mA of anodic current was applied for 24 min and the reaction was left to react for an additional hour. Under inert atmosphere, aliquots for NMR and GPC analysis were taken at timepoints prior to a change in stimuli.

Procedure for Temporal Control Over Photocontrolled Radical Polymerization under Optimized Switchable Polymerization Conditions

To an oven dried electrochemical cell, a magnetic stir bar was added to both the working and counter compartment. The cell was equipped with a stainless steel wire anode and stainless steel wire cathode and then sealed with the cell caps and rubber septa (Figure 4.19a,b). The electrochemical cell was then evacuated and backfilled with positive pressure of nitrogen. Once the electrochemical cell had cooled to room temperature, 0.050 mL of a stock solution of ferrocene in DCM (0.084 M, 0.78 mg, 0.0042 mmol, 0.022 mol% relative to IBVE) was added to the working compartment and Bu_4NClO_4 (205 mg, 0.60 mmol) was added to both the working and counter compartments. The cell was then evacuated and backfilled with positive pressure of nitrogen three

times. Then the working compartment was charged with isobutyl vinyl ether (2.5 mL, 19.2 mmol, 100 equiv), methyl acrylate (1.7 mL, 19.0 mmol, 100 equiv), 1.0 mL of a stock solution of Ir(ppy)₃ in DCM (4.58 mM, 0.042 mmol, 0.024 mol% relative to IBVE), 0.38 mL of a stock solution of **1b** in DCM (0.5 M, 0.19 mmol, 1 equiv), and 0.4 mL of DCM. The counter compartment was charged with 6.0 mL of DCM. The leads of the DC power supply were connected to the electrodes, and a blue LED kessil lamp was situated 3 cm away from the working compartment. Polymerization was initiated by irradiating the solution for 1 h followed by a 1 h off period. The solution was then irradiated for an additional 3 h followed by a 1.5 h off period. The reaction was reversibly terminated after the second off period. Under inert atmosphere, aliquots for NMR and GPC analysis were taking at timepoints prior to a change in stimuli.

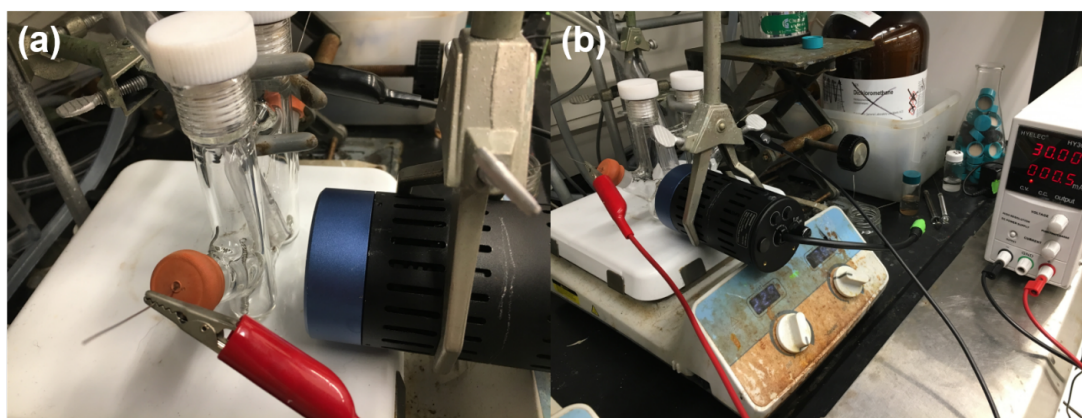


Figure 4.19. Electrochemical cell setup for dual electrochemical and photochemical switching. (a) Side-view of electrochemical cell and Kessil lamp. (b) View of electrochemical cell, DC power source, and Kessil lamp.

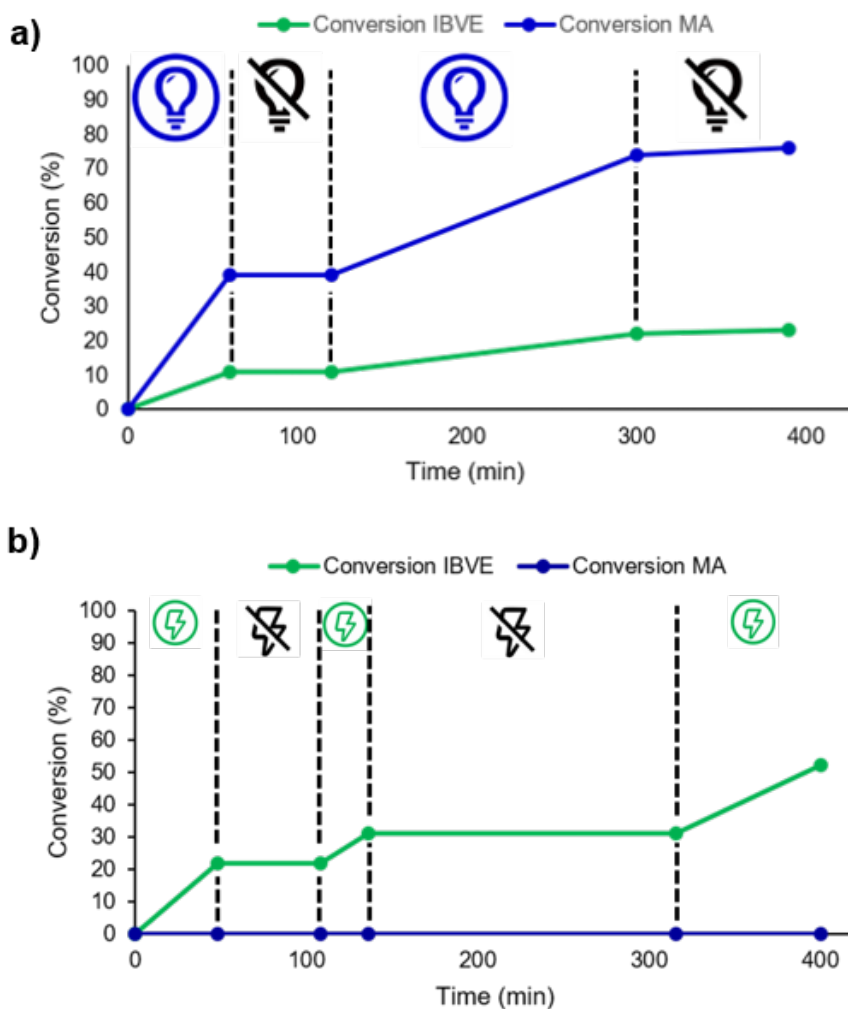


Figure 4.20 Conversion vs. Time plot Illustrating Temporal Control over (a) Photochemical and (b) Electrochemical Polymerizations.

Procedure for Diblock Copolymer Synthesis of Methyl Acrylate and Isobutyl Vinyl Ether (p(IBVE-*b*-MA), Figure 4.5.c.i)

To an oven dried electrochemical cell, a magnetic stir bar was added to both the working and counter compartment. The cell was equipped with a stainless steel wire anode and stainless steel wire cathode and then sealed with the cell caps and rubber septa. The electrochemical cell was then evacuated

and backfilled with positive pressure of nitrogen. Once the electrochemical cell had cooled to room temperature, 0.050 mL of a stock solution of ferrocene in DCM (0.084 M, 0.78 mg, 0.0042 mmol, 0.022 mol% relative to IBVE) was added to the working compartment and Bu_4NClO_4 (205 mg, 0.60 mmol) was added to both the working and counter compartments. The cell was then evacuated and backfilled with positive pressure of nitrogen three times. Then the working compartment was charged with isobutyl vinyl ether (2.5 mL, 19.2 mmol, 100 equiv), methyl acrylate (1.7 mL, 19.0 mmol, 100 equiv), 1.0 mL of a stock solution of $\text{Ir}(\text{ppy})_3$ in DCM (4.58 mM, 0.042 mmol, 0.022 mol% relative to MA), 0.38 mL of a stock solution of **1b** in DCM (0.5 M, 0.19 mmol, 1 equiv), and 0.4 mL of DCM. The counter compartment was charged with 6.0 mL of DCM. The leads of the DC power supply were connected to the electrodes, and a blue LED kessil lamp was situated 3 cm away from the working compartment. Polymerization was initiated by applying an anodic current of 0.5 mA for 5 min followed by a reaction period of 2 h; this polymerization was then reversibly terminated by applying a cathodic current of -0.5 mA for 10 min. The reaction was then irradiated with blue LEDs for 3.5 h with compressed air blowing over the reaction vessel to cool the reaction. Under inert atmosphere, aliquots for NMR and GPC analysis were taken at timepoints prior to a change in stimuli. GPC traces of the polymers before and after chain extension are shown in Figure 4.21. $M_{n,\text{Theo}}$ (kg/mol) = 16.5, $M_{n,\text{Exp}}$ (kg/mol) = 12.5, $D = 1.40$.

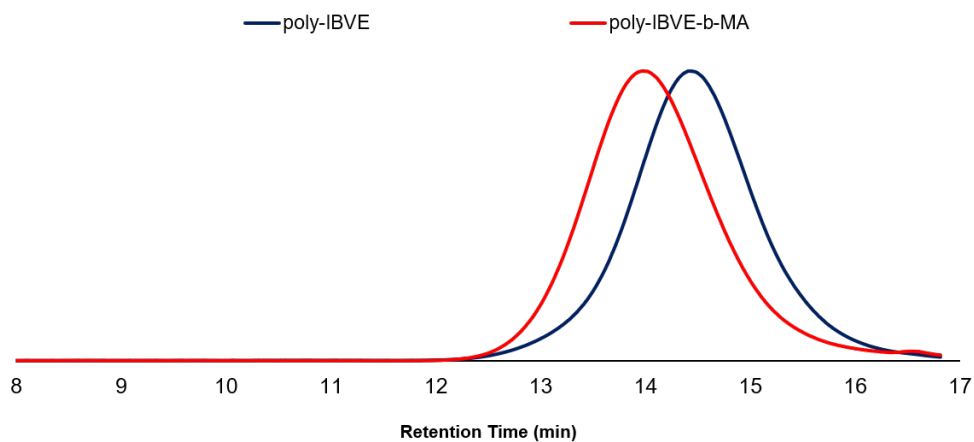


Figure 4.21. GPC traces of poly(*IBVE-b-MA*)

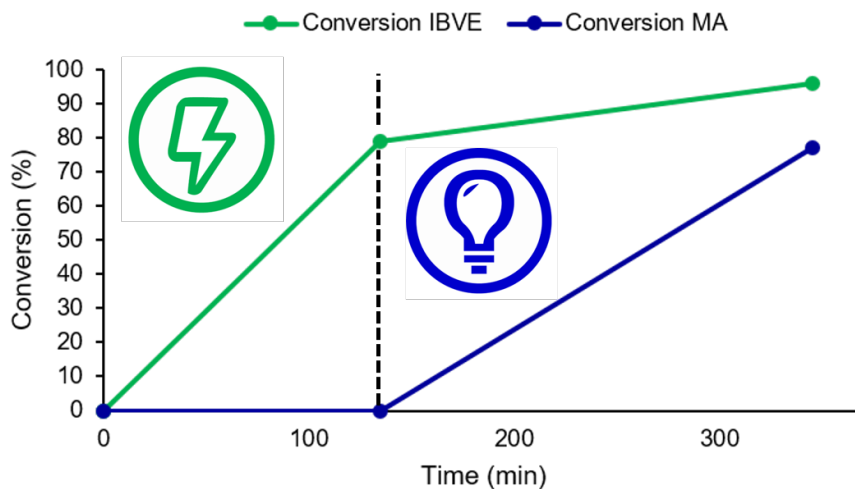


Figure 4.22. Conversion vs. Time of IBVE (green line) and MA (blue line) for dual stimuli switching to generate poly(*IBVE-b-MA*)

Procedure for Diblock Copolymer Synthesis of Methyl Acrylate and Isobutyl Vinyl Ether (p(MA-*b*-IBVE), Figure 4.5.c.ii)

To an oven dried electrochemical cell, a magnetic stir bar was added to both the working and counter compartment. The cell was equipped with a stainless steel wire anode and stainless steel wire cathode and then sealed with the cell caps and rubber septa. The electrochemical cell was then evacuated and backfilled with positive pressure of nitrogen. Once the electrochemical cell had cooled to room temperature, 0.050 mL of a stock solution of ferrocene in DCM (0.084 M, 0.78 mg, 0.0042 mmol, 0.022 mol% relative to IBVE) was added to the working compartment and Bu₄NClO₄ (205 mg, 0.60 mmol) was added to both the working and counter compartments. The cell was then evacuated and backfilled with positive pressure of nitrogen three times. The working compartment was then charged with isobutyl vinyl ether (2.5 mL, 19.2 mmol, 100 equiv), methyl acrylate (1.7 mL, 19.0 mmol, 100 equiv), 1.0 mL of a stock solution of Ir(ppy)₃ in DCM (4.58 mM, 0.042 mmol, 0.022 mol% relative to MA), 0.38 mL of a stock solution of **1b** in DCM (0.5 M, 0.19 mmol, 1 equiv), and 0.4 mL of DCM. The counter compartment was charged with 6.0 mL of DCM. The leads of the DC power supply were connected to the electrodes, and a blue LED kessil lamp was situated 3 cm away from the working compartment. Polymerization was initiated by irradiating the solution for 30 min. The light was then turned off and an anodic current of 0.5 mA was applied for 5 min; the reaction was then stirred for 2 h. The reaction was then reversibly terminated

by applying a cathodic current of -0.5 mA for 10 min. Under inert atmosphere, aliquots for NMR and GPC analysis were taken at timepoints prior to a change in stimuli. GPC traces of the polymers before and after chain extension are shown in Figure 4.23. $M_{n, \text{Theo}}$ (kg/mol) = 11.1, $M_{n, \text{Exp}}$ (kg/mol) = 8.0, $D = 1.35$.

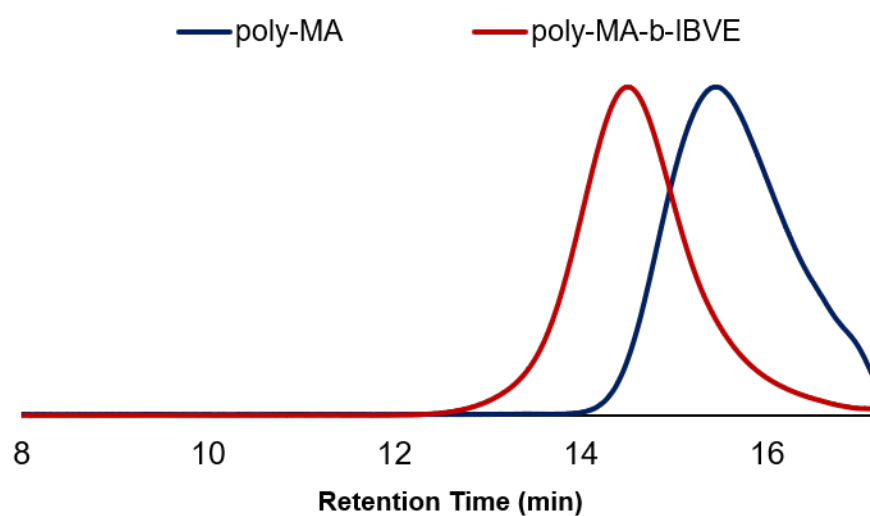


Figure 4.23. GPC traces of poly(MA-*b*-IBVE)

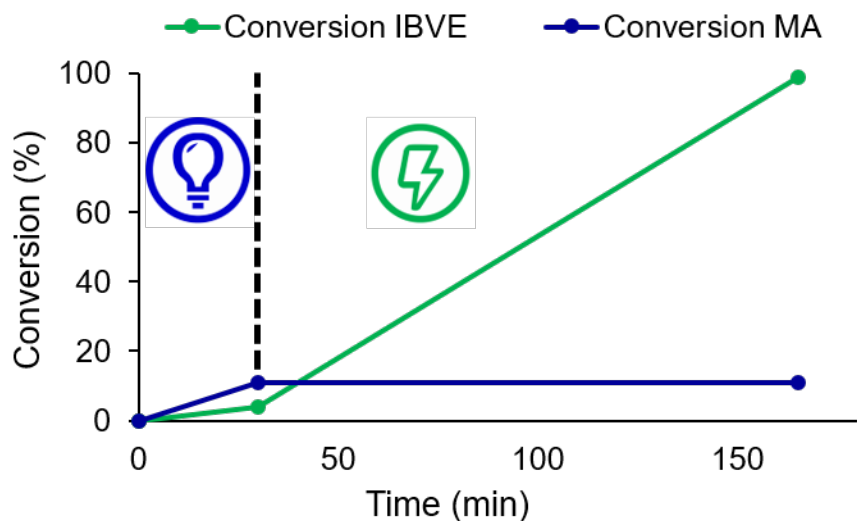


Figure 4.24. Conversion vs. Time of IBVE (green line) and MA (blue line) for dual stimuli switching to generate poly(MA-*b*-IBVE)

Procedure for Triblock Copolymer Synthesis of Methyl Acrylate and Isobutyl Vinyl Ether (p(IBVE-*b*-MA-*b*-IBVE), Figure 4.5c.iii)

To an oven dried electrochemical cell, a magnetic stir bar was added to both the working and counter compartment. The cell was equipped with a stainless steel wire anode and stainless steel wire cathode and then sealed with the cell caps and rubber septa. The electrochemical cell was then evacuated and backfilled with positive pressure of nitrogen. Once the electrochemical cell had cooled to room temperature, 0.050 mL of a stock solution of ferrocene in DCM (0.084 M, 0.78 mg, 0.0042 mmol, 0.022 mol% relative to IBVE) was added to the working compartment and Bu₄NClO₄ (205 mg, 0.60 mmol) was added to both the working and counter compartments. The cell was then evacuated and backfilled with positive pressure of nitrogen three times. The working

compartment was then charged with isobutyl vinyl ether (2.5 mL, 19.2 mmol, 100 equiv), methyl acrylate (1.7 mL, 19.0 mmol, 100 equiv), 1.0 mL of a stock solution of Ir(ppy)₃ in DCM (4.58 mM, 0.042 mmol, 0.022 mol% relative to MA), 0.38 mL of a stock solution of **1b** in DCM (0.5 M, 0.19 mmol, 1 equiv), and 0.4 mL of DCM. The counter compartment was charged with 6.0 mL of DCM. The leads of the DC power supply were connected to the electrodes, and a blue LED kessil lamp was situated 3 cm away from the working compartment. Cationic polymerization was initiated by applying an anodic current of 0.5 mA for 2 min and subsequent stirring for 1 h. In order to reversibly terminate the reaction, a cathodic current of -0.5 mA was applied for 4 min and proceeded by a 1 h off period. At this time, radical polymerization was initiated by irradiating the solution with blue LEDs for 1.5 h and proceeded by a 2.5 h off period. The last block was synthesized by applying an anodic current of 0.5 mA for 6 min and subsequent stirring for 6 h. Then a cathodic current of -0.5 mA was applied for 12 min. Under inert atmosphere, aliquots for NMR and GPC analysis were taken at timepoints prior to a change in stimuli. GPC traces of the polymers before and after chain extension are shown in Figure 4.25. $M_{n, \text{Theo}}$ (kg/mol) = 15.7, $M_{n, \text{Exp}}$ (kg/mol) = 12.4, $D = 1.40$.

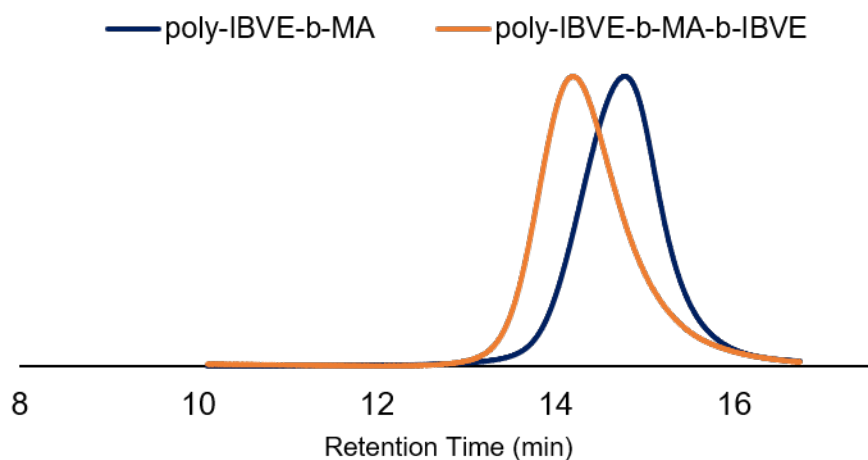


Figure 4.25. GPC Traces of poly(IBVE-*b*-MA-*b*-IBVE)

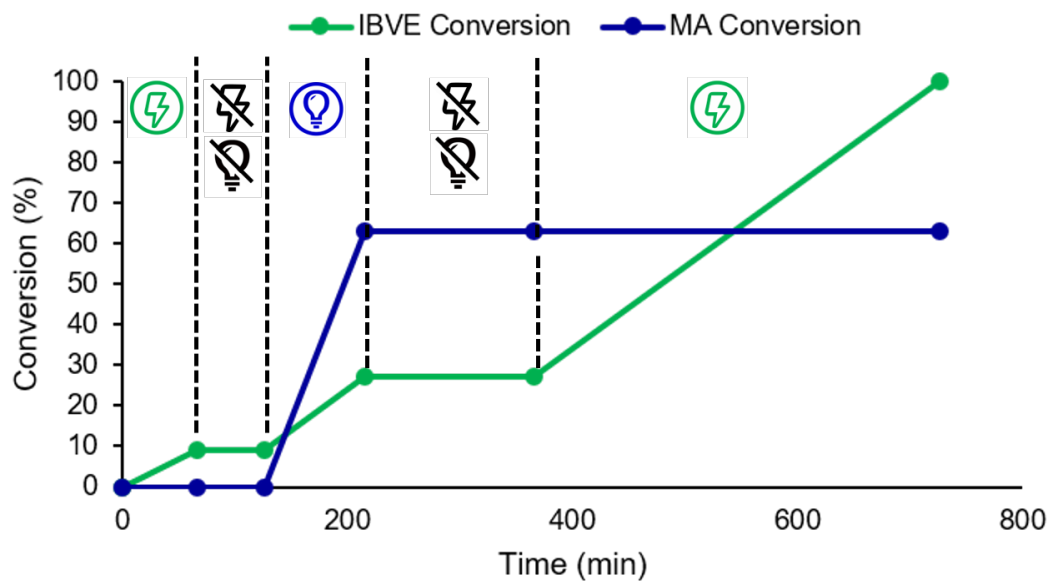


Figure 4.26. Conversion vs. Time of IBVE (green line) and MA (blue line) for dual stimuli switching to generate poly(IBVE-*b*-MA-*b*-IBVE)

Procedure for Tetrablock Copolymer Synthesis of Methyl Acrylate and Isobutyl Vinyl Ether (p(IBVE-*b*-MA-*b*-IBVE-*b*-MA), Figure 4.5.c.iv)

To an oven dried electrochemical cell, a magnetic stir bar was added to both the working and counter compartment. The cell was equipped with a stainless steel wire anode and stainless steel wire cathode and then sealed with the cell caps and rubber septa. The electrochemical cell was then evacuated and backfilled with positive pressure of nitrogen. Once the electrochemical cell had cooled to room temperature, 0.050 mL of a stock solution of ferrocene in DCM (0.084 M, 0.78 mg, 0.0042 mmol, 0.022 mol% relative to IBVE) was added to the working compartment and Bu_4NClO_4 (205 mg, 0.60 mmol) was added to both the working and counter compartments. The cell was then evacuated and backfilled with positive pressure of nitrogen three times. The working compartment was then charged with isobutyl vinyl ether (2.5 mL, 19.2 mmol, 100 equiv), methyl acrylate (1.7 mL, 19.0 mmol, 100 equiv), 1.0 mL of a stock solution of $\text{Ir}(\text{ppy})_3$ in DCM (4.58 mM, 0.042 mmol, 0.022 mol% relative to MA), 0.38 mL of a stock solution of **1b** in DCM (0.5 M, 0.19 mmol, 1 equiv), and 0.4 mL of DCM. The counter compartment was charged with 6.0 mL of DCM. The leads of the DC power supply were connected to the electrodes, and a blue LED kessil lamp was situated 3 cm away from the working compartment. Cationic polymerization was initiated by applying 0.5 mA of anodic current for 2 min and subsequent stirring for 42 min. The reaction was then reversibly terminated by

applying a cathodic current of -0.5 mA for 4 min and letting it stir for 180 min. The radical polymerization was then initiated by irradiation with blue LEDs for 1 h. Next, an anodic current of 0.5 mA was applied for 7 min and the reaction was stirred for an additional 2 min. The cationic polymerization was reversibly terminated by applying a cathodic current of -0.5 mA for 14 min. The radical polymerization was then reinitiated by irradiating the solution with blue LEDs for 12 h. Under inert atmosphere, aliquots for NMR and GPC analysis were taken at timepoints prior to a change in stimuli. GPC traces of the polymers before and after chain extension are shown in Figure 4.27. $M_{n, \text{Theo}}$ (kg/mol) = 14.7, $M_{n, \text{Exp}}$ (kg/mol) = 13.4, $D = 1.33$.

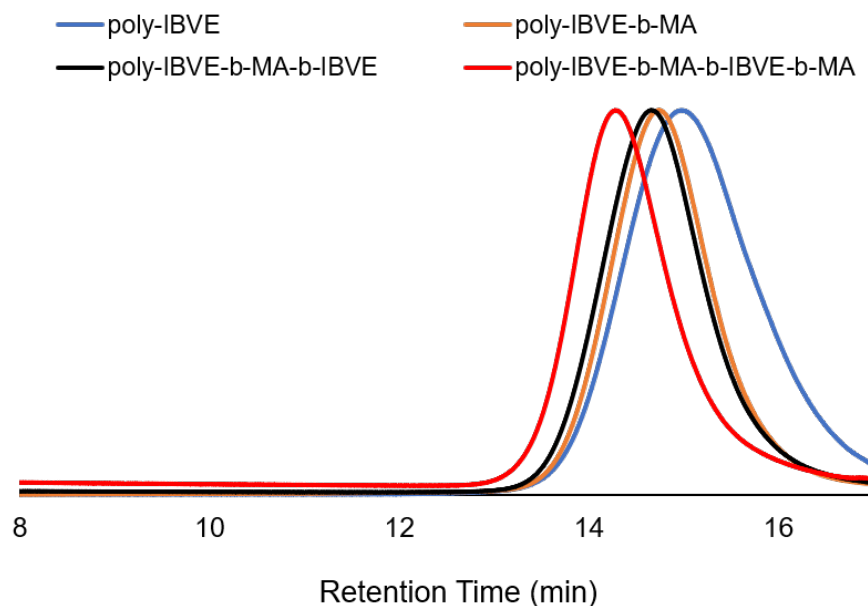


Figure 4.27. GPC Traces of poly(IBVE-*b*-MA-*b*-IBVE-*b*-MA)

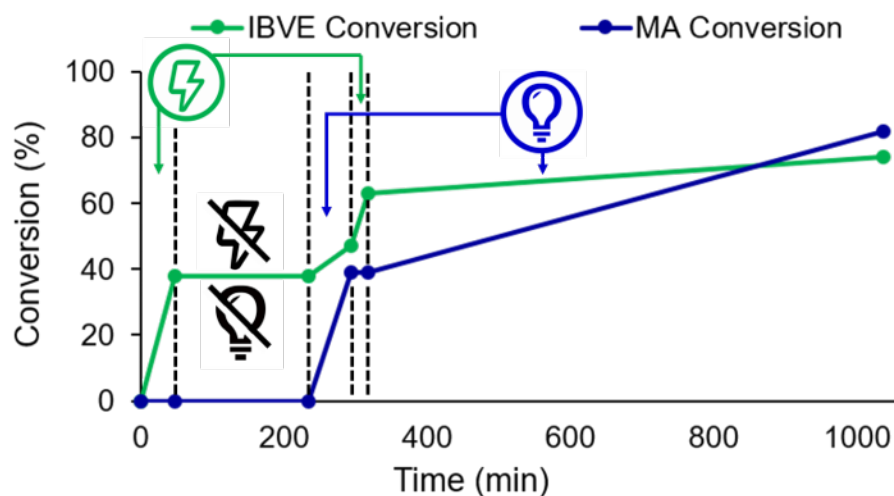


Figure 4.28. Conversion vs. Time of IBVE (green line) and MA (blue line) for dual stimuli switching to generate poly(IBVE-*b*-MA-*b*-IBVE-*b*-MA)

Procedure for Pentablock Copolymer Synthesis of Methyl Acrylate and Isobutyl Viny Ether (p(IBVE-*b*-MA-*b*-IBVE-*b*-MA-*b*-IBVE), Figure 4.5.c.v)

To an oven dried electrochemical cell, a magnetic stir bar was added to both the working and counter compartment. The cell was equipped with a reticulated vitreous carbon anode and reticulated vitreous carbon cathode and then sealed with the cell caps and rubber septa. The electrochemical cell was then evacuated and backfilled with positive pressure of nitrogen. Once the electrochemical cell had cooled to room temperature, 0.050 mL of a stock solution of ferrocene in DCM (0.084 M, 0.78 mg, 0.0042 mmol, 0.022 mol% relative to IBVE) was added to the working compartment and Bu₄NClO₄ (205 mg, 0.60 mmol) was added to both the working and counter compartments. The

cell was then evacuated and backfilled with positive pressure of nitrogen three times. The working compartment was then charged with isobutyl vinyl ether (2.5 mL, 19.2 mmol, 100 equiv), methyl acrylate (1.7 mL, 19.0 mmol, 100 equiv), 1.0 mL of a stock solution of Ir(ppy)₃ in DCM (4.58 mM, 0.042 mmol, 0.022 mol% relative to MA), 0.19 mL of a stock solution of **1b** in DCM (1.0 M, 0.19 mmol, 1 equiv), and 0.6 mL of DCM. The counter compartment was charged with 6.0 mL of DCM. The leads of the DC power supply were connected to the electrodes, and a blue LED kessil lamp was situated 3 cm away from the working compartment. Cationic polymerization was initiated by applying 0.6 mA of anodic current for 5 min and subsequent stirring for 10 min. The reaction was then reversibly terminated by applying a cathodic current of -0.6 mA for 10 min. The radical polymerization was then initiated by irradiation with blue LEDs for 32 min. Next, an anodic current of 0.6 mA was applied for 5 min and the reaction was stirred for an additional 45 min. The cationic polymerization was reversibly terminated by applying a cathodic current of -0.6 mA for 10 min. The radical polymerization was then reinitiated by irradiating the solution with blue LEDs for 66 min. Next, an anodic current of 0.6 mA was applied for 10 min and the reaction was stirred for an additional 2h 45 min. The cationic polymerization was reversibly terminated by applying a cathodic current of -0.6 mA for 20 min. Under inert atmosphere, aliquots for NMR and GPC analysis were taken at timepoints prior to a change in stimuli. GPC traces of the polymers before and

after chain extension are shown in Figure 4.29. $M_{n, \text{Theo}}$ (kg/mol) = 9.5, $M_{n, \text{Exp}}$ (kg/mol) = 11.0, $D = 1.24$.

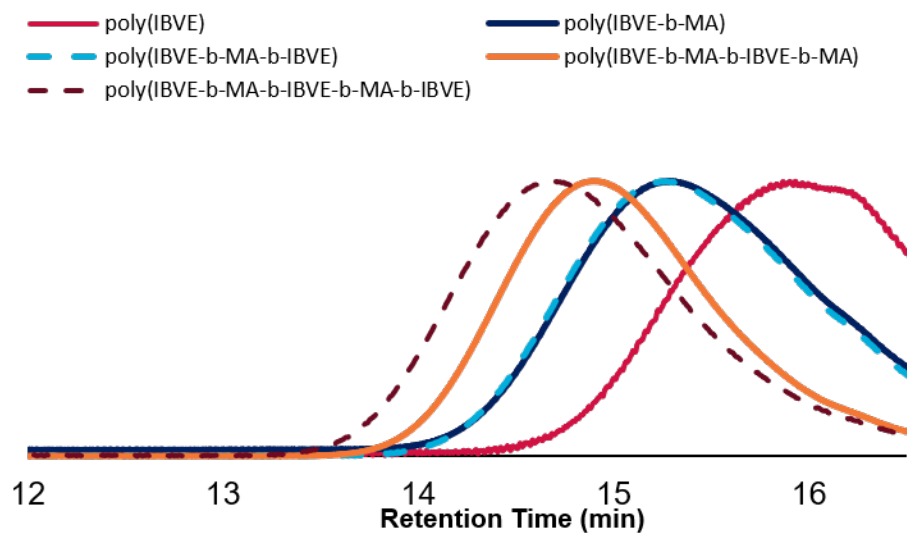


Figure 4.29. GPC traces of poly(IBVE-*b*-MA-*b*-IBVE-*b*-MA-*b*-IBVE)

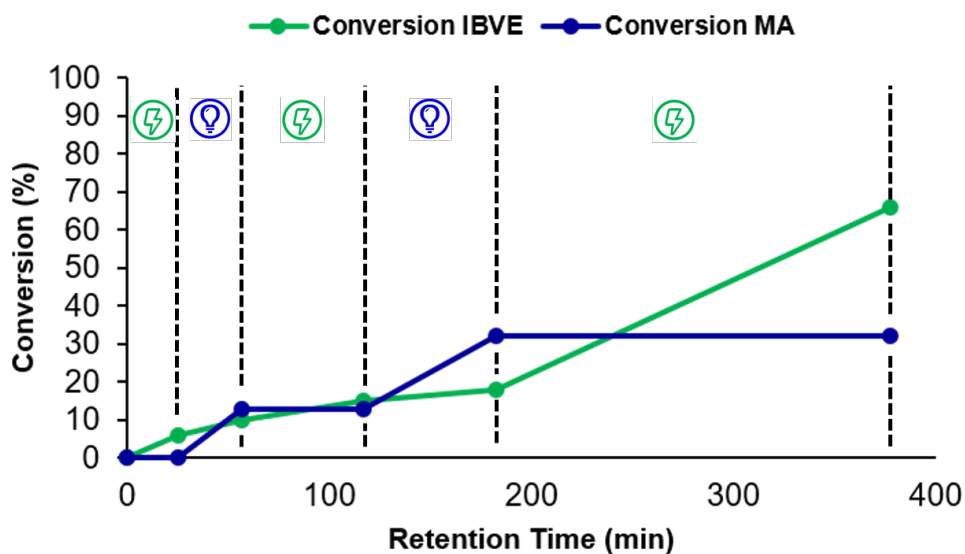


Figure 4.30. Conversion vs. Time of IBVE (green line) and MA (blue line) for dual stimuli switching to generate poly(IBVE-*b*-MA-*b*-IBVE-*b*-MA-*b*-IBVE)

Procedure for Hexablock Copolymer Synthesis of Methyl Acrylate and Isobutyl Vinyl Ether (p(MA-*b*-IBVE-*b*-MA-*b*-IBVE-*b*-MA-*b*-IBVE), Figure 5.c.vi)

To an oven dried electrochemical cell, a magnetic stir bar was added to both the working and counter compartment. The cell was equipped with a stainless steel wire anode and stainless steel wire cathode and then sealed with the cell caps and rubber septa. The electrochemical cell was then evacuated and backfilled with positive pressure of nitrogen. Once the electrochemical cell had cooled to room temperature, 0.050 mL of a stock solution of ferrocene in DCM (0.084 M, 0.78 mg, 0.0042 mmol, 0.022 mol% relative to IBVE) was added to the working compartment and Bu_4NClO_4 (205 mg, 0.60 mmol) was added to both the working and counter compartments. The cell was then evacuated and backfilled with positive pressure of nitrogen three times. The working compartment was then charged with isobutyl vinyl ether (2.5 mL, 19.2 mmol, 100 equiv), methyl acrylate (1.7 mL, 19.0 mmol, 100 equiv), 1.0 mL of a stock solution of $\text{Ir}(\text{ppy})_3$ in DCM (4.58 mM, 0.042 mmol, 0.022 mol% relative to MA), 0.19 mL of a stock solution of **1b** in DCM (1.0 M, 0.19 mmol, 1 equiv), and 1.6 mL of DCM. The counter compartment was charged with 8.0 mL of DCM. The leads of the DC power supply were connected to the electrodes, and a blue LED kessil lamp was situated 3 cm away from the working compartment. The radical polymerization was initiated by irradiation with blue LEDs for 1 h. Next, an anodic current of 0.4 mA was applied for 6 min and the reaction was stirred for

an additional 15 min. The cationic polymerization was reversibly terminated by applying a cathodic current of -0.4 mA for 12 min. The radical polymerization was then reinitiated by irradiating the solution with blue LEDs for 50 min. Next, an anodic current of 0.4 mA was applied for 6 min and the reaction was stirred for an additional 15 min. The cationic polymerization was reversibly terminated by applying a cathodic current of -0.4 mA for 12 min. The radical polymerization was then reinitiated by irradiating the solution with blue LEDs for 30 min. Next, an anodic current of 0.4 mA was applied for 6 min and the reaction was stirred for an additional 30 min. The cationic polymerization was then reversibly terminated by applying a cathodic current of -0.4 mA for 12 min. Under inert atmosphere, aliquots for NMR and GPC analysis were taken at timepoints prior to a change in stimuli. GPC traces of the polymers before and after chain extension are shown in Figure 4.31. $M_{n, \text{Theo}}$ (kg/mol) = 11.7, $M_{n, \text{Exp}}$ (kg/mol) = 9.7, $D = 1.41$.

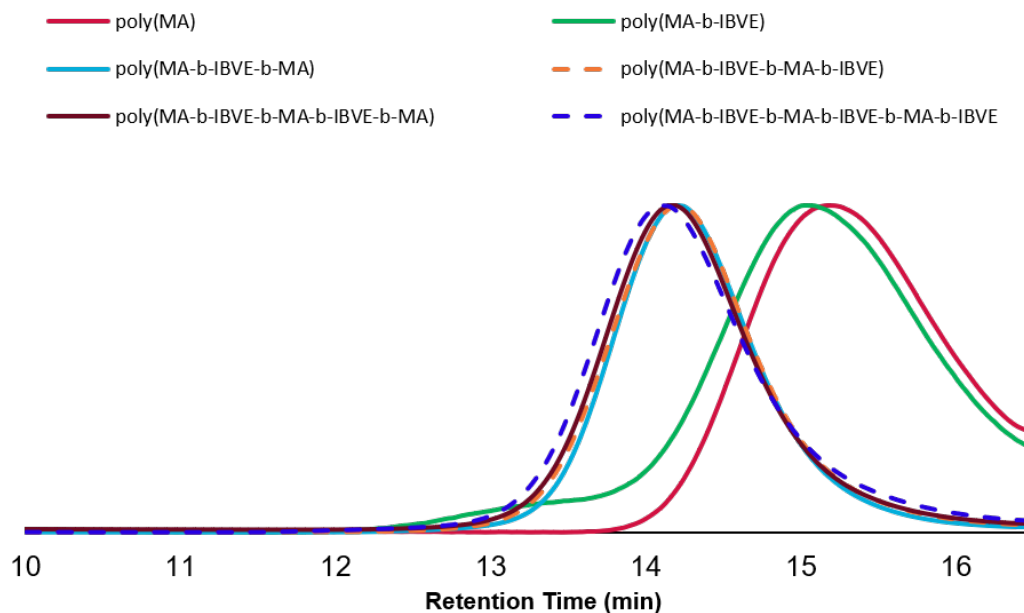


Figure 4.31. GPC Traces of poly(MA-*b*-IBVE-*b*-MA-*b*-IBVE-*b*-MA-*b*-IBVE)

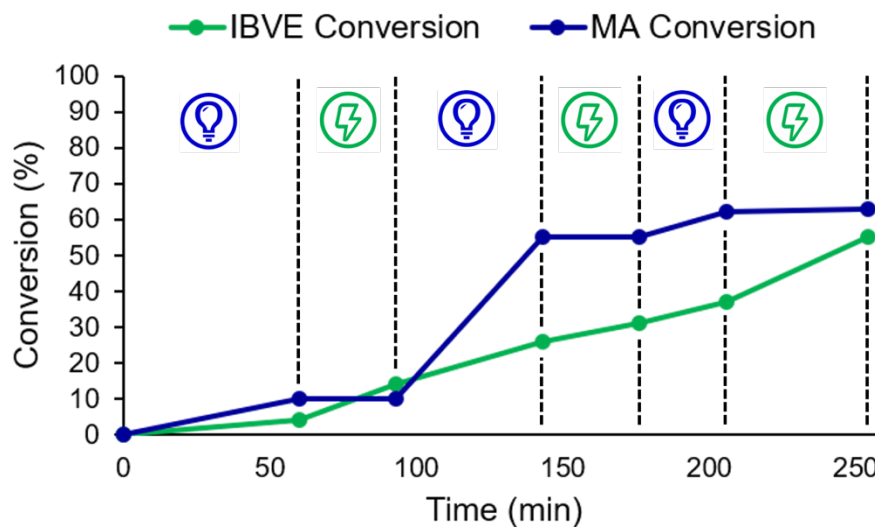


Figure 4.32. Conversion vs. Time of IBVE (green line) and MA (blue line) for dual stimuli switching to generate poly(MA-*b*-IBVE-*b*-MA-*b*-IBVE-*b*-MA-*b*-IBVE)

References.

- (1) Kottisch, V., Michaudel, Q., and Fors, B. P. *J. Am. Chem. Soc.* **2015**, *138*, 15535.
- (2) An induction period is observed which corresponds to the amount of time it takes to generate sufficient ferrocenium to initiate polymerization.

CHAPTER 5

INTRODUCTION TO THE DESIGN AND PERFORMANCE OF AMORPHOUS ORGANIC ELECTRODES

5.1 Introduction

The ways which we obtain access to energy and the venues in which we use energy is constantly evolving. With an increasing global population and an ever climbing standard of living, energy demand is expected to double by 2050.¹ Rising temperatures and elevating air pollution are cause for concern over potential climate change, environmental stability, and public health concerns. Currently, renewable energies account for 19% of electricity generation.¹ By 2050, energy sourced from renewable sources is expected to double. However, incorporation of renewable energy into the grid is challenging, due to the intermittent nature of wind and solar sources. Electrochemical energy storage (EES) systems could alleviate the strain of variable energy sources by providing storage when energy production is high and an energy source when demand exceeds production.

EES systems can also play role in the mobile use of energy. Currently, transportation sector accounts for 28% of greenhouse gas emissions.¹ Electric vehicles can approach carbon neutrality, so long as the electricity is sourced from renewable venues (wind, solar). Vehicles powered solely by EES systems, demand high energy densities (greater range), as well as high power densities

(faster acceleration and charging). Lithium ion (Li-ion) batteries continue to be the most practical and economic EES system to address these global challenges.

Li-ion batteries can be improved by increasing the energy density and power density and remains a grand challenge in the field. Electrolyte, separators, and electrode material all have an impact on battery performance. However, a focus will be given to electrode material, specifically the cathode (positive electrode) as electrode materials represent a significant portion of the cost and size of a Li-ion battery. Electrodes also determines the amount of energy stored in a battery and the rate at which a battery can be charged and discharged, while being held to limitations from the electrolyte (i.e. electrochemical stability window, viscosity, and ionic conduction).

5.2 Discussion

Battery Materials (Traditional History, characteristics, and consequences)

Since their collaborative invention by Stanley Whittingham, John B. Goodenough, and Akira Yoshina, many of the original foundations have remained the same. Traditional cathode materials, like LiCoO_2 , are crystalline inorganic materials. During the discharge process, the CoO_2 is reduced while Li-ions intercalate into the layers of the metal oxide. During the charge process, the reverse reaction occurs, LiCoO_2 oxidation is accompanied with Li-ion deintercalation and subsequent intercalation into the anode. The intercalation

process is kinetically limiting in charging and discharging owing to slow ion diffusion. This limits the rate at which Li-ion batteries can charge and discharge to the order of hours. Many new materials have been discovered over the last decade, most retaining the intercalation process.

Over the last two decades, interest in alternative cathode materials based on organic small molecules and polymers have shown promise in designing Li-ion batteries which can charge and discharge on significantly faster time scales. Owing to weaker intermolecular interactions (van der Waals forces), organic materials can support facile ion diffusion which allows energy to be distributed more quickly with less polarization. Additionally, amorphous organic materials can lead to even faster ion diffusion by providing multiple dimensions for ion transport. Amorphous organic materials can be advantageous electrode materials for applications which demand fast charging and discharging.

Key Parameters in the Design of Fast Charging Cathodes

To enable fast charging batteries, the key metric to improve is power density. Power density (P_d) can be defined as:

$$P_d = E_d \times \frac{1}{t} \quad (1)$$

where E_d is energy density, t is time of discharge. Therefore high power density materials must be able to transfer a large amount of energy on a short timescale. A significant number of factors and variables determine the rate which a battery can be charged and discharged, this review focuses on strategies which can maximize the electrode power density. Since the power

density of a battery is determined by the product of energy density and the inverse of time of discharge, we will discuss factors which influence the energy density and then focus on how energy density is affected by the time of discharge.

The energy density of a cathode is a product of the amount of charge stored and the potential at which the charge is stored. It can be defined as

$$E_d = C_{sp} \times V \quad (2),$$

where C_{sp} is the specific capacity and V is the voltage difference between the anode and the cathode. The operating voltage of a battery is determined by the potential difference between the anode and the cathode. Significant efforts have been made to tailor cathode structures to increase the standard operating potentials. Organic materials are uniquely suited to tune electronic character through electron withdrawing or electron donating groups to stabilize or destabilize oxidation states.^{2,3} This provides a convenient handle to tune the working potential of electrode materials, although often at the capacitive cost of additional mass. Taking advantage of resonance delocalization, the effect of electron withdrawing groups can be emphasized without increasing the mass of the electrode.⁴⁻⁶ The synthetic toolbox available to tune organic structures enables a variety of approaches to precisely increase the working potential of the resulting electrode.

The operating potential of Li-ion batteries are limited by the electrochemical stability window of electrolytes, approximately 4.5 V vs. Li^+/Li .

Therefore, any further improvements to energy density are dependent on increasing the amount of charge stored, otherwise referred to as the specific capacity (C_{sp}). Specific capacity can be defined as

$$C_{sp} = \frac{nF}{MW} \quad (3),$$

where n is the number of electrons stored per mole, F is faradays constant, and MW is the molecular weight of the material. The goal is simple: increase the number of electrons that can be stored while minimizing the molar mass. The energy density of a material can be made large by designing materials which have large specific capacities and high operating potentials. The factor which distinguishes power density from energy density is the inverse relationship with time. This rate dependence which determines the power density will be the focus of the remainder of this review.

Discharging over a shorter amount of time corresponds to an increase in current density and leads to greater polarization in the cell. Polarization is a form of overpotential, owing to kinetic limitations which prevent the electrochemical reaction from occurring at its thermodynamic potential. The kinetics of an electrochemical reaction are dependent on the activation energy barrier to electron transfer. Polarization leads to (1) decreased cell voltage with increasing rate of discharge, and (2) loss of capacity from material isolation or electrochemical irreversibility. Irreversibility occurs from the chemical and physical changes associated with the charge/discharge process and can be increasingly problematic if a phase change occurs with the redox reaction.[4]

Therefore, when designing cathode materials for high power density applications, it is important to minimize polarization.

Polarization in batteries can be attributed to three causes: (1) ohmic polarization from resistance within and between the cell components, (2) activation polarization related to the charge transfer processes required for the electrochemical reaction, or (3) concentration polarization arising from limitations in mass transport. Ohmic polarization arises from electrolyte resistance and resistance stemming from electrical contacts of the cell. These contributions are typically small relative to the total polarization in the cell. The other two sources of polarizations arise from resistance in the transport of electrons and ions through the electrode and are often the limiting factors in rate performance. Thus, it is essential to understand the source of this polarization and design materials which can support electron and ion transport.

Classical theory of electron transfer describes the approach of reacting species close enough to an electrode surface (tenths of a nanometer) that electrons can tunnel between the electrode and the active species. This is described by the heterogeneous electron transfer rate constant k^0 , which is a measure of the kinetic facility of a redox reaction. Facile electron transfer reactions with no accompanied molecular rearrangement are associated with large k^0 values, while small k^0 are indicative of sluggish electron transfer reactions involving significant molecular rearrangement or a multistep mechanism.^{7,8} Materials with a large heterogeneous electron transfer rate

constant undergo minimal phase transitions during electron transfer and should support fast charging and discharging.

Charge transport in solid state organic electrode materials can be accomplished by electron exchange reaction between neighboring redox sites (electron hopping) or by the movement of electrons through a delocalized, conjugated system.⁹⁻¹⁴ Even in a fully conjugated system, it is expected that significant charge transport still occurs by an electron hopping mechanism. An electron hopping mechanism is only operative upon generation of charge carriers. This is accompanied by an increase in conductivity, by several orders of magnitude, when organic materials are doped from the initially insulating neutral state.¹⁵⁻¹⁷

Since electron exchange within the active material is often sluggish, electron transport is supported by the addition of carbon-based materials (carbon black, carbon nanotubes) to the electrode composite. Resistance in the conductive carbon additives is small and provides additional pathways for fast electron transport to redox active sites. This again stresses the importance of high values of k^0 for facile charge transport in the electrode.

Despite attempts to improve intrinsic conductivity, many organic electrode materials are still insulating in nature, and require large amounts of conductive additives to support charge transport in a battery. Supplementing a charge storage material with excess carbon decreases the energy density of the electrode, since conductive additives contribute to mass in the cell without

contributing significantly to stored charge. If carbon must be added to improve conductivity, high aspect ratio materials, such as carbon nanotubes and graphene oxide, are the most effective, as they can lower the percolation threshold resulting in an electrode which exhibits conductivity more similar to the carbon additive than the insulating storage material.^{18,19} Ultimately, it is most beneficial to design conductive storage materials which do not necessitate carbon additives.

Many approaches have been taken to improve the electron transfer properties of an electrode material. Redox functionalized conductive polymers can deliver high energy densities due to the faradaic events at fast rates owing to the high conductivity of doped conducting polymers.²⁰⁻²⁷ Alternatively, redox active groups can be covalently linked to graphene or carbon supports by in situ polymerization or click chemistry.^{28,29} However, each of these methods relies on additional mass to support electron transfer without increasing the number of faradaic reactions, decreasing the capacity of the electrode.

An electron transfer to or from a species in solution generates a charged species which is charge balanced by a corresponding ion from solution. During linear sweep potentiometric experiments of dissolved species, the electrolyte concentration is usually orders of magnitude greater than the species of interest, so that the diffusion kinetics of the species of interest can be studied. However, in solid state electrode materials the redox active species are largely immobilized and diffusion limitations are largely a measure of counterion

transport. Charge transport is complicated by the dependence of electron transport on the transport of ions to the redox active species.

Although most battery materials suffer from poor conductivity, nearly all cathode materials are limited by diffusion of ions through electrode materials. Therefore, concentration polarization is one of the largest inhibitors of rate performance. The movement of counterions is necessary in order to maintain charge neutrality and prevent the generation of an electric field across the electrode. The strong interactions in crystal structures of inorganic electrode materials make it difficult for solvated ions to quickly move through for charge compensation. However, due to the weaker van der Waals interactions in organic materials, many organic electrode materials can achieve significantly higher ionic diffusivity than their inorganic counterparts. While the low density of organic materials may negatively impact their volumetric energy densities, it can also be significantly advantageous for ionic mobility in the solid state. The more flexible structure of organic polymers and larger interlayer spacing allow for faster ion diffusion and reduced volumetric and structural changes upon charge/discharge, ultimately enabling higher rate capabilities and higher power densities.^{30,31} Still, diffusion is often rate limiting factor at high rates and hinders the performance. Thus, it is necessary to address ion diffusion limitations for high rate performance.^{10,32-35}

Diffusion in electrode materials is an inherently complex process which is effected by a number of factors: the nature of the electrolyte phase, the solid-

liquid interface, the tortuosity of diffusion paths, solvent swelling of the active material, and the size and shape distribution of the particles. However, under the assumption that solid state diffusion through the particle is the rate limiting process, we need only consider the following relationship:

$$t = \phi^2/D \quad (5),$$

where t is the time of charge or discharge, ϕ is the diffusion length, and D is the diffusion coefficient. Thus, at a given discharge rate, the diffusion pathlength must exceed the particles radius otherwise only a fraction of the materials capacity will be accessed. This can be ensured by decreasing the particle size or by increasing the diffusion coefficient of ions within the material.

Decreasing particle size has been thoroughly investigated in both inorganic and organic electrode materials as a method to alleviate diffusional limitations.³⁶ Smaller particles ensure ions access to the entirety of the material on shorter timescales. In addition, decreasing the size of the crystallites has been shown to relieve stress associated with ion insertion, improving lifetime while supporting faster ion diffusion and decreasing polarization.³⁷ These nanoscaled materials are classified by the number of nano-sized dimensions. Thin films (2D materials), nanorods and nanowires (1D), and nanoparticles (0D) have all been investigated as high rate electrode materials. Nanostructure porous and high surface area 3D materials, often in the form of porous polymers or covalent organic frameworks (COFs).^{21,38-43} Additionally, redox active organic materials on nanostructured carbons such as carbon nanotubes or

graphene sheets also offer improved electronic conductivity and shortened diffusion pathlengths.^{28,44} The increased surface area of the composite increases the contact area of the cathode with the electrolyte, and allows for fast ion transport.⁴⁵ Reducing ion pathlength in organic materials by all of these methods has been very successful at improving rate performance.

Along with decreasing pathlength, improving the diffusion coefficient of ions can also result in materials with excellent high rate performance. It is the authors opinion that this approach is not well understood and taken less often than nanoengineering materials. A wide variety of approaches have been employed with varying degrees of success at improving rate performance. Creating expanded structures with large ion diffusion pathways allow for facile ion transport and avoid phase transformations upon accommodation of ions.^{30,46} Increasing the flexibility of structure has been proposed to improve ion mobility, rate capabilities, and cycle lifetimes by reducing the strain from ion insertion without necessitating major structural rearrangement.⁴⁷⁻⁴⁹ Additionally, increasing the number of pathways accessible for ion transport through a material has been shown to be effective at achieving high rate capabilities.^{50,51}

In addition to affecting electronic conductivity, π - π interactions have been shown to affect ionic conductivity as well. Aromatic π stacking between molecules often leads to layered structures with discrete pathways for ionic transport. This has been suggested to facilitate fast ionic diffusion and yield high diffusion coefficients in some systems.⁵²⁻⁵⁴ However, others have shown

diffusion is slow in systems with strong π - π stacking interactions.^{34,55} In these instances, it is suggested that strong π - π stacking restricts ion movement and ions are forced to travel through different pathways generated in the material around the regions of π - π stacking.⁵² The relationship between ion transport and π - π interactions seems to vary among systems.

Amorphous materials provide unique advantages for improving ionic transport in the solid state. While crystalline materials have long been the phase of choice for energy storage, they suffer several shortcomings. In a crystalline system, the storage capacity is affected by crystallite orientation, exposure of redox active sites, and phase transitions associated with ion intercalation.^{56,57} These elements become increasingly problematic at high rates of charge/discharge as they raise the activation energy barrier and impose kinetic limitations. By imbedding defects in a structure through amorphization, new, isotropic pathways and sites for ion transport and storage are made available.⁵⁸⁻⁶⁰ The reduced ordering in the structure of amorphous materials reduces the entropic penalty of intercalating of ions, reducing the activation energy barrier to ion transport.⁶¹⁻⁶³ In most cases, improved flexibility and diffuse structures of amorphous materials can tolerate the stress imposed during the ion transport than crystalline materials. Amorphous materials can also reduce or eliminate structural rearrangement and phase changes associated with redox reactions.^{64,65} It is this author's opinion that the benefits of amorphous materials,

in terms of improved ionic diffusivity, has shown to be well worth more focused attention as materials for energy storage applications.

Organic materials also offer an opportunity to utilize alternative charge compensating ions. There have been a number of examples of organic electrode materials which display impressive rate performances using ions alternative to Li^+ , despite the increase in the ionic radius. This is in part due to the smaller solvation shell of larger ions which decreases the activation energy barrier to ion transport and enthalpic cost of disrupting solvation shells.^{66,67} Pairing organic structures with soft ions, such as tetrabutyl ammonium and larger anions, has also led to higher diffusion coefficient relative to pairing with hard, compact ions, like lithium ions.⁶⁸⁻⁷⁰ Abruña and coworkers have shown that k^0 decreases with increasing strength of ionic interaction between the redox active unit and charge compensating ion.⁷¹ In a separate system it was shown that the diffusion coefficient of Mg^{2+} is five-fold slower than tetrabutylammonium (TBA^+) due to the stronger electrostatic interactions between the small densely charged Mg^{2+} and the reduced redox sites.⁷²

In the following chapters, contributions in the synthesis and understanding of materials based around heterocyclic aromatic storage sites (phenothiazine, phenazine, triarylamine) for energy storage applications are presented.

5.3 References

- (1) *Annual Energy Outlook 2020*; U. S. Energy Information Administration; U.S. Government Printing Office: Washington DC, 2020
- (2) Liang, Y.; Zhang, P.; Yang, S.; Tao, Z.; Chen, J. *Adv. Energy Mater.* **2013**, *3*, 600.
- (3) Lu, Y.; Zhang, Q.; Li, L.; Niu, Z.; Chen, J. *Chem* **2018**, *4*, 2786.
- (4) Wu, D.; Xie, Z.; Zhou, Z.; Shen, P.; Chen, Z. *J. Mater. Chem. A*, **2015**, *3*, 19137.
- (5) Gottis, S.; Barrès, A. L.; Dolhem, F.; Poizot, P. *ACS Appl. Mater. Interfaces*, **2014**, *6*, 10870.
- (6) Patil, N.; Aqil, A.; Ouhib, F.; Admassie, S.; Inganäs, O.; Jérôme, C.; Detrembleur, C. *Adv. Mater.* **2017**, *29*, 1703373.
- (7) Kojima, H.; Bard, A. J. *J. Am. Chem. Soc.* **1975**, *97*, 6317.
- (8) Bard, A. J.; Faulkner, L. R. *Kinetics of Electrode Reactions. Electrochemical Methods Fundamentals and Applications*, Edition Two; John Wiley & Sons, Inc.: New York, NY. 2001; 87.
- (9) Dalton, E. F.; SurrIDGE, N. A.; Jernigan, J.C.; Wilbourn, K. O.; Facci, J. S.; Murray, R.W. *Chem. Phys.* **1990**, *141*, 143.
- (10) Kaufman, F. B.; Schroeder, A. H.; Engler, E. M.; Kramer, S. R.; Chambers, J. Q. *J. Am. Chem. Soc.* **1980**, *102*, 483.
- (11) Abruña, H. D. *Coord. Chem. Rev.* **1988**, *86*, 135.
- (12) Dahms, H. *J. Phys. Chem.* **1968**, *72*, 362.

- (13) Ruff, I.; Friedrich, V. J. *J. Phys. Chem.* **1971**, *75*, 3297.
- (14) Ruff, I.; Friedrich, V. J.; Demeter, K.; Csillag, K. *J. Phys. Chem.* **1971**, *75*, 3303.
- (15) Morishima, Y.; Akihara, I.; Nozakura, S.I. *J. Polym. Sci., Polym. Lett. Ed.* **1985**, *23*, 651.
- (16) Chiang, C. K.; Fincher Jr, C. R.; Park, Y. W.; Heeger, A. J.; Shirakawa, H.; Louis, E. J.; Gau, S. C.; MacDiarmid, A. G. *Phys. Rev. Lett.* **1977**, *39*, 1098.
- (17) Pickup, P. G.; Murray, R. W. *J. Am. Chem. Soc.* **1983**, *105*, 4510.
- (18) Kim, H.; Abdala, A. A.; Macosko, C. W. *Macromolecules*, **2010**, *43*, 6515.
- (19) Bauhofer, W.; Kovacs, J. Z. *Compos. Sci. Technol.* **2009**, *69*, 1486.
- (20) Bidan, G.; Deronzier, A.; Moutet, J. C. *J. Chem. Soc. ChemComm.* **1984**, *17*, 1185.
- (21) Lin, C. H.; Chou, W. J.; Lee, J. T. *Macromol. Rapid Commun.* **2012**, *33*, 107.
- (22) Liang, Y.; Chen, Z.; Jing, Y.; Rong, Y.; Facchetti, A.; Yao, Y. *J. Am. Chem. Soc.* **2015**, *137*, 4956.
- (23) Casado, N.; Hernández, G.; Veloso, A.; Devaraj, S.; Mecerreyes, D.; Armand, M. *ACS Macro Lett.* **2016**, *5*, 59.
- (24) Shen, L.; Mizutani, M.; Rodríguez-Calero, G. G.; Hernández-Burgos, K.; Truong, T.-T.; Coates, G. W.; Abruña, H. D. *J. Electrochem. Soc.* **2017**, *164*, A1946.

- (25) Rodríguez-Calero, G. G.; Conte, S.; Lowe, M. A.; Gao, J.; Kiya, Y.; Henderson, J. C.; Abruña, H. D. *Electrochim. Acta*, **2015**, *167*, 55.
- (26) Conte, S.; Rodríguez-Calero, G. G.; Burkhardt, S. E.; Lowe, M. A.; Abruña, H. D. *RSC Adv.* **2013**, *3*, 1957.
- (27) Häupler, B.; Rössel, C.; Schwenke, A.M.; Winsberg, J.; Schmidt, D.; Wild, A.; Schubert, U.S. *NPG Asia Mater.* 2016, *8*, e283.
- (28) Ernould, B.; Bertrand, O.; Minoia, A.; Lazzaroni, R.; Vlad, A.; Gohy, J. F. *RSC Adv.* **2017**, *7*, 17301.
- (29) Li, Y.; Jian, Z.; Lang, M.; Zhang, C.; Huang, X. *ACS Appl. Mater. Interfaces*, **2016**, *8*, 17352.
- (30) Zhang, Y. Y.; Sun, Y. Y.; Du, S. X.; Gao, H. J.; Zhang, S. B. *Appl. Phys. Lett.* **2012**, *100*, 091905.
- (31) Ogihara, N.; Yasuda, T.; Kishida, Y.; Ohsuna, T.; Miyamoto, K.; Ohba, N. *Angew. Chem. Int. Ed.* **2014**, *53*, 11467.
- (32) Majda, M.; Faulkner, L. R. *J. Electroanal. Chem. Interf. Electrochem.* **1984**, *169*, 97.
- (33) Pearce, P. J.; Bard, A. J. *J. Electroanal. Chem. Interf. Electrochem.* **1980**, *114*, 89.
- (34) Niu, Z.; Wu, H.; Liu, L.; Dai, G.; Xiong, S.; Zhao, Y.; Zhang, X. *J. Mater. Chem. A.* **2019**, *7*, 10581.
- (35) Chen, X.; He, P.; Faulkner, L. R. *J. Electroanal. Chem.* **1987**, *222*, 223.

- (36) Arico, A. S.; Bruce, P.; Scrosati, B.; Tarascon, J. M.; Van Schalkwijk, W. *Nat. Mater.* **2011**, *4*, 336.
- (37) Luo, C.; Huang, R.; Kevorkyants, R.; Pavanello, M.; He, H.; Wang, C. *Nano Lett.* **2014**, *14*, 1596.
- (38) Xu, F.; Chen, X.; Tang, Z.; Wu, D.; Fu, R.; Jiang, D. *ChemComm.* **2014**, *50*, 4788.
- (39) Zhang, C.; Yang, X.; Ren, W.; Wang, Y.; Su, F.; Jiang, J. X. *J. Power Sources*, **2016**, *317*, 49.
- (40) Zhang, S.; Huang, W.; Hu, P.; Huang, C.; Shang, C.; Zhang, C.; Yang, R.; Cui, G. *J. Mater. Chem. A* **2015**, *3*, 1896.
- (41) Zhan, X.; Chen, Z.; Zhang, Q. *J. Mater. Chem. A* **2017**, *5*, 14463.
- (42) Mulzer, C. R.; Shen, L.; Bisbey, R. P.; McKone, J. R.; Zhang, N.; Abruña, H. D.; Dichtel, W. R. *ACS Cent. Sci.* **2016**, *2*, 667.
- (43) Vitaku, E.; Gannett, C. N.; Carpenter, K. L.; Shen, L.; Abruña, H. D.; Dichtel, W. R. *J. Am. Chem. Soc.* **2020**, *142*, 16.
- (44) Su, Y.; Liu, Y.; Liu, P.; Wu, D.; Zhuang, X.; Zhang, F.; Feng, X. *Angew. Chem. Int. Ed.* **2015**, *54*, 1812.
- (45) Song, Z.; Xu, T.; Gordin, M. L.; Jiang, Y. B.; Bae, I. T.; Xiao, Q.; Zhan, H.; Liu, J.; Wang, D. *Nano Lett.* **2012**, *12*, 2205.
- (46) Wang, L.; Zhang, H.; Mou, C.; Cui, Q.; Deng, Q.; Xue, J.; Dai, X.; Li, J. *Nano Res.* **2015**, *8*, 523.

- (47) Park, Y.; Shin, D. S.; Woo, S. H.; Choi, N. S.; Shin, K. H.; Oh, S. M.; Lee, K. T.; Hong, S. Y. *Adv. Mater.* **2012**, *24*, 3562.
- (48) Fédèle, L.; Sauvage, F.; Gottis, S.; Davoisne, C.; Salager, E.; Chotard, J.N.; Becuwe, M. *Chem. Mater.* **2017**, *29*, 546.
- (49) Bai, Y.; Fu, W.; Chen, W.; Chen, Z.; Pan, X.; Lv, X.; Wu, J.; Pan, X.; *J. of Mater. Chem. A* **2019**, *7*, 24454.
- (50) Chen, D.; Avestro, A. J.; Chen, Z.; Sun, J.; Wang, S.; Xiao, M.; Erno, Z.; Algaradah, M. M.; Nassar, M. S.; Amine, K.; Meng, Y. *Adv. Mater.* **2015**, *27*, 2907.
- (51) Dai, G.; Liu, Y.; Niu, Z.; He, P.; Zhao, Y.; Zhang, X.; Zhou, H. *Matter*, **2019**, *1*, 945.
- (52) Tang, M.; Zhu, S.; Liu, Z.; Jiang, C.; Wu, Y.; Li, H.; Wang, B.; Wang, E.; Ma, J.; Wang, C. *Chem*, **2018**, *4*, 2600.
- (53) Wang, C.; Xu, Y.; Fang, Y.; Zhou, M.; Liang, L.; Singh, S.; Zhao, H.; Schober, A.; Lei, Y. *J. Am. Chem. Soc.* **2015**, *137*, 3124.
- (54) Bai, Y.; Fu, W.; Chen, W.; Chen, Z.; Pan, X.; Lv, X.; Wu, J.; Pan, X. *J. Mater. Chem. A* **2019**, *7*, 24454
- (55) Otteny, F.; Perner, V.; Wassy, D.; Kolek, M.; Bieker, P.; Winter, M.; Esser, B. *ACS Sustainable Chem. Eng.* **2020**, *8*, 238.
- (56) Mathew, V.; Kim, S.; Kang, J.; Gim, J.; Song, J.; Baboo, J.P.; Park, W.; Ahn, D.; Han, J.; Gu, L.; Wang, Y. *NPG Asia Mater.* **2014**, *6*, e138.
- (57) Uchaker, E.; Cao, G. *Chem. Asian J.* **2015**, *10*, 1608.

- (58) Ku, J. H.; Ryu, J. H.; Kim, S. H.; Han, O. H.; Oh, S. M. *Adv. Func. Mater.* **2012**, *22*, 3658.
- (59) Chae, O. B.; Kim, J.; Park, I.; Jeong, H.; Ku, J. H.; Ryu, J. H.; Kang, K.; Oh, S. M. *Chem. Mater.* **2014**, *26*, 5874.
- (60) Walter, M.; Kravchyk, K. V.; Böfer, C.; Widmer, R.; Kovalenko, M. V. *Adv. Mater.* **2018**, *30*, 1705644.
- (61) Uchaker, E.; Zheng, Y. Z.; Li, S.; Candelaria, S. L.; Hu, S.; Cao, G. Z. *J. Mater. Chem. A*, **2014**, *2*, 18208.
- (62) Tian, F.; Radin, M. D.; Siegel, D.J. *Chem. Mater.* **2014**, *26*, 2952.
- (63) Acker, P.; Rzesny, L.; Marchiori, C. F.; Araujo, C. M.; Esser, B. *Adv. Func. Mater.* **2019**, *29*, 1906436.
- (64) Seo, D. H.; Kim, H.; Kim, H.; Goddard, W. A.; Kang, K. *Energy Environ. Sci.*, **2011**, *4*, 4938.
- (65) Suga, T.; Ohshiro, H.; Sugita, S.; Oyaizu, K.; Nishide, H. *Adv. Mater.* **2009**, *21*, 1627.
- (66) Komaba, S.; Hasegawa, T.; Dahbi, M.; Kubota, K. *Electrochem. Commun.* **2015**, *60*, 172.
- (67) Zhao, Q.; Wang, J.; Lu, Y.; Li, Y.; Liang, G.; Chen, J. *Angew. Chem. Int. Ed.* **2016**, *55*, 12528.
- (68) Armand, M. B. Intercalation Electrodes. in *Materials for Advanced Batteries*, First Edition; Murphy, D. W., Ed.; Springer US: Boston, MA, 1980; *2*, 145.

- (69) Burgess, M.; Hernández-Burgos, K.; Cheng, K. J.; Moore, J. S.; Rodríguez-López, J. *Analyst*, **2016**, *141*, 3842.
- (70) Hernández-Burgos, K.; Barton, Z. J.; Rodríguez-López, J. *Chem. Mater.* **2017**, *29*, 8918.
- (71) Hernández-Burgos, K.; Rodríguez-Calero, G. G.; Zhou, W.; Burkhardt, S. E.; Abruña, H. D. *J. Am. Chem. Soc.*, **2013**, *135*, 14532.
- (72) Hernández-Burgos, K.; Rodríguez-Calero, G. G.; Zhou, W.; Burkhardt, S. E.; Abruña, H. D. *J. Am. Chem. Soc.* **2013**, *135*, 14532.

CHAPTER 6

PHENOTHIAZINE-BASED POLYMER CATHODE MATERIALS WITH ULTRA-HIGH POWER DENSITIES FOR LITHIUM ION BATTERIES

6.1 Abstract

Lithium ion batteries (LIBs) currently deliver the highest energy density of any known secondary electrochemical energy storage system. However, new cathode materials, which can deliver both high energy and power densities, are needed to improve LIBs. Herein, we report on the synthesis of a new organic-based redox active material centered about phenothiazine and phenylenediamine units. Improved coulombic efficiencies and greater capacity retention during cycling are observed through the copolymerization of a phenothiazine based monomer that yield cross-linked materials. As the positive electrode in Li-coin cells, high specific capacities (150 mAh/g) are delivered at very positive operating voltages (2.8–4.3 V vs Li⁺/Li), yielding high energy densities. The material has low charge transfer resistance as verified by electrochemical impedance spectroscopy, which contributes in delivering previously unseen power densities in coin cells for all organic electrical energy storage devices. Excellent retention of capacity (82%) is observed at ultra-fast discharge rates (120 C).

6.2 Introduction

Organic and polymeric materials are excellent candidates for next generation electrode materials in high-power and high-energy density

electrochemical energy storage applications, namely lithium ion batteries (LIBs).¹⁻³ Relative to traditional metal oxide cathodes, organic materials are structurally tunable, environmentally benign, and elementally abundant, lending to their continued study as cathodes. Polymers centered about conductive,^{4,5} carbonyl-based,⁶⁻⁹ nitroxide radicals,^{10,11} and organosulfur¹²⁻¹⁴ functionalities have shown exceptional performance and promise as cathodes in LIBs (See Chapter 6.6.Appendix, Figure 6.7). However, designing organic cathodes which exhibit both high power density, characteristic of capacitors, with high energy density, often associated with batteries, remains intrinsically challenging.

In the quest for high energy density organic cathodes, p-type polymers are particularly enticing, owing in part to their high operating voltages.¹⁵⁻¹⁸ Recently reported phenothiazine-based p-type polymer cathodes exhibit stable cycling and high working voltages.¹⁹⁻²¹ However low capacities are delivered due to only a single electron oxidation per repeat unit. Encouraged by these reports, we sought to design a class of phenothiazine main-chain polymers which would undergo multiple electron oxidations and deliver high capacities (Figure 6.1). Incorporation of redox functionality directly into the main chain minimizes supporting mass per redox event, affording high theoretical gravimetric capacities. Furthermore, a partially conjugated structure should provide a framework for low resistance toward electronic conduction throughout the cathode. Adhering to these design principles, we present a redox-active

phenothiazine centered polymer cathode, which effectively couples high energy- and power-densities.

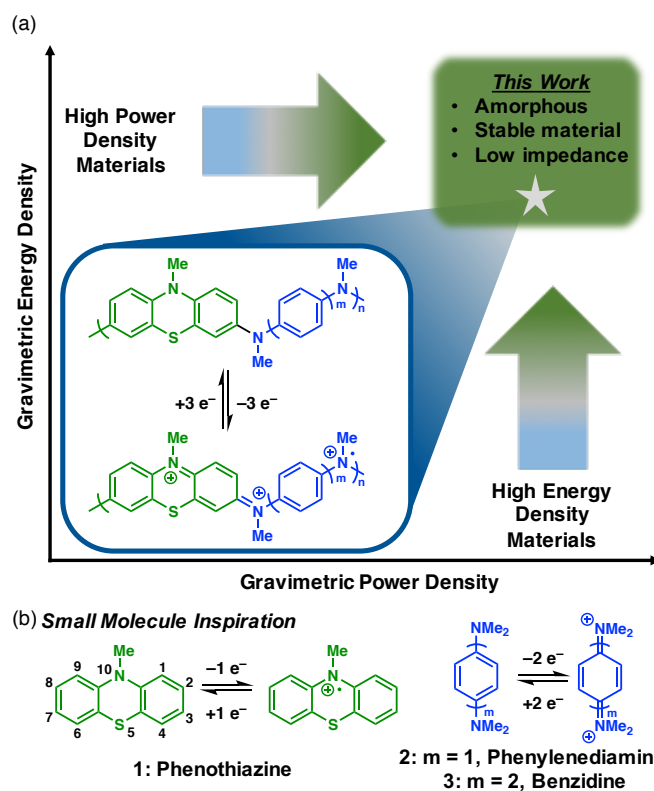


Figure 6.1. (a) Charged and discharged states of high energy density and high power density Poly(N-methylphenothiazine dimethylphenylenediamine) (PT-DMPD, m=1) and poly(N-methylphenothiazine benzidine) (PT-BZ, m=2). (b) The oxidized and reduced states of the small molecule basis.

Through rational design, we sought to synthesize phenothiazine based polymer cathodes capable of delivering high power densities at fast charging and discharging rates. We hypothesized that copolymerization of N-methylphenothiazine (**1**) with electron rich and redox active aryl diamines would afford polymers with high theoretical capacities and stable charged states by

mimicking the stabilized oxidized state of methylene blue. Two aryl amines, *N,N,N',N'*-tetramethyl-*p*-phenylenediamine (**2**) and *N,N,N',N'*-tetramethylbenzidine (**3**), were natural candidates considering their multiple oxidation events to a stabilized quinoidal dication at potentials greater than 3.3 V vs Li⁺/Li.²² We further hypothesized that copolymerization through the 3 and 7 positions of phenothiazine would facilitate fast charging and discharging rates, since partial conjugation throughout the entire backbone would allow for facile electron transfer to and from the current collector.

6.3 Results and Discussion

Poly(*N*-methylphenothiazine dimethylphenylenediamine) (PT-DMPD) and poly(*N*-methylphenothiazine benzidine) (PT-BZ) were synthesized from inexpensive starting materials using Buchwald-Hartwig cross-coupling of 3,7-dibromo-*N*-methylphenothiazine (**1a**) with dimethylphenylenediamine (**2a**) or dimethylbenzidine (**3a**) (Figure 6.2.a).^{23,24} The resulting linear polymers were insoluble in their neutral state, and their electrochemical properties were probed using cyclic voltammetry (CV), measured as slurries in a solution of LiPF₆ (1 M) in ethylene carbonate/diethyl carbonate (EC/DEC). The neutral and oxidized redox states of PT-DMPD are displayed in Figure 6.1. The three discrete redox couples of each polymer were observed by CV (Figure 6.2.b), occurring at 3.3, 3.6, and 4.3 V vs Li⁺/Li.²⁵ These redox couples are among the highest in organic electrodes reported for electrical energy storage applications.

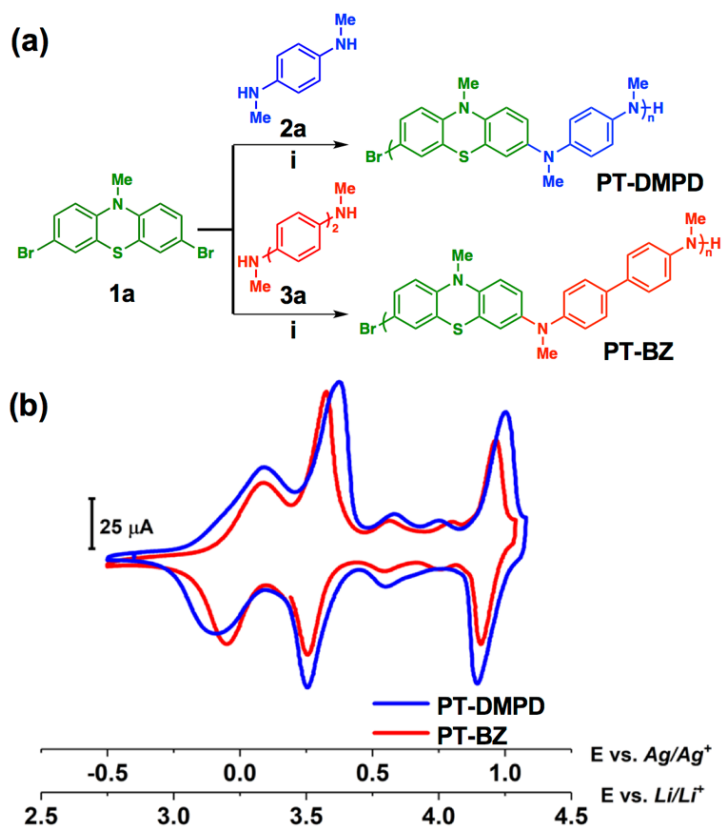


Figure 6.2. (a) General synthetic strategy towards PT-DMPD and PT-BZ polymers using Buchwald-Hartwig coupling. i: NaOtBu, RuPhos (3 mol%), RuPhos Pd G2 (3 mol%), Toluene, 80 °C. (b) Neutral and oxidized states of PT-DMPD (c) Slurry CV of PT-DMPD and PT-BZ in LiPF₆ (1 M) in EC/DEC at 20 mVs⁻¹.

Coin cells employing PT-DMPD or PT-BZ as the cathode and Li metal as the anode were assembled to explore the performance of the polymers in devices. Due to the limited stability window of the electrolyte medium (EC/DEC), only the first two redox couples were accessed in coin cell cycling (See Chapter 6.6 Appendix: Figure 6.8). Coin cells were prepared on carbon felt current collectors with 0.55 mg/cm² active material loading (See Chapter 6.6 Appendix for coin cell fabrication). Figure 6.3.a displays the first cycle charge-discharge

curves of PT-DMPD and PT-BZ at 1 C, over the voltage range from 2.8 to 4.3 V. Both exhibit reversible two-stage charge-discharge behavior, which is consistent with the two major redox couples observed in the CV. The discharge

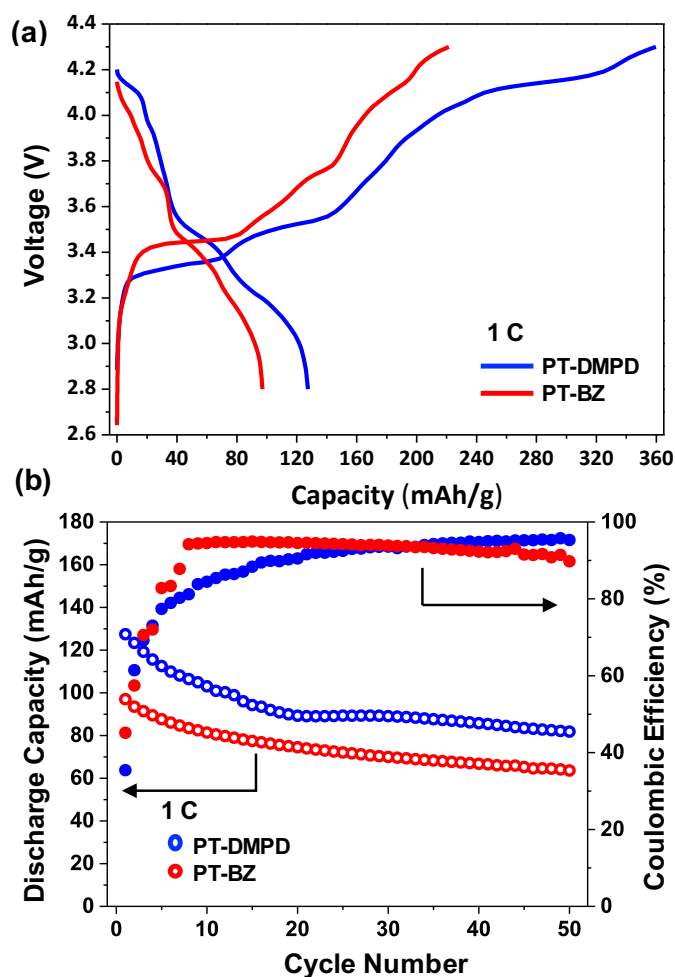


Figure 6.3. (a) Initial charge–discharge curves of coin cells, prepared with 0.55 mg/cm² loading of PT-DMPD and PT-BZ, at 1 C. (b) Cycling performance of the PT-DMPD and PT-BZ cells at 1 C.

capacities of PT-DMPD and PT-BZ were 128 mAh/g and 97 mAh/g, representing 82% and 76% of theoretical capacity, respectively. However, both

materials exhibited a relatively low coulombic efficiency (35% for PT-DMPD and 44% for PT-BZ). The cycling performances of the PT-DMPD and PT-BZ cathode materials are shown in Figure 6.3.b. Both cells were cycled at 25 °C over the same voltage range at 1 C. The discharge capacity of PT-DMPD was 82 mAh/g after 50 cycles (64% retention), while that of PT-BZ was 64 mAh/g after 50 cycles (66% retention). Since the PT-DMPD polymer exhibited higher capacity than PT-BZ polymer, further work focused on the former.

We hypothesized that the low coulombic efficiency and capacity fade upon cycling were caused by dissolution of the polymer upon oxidation. This dissolution could be observed visually as green dissolved polymer diffused away from the electrode during CV cycling. To address these limitations, a second class of increasingly cross-linked materials was synthesized to generate polymers with decreased solubility in the electrolyte medium (Figure 6.4.a). This class of cross-linked cathode materials are referenced according to the mole percentage of cross-linker relative to **1a**. The first charge-discharge cycle of PT-DMPD, PT-DMPD (5% cross-linked, 5% CL), PT-DMPD (10% CL), and PT-DMPD (33% CL) at 5 C are shown in Figure 6.4.b. Increased discharge capacities trended with an increase in mol percentage of cross-linker, with PT-DMPD (10% CL) exhibiting the highest discharge capacity of 150 mAh/g (97% of the theoretical value of PT-DMPD). In addition, a decrease in charging capacity lead to significant improvements in coulombic efficiency with increasing copolymerization of cross-linker. It is likely that the decrease in charging capacity results from either a suppression of polymer degradation or a decrease

in small, soluble oligomers, which can act as electron shuttles between electrodes during charging.²⁶⁻²⁸ The coulombic efficiency at 5 C increases from 49% to 82% between linear (no cross-linker) and 33% cross-linked polymer. By limiting dissolution through cross-linking, both the capacity and coulombic efficiency were greatly improved.

The cycling performance of PT-DMPD, PT-DMPD (5% CL), PT-DMPD (10% CL) and PT-DMPD (33% CL) materials was investigated between 2.8 and 4.3 V at 5 C, as shown in Figure 6.4.c. Increasing the mol percentage of cross-linker resulted in materials exhibiting better cycling performance when compared to linear PT-DMPD. As the mol percentage of cross-linker increased from 0% to 5% to 10% to 33%, the capacity retention after 50 cycles increased from 65% to 73% to 74% to 82%, respectively. These results suggest that dissolution of the polymer from the cathode was mitigated in the cross-linked materials. For use in high power applications, the proposed materials must be able to deliver high discharge capacities at fast discharge rates. To better understand the relationship between mol% cross-linker and the materials capacity retention at increasing discharge rates, the rate capabilities of PT-DMPD (10% CL) and PT-DMPD (33% CL), the two materials displaying the highest discharge capacities, were investigated between 2.8 and 4.3 V. Figure 6.5 compares the discharge capacities of these materials charged at 1 C and discharged at C- rates of 1, 5, 10, 20, 40, 60, and 120 C. Significantly, excellent capacity retention (82%) was observed in PT-DMPD (10% CL) between even the most extreme discharging rates, 1 C to 120 C.

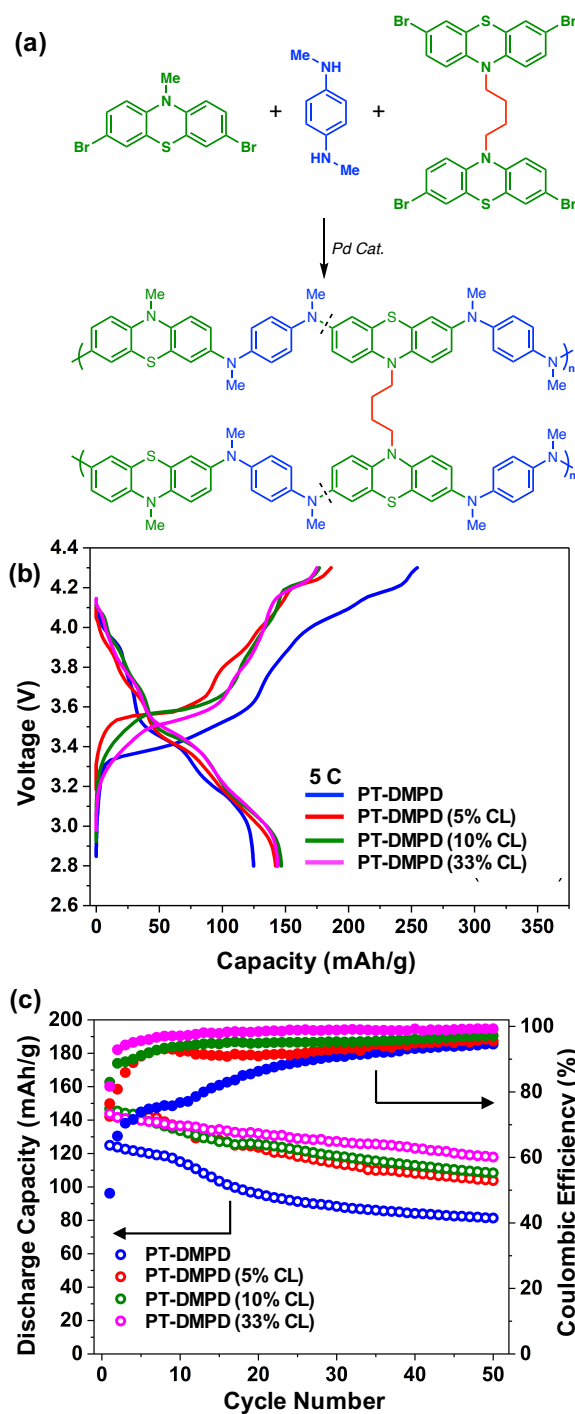


Figure 6.4. (a) Cross-linker (CL) structure and material design. (b) Initial charge-discharge of PT-DMPD, PT-DMPD (5% CL), PT-DMPD (10% CL), and PT-DMPD (33% CL) at 5 C. **c.** Cycling performance of coin cells with 0.55 mg/cm² loading of PT-DMPD, PT-DMPD (5% CL), PT-DMPD (10% CL), and PT-DMPD (33% CL) at 5 C.

While similar capacities are observed at the lower rates for both materials, an apparent decrease in capacity is evident in PT-DMPD (33% CL) at higher discharge rates. We attribute this to a decrease in the rate of counterion transport through the more densely cross-linked material. Notably, the PT-DMPD (10% CL) material retained a very high discharge capacity of 122 mAh/g at the ultrahigh C-rate of 120 C.²⁹

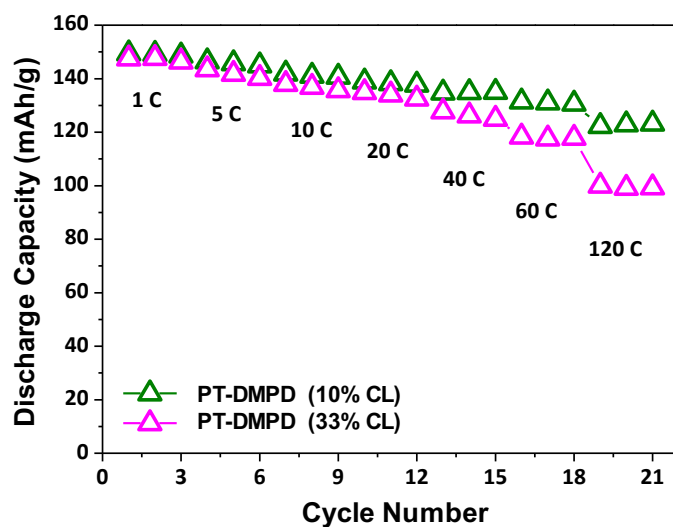


Figure 6.5. Discharge capacities of PT-DMPD (10% CL) and PT-DMPD (33% CL) at C-rates from 1 C to 120 C.

Encouraged by the fast discharge rates exhibited by these materials, electrochemical impedance spectroscopy (EIS) was used to measure the charge transfer resistance of PT-DMPD (10% CL) in a coin cell to explore the origin of the ultrahigh-rate behavior.³⁰⁻³² In impedance measurements, a high frequency semicircle is attributed to the double layer and the kinetics of the active material (Figure 6.6). In addition, the low frequency behavior is attributed

to transport effects. The high frequency semicircle was fit to a simplified Randles model, and the charge transfer resistances obtained are given as an inset.

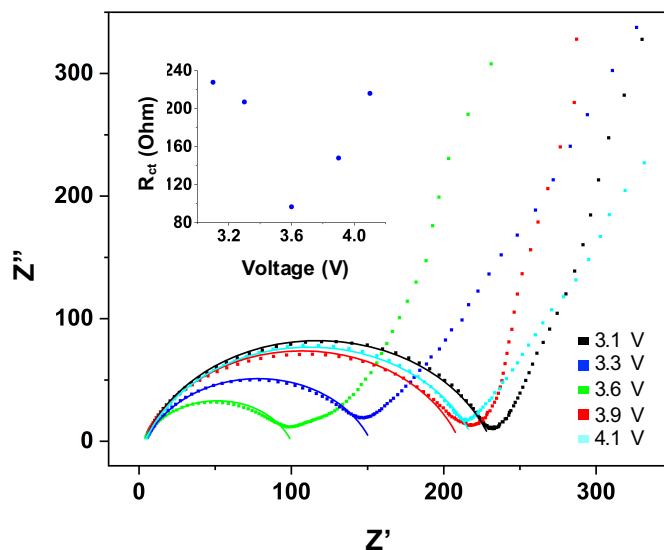


Figure 6.6. Electrochemical impedance spectra of PT-DMPD (10% CL) at various charge states reflects fast charge transfer kinetics dependent on the oxidation state of the polymer. Inset shows the charge transfer resistance (R_{ct}) as a function of potential of the device.

As expected, the charge transfer resistance was a function of the oxidation state of the polymer. The charge transfer resistances near the redox couple around 3.6 V are much lower than the charge transfer resistances near 4.1 V and 3.1 V. Overall, the charge transfer resistance was between 80 Ω and 230 Ω . When compared to literature reports, these values are similar or lower than comparable systems, reflecting fast charge transfer kinetics.^{7,9,30-34} This facile kinetic behavior allows the battery to operate at high C-rates without excessive overpotentials. The low overpotentials, in turn, are one of the reasons

for the high rate cycling capability without significant loss of capacity. The low charge transfer resistance of this material is exemplified by retention of capacity and stable cycling in coin cells with 75% active material loading (Figure 6.10).

6.4 Conclusion

In conclusion, we have designed, synthesized, and tested a class of high-energy phenothiazine-derived redox-active polymers that deliver high capacities at ultra-fast discharge rates and high operating voltages in lithium ion batteries. The initial capacity fade, due to electrode dissolution, was largely mitigated through the implementation of cross-linked materials, which led to dramatically improved cycling performance, discharge capacity, and coulombic efficiency without compromising the material's rate capability. PT-DMPD (10% CL) retained 82% capacity at an unparalleled 120 C rate. These results validate our design principles, and are highly instructive for future discoveries of organic electrodes with competitive energy densities and superior power densities for electrical energy storage applications.

6.5 References

- (1) Novak, P.; Müller, K.; Santhanam, K. S. V.; Haas, O. *Chem. Rev.* **1997**, 97, 207.
- (2) Liang, Y.; Tao, Z.; Chen, J. *Adv. Energy Mater.* **2012**, 2, 742.
- (3) Schon, T. B.; McAllister, B. T.; Li, P.-F.; Seferos, D. S. *Chem. Soc. Rev.* **2016**, 45, 6345.
- (4) Snook, G. A.; Kao, P.; Best, A. S. *J. Power Sources* **2011**, 196, 1–12.

- (5) Hudak, N. S. *J. Phys. Chem. C* **2014**, *118*, 5203–5215.
- (6) Zhang, H.; Deng, Q.; Zhou, A.; Liu, X.; Li, J. *J. Mater. Chem. A* **2014**, *2*, 5696.
- (7) Song, Z.; Qian, Y.; Gordin, M. L.; Tang, D.; Xu, T.; Otani, M.; Zhan, H.; Zhou, H.; Wang, D. *Angew. Chem., Int. Ed.* **2015**, *54*, 13947.
- (8) Liang, Y.; Chen, Z.; Jing, Y.; Rong, Y.; Facchetti, A.; Yao, Y. *J. Am. Chem. Soc.* **2015**, *137*, 4956.
- (9) Wang, S.; Wang, Q.; Shao, P.; Han, Y.; Gao, X.; Ma, L.; Yuan, S.; Ma, X.; Zhou, J.; Feng, X.; Wang, B. *J. Am. Chem. Soc.* **2017**, *139*, 4258.
- (10) Lin, H.-C.; Li, C.-C.; Lee, J.-T. *J. Power Sources* **2011**, *196*, 8098.
- (11) Wang, Y.-H.; Hung, M.-K.; Lin, C.-H.; Lin, H.-C.; Lee, J.-T. *Chem. Commun.* **2011**, *47*, 1249.
- (12) Sarukawa, T.; Oyama, N. *J. Electrochem. Soc.* **2010**, *157*, F23.
- (13) Kiya, Y.; Iwata, A.; Sarukawa, T.; Henderson, J. C.; Abruña, H. D. *J. Power Sources* **2007**, *173*, 522.
- (14) Davoglio, R. A.; Biaggio, S. R.; Rocha-Filho, R. C.; Bocchi, N. *J. Power Sources* **2010**, *195*, 2924.
- (15) Happler, B.; Burges, R.; Friebe, C.; Janoschka, T.; Schmidt, D.; Wild, A.; Schubert, U. S. *Macromol. Rapid Commun.* **2014**, *35*, 1367.
- (16) Imada, Y.; Nakano, H.; Furukawa, K.; Kishi, R.; Nakano, M.; Maruyama, H.; Nakamoto, M.; Sekiguchi, A.; Ogawa, M.; Ohta, T.; Yamamoto, Y. *J. Am. Chem. Soc.* **2016**, *138*, 479.

- (17) Speer, M. E.; Kolek, M.; Jassoy, J. J.; Heine, J.; Winter, M.; Bieker, P. M.; Esser, B. *Chem. Commun.* **2015**, *51*, 15261.
- (18) Peng, C.; Ning, G.-H.; Su, J.; Zhong, G.; Tang, W.; Tian, B.; Su, C.; Yu, D.; Zu, L.; Yang, J.; Ng, M.-F.; Hu, Y.-S.; Yang, Y.; Armand, M.; Loh, K. P. *Nat. Energy* **2017**, *2*, 17074.
- (19) Golriz, A.; Suga, T.; Nishide, H.; Berger, R.; Gutmann, J. S. *RSC Adv.* **2015**, *5*, 22947.
- (20) Kolek, M.; Otteny, F.; Schmidt, P.; Mück-Lichtenfeld, C.; Einholz, C.; Becking, J.; Schleicher, E.; Winter, M.; Bieker, P.; Esser, B. *Energy Environ. Sci.* **2017**, *10*, 2334.
- (21) Godet-Bar, T.; Lepretre, J.-C.; Le Bacq, O.; Sanchez, J.-Y.; Deronzier, A.; Pasturel, A. *Phys. Chem. Chem. Phys.* **2015**, *17*, 25283.
- (22) (a) Truong, T.-T.; Coates, G. W.; Abruña, H. D. *Chem. Commun.* **2015**, *51*, 14674.
- (23) Maiti, D.; Fors, B. P.; Henderson, J. L.; Nakamura, Y.; Buchwald, S. L. *Chem. Sci.* **2011**, *2*, 57.
- (24) Kinzel, T.; Zhang, Y.; Buchwald, S. L. *J. Am. Chem. Soc.* **2010**, *132*, 14073.
- (25) We hypothesize the two small redox couples at 3.6 and 4.0 V vs Li/Li⁺ correspond to redox active end groups of the polymers.
- (26) Peled, E.; Sternberg, Y.; Gorenshtein, A.; Lavi, Y. *J. Electrochem. Soc.* **1989**, *136*, 1621.

- (27) Mikhaylik, Y. V.; Akridge, J. R. Polysulfide Shuttle Study in the Li/S Battery System. *J. Electrochem. Soc.* 2004, 151, A1969–A1976. (28)
- (28) Diao, Y.; Xie, K.; Xiong, S.; Hong, X. *J. Power Sources* **2013**, 235, 181.
- (29) By comparison, the reported materials retain 82% of initial capacity (150 mAh/g) at 120 C, whereas the phenothiazine-based material reported in 20 retains 52% of initial capacity (79 mAh/g) at 100 C.
- (30) Bhosale, M. E.; Krishnamoorthy, K. *Chem. Mater.* **2015**, 27, 2121.
- (31) Zhang, K.; Guo, C.; Zhao, Q.; Niu, Z.; Chen, J. *Adv. Sci.* **2015**, 2, 1500018.
- (32) Wu, H.; Shevlin, S. A.; Meng, Q.; Guo, W.; Meng, Y.; Lu, K.; Wei, Z.; Guo, Z. *Adv. Mater.* **2014**, 26, 3338.
- (33) Song, Z.; Qian, Y.; Liu, X.; Zhang, T.; Zhu, Y.; Yu, H.; Otani, M.; Zhou, H. *Energy Environ. Sci.* **2014**, 7, 4077.

6.6 Appendix

Materials and Reagents

Toluene, dichloromethane (DCM), and tetrahydrofuran (THF) were purchased from J.T. Baker and purified by vigorous purging with argon for 2 hours, followed by passing through two packed columns of neutral alumina under argon pressure. BrettPhos (96%), BrettPhos Pd G3 (95%), RuPhos (95%), RuPhos Pd G2, sodium *tert*-butoxide (NaOtBu), potassium *tert*-butoxide (KOtBu), methylamine (40% in water), hydrazine (anhydrous), 4,4-dibromobiphenyl, 4-bromo-*N,N'*-dimethylaniline (97%), *N*-methyl-aniline, 1,4-

dibromobenzene (98%), and copper powder (99%) were purchased from Sigma Aldrich and used as received. 4,4'-dibromobiphenyl (98%), 1,4-dibromobutane (99%), phenothiazine (98%+), iodomethane (99.5%), and methylamine (2M in THF) were purchased from Alfa Aesar, and used as received. Anhydrous magnesium sulfate was purchased from EMD Chemicals. *N*-Bromosuccinimide (NBS) was purchased from Oakwood Chemicals and recrystallized from DI water before use. Sodium sulfite was purchased from Fischer Scientific. Tetrabutylammonium perchlorate was purchased from TCI American (>98%) and recrystallized from ethyl acetate three times to obtain white crystals. Acetonitrile (ACS Grade), from Fischer Scientific, was dried over activated 4 Å molecular sieves. 1-Methyl-2-pyrrolidinone (NMP, anhydrous, 99.5%) was purchased from Sigma Aldrich and used without further purification.

General Analytical Information:

Nuclear magnetic resonance (NMR) spectra were recorded on a Mercury 300 MHz, a Varian 400 MHz, or a Bruker 500 MHz. Infrared spectra were recorded on a Bruker Hyperion FT-IR Spectrometer with an ATR objective. Gel Permeation Chromatograms were acquired on a Waters Ambient Temperature GPC. THF was used as the eluent and number-average molecular weights (M_n), weight-average molecular weights (M_w), and dispersities (\mathcal{D}) were calculated from refractive index chromatograms against polystyrene standards.

All electrochemical measurements were performed in a three-compartment glass cell with medium porosity glass frits separating the compartments. An Ag/Ag⁺ reference electrode and a Pt wire counter electrode

were used, unless otherwise specified. All potentials are referenced to an Ag/Ag⁺ reference electrode, which is 0.50 V vs NHE. All 3-mm glassy carbon (GC) electrodes were homemade, in which a glassy carbon slug was press-fitted into a Teflon casing. Prior to the experiment, solutions were subjected to 10 minutes of sparging with Ar or N₂ to prevent undesirable side-reactions and oxygen reduction over the applied potential window.

The following procedure was taken to clean GC electrodes before use. Electrodes were sonicated in ethanol for 30 seconds before polishing with diamond paste and MetaDi Fluid (Buehler). Following polishing, the electrodes were sonicated in ethanol again for 30 seconds and dried with an IR lamp.

Electrochemical Experimental:

Electrochemical Tests:

Electrochemical measurements were carried out in CR 2032 coin cells assembled in an argon filled glove box (residual water and oxygen were 0.5 ppm and 0.1 ppm, respectively) with lithium metal as the anode. The working cathode was fabricated with 30 wt% active material (0.55 mg/cm²), 60 wt% Super P carbon, and 10 wt% poly(vinylidene fluoride) (PVDF) as binder. The high loading cathode was fabricated with 75 wt% active material, 15 wt% Super P carbon, and 10 wt% poly(vinylidene fluoride) (PVDF) as binder. The resulting slurry was coated onto a carbon paper current collector. The coated electrode was dried for 12 h at 100 °C in a vacuum oven. The counter electrode was Li metal. The two electrodes were separated by a polypropylene separator

(Celgard 2300). The electrolyte was 1.0 M LiPF₆ in a 1:1 ratio of EC (ethylene carbonate) to DEC (diethyl carbonate). Galvanostatic charge/discharge of the coin cells was carried out using an Arbin BT-2000 battery tester with a constant charge-discharge current rate and a voltage range of 2.8 to 4.3 V vs. Li/Li⁺ at 25 °C.

Electrochemical Impedance Spectroscopy (EIS):

Electrochemical impedance spectroscopy measurements using a Solartron 1280-B potentiostat, were performed on a lithium coin cell with PT-DMPD (10% CL) as cathode. Impedance measurements were taken at 3.1, 3.3, 3.6, 3.9 and 4.1 V vs. Li/Li⁺ after 3600 s of pretreatment at the respective potentials from 0.001 - 20000 Hz. AC amplitude of the measurements were 10 mV.

Slurry Preparation:

2.0 mg of bulk polymer, 2.5 mg of carbon black and 0.5 mg of PVDF were mixed in a 5 mL vial with 1 mL NMP. Such a composition yields a composite loading of 5 mg mL⁻¹. The mixture was sonicated for 1 h until the mixture was homogeneously dispersed in solvent, 10 µL of ink were drop-casted onto the GC surface to create a polymer loading of 0.28 mg cm⁻². Even though the powdered polymers were insoluble in conventional organic solvents, when oxidized the polymers become slightly soluble in EC/DEC, as the slurry on the GC dissolved

as the materials became oxidized. Since materials were lost during cycling, scan rate dependence and other quantitative analysis were not performed on

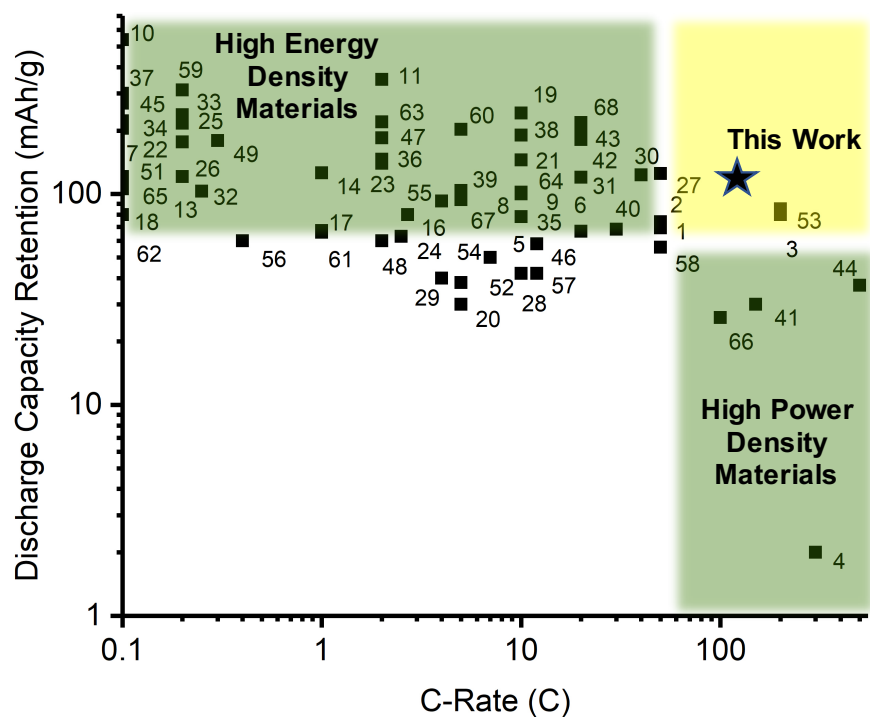


Figure 6.7. A plot of the retained capacity retention at the highest reported rates of a representative number of organic cathode materials. References are listed below.

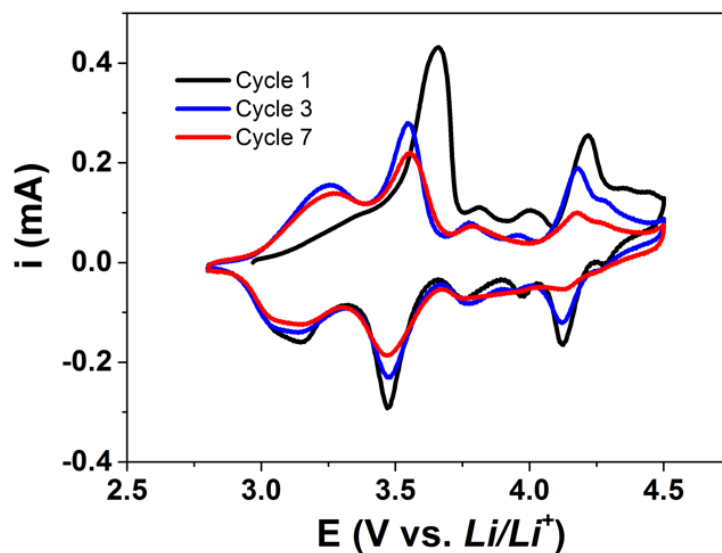


Figure 6.8. CV cycling the full potential window of 10% CL PT-DMPD in 1 M LiPF₆ in EC/DEC in a coin cell at 0.2 mVs⁻¹. In the 1st cycle, there is likely a kinetic barrier in “breaking in” the electrode material to be incorporated with anions in the first cycle, as the total charge in the first cycle approximates to the charge involved in the first two redox.

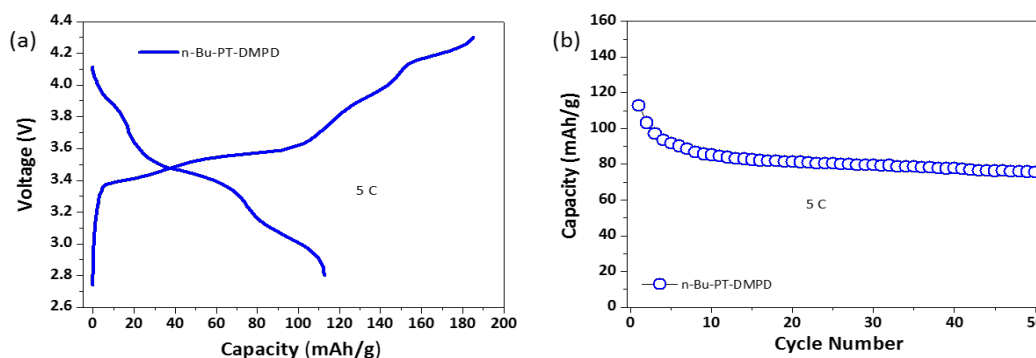


Figure 6.9. Poly(*N*-nbutylphenothiazine dimethylphenylenediamine) (*n*BuPT-DMPD) was synthesized in an attempt to make soluble derivatives of PT-DMPD polymers for more complete characterization. Detailed synthesis and characterization of *n*BuPT-DMPD are presented in the synthesis section later in the SI. (a) Initial charge–discharge curves of the *n*BuPT-DMPD cell at 5 C between 2.8 and 4.3 V. (b) Cycling performance of the *n*BuPT-DMPD cell at 5 C between 2.8 and 4.3 V. processes in the subsequent cycles.

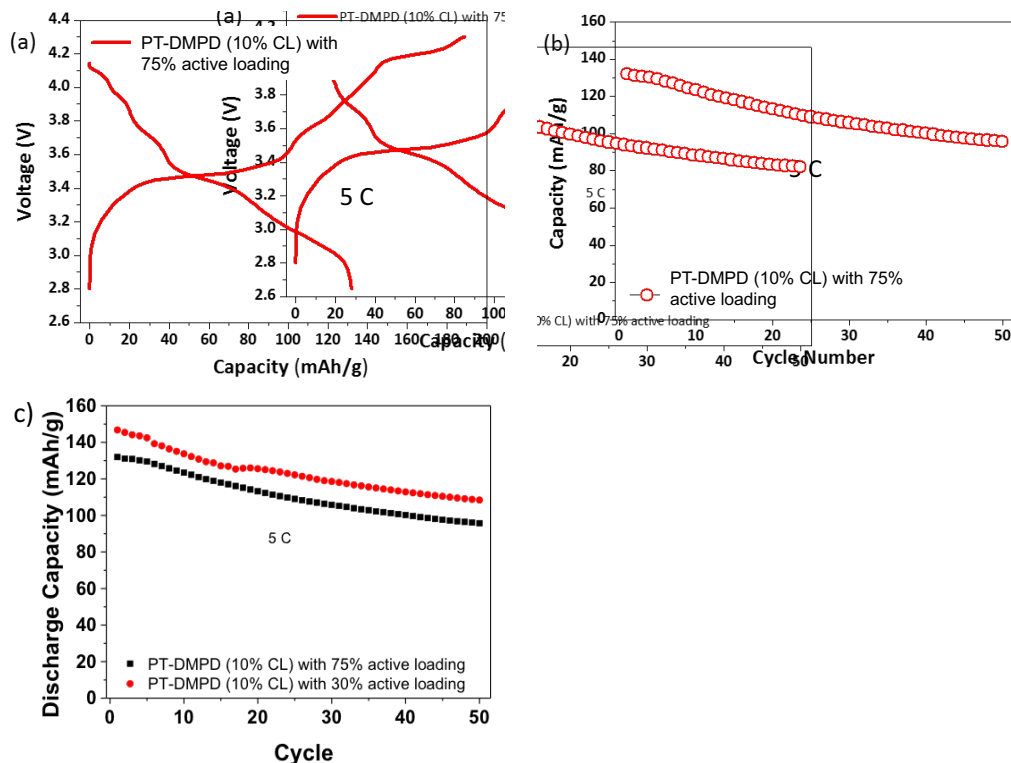


Figure 6.10. (a) Initial charge–discharge curves of the PT-DMPD (10% CL) cell with 75% active material loading at 5 C between 2.8 and 4.3 V. (b) Cycling performance of the PT-DMPD (10% CL) cell with 75% active loading at 5 C between 2.8 and 4.3 V. (c) Cycling of PT-DMPD (10% CL) cell with 75% active loading at 5C and PT-DMPD (10% CL) cell with 30 % active loading at 5 C.

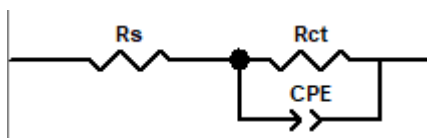


Figure 6.11. Equivalent circuit model for electrochemical impedance spectroscopy data

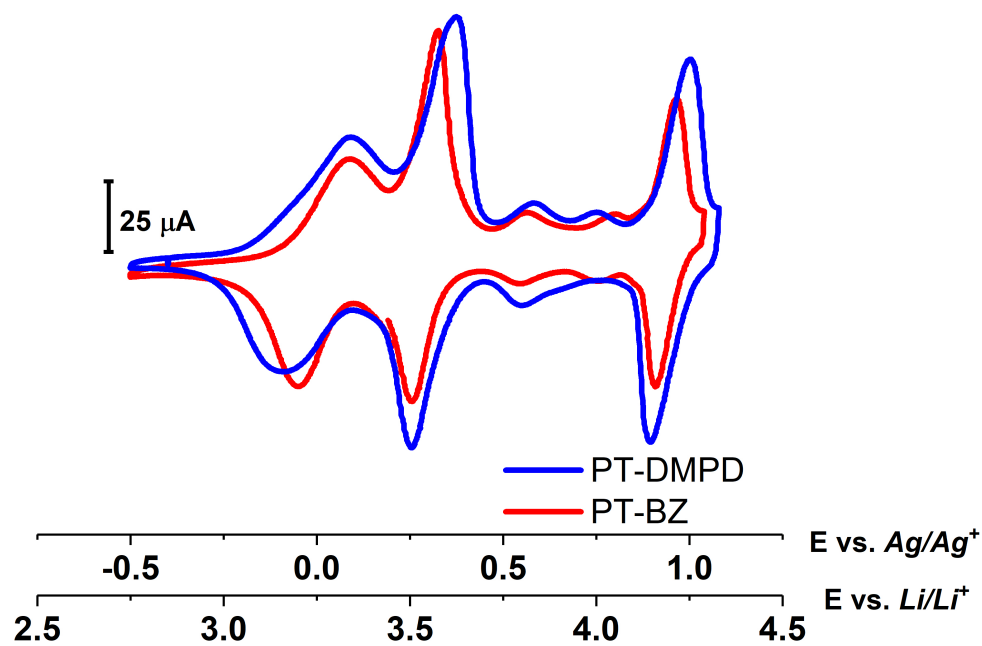


Figure 6.12. CV of PT-BZ and PT-DMPD in units of current density.

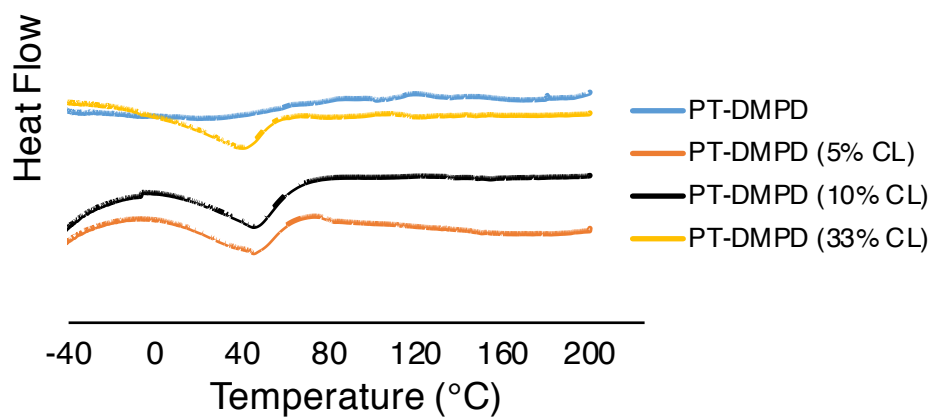


Figure 6.13. DSC Traces of the PT-DMPD, PT-DMPD (5% CL), PT-DMPD (10% CL), and PT-DMPD (33% CL). A T_g around 45 °C is observed in the cross-linked materials but the absence of any T_m suggests the material is amorphous.

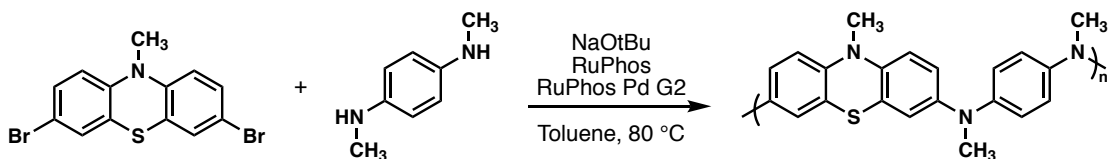
Table 6.1. Discharge capacities of the PT-DMPD (10% CL) sample and the PT-DMPD (33% CL) sample at different rates and the corresponding capacity retentions (Note: retention at 1 C is defined as 100%).

Rates	PT-DMPD (10% CL)		PT-DMPD (33% CL)	
	Discharge capacity (mAh/g)	Capacity retention (%)	Discharge capacity (mAh/g)	Capacity retention (%)
1 C	149.4	100	147.5	100
5 C	146.4	98.0	143.5	97.3
10 C	141.9	95.0	138.0	93.6
20 C	138.9	93.0	134.9	91.5
40 C	134.7	90.2	127.8	86.6
60 C	131.5	88.0	118.3	80.2
120 C	122.3	81.9	100.0	67.8

Table 6.2. Values of circuit elements and estimated errors in Electrochemical Impedance Spectroscopy

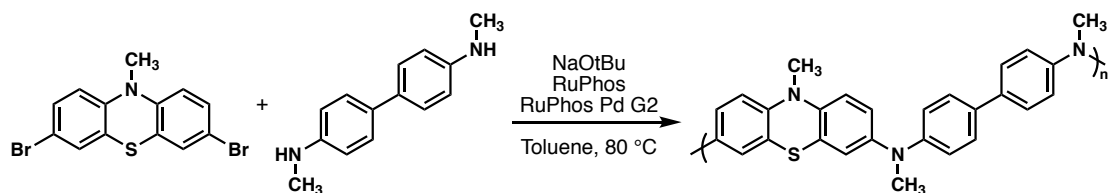
Potential	R _{ct}	R _{ct} (Error%)	CPE-T (X 10 ⁻⁵)	CPE-T (Error%)	CPE-P	CPE-P (Error%)	R _s	R _s (Error%)
3.1V	228	0.3	2.32	1.5	0.80	0.2	3.42	1.3
3.3V	207	0.5	2.52	2.3	0.79	0.3	3.40	1.9
3.6V	97	0.8	3.75	4.8	0.76	0.7	3.19	3.4
3.9V	148	0.7	3.56	3.4	0.77	0.5	4.09	2.1
4.1V	216	0.2	3.24	0.9	0.79	0.1	4.00	0.6

Synthesis and Characterization of Monomers and Polymers



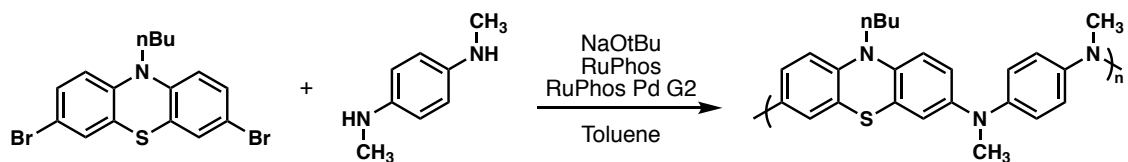
PT-DMPD Polymer:

A flame dried 30 mL reaction tube was equipped with a magnetic stir bar and charged with 3,7-dibromo-*N*-methyl-phenothiazine (204 mg, 0.550 mmol, 1 equiv), *N,N'*-dimethyl-paraphenylenediamine (75 mg, 0.55 mmol, 1 equiv), RuPhos ligand (7.5 mg, 0.017 mmol, 0.03 equiv), RuPhos Pd G2 precatalyst (13 mg, 0.017 mmol, 0.03 equiv), and NaOtBu (170 mg, 1.65 mmol, 3 equiv). The reaction tube was evacuated and backfilled with N₂ three times and toluene (2 mL) was added via syringe. The reaction was stirred at 80 °C overnight. The mixture was allowed to cool to room temperature, and diluted into a 200 mL biphasic solution consisting of equal parts water and DCM. The insoluble polymer was filtered off and washed with an additional 100 mL of water and subsequently 100 mL of DCM. The polymer was dried under vacuum, yielding 128 mg of tan powder. IR (ATR, cm⁻¹): 1511, 1468, 1321, 1250, 1133, 1112, 1078, 914, 852, 821. Elemental Anal. Found: C, 67.29; H, 5.55; Br, 3.64. (This analysis is consistent with a polymer with an M_n ~ 2.5 kg/mol.)



PT-BZ Polymer:

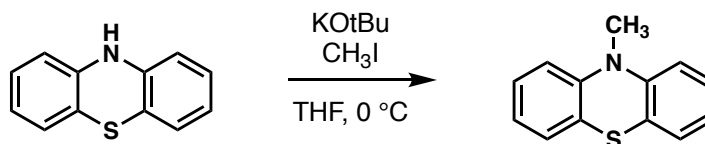
A flame dried 30 mL reaction tube was equipped with a magnetic stir bar and charged with 3,7-dibromo-*N*-methyl-phenothiazine (371 mg, 1.00 mmol, 1 equiv), *N,N'*-Dimethyl-4,4'-diaminobiphenyl (212.3 mg, 1 mmol, 1 equiv), RuPhos ligand (4.6 mg, 0.010 mmol, 0.010 equiv), RuPhos Pd G2 precatalyst (7.8 mg, 0.010 mmol, 0.010 equiv), and NaOtBu (288 mg, 3.00 mmol, 3 equiv). The reaction tube was evacuated and backfilled with N₂ three times and toluene (3 mL) was added via syringe. The reaction was heated to 80 °C and stirred for 10.5 hours. The mixture was allowed to cool to room temperature, and diluted into a 200 mL biphasic solution consisting of equal parts water and DCM. The insoluble polymer was filtered off and washed with an additional 100 mL of water and subsequently 100 mL of DCM. The polymer was dried under vacuum, yielding 415 mg of a yellow powder. IR (ATR, cm⁻¹): 3008, 2961, 2931, 2877, 1736, 1463, 1283, 751 cm⁻¹.



nBu-PT-DMPD Polymer:

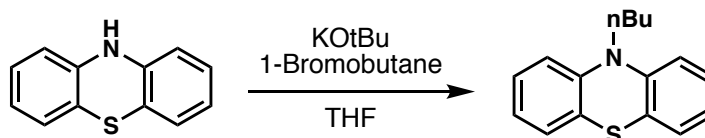
A flame dried 30 mL reaction tube was equipped with a magnetic stir bar and charged with 3,7-dibromo-*N*-butylphenothiazine (413 mg, 1.0 mmol, 1 equiv), *N,N'*-Dimethyl-*p*-phenylenediamine (136 mg, 1.00 mmol, 1 equiv), RuPhos ligand (9.3 mg, 0.02 mmol, 0.02 equiv), RuPhos Pd G2 precatalyst (15.5 mg, 0.0200 mmol, 0.02 equiv), and NaOtBu (212 mg, 2.20 mmol, 2.20 equiv). The reaction tube was evacuated and backfilled with N₂ three times and toluene (4 mL) was added via syringe, and the reaction was heated to 80 °C and stirred for 20 hours. The mixture was diluted in DCM and washed three times with water. The organic layer was concentrated and dried under vacuum, yielding 173.2 mg. ¹H NMR (CDCl₃) - Polymer was reduced with pentafluorophenylhydrazine: δ: 6.70-6.87 (10H, mult), 3.75 (2H, s), 3.18 (6H, s), 1.75 (2H, s), 2.19 (2H, mult), 0.93 (3H, t).

GPC Sample Preparation: Sonication with pentafluorophenylhydrazine in THF solubilized polymer for GPC analysis. M_n = 8.4 kg/mol, Dispersity = 1.9



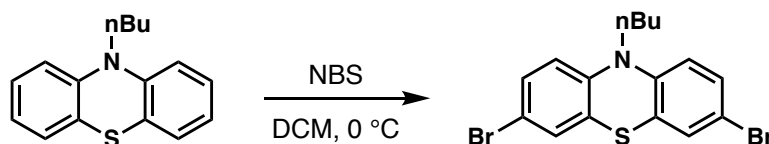
N-methylphenothiazine (1):

Phenothiazine (8.967 g, 45.00 mmol, 1 equiv) and KOtBu (7.574 g, 67.50 mmol, 1 equiv) were added to a round bottom flask and the flask was evacuated and backfilled with N₂ three times. Dry THF (90 mL) was added via cannula transfer and stirred at 0 °C for 15 minutes under a nitrogen atmosphere. Iodomethane (5.6 mL, 90 mmol, 2 equiv) at room temperature, was added and the reaction was allowed to proceed for 15 hours. The reaction was quenched with DI water and extracted with DCM. The organic layer was collected, dried with MgSO₄, and concentrated in vacuo. The product was purified by silica column chromatography (1:20 DCM:Hexanes), yielding 7.967 g (83% yield). ¹H NMR (CDCl₃, 500 MHz) δ: 7.16 (mult, 4H), 6.92 (td, 2H), 6.82, (d, 2H), 3.38 (s, 3H). ¹³C NMR (CDCl₃, 125 MHz) δ: 145.83, 127.42, 127.15, 123.41, 122.44, 114.06, 35.31. IR(ATR, cm⁻¹): 3053, 2879, 2816, 1591, 1567, 1454, 1443, 1330, 1135, 745. ⁶⁹



N-Butylphenothiazine:

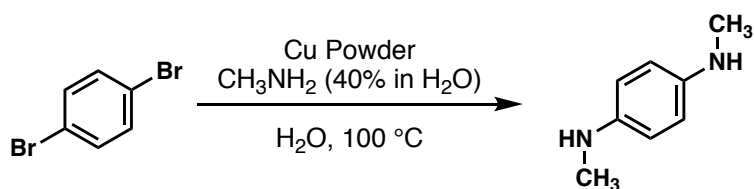
Phenothiazine (1.992 g, 10.00 mmol, 1 equiv) and KOtBu (1.683 g, 15.00 mmol, 1.5 equiv) were added to a round bottom flask and the flask was evacuated and backfilled with N₂ three times. Dry THF (90 mL) was added via cannula transfer and stirred for 15 minutes under a nitrogen atmosphere. 1-Bromobutane (1.07 mL, 10.0 mmol, 1 equiv) at room temperature, was added and the reaction was allowed to proceed overnight. The reaction was quenched with DI water, extracted with DCM, and washed with Na₂SO₃. The organic layer was collected, dried with MgSO₄, and concentrated in vacuo. The product was purified by silica column chromatography (1:4 DCM:Hexanes), yielding 1.50 g (59% yield). ¹H NMR (CDCl₃, 500 MHz) δ: 7.14 (mult, 4H), 6.88 (mult, 4H), 3.85 (t, 2H), 1.79 (quint, 2H), 1.46 (mult, 2H), 0.94 (t, 3H).⁷⁰



3,7-Dibromo-N-butylphenothiazine:

N-Butylphenothiazine (1.500 g, 5.873 mmol, 1 equiv) was charged to a round bottom flask and the flask was evacuated and backfilled with N₂ three times. Dry DCM (60 mL) was added to the flask and the temperature reduced to 0 °C. While stirring, NBS (2.085, 11.72 mmol, 2.0 equiv) was added under positive nitrogen pressure. The solution turned dark purple over the course of one hour. The reaction was allowed to proceed overnight. Reaction was diluted

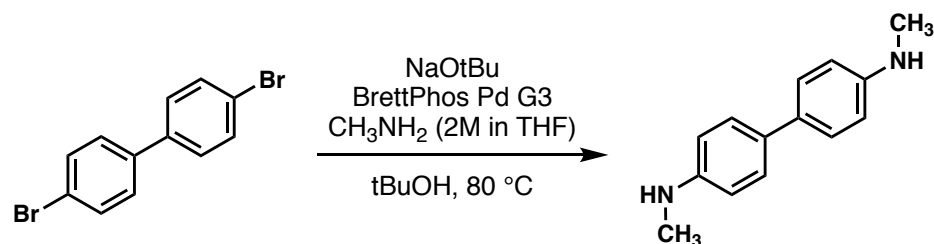
in DCM and shaken with saturated Na₂SO₃. Upon shaking, the organic layer turned light orange. The organic layer was washed with DI water three times. Organic layer was dried with MgSO₄ and concentrated. The product was purified by silica column chromatography (1:4 DCM:Hexanes), yielding 1.86 g (77% yield). ¹H NMR (CDCl₃, 500 MHz) δ: 7.21-7.25 (4H, mult), 6.69 (2H, d), 3.77 (2H, t), 1.73 (2H, quint), 1.43 (2H, mult), 0.92 (3H, t). ¹³C NMR (CDCl₃, 125 MHz) δ: 144.2, 130.1, 129.7, 126.5, 116.7, 114.8, 47.3, 28.8, 20.0, 13.7. IR (ATR, cm⁻¹): 3079, 3058, 2990, 2961, 2883, 2817, 1458, 1265, 748, 541 cm⁻¹.⁷¹



***N, N'*-Dimethyl-diaminobenzene (2a):**

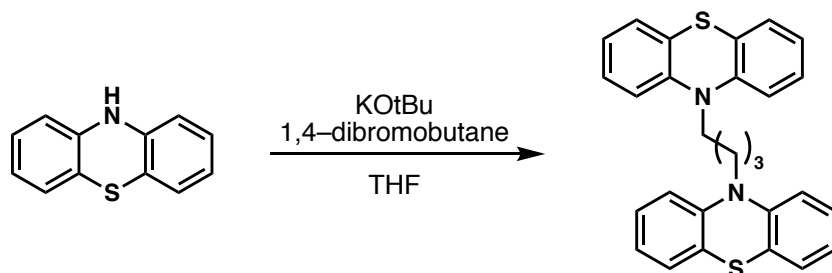
Dibromobenzene (2.359 g, 10.00 mmol, 1 equiv), methylamine (40% in water) (4.35 mL, 50.0 mmol, 5 equiv), Cu powder (32 mg, 0.50 mmol, 0.05 equiv) and 1 mL DI water were charged to a 25 mL Teflon sealed reaction tube. The reaction was stirred at 100 °C for 16 hrs. Product was extracted with EtOAc and washed with DI water. The crude product was purified by silica column chromatography (6:4 EtOAc:Hexanes), yielding 463 mg (34% yield). The isolated product is highly susceptible to oxidation, making characterization via ¹H NMR challenging. Hydrazine was added in order to confirm product identity and purity. ¹H NMR (CDCl₃, 300 MHz) δ: 6.59 (4H, s), 2.80 (6H, s). (Hydrazine was added to reduce product for NMR). ¹³C NMR (CDCl₃, 125 MHz) δ: 141.89,

114.30, 31.93 (Hydrazine was added to reduce product for NMR) IR ATR, cm^{-1}): 3377, 3339, 3019, 2981, 2863, 2799, 1513, 1471, 1446, 1246, 1153, 817.^{72,73}



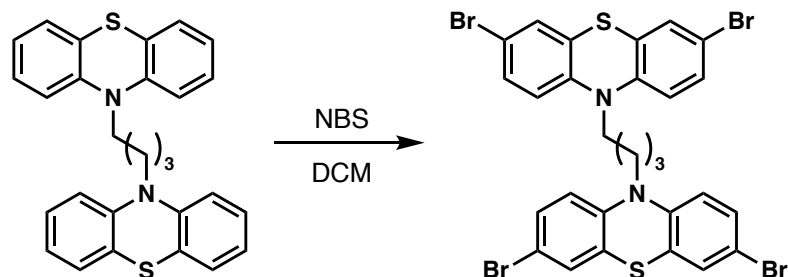
N,N'-dimethyl-benzidine (3a):

4,4'-Dibromobiphenyl (312 mg, 1.00 mmol, 1 equiv), NaOtBu (288 mg, 3.00 mmol, 3 equiv), and BrettPhos Pd G3 (4.5 mg, 0.005 mmol, 0.005 equiv) were charged to a 20 mL reaction tube. The reaction tube was evacuated and backfilled with N₂ three times. Methylamine (2M in THF) (2 mL, 4 mmol, 4 equiv) and *tert*-butanol (1 mL) were added via syringe. Reaction was allowed to proceed at 80 °C for 18 hours. Product was extracted with diethyl ether, washed with water three times, and concentrated in vacuo. Purification by silica column chromatography (4:6 Diethyl Ether:Hexanes) yielded 146 mg (69%) of the desired product. ¹H NMR (CDCl₃, 500 MHz) δ : 7.41 (d, 4H), 6.68 (d, 4H), 2.88 (s, 6H). ¹³C NMR (CDCl₃, 125 MHz) δ : 147.90, 130.72, 127.16, 112.77, 30.94. IR (ATR, cm^{-1}): 3406, 3272, 3020, 2876, 1609, 1504, 1322, 1282, 1249, 1179, 1153, 809.⁷⁴



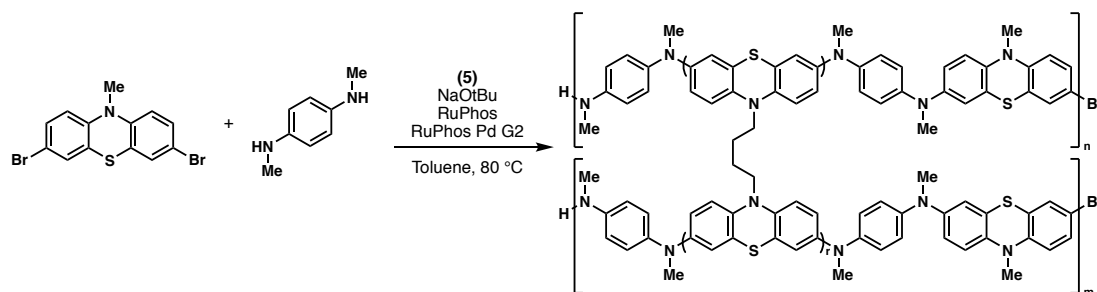
1,4-Di(10H-phenothiazin-10-yl)butane (4):

Phenothiazine (1.993 g, 10.00 mmol, 2.5 equiv) and KOtBu (1.345 g, 12.00 mmol, 3 equiv) were added to a round bottom flask and the flask was evacuated and backfilled three times with N₂. Dry THF (16 mL) was added and the solution stirred for 15 minutes. 1,4-Dibromobutane (0.48 mL, 4.0 mmol, 1 equiv) was added and the reaction proceeded overnight. Reaction was quenched with DI water, causing the desired product to precipitate from solution. The precipitate was filtered and washed with cold ethanol, removing all color from the pure white product. Upon drying under vacuo, 1.283 g (71% yield) desired product was obtained. ¹H NMR (500 MHz, CDCl₃) δ: 7.10 (mult, 8H), 6.89 (t, 4H), 6.79 (d, 4H), 3.87 (s, 4H), 1.94 (quint, 4H). ¹³C NMR (125 MHz, CDCl₃) δ: 145.12, 127.45, 127.21, 125.25, 122.44, 115.51, 46.60, 23.93. IR (ATR, cm⁻¹): 3055, 2935, 2850, 1590, 1567, 1484, 1449, 1440, 1311, 1179, 1052, 746. MS (DART) m/z: [M]⁺ Calcd for C₂₈H₂₄N₂S₂ 452.138; Found 452.138.



1,4-Bis(3,7-dibromo-10H-phenothiazin-10-yl)butane (5):

1,4-Di(10H-phenothiazin-10-yl)butane (**4**) (272 mg, 0.600 mmol, 1 equiv) and NBS (641 mg, 3.60 mmol, 6 equiv) were charged to a 25 mL reaction tube. The reaction tube was evacuated and backfilled three times with N₂. The reaction vessel was wrapped in aluminum foil to block any light from entering. THF (5 mL) was added and the reaction stirred at room temperature overnight. The reaction was diluted in DCM and quenched with 50 mL saturated Na₂SO₃. The biphasic solution was stirred for 30 minutes and the organic layer turned from dark purple to light yellow. The organic layer was washed with water and concentrated under vacuo. Purification by silica column chromatography (2:8 DCM:Hexanes) yielded 115 mg (25% yield) white crystalline product. ¹HNMR (CDCl₃, 500 MHz) δ: 7.20 (mult, 8H), 6.59 (t, 4H), 3.78 (s, 4H), 1.85 (unresolved quintet, 4H). ¹³C NMR (125 MHz, CDCl₃) δ: 143.87, 130.17, 129.82, 127.09, 116.88, 114.99, 46.56, 23.21. IR (ATR, cm⁻¹): 3058, 2915, 2848, 1449, 1385, 1325, 864, 796, 748, 542. MS (DART) m/z: [M]⁺ Calcd for C₂₈H₂₀N₂S₂Br₄ 768.779; Found 768.782.



PT-DMPD (5% CL) Polymer:

3,7-Dibromo-*N*-methylphenothiazine (334.0 mg, 0.9000 mmol, 0.9 equiv), *N,N'*-dimethyl-diaminobenzene (136.2 mg, 1.000 mmol, 1.0 equiv), **(5)** (38.4 mg, 0.05 mmol, 0.05 equiv), NaOtBu (240.3 mg, 2.500 mmol, 2.5 equiv), RuPhos (9.3 mg, 0.020 mmol, 0.02 equiv) and RuPhos Pd G2 (15.5 mg, 0.0200 mmol, 0.02 equiv) were charged to a 30 mL reaction tube. The reaction tube was evacuated and backfilled three times with N₂ and degassed (by sparging with N₂), and then dry toluene (5 mL) was added. The reaction was heated to 80 °C and stirred overnight. The mixture was allowed to cool to room temperature, and diluted into a 200 mL biphasic solution consisting of equal parts water and DCM. The insoluble polymer was filtered off and washed with an additional 100 mL of water and subsequently 100 mL of DCM. 178 mg light green polymer was collected after drying under vacuo. IR (ATR, cm⁻¹): 1508, 1466, 1319, 1250, 1134, 1110, 1070, 856, 822, 745.

PT-DMPD (10% CL) Polymer:

3,7-dibromo-*N*-methylphenothiazine (311.7 mg, 0.8399 mmol, 0.84 equiv), *N,N'*-dimethyl-diaminobenzene (136.2 mg, 1.000 mmol, 1.0 equiv), **(5)** (64.4 mg, 0.0838 mmol, 0.084 equiv), NaOtBu (211.4 mg, 2.200 mmol, 2.5

equiv), RuPhos (9.3 mg, 0.020 mmol, 0.02 equiv) and RuPhos Pd G2 (15.5 mg, 0.0200 mmol, 0.02 equiv) were charged to a 30 mL reaction tube. The reaction tube was evacuated and backfilled three times with N₂ and degassed (by sparging with N₂), dry toluene (5 mL) was added. The reaction was heated to 80 °C and stirred overnight. The mixture was allowed to cool to room temperature, and diluted into a 200 mL biphasic solution consisting of equal parts water and DCM. The insoluble polymer was filtered off and washed with an additional 100 mL of water and subsequently 100 mL of DCM. 214 mg light green polymer was collected after drying under vacuo.

PT-DMPD (33% CL) Polymer:

3,7-dibromo-*N*-methylphenothiazine (222.7 mg, 0.6001 mmol, 0.6 equiv), *N,N'*-dimethyl-diaminobenzene (136.2 mg, 1.000 mmol, 1.0 equiv), **(5)** (153.6 mg, 0.2000 mmol, 0.2 equiv), NaOtBu (211.4 mg, 2.200 mmol, 2.5 equiv), RuPhos (9.3 mg, 0.020 mmol, 0.02 equiv) and RuPhos Pd G2 (15.5 mg, 0.0200 mmol, 0.02 equiv) were charged to a 30 mL reaction tube. The reaction tube was evacuated and backfilled three times with N₂ and degassed (by sparging with N₂), dry toluene (5 mL) was added. The reaction was heated to 80 °C and stirred overnight. The mixture was allowed to cool to room temperature, and diluted into a 200 mL biphasic solution consisting of equal parts water and DCM. The insoluble polymer was filtered off and washed with an additional 100 mL of water and subsequently 100 mL of DCM. 309 mg light green polymer was collected after drying under vacuo.

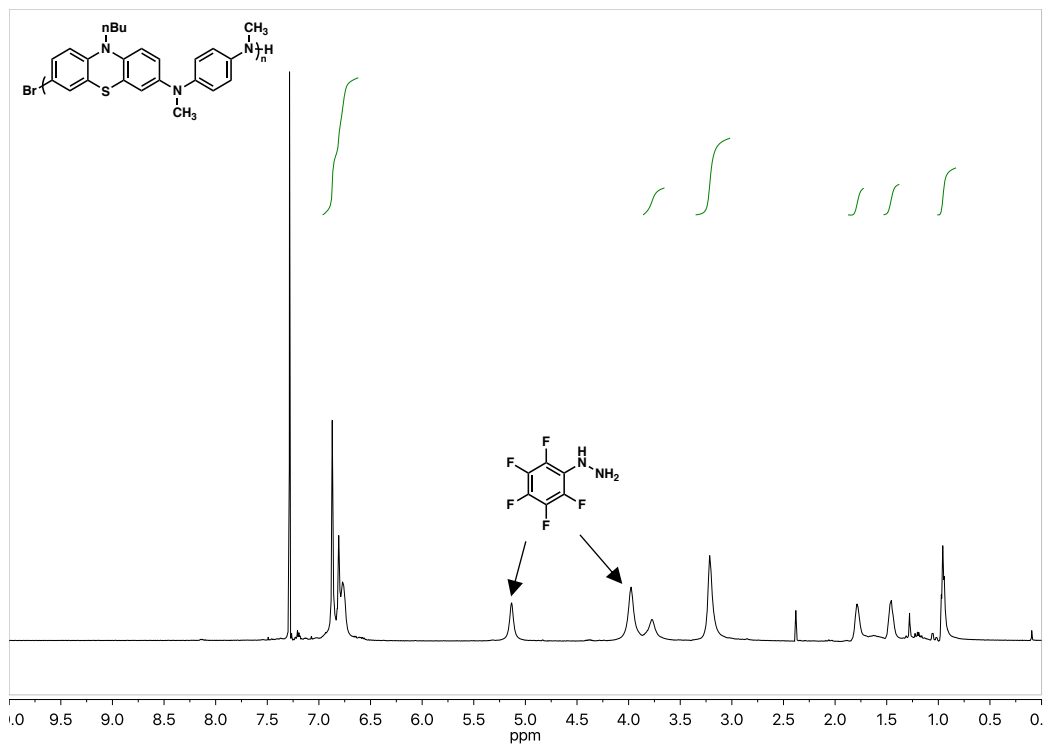


Figure 6.14. ^1H NMR spectrum of *n*Bu-PT-DMPD

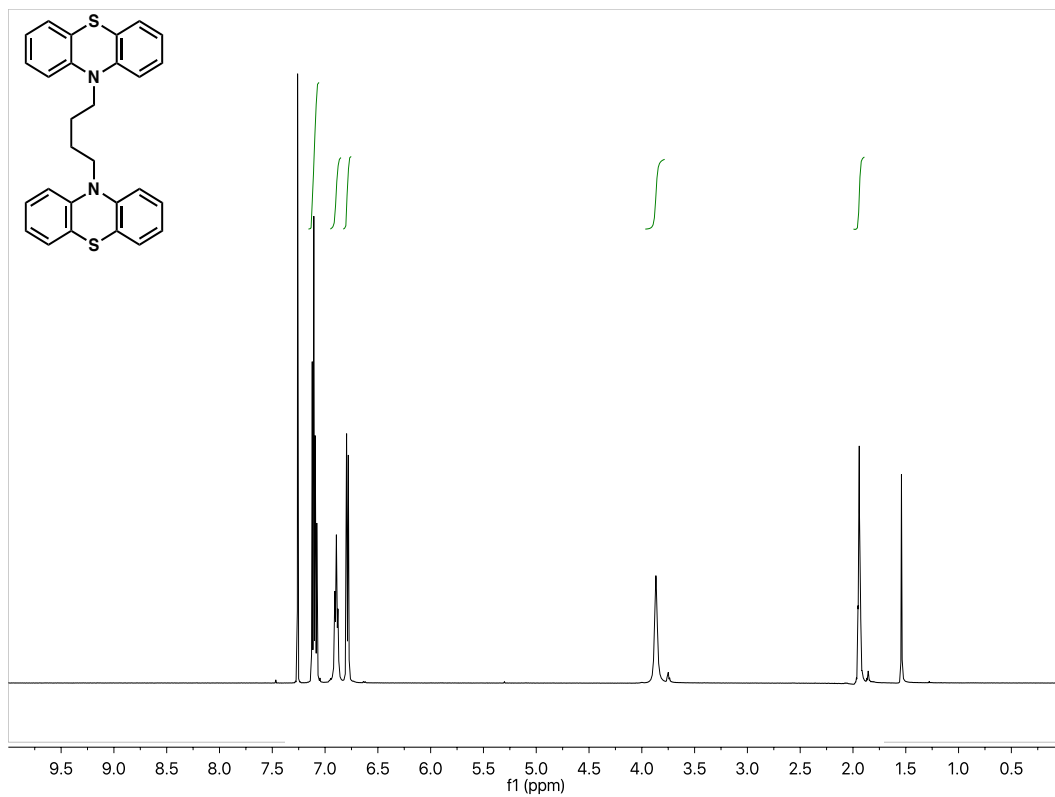


Figure 6.15. ^1H NMR spectrum of 1,4-di(10H-phenothiazin-10-yl)butane (4)

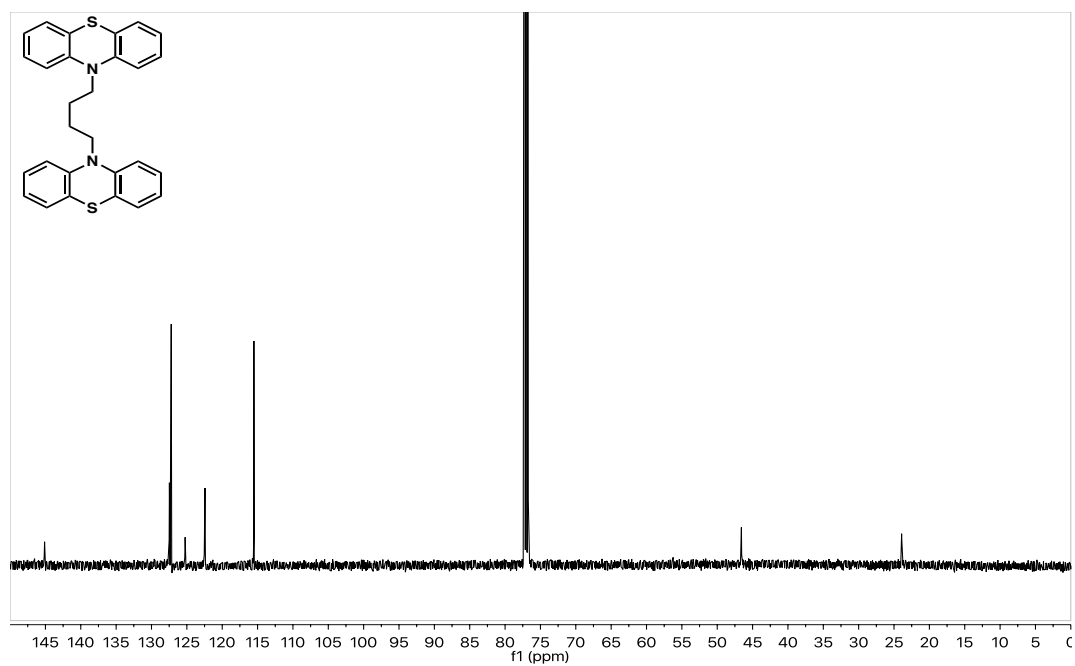


Figure 6.16. ^{13}C NMR spectrum of 1,4-di(10H-phenothiazin-10-yl)butane (4)

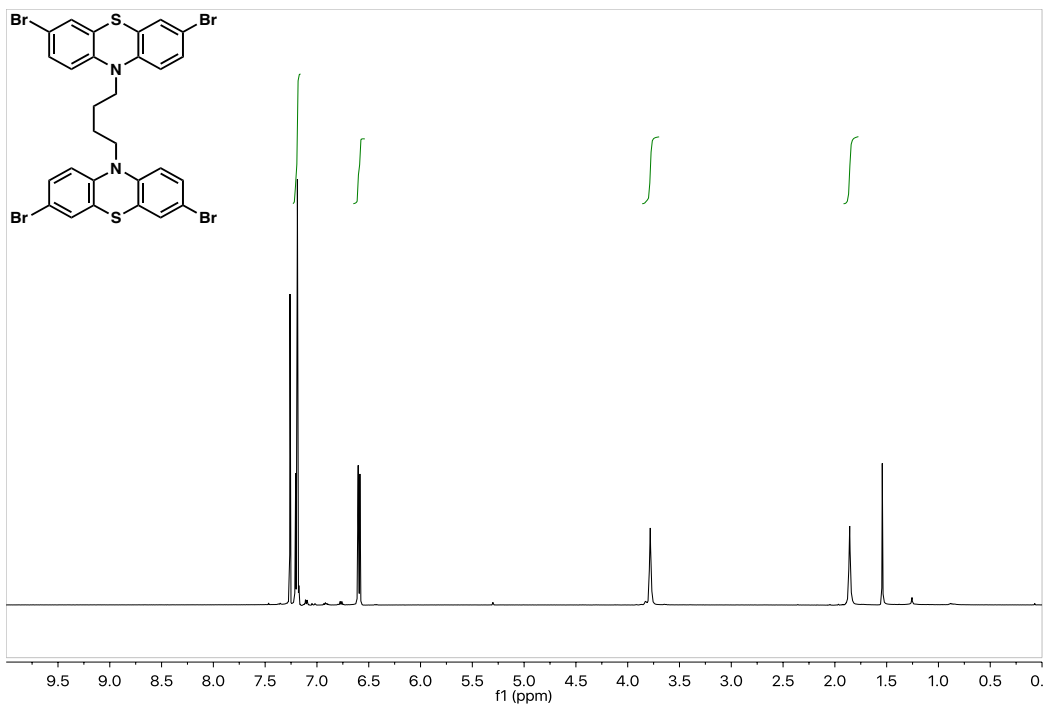


Figure 6.17. ¹H NMR spectrum of 1,4-bis(3,7-dibromo-10H-phenothiazin-10-yl)butane (5)

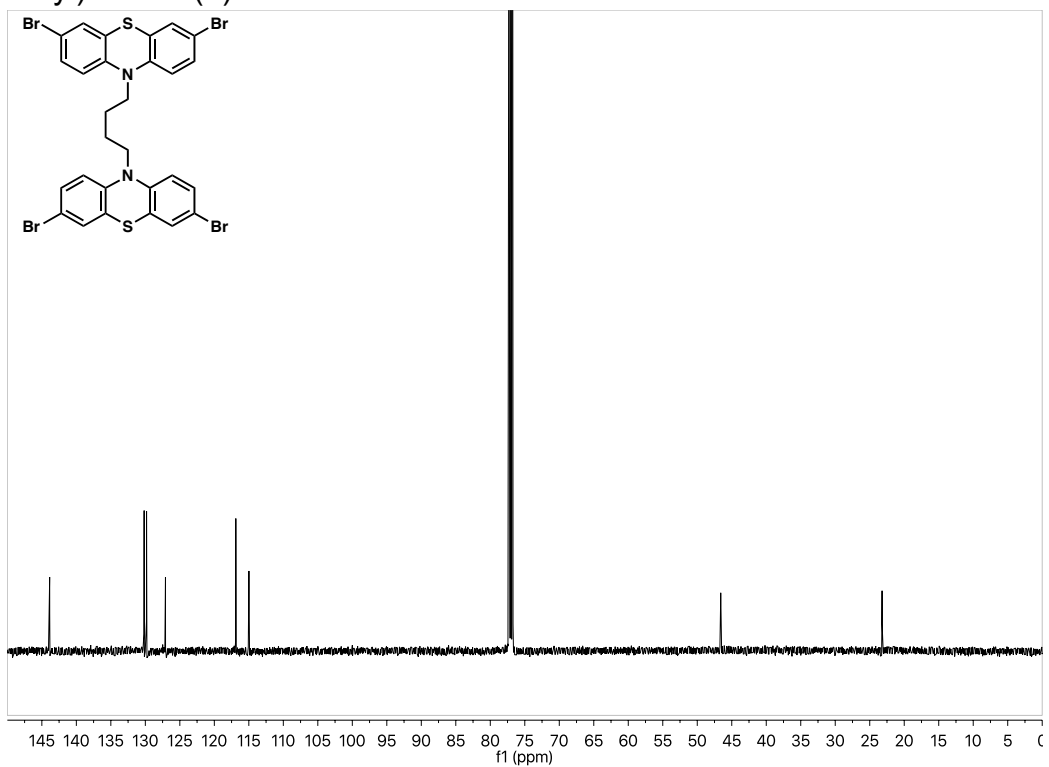


Figure 6.18. ¹³C NMR spectrum of 1,4-bis(3,7-dibromo-10H-phenothiazin-10-yl)butane (5)

2.6.1 Appendix References

- (1) Lin, H.-C.; Li, C.-C.; Lee, J.-T. *J. Power Sources* **2011**, *196*, 8098.
- (2) Wang, Y. H.; Hung, M. K.; Lin, C. H.; Lin, H. C.; Lee, J. T. *Chem. Commun.* **2011**, *47*, 1249.
- (3) Guo, W.; Yin, Y.-X.; Xin, S.; Guo, Y.-G.; Wan, L.-J. *Energy Environ. Sci.* **2012**, *5*, 5221.
- (4) Choi, W.; Ohtani, S.; Oyaizu, K.; Nishide, H.; Geckeler, K. E. *Adv. Mater.* **2011**, *23*, 4440.
- (5) Yoshihara, S.; Katsuta, H.; Isozumi, H.; Kasai, M.; Oyaizu, K.; Nishide, H. *J. Power Sources* **2011**, *196*, 7806.
- (6) Dai, Y.; Zhang, Y.; Gao, L.; Xu, G.; Xie, J. *J. Electrochem. Soc.* **2011**, *158*, A291.
- (7) Kiya, Y.; Iwata, A.; Sarukawa, T.; Henderson, J. C.; Abruña, H. D. *J. Power Sources* **2007**, *173*, 522.
- (8) Davoglio, R. A.; Biaggio, S. R.; Rocha-Filho, R. C.; Bocchi, N. *J. Power Sources* **2010**, *195*, 2924.
- (9) Sarukawa, T.; Oyama, N. *J. Electrochem. Soc.* **2010**, *157*, F23.
- (10) Fanous, J.; Wegner, M.; Grimminger, J.; Andresen, Ä.; Buchmeiser, M. R. *Chem. Mater.* **2011**, *23*, 5024.
- (11) Simmonds, A. G.; Griebel, J. J.; Park, J.; Kim, K. R.; Chung, W. J.; Oleshko, V. P.; Kim, J.; Kim, E. T.; Glass, R. S.; Soles, C. L.; Sung, Y.-E.; Char, K.; Pyun, J. *ACS Macro Lett.* **2014**, *3*, 229.
- (12) Geng, J.; Bonnet, J.-P.; Renault, S.; Dolhem, F.; Poizot, P. *Energy Environ. Sci.* **2010**, *3*, 1929.
- (13) Song, Z.; Zhan, H.; Zhou, Y. *Angew. Chem. Int. Ed. Engl.* **2010**, *49*, 8444.

- (14) Zeng, R.-H.; Li, X.-P.; Qiu, Y.-C.; Li, W.-S.; Yi, J.; Lu, D.-S.; Tan, C.-L.; Xu, M.-Q. *Electrochem. Commun.* **2010**, *12*, 1253.
- (15) Renault, S.; Geng, J.; Dolhem, F.; Poizot, P. *Chem. Commun.* (Cambridge, U. K.) **2011**, *47*, 2414.
- (16) Lei, Z.; Wei-kun, W.; An-bang, W.; Zhong-bao, Y.; Shi, C.; Yu-Sheng, Y. *J. Electrochem. Soc.* **2011**, *158*, A991.
- (17) Pirnat, K.; Dominko, R.; Cerc-Korosec, R.; Mali, G.; Genorio, B.; Gaberscek, M., *J. Power Sources* **2012**, *199*, 308.
- (18) Lee, M.; Hong, J.; Seo, D. H.; Nam, D. H.; Nam, K. T.; Kang, K.; Park, C. B. *Angew. Chem. Int. Ed. Engl.* **2013**, *52*, 8322.
- (19) Lee, M.; Hong, J.; Kim, H.; Lim, H. D.; Cho, S. B.; Kang, K.; Park, C. B. *Adv. Mater.* **2014**, *26*, 2558.
- (20) Wan, W.; Lee, H.; Yu, X.; Wang, C.; Nam, K.-W.; Yang, X.-Q.; Zhou, H. *RSC Adv.* **2014**, *4*, 19878.
- (21) Li, H.; Duan, W.; Zhao, Q.; Cheng, F.; Liang, J.; Chen, J. *Inorg. Chem. Front.* **1**, 193.
- (22) Iordache, A.; Maurel, V.; Mouesca, J.-M.; Pécaut, J.; Dubois, L.; Gutel, T. *J. Power Sources* **2014**, *267*, 553.
- (23) Kim, H.; Seo, D. H.; Yoon, G.; Goddard, W. A., 3rd; Lee, Y. S.; Yoon, W. S.; Kang, K. *J. Phys. Chem. Lett.* **2014**, *5*, 3086.
- (24) Gottis, S.; Barres, A. L.; Dolhem, F.; Poizot, P. *ACS Appl. Mater. Interfaces* **2014**, *6*, 10870.
- (25) Shimizu, A.; Kuramoto, H.; Tsujii, Y.; Nokami, T.; Inatomi, Y.; Hojo, N.; Suzuki, H.; Yoshida, J.-I. *J. Power Sources* **2014**, *260*, 211.

- (26) Vadehra, G. S.; Maloney, R. P.; Garcia-Garibay, M. A.; Dunn, B. *Chem. Mater.* **2014**, *26*, 7151.
- (27) Liang, Y.; Zhang, P.; Yang, S.; Tao, Z.; Chen, J. *Adv. Energy Mater.* **2013**, *3*, 600.
- (28) Kim, J.; Kim, J.; Lee, J.; Song, H.-K.; Yang, C. *ChemElectroChem* **2014**, *1*, 1618.
- (29) Shen, Y. F.; Yuan, D. D.; Ai, X. P.; Yang, H. X.; Zhou, M. *Electrochem. Commun.* **2014**, *49*, 5.
- (30) Song, Z.; Qian, Y.; Liu, X.; Zhang, T.; Zhu, Y.; Yu, H.; Otani, M.; Zhou, H. *Energy Environ. Sci.* **2014**, *7*, 4077.
- (31) Wu, H.; Shevlin, S. A.; Meng, Q.; Guo, W.; Meng, Y.; Lu, K.; Wei, Z.; Guo, Z. *Adv. Mater.* **2014**, *26*, 3338.
- (32) Tian, D.; Zhang, H.-Z.; Zhang, D.-S.; Chang, Z.; Han, J.; Gao, X.-P.; Bu, X.-H. *RSC Adv.* **2014**, *4*, 7506.
- (33) Shimizu, A.; Tsujii, Y.; Kuramoto, H.; Nokami, T.; Inatomi, Y.; Hojo, N.; Yoshida, J.-I. *Energy Technol.* **2014**, *2*, 155.
- (34) Fédèle, L.; Sauvage, F.; Bécuwe, M. *J. Mater. Chem. A* **2014**, *2*, 18225.
- (35) Wu, H.; Meng, Q.; Yang, Q.; Zhang, M.; Lu, K.; Wei, Z. *Adv. Mater.* **2015**, *27*, 6504.
- (36) Zhang, K.; Guo, C.; Zhao, Q.; Niu, Z.; Chen, J. *Adv Sci (Weinheim, Ger.)* **2015**, *2*, 1500018.
- (37) Hernández, G.; Casado, N.; Coste, R.; Shanmukaraj, D.; Rubatat, L.; Armand, M.; Mecerreyes, D. *RSC Adv.* **2015**, *5*, 17096.
- (38) Haupler, B.; Hagemann, T.; Friebe, C.; Wild, A.; Schubert, U. S. *ACS Appl. Mater. Interfaces* **2015**, *7*, 3473.

- (39) Schmidt, D.; Häupler, B.; Stolze, C.; Hager, M. D.; Schubert, U. S. *J. Polym. Sci., Part A: Polym. Chem.* **2015**, *53*, 2517.
- (40) Bhosale, M. E.; Krishnamoorthy, K. *Chem. Mater.* **2015**, *27*, 2121.
- (41) Chen, D.; Avestro, A. J.; Chen, Z.; Sun, J.; Wang, S.; Xiao, M.; Erno, Z.; Algaradah, M. M.; Nassar, M. S.; Amine, K.; Meng, Y.; Stoddart, J. F. *Adv. Mater.* **2015**, *2*, 2907.
- (42) Song, Z.; Qian, Y.; Gordin, M. L.; Tang, D.; Xu, T.; Otani, M.; Zhan, H.; Zhou, H.; Wang, D. *Angew. Chem. Int. Ed. Engl.* **2015**, *54*, 13947.
- (43) Song, Z.; Qian, Y.; Zhang, T.; Otani, M.; Zhou, H. *Adv. Sci. (Weinheim, Ger.)* **2015**, *2*, 1500124.
- (44) Liang, Y.; Chen, Z.; Jing, Y.; Rong, Y.; Facchetti, A.; Yao, Y. *J. Am. Chem. Soc.* **2015**, *137*, 4956.
- (45) Vlad, A.; Arnould, K.; Ernould, B.; Sieuw, L.; Rolland, J.; Gohy, J.-F. *J. Mater. Chem. A* **2015**, *3*, 11189.
- (46) Xu, F.; Jin, S.; Zhong, H.; Wu, D.; Yang, X.; Chen, X.; Wei, H.; Fu, R.; Jiang, D. *Sci. Rep.* **2015**, *5*, 8225.
- (47) Wu, J.; Rui, X.; Wang, C.; Pei, W.-B.; Lau, R.; Yan, Q.; Zhang, Q. *Adv. Energy Mater.* **2015**, *5*, 1402189.
- (48) Oltean, V. A.; Renault, S.; Brandell, D. *Electrochem. Commun.* **2016**, *68*, 45.
- (49) Xu, F.; Xia, J.; Shi, W. *Electrochem. Commun.* **2015**, *60*, 117.
- (50) Lakraychi, A. E.; Dolhem, F.; Djedāini-Pilard, F.; Thiam, A.; Frayret, C.; Becuwe, M. *J. Power Sources* **2017**, *359*, 198.
- (51) Wang, S.; Wang, Q.; Shao, P.; Han, Y.; Gao, X.; Ma, L.; Yuan, S.; Ma, X.; Zhou, J.; Feng, X.; Wang, B. *J. Am. Chem. Soc.* **2017**, *139*, 4258.

- (52) Xu, F.; Chen, X.; Tang, Z.; Wu, D.; Fu, R.; Jiang, D. *Chem. Commun.* **2014**, *50*, 4788.
- (53) Kim, J.; Park, H. S.; Kim, T. H.; Kim, S. Y.; Song, H. K. *Phys Chem. Chem. Phys.* **2014**, *16*, 5295.
- (54) Haupler, B.; Burges, R.; Friebe, C.; Janoschka, T.; Schmidt, D.; Wild, A.; Schubert, U. S. *Macromol Rapid Commun.* **2014**, *35*, 1367.
- (55) Su, C.; Yang, F.; Ji, L.; Xu, L.; Zhang, C. *J. Mater. Chem. A* **2014**, *2*, 20083.
- (56) Zhu, H.; Yin, J.; Zhao, X.; Wang, C.; Yang, X. *Chem. Commun.* **2015**, *51*, 14708.
- (57) Imada, Y.; Nakano, H.; Furukawa, K.; Kishi, R.; Nakano, M.; Maruyama, H.; Nakamoto, M.; Sekiguchi, A.; Ogawa, M.; Ohta, T.; Yamamoto, Y. *J. Am. Chem. Soc.* **2016**, *138*, 479.
- (58) Golriz, A. A.; Suga, T.; Nishide, H.; Berger, R.; Gutmann, J. S. *RSC Adv.* **2015**, *5*, 22947.
- (59) Zhang, S.; Huang, W.; Hu, P.; Huang, C.; Shang, C.; Zhang, C.; Yang, R.; Cui, G. *J. Mater. Chem. A* **2015**, *3*, 1896.
- (60) Wu, J.; Rui, X.; Long, G.; Chen, W.; Yan, Q.; Zhang, Q. *Angew. Chem. Int. Ed.* **2015**, *54*, 7354.
- (61) Speer, M. E.; Kolek, M.; Jassoy, J. J.; Heine, J.; Winter, M.; Bieker, P. M.; Esser, B. *Chem. Commun.* **2015**, *51*, 15261.
- (62) Godet-Bar, T.; Lepretre, J. C.; Le Bacq, O.; Sanchez, J. Y.; Deronzier, A.; Pasturel, A. *Phys. Chem. Chem. Phys.* **2015**, *17*, 25283.
- (63) Bitenc, J.; Pirnat, K.; Mali, G.; Novosel, B.; Randon Vitanova, A.; Dominko, R. *Electrochem. Commun.* **2016**, *69*, 1.

- (64) Xiang, J.; Sato, K.; Tokue, H.; Oyaizu, K.; Ho, C.-L.; Nishide, H.; Wong, W.-Y.; Wei, M. *Eur. J. Inorg. Chem.* **2016**, *7*, 1030.
- (65) Deunf, É.; Jiménez, P.; Guyomard, D.; Dolhem, F.; Poizot, P. *Electrochem. Commun.* **2016**, *72*, 64.
- (66) Kolek, M.; Otteny, F.; Schmidt, P.; Mück-Lichtenfeld, C.; Einholz, C.; Becking, J.; Schleicher, E.; Winter, M.; Bieker, P.; Esser, B. *Energy Environ. Sci.* **2017**, *10*, 2334.
- (67) Wild, A.; Strumpf, M.; Häupler, B.; Hager, M. D.; Schubert, U. S. *Adv. Energy Mater.* **2017**, *7*, 1601415.
- (68) Peng, C.; Ning, G.-H.; Su, J.; Zhong, G.; Tang, W.; Tian, B.; Su, C.; Yu, D.; Zu, L.; Yang, J.; Ng, M.-F.; Hu, Y.-S.; Yang, Y.; Armand, M.; Loh, K. P. *Nature Energy* **2017**, *2*, 17074.
- (69) Yang, C.-J.; Chang, Y. J.; Watanabe, M.; Hon, Y.-S. Chow, T. J. *J. Mater. Chem.* **2012**, *22*, 4040.
- (70) Zhao, S.; Kang, J.; Du, Y.; Kang, J.; Xiaoni, Z.; Xu, Y.; Chen, R.; Wang, Q.; Shi, X. *J. Heterocyclic Chem.* **2014**, *51*, 683.
- (71) Jo, M.-Y.; Lim, Y.-H.; Ahn, B.-H.; Lee, G.-D.; Kim, J.-H. *Bull. Korean. Chem. Soc.* **2012**, *33*, 492.
- (72) Jiao, J.; Zhang, X.-R.; Chang, N.-H.; Wang, J.; Wei, J.-F.; Shi, X.-Y.; Chen, Z.-G. *J. Org. Chem.* **2011**, *76*, 1180.
- (73) Lewis, F. D.; Kurth, T. L.; Delos Santos, G. B. *J. Phys. Chem. B.* **2005**, *109*, 4893.
- (74) Seth, K.; Raha Roy, S.; Chakraborti, A. K. *Chem. Commun.* **2016**, *52*, 922.

CHAPTER 7
ELUCIDATION OF THE ELECTROCHEMICAL BEHAVIOR OF
PHENOTHIAZINE-BASED POLYAROMATIC AMINES

7.1 Abstract

Polyarylamines with discrete redox active groups in the polymer backbone represent a promising class of cathode materials for electrical energy storage applications. In this area, our group recently reported a set of phenothiazine-based polymers that exhibit both high capacities and power densities. In order to rationally improve the properties of these electrode materials, a fundamental understanding of their electrochemical properties is indispensable. Herein, we probe the electrochemical behavior of our phenothiazine-based systems by synthesizing small molecule analogs using C–N cross-coupling. Additionally, electropolymerization of a class of these small molecule phenothiazines yields thin films that were then characterized with an electrochemical quartz crystal microbalance. Analysis of these materials provides insights into the number of electrons accessed from each repeat unit in our polymer backbone during electrochemical cycling, as well as counter ion transport dynamics.

7.2 Introduction

Polymeric organic cathodes are promising alternatives to inorganic materials, owing to their high elemental abundance and their ability to tolerate

fast charge rates due to facile ion transport in amorphous materials.¹⁻³ Many polymerization methods used to synthesize organic cathodes afford materials with insulating backbones and excess mass that does not contribute to charge storage.⁴⁻⁶ This limits electron mobility to the current collector, hindering charge-discharge rates, and decreases the energy density of the organic cathode. Polyanilines are one class of materials that have the potential to overcome these limitations as they can be doped to achieve modest conductivity; however, upon discharge a continuous voltage drop is observed. We reasoned that incorporation of discrete redox active heterocycles into the polyaromatic amine backbone could circumvent the voltage drop and provide cathode materials with high energy and power densities.

Phenothiazines and phenylenediamines are two classes of molecules that display reversible redox processes at high voltages relative to Li/Li⁺.^{4,7-16} Using Buchwald-Hartwig C–N cross-coupling chemistry,^{17,18} we envisioned that we could efficiently incorporate these units into a polyamine backbone to provide a new class of cathode materials.^{19,20} Using this strategy, completely insoluble materials, **P1** and **P2**, were obtained by cross-coupling dialkylphenylene diamines (**2** and **3**) with 3,7-dibromo-10-methylphenothiazine (**1**) (Figure 7.1.a) in a step growth polymerization using a RuPhos-based Pd precatalyst that was developed by Buchwald and coworkers.²¹ The polymers made from both phenylene diamine (**P1**) and benzidine (**P2**) showed multiple reversible redox couples. Additionally, lithium half-cells that incorporated these

polymers displayed specific capacities up to 150 mAhg^{-1} and could be discharged at 120 C while maintaining 81% of their capacity. These results demonstrated that main chain polymers consisting of phenothiazine and phenylene diamine lead to materials with high capacities and high power densities.

To improve these cathode materials we need a fundamental understanding of their electrochemical properties. For both polymers, **P1** and **P2**, solid state cyclic voltammetry (CV) displayed three main oxidations (-0.1 , 0.3 and 0.9 V) and two smaller redox couples ($0.6 - 0.9 \text{ V}$) (Figure 7.1.b). The presence of the latter two redox couples was unexpected. Full characterization of these two polymers was difficult due to their insolubility and inhomogeneity in chain lengths. In this manuscript, we synthesized and fully characterized small molecule analogs of these materials to gain a better understanding of their electrochemical behavior. Specifically, we synthesized phenothiazine based compounds that represents one and a half repeat units in the polymer backbone and fully characterize their redox processes. Further, we synthesized a small molecule analog that could be electrochemically polymerized to give **P2** on the surface of an electrode. We used such an approach to deposit films on the surface of a quartz crystal microbalance. This enables us to accurately quantify the number of oxidation events that are occurring per repeat unit on the polymer backbone, as well as characterize ionic transport and solvation dynamics.

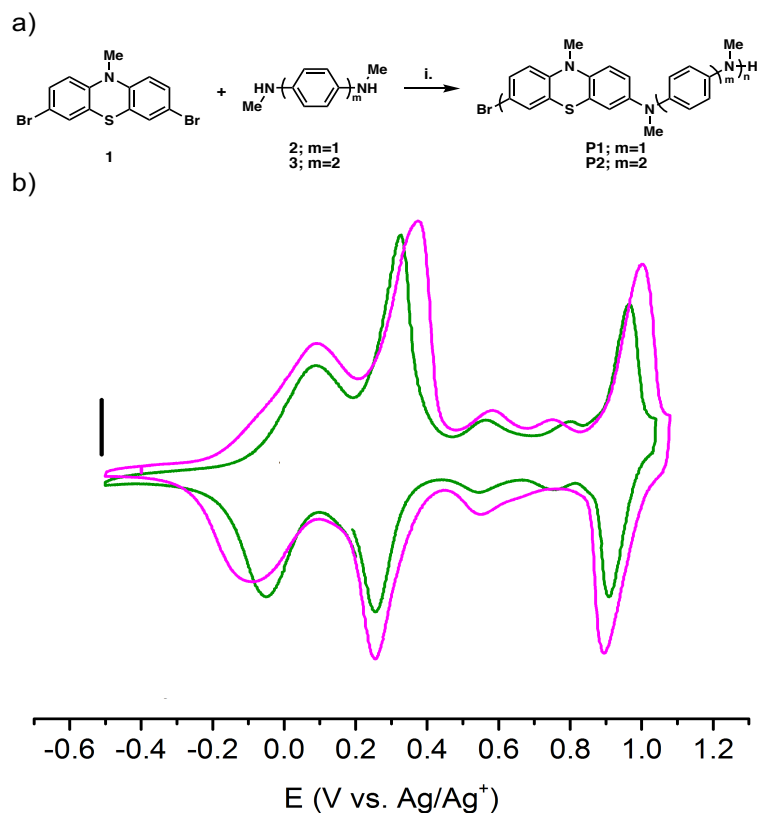


Figure 7.1. a) Synthesis of **P1** and **P2**; i. NaOtBu, RuPhos, RuPhos Pd G2 precatalyst, toluene, 80 °C
b) Slurry CV of **P1** (pink) and **P2** (green) in 1 M LiPF₆/MeCN at 20 mVs⁻¹ (scale bar 25 μA).

7.3 Results and Discussion

7.3.1 Synthesis of Redox Active Small Molecule

To investigate the redox properties of these polyphenothiazines, we targeted **C1**, a small molecule analog of **P1** that represents one and a half repeat units of the polymer backbone.²²⁻²⁶ Using two consecutive C–N cross-coupling reactions we were able to efficiently synthesize this molecule (Figure 7.2.a). First, 4-bromo-*N,N*-dimethyl aniline (**4**) was coupled with methyl amine

using a catalyst system developed by Buchwald and coworkers to yield the phenylene diamine **5**.^{27,28} A second cross-coupling between **1** with **5**, using a RuPhos-based Pd catalyst, gives **C1** in 67% yield.^{29,30} The small molecule analog, **C1**, quickly oxidizes in air; therefore, **C1** was kept under nitrogen and electrochemical studies were conducted in deoxygenated solvents.

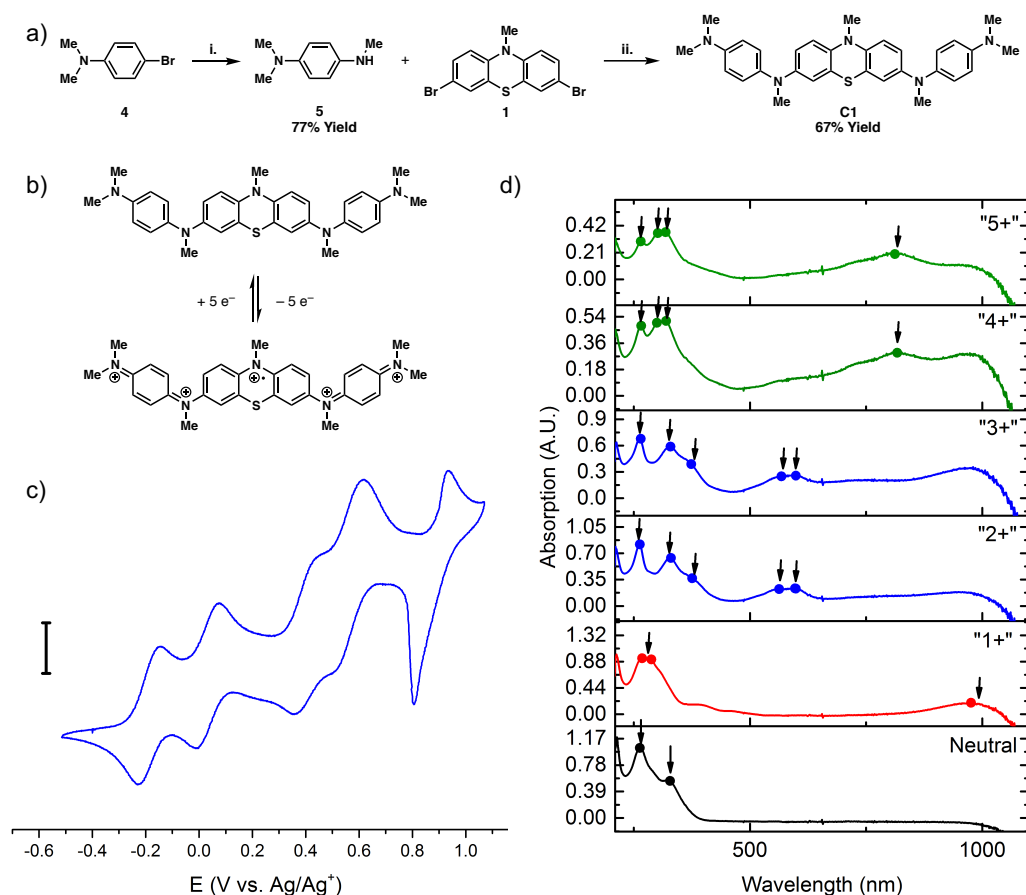


Figure 7.2. a) Synthesis of **C1**; i. NaOtBu, BrettPhos, BrettPhos Pd G3 precatalyst, methylamine, *t*BuOH, 80 °C; ii. NaOtBu, RuPhos, RuPhos Pd G2 precatalyst, dioxane, 80 °C; b) Oxidation of **C1** to the pentacationic state; c) CV of 0.5 mM **C1** in 0.1 M TBAP in 1:1 MeCN/DCM at 20 mVs⁻¹ (scale bar 5 μ A); d) UV-Visible absorption spectra of **C1** in each redox state; arrows indicate the major absorptions.

The CV of **C1** shows five reversible redox couples between -0.5 and 1.1 V vs. Ag/Ag⁺ (Figures 7.2.b and 7.2.c). The first four redox couples appear reversible, while the fifth oxidation is followed by adsorption onto the electrode. This degree of redox activity is rarely observed in soluble organic molecules. As **C1** is comprised of 1.5 repeat units of **P1**, four to five redox events were expected. The presence of five reversible redox events shows that the structural units of **P1** are indeed stable in a highly oxidized state.

The spectrochemical signature of **C1** in each oxidation state was characterized *in situ* (Fig. 7.2.d). We observed that the neutral and monocationic states exhibit distinct electronic absorption spectra, while similar absorption behavior was observed between the di- and tricationic states and between the tetra- and pentacationic states. In the UV region, distinct sets of electronic absorptions were observed in the neutral state, distinguished by absorptions at 263 and 328 nm, and in the monocationic state, at 268 and 288 nm. In the 400–800 nm region, di- and tricationic states show absorptions at 588 nm, while tetra- and pentacationic states exhibit absorptions at 817 nm.

7.3.2 Electropolymerization of Thin-Film P2-TF

When analyzing **P1** in a Li half-cell, we observed good agreement between theoretical and experimental capacity, if only two electrons are exchanged during charge and discharge. To further support our observation that we could efficiently access the first two redox couples of our polymers in the Li

which would allow us to accurately quantify the number of counterions transported in and out of the film when oxidized and reduced. This experiment would give us evidence for the number of electrons accessed from each repeat unit during cycling.

We proposed that we could deposit **P2** as a thin film (**P2-TF**) on an electrode surface through the electrochemical oxidative step growth polymerization of monomer **C2** (Figure 7.3.b), based on the fact that the electrochemical dimerization of anilines to benzidine is a well-studied and highly efficient reaction.^{14,31} To test our strategy, we synthesized monomer **C2** in 71% yield by coupling N-methylaniline with **1** (Figure 7.3.a). **C2** exhibited two highly reversible redox couples at 0.0 and 0.3 V (Figures 7.3.b and 7.3.c) and efficiently polymerized into a thin film upon a third oxidation at 1.3 V, which can be observed by an increase in current in subsequent cycles. In dichloromethane (DCM), adsorptive behavior is observed at high concentration, and deposition on the electrode can be monitored during sequential scans (Figure 7.3d). The coupling reaction can also be monitored spectroscopically (Figure 7.3e). The neutral, 1⁺ and 2⁺ states of the monomer can be clearly seen as the potential of the electrode is swept from -0.4 to 1.2 V. The coupled species between two tricationic **C2** species (**C2**³⁺) is observed when sweeping the potential in the reverse direction between 1.2 and 0.8 V, which is followed by polymer deposition on the electrode surface. Sweeping the potential to more negative values, any uncoupled **C2**³⁺ is reduced to the dication state, which can be

observed between 0.8 to 0.2 V. Once the potential of electrode is swept past 0.2 V, the characteristic spectral peak of **C2**²⁺ at approximately 850 nm recedes. Continuing to sweep between 0.2 and -0.4 V, the spectral signature of the 1⁺ oxidation state is observed before being reduced to neutral **C2** at -0.2 V.

7.3.3 Electrochemical Quartz Crystal Microbalance

With efficient conditions for the electrochemical formation of **P2-TF**, we set out to deposit a thin film on a quartz crystal microbalance electrode to perform electrochemical quartz crystal microbalance (EQCM) analysis during cycling.³² EQCM enables monitoring of the mass changes associated with ion movement and viscoelastic changes in a thin-film during electrochemical processes.³³⁻³⁵ Numerous studies have employed this method to elucidate transport dynamics in thin-film materials. To probe the redox mechanisms of **P2-TF** we employed EQCM to monitor the anion flux into the film as the polymer was oxidized in electrolyte solution. This enables us to determine the approximate number of electrons exchanged per repeat unit in **P2-TF**, and by extension **P1**, and **P2**.

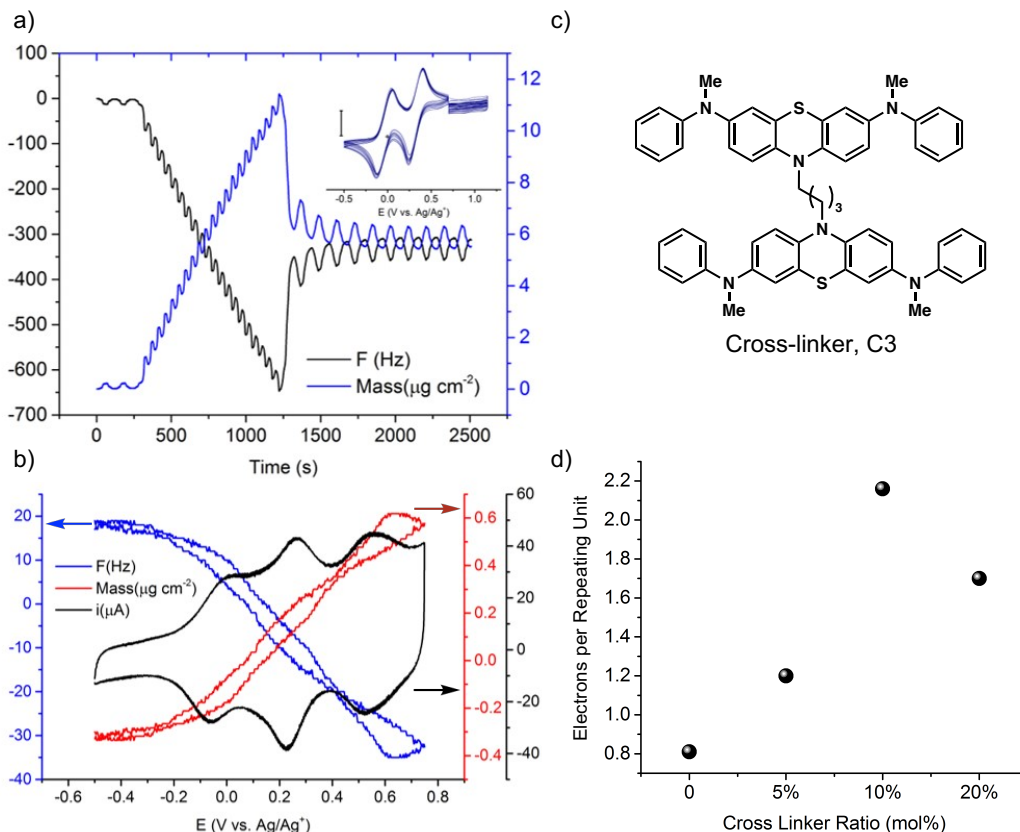


Figure 7.4. a) Frequency and mass changes during electropolymerization of **C2** on a QCM Au electrode. Inset shows the CV profile during the electropolymerization, polymerization was achieved by cycling between 0.7 – 1.15 V to accelerate film deposition (10 mM **C2** in 1 M TBAP/DCM, scale bar: 500 μA); b) The simultaneous change in frequency and mass during cycling of **P2-TF** in fresh electrolyte, 0.1 M TBAP/MeCN at 20 mVs^{-1} ; c) Chemical structure of cross-linker **C3**; d) The number of electrons exchanged during film cycling as a function of the amount of **C3** present during electropolymerization.

The EQCM experiment was divided into two parts: electropolymerization and film cycling (Figure 7.4.a). Polymer film mass was established by the frequency change of the QCM electrode in solution, before and after electropolymerization. Frequency and mass changes are minimal during the first two redox couples. However, when the potential of the gold electrode was scanned to 1.10 V, a sudden and large decrease in frequency, and increase in mass, associated with film deposition were observed, as seen in Figure 7.4.a through 1250 seconds. Typically, twenty cycles of electropolymerization yielded a film-thickness of 40 – 50 nm, as measured by contact profilometry. This yielded a mass loading in the range of a few $\mu\text{g cm}^{-2}$.

Upon completion of electropolymerization, **P2-TF** was subjected to cycling in blank electrolyte solution containing no monomer. During film cycling, frequency and mass changes are attributed to anion movement into and out of the polymer film, between 1250 and 2500 seconds in Figure 4a. Upon cycling the potential of the electrode between – 0.6 to 0.8 V the frequency decreased, corresponding to an increase in mass, which was attributed to an influx of charge compensating perchlorate ions into the polymer film (Figure 7.4.b). During the reverse scan, an increase in frequency, corresponding to a decrease in mass, is observed as anions diffuse out of **P2-TF**. Simultaneous resistance measurements indicate no significant changes in the viscoelastic properties during potential cycling. This confirms the rigid film nature of the **P2-TF**, and

allows for the direct application of the Sauerbrey equation, which correlates frequency changes to a change in mass on the QCM electrode.

Only the first two redox couples near 0.0 and 0.3 V could be studied, since the electrochemical stability of the gold electrode of the QCM does not allow potential sweeps beyond 0.8 V vs. Ag/Ag⁺. When the thin film is oxidized to the dication, approximately 0.8 counterions diffuse into the thin film, which is in contrast to our expectation that two counterions would be brought in during cycling to account for the two redox couples in the CV (Figure 7.4.d).

We hypothesized that this discrepancy in the capacity of our Li half-cells and EQCM studies could be explained by two scenarios: the film is not fully accessed by ions, leading to an underestimation of anions transported in, or a portion of the film was dissolving away while the electrode was washed. Film cycling in the presence of ferrocene, as a redox shuttle, could aid in unclogging any electronically or ionically isolated portions of film. However, no sign of unclogging or improvement of film accessibility was observed (Figure 7.15). Therefore, we hypothesized that if the film was indeed washing away when rinsed with acetone after the film was deposited, incorporation of a cross-linker could improve the polymer's adherence to the gold electrode (Figure 7.4.c). It is important to mention that we observed similar behavior in our Li half-cells. The linear polymer of **P1** showed significant capacity fade after every charging cycle due to dissolution of the active material. In our initial coin cell study we

demonstrated that cross-linking of the polymer film mitigated dissolution of the polymers.

Electropolymerization of **C2** with varying amounts of cross-linker **C3** to cross-link the thin film in the EQCM experiment could prevent dissolution of the thin film during washing. No difference was observed during electropolymerization or film cycling, as the addition of the cross-linker did not alter the polymer's redox activity (only a butyl-chain differentiates the cross-linker from the monomer, as shown in Fig 7.4.c). With incremental addition of cross-linker **C3** to the electropolymerization solution, the number of electrons exchanged increased to 2.17 per repeating unit at 10 mol% **C3**. At higher loadings of **C3** (20 mol%), a decrease in electrons exchanged per repeat unit was observed. This decrease at higher cross-linker content is likely due to transport limitations arising from the highly cross-linked network (Figure 7.4.d). These experiments are in good agreement with our coin cell studies where we found that the optimal cathode material contained 10% cross-linker. Moreover, these results suggest that two electrons are exchanged per repeat unit during potential sweeps through the first two redox couples. This is in excellent agreement with our previous study which showed an experimental capacity of 150 mAh g⁻¹ in agreement with the theoretical capacity for two electron energy storage in **P1** (152 mAh g⁻¹).

7.4 Conclusion

This study provides a thorough and comprehensive analysis of the electrochemical and spectrochemical behavior of two charge storing polymers synthesized by palladium-catalyzed C–N cross-coupling reactions. The investigation of the small molecule analog **C1**, provided confidence that the charge storing units in **P1** are stable in all accessible oxidation states. Analysis of the core structure of **P2** in a thin film provided evidence that nearly quantitative oxidation of the first two redox couples contributes to the experimental capacity observed in these phenothiazine based polyaromatic amines. The electropolymerization of cross-linked **P2-TF** was analyzed by EQCM and cycling the potential between the first two redox processes showed that 2.18 electrons are accessed per repeat unit. Through the analysis of small molecule and thin film analogs, the spectrochemical and electrochemical properties of a series of redox active polymer cathode materials were probed.

7.5 References

- (1) Zhao, Q.; Guo, C.; Lu, Y.; Liu, L.; Liang, J.; Chen, J.; *Ind. Eng. Chem. Res.* **2016**, *55*, 5795.
- (2) Schon, T. B.; McAllister, B. T.; Li, P.-F.; Seferos, D. S.; *Chem. Soc. Rev.* **2016**, *45*, 6345.
- (3) Novák, P.; Müller, K.; Santhanam, K. S. V.; Haas, O. *Chem. Rev.* **1997**, *97*, 207.

- (4) Conte, S.; Rodriguez-Calero, G. G.; Burkhardt, S. E.; Lowe, M. A.; Abruña, H. D.; *RSC Adv.* **2013**, *3*, 1957.
- (5) Y. Liang, Y.; Z. Tao, Z.; J. Chen, J. *Adv. Energy Mater.* **2012**, *2*, 742.
- (6) Muench, S.; Wild, A.; Friebe, C.; Häupler, B.; Janoschka, T.; Schubert, U. S. *Chem. Rev.* 2016, *116*, 9438.
- (7) Golriz, A. A.; Suga, T.; Nishide, H.; Berger, R.; Gutmann, J. S. *RSC Adv.* **2015**, *5*, 22947
- (8) Kolek, M.; Otteny, F.; Schmidt, P.; Mück-Lichtenfeld, C.; Einholz, C.; Becking, J.; Schleicher, E.; Winter, M.; Beiker, P.; Esser, B. *Energy Environ. Sci.* **2017**, *10*, 2334.
- (9) Godet-Bar, T.; Lepretre, J.-C.; Le Bacq, O.; Sanchez, J.-Y.; Deronzier, A.; Pasturel, A. *Phys. Chem. Chem. Phys.* **2015**, *17*, 25283.
- (10) Kowalski, J. A.; Casselman, M. D.; Kaur, A. P.; Milshtein, J. D.; Elliot, C. F.; Modekrutti, S.; Attanayake, N. H.; Zhang, N.; Parkin, S. R.; Risko, C.; Brushett, F. R.; Odom, S. A. *J. Mater. Chem. A.* **2017**, *5*, 24371.
- (11) Kong, X.; Kulkarni, A. P.; Jenekhe, S. A. *Macromolecules* **2003**, *36*, 8992.
- (12) Golriz, A. A.; Kaule, T.; Untch, M. B.; Kolman, K.; Berger, R.; Gutmann, J. S. *ACS Appl. Mater. Interfaces* **2013**, *5*, 2485.
- (13) Fungo, F.; Jenekhe, S. A.; Bard, A. J. *Chem. Mater.* **2003**, *15*, 1264.
- (14) Truong, T.-T.; Coates, G. W.; Abruña, H. D. *Chem. Commun.* **2015**, *51*, 14674.

- (15) Yang, H.; Wipf, D. O.; Bard, A. J. *J. Electroanal. Chem.* **1992**, 331, 913.
- (16) Mizoguchi, T.; Adams, R. N. *J. Am. Chem. Soc.* **1962**, 84, 2058.
- (17) Ruiz-Castillo, P.; Buchwald, S. L. *Chem. Rev.* **2016**, 116, 12564.
- (18) Hartwig, J. F. *Synlett*, **2006**, 0, 1283.
- (19) Singer, R. A.; Sadighi, J. P.; Buchwald, S. L. *J. Am. Chem. Soc.* **1998**, 120, 213.
- (20) Zhang, X.-X.; Sadighi, J. P.; Mackewitz, T. W.; Buchwald, S. L. *J. Am. Chem. Soc.* **2000**, 122, 7606.
- (21) Peterson, B. M.; Ren, D.; Shen, L.; Wu, Y.-C. M.; Ulgut, B.; Coates, G. W.; Abruña, H. D.; Fors, B. P. *ACS Appl. Energy Mater.* **2018**, 1, 3560.
- (22) Etori, H.; Kanbara, T.; Yamamoto, T. *Chem. Lett.* **1994**, 23, 461.
- (23) Nguyen, P.; Gómez-Elipe, P.; Manners, I. *Chem. Rev.* **1999**, 99, 1515.
- (24) Naka, K.; Uemura, T.; Chujo, Y. *Macromolecules* **2000**, 33, 6965.
- (25) Rulkens, R.; Lough, A. J.; Manners, I. *J. Am. Chem. Soc.* **1994**, 116, 797.
- (26) Rulkens, R.; Lough, A. J.; Manners, I.; Lovelace, S. R.; Grant, C.; Geiger, W. E. *J. Am. Chem. Soc.* **1996**, 118, 12683.
- (27) Fors, B. P.; Watson, D. A.; Briscoe, M. R.; Buchwald, S. L. *J. Am. Chem. Soc.* **2008**, 130, 13552.
- (28) Bruno, N. C.; Trudge, M. T.; Buchwald, S. L. *Chem. Sci.* **2013**, 4, 916.
- (29) Maiti, D.; Fors, B. P.; Henderson, J. L.; Nakamura, Y.; Buchwald, S. L. *Chem. Sci.* **2011**, 2, 57.

- (30) Kinzel, T.; Zhang, Y.; Buchwald, S. L. *J. Am. Chem. Soc.* **2010**, *132*, 14073.
- (31) Wei, D.; Kvarnström, C.; Lindfors, T.; Kronberg, L.; Sjöholm, R.; Ivaska, A. *Synth. Met.* **2006**, *156*, 541.
- (32) Buttry, D. A.; Ward, M. D. *Chem. Rev.* **1992**, *92*, 1355.
- (33) Borjas, R.; Buttry, D. A. *Chem. Mater.* **1991**, *3*, 872.
- (34) Hillman, A. R.; Loveday, D. C.; Bruckenstein, S. *Langmuir* **1991**, *7*, 191.
- (35) John, J.; Hugar, K. M.; Rivera-Meléndez, J.; Kostalik, H. A.; Rus, E. D.; Wang, H.; Coates, G. W.; Abruña, H. D. *J. Am. Chem. Soc.* **2014**, *136*, 5309.

7.6 Experimental

General Methods

Toluene, DCM, and THF were purchased from J.T. Baker and were purified by vigorous purging with argon for 2 h, followed by passing through two packed columns of neutral alumina under argon pressure. BrettPhos (96%), BrettPhos Pd G3 (95%), RuPhos (95%), RuPhos Pd G2, sodium *tert*-butoxide (NaOtBu), potassium *tert*-butoxide (KOtBu), anhydrous hydrazine, 4-bromo-*N,N'*-dimethylaniline (97%), and methylaniline were purchased from Sigma Aldrich and used as received. 1,4-dibromobutane (99%), phenothiazine (98%+), iodomethane (99.5%), and methylamine (2 M in THF) were purchased from Alfa Aesar and used as received. Anhydrous magnesium sulfate (MgSO₄)

was purchased from EMD Chemicals. *N*-Bromosuccinimide was purchased from Oakwood Chemicals and recrystallized from DI water before use as a brominating agent. Sodium sulfite (Na_2SO_3) was purchased from Fischer Scientific and used as received. Tetrabutylammonium perchlorate (TBAP) was purchased from TCI (>98%), and recrystallized from ethyl acetate (EtOAc) three times to obtain white crystal. Acetonitrile (MeCN) was purchased from Fisher (ACS grade) dried over activated 4 Å molecular sieves. 1-Methyl-2-pyrrolidinone (NMP, anhydrous, 99.5%) was purchased from Sigma Aldrich and used as received.

Nuclear magnetic resonance (NMR) spectra were recorded on a Mercury 300 MHz, a Varian 400 MHz or a Bruker 500 MHz. Cyclic voltammetric analysis on glassy carbon electrodes were performed on a Hokuto Denko HABF1050m potentiostat/galvanostat controlled by LabView program. UV-vis spectroscopy experiments were carried out using an Agilent/HP 8453 UV-visible spectroscopy system. Frequency, mass, and resistance data were measured on a Model QCM 200 Quartz Crystal Microbalance Digital Controller from Stanford Research Systems and processed by a SRS LabVIEW program. The temperature of the electrochemical system was controlled by a Fisher Scientific thermostat (Model No. 9101). 5 MHz AT-cut quartz crystals sputtered with gold were obtained from Maxtek, with a front electrode area of 1.37 cm² and used for EQCM experiments. Polymer **P1**, **P2** and small molecules 10-methylphenothiazine, 3,7-dibromo-10-methylphenothiazine (**1**), *N,N'*-dimethyl-

p-phenylenediamine (**2**), *N,N'*-dimethylbenzidine (**3**), 1,4-bis(3,7-dibromo-10*H*-phenothiazin-10-yl)butane were synthesized by literature procedures.²¹

***N,N,N'*-Trimethyl-*p*-phenylenediamine (**5**)**

4-Bromo-*N,N*-dimethylaniline (600 mg, 3 mmol, 1 equiv), NaOtBu (432.5 mg, 4.5 mmol, 1.5 equiv), BrettPhos (16.1 mg, 0.03 mmol, 0.01 equiv), BrettPhos Pd G3 (27.21 mg, 0.03 mmol, 0.01 equiv), and a magnetic stir bar were charged to a flame dried, 20 mL reaction tube and sealed with a Teflon cap. A nitrogen atmosphere was established and methylamine (2M in THF) (3 mL, 6 mmol, 2 equiv) and *tert*-butanol (6 mL) were added. The reaction was stirred at 80 °C for 7 hours. The reaction mixture was extracted into ethyl acetate (EtOAc) and washed with water. The organic layer was dried with MgSO₄ and concentrated. Purification by silica column chromatography (4:6 EtOAc:Hexanes) yielded 346 mg (77% yield) of the desired product. ¹H NMR (CDCl₃, 500 MHz): δ 6.77 (d, 2H), 6.62 (d, 2H), 2.83 (s, 6H), 2.81 (s, 3H). ¹³C NMR (CDCl₃, 126 MHz): δ 144.15, 142.06, 115.99, 113.89, 42.36, 31.74. IR (ATR, cm⁻¹): 3397, 3022, 2941, 2873, 2799, 1520, 1476, 1447, 1304, 815.

***N',N'*-(10-methyl-10*H*-phenothiazine-3,7-diyl)bis(*N',N',N'*-trimethylbenzene-1,4-diamine) (**C1**)**

3,7-Dibromo-*N*-methylphenothiazine (93 mg, 0.25 mmol, 1 equiv), *N,N,N'*-trimethyl-1,4-diaminobenzene (115 mg, 0.75 mmol, 3 equiv), NaOtBu (75 mg, 0.75 mmol, 3 equiv), RuPhos (2.3 mg, 2.5 μmol, 0.01 equiv), RuPhos Pd

G2 (3.8 mg, 2.5 μmol , 0.01 equiv), and a magnetic stir bar were charged to a flame dried, 20 mL reaction tube and sealed with a Teflon cap. A nitrogen atmosphere was established and dioxane (2 mL) was added via syringe. The reaction was stirred at 80 °C for 16 hours. After cooling, the reaction was diluted with EtOAc and washed with DI water. The organic layer was dried with MgSO_4 and concentrated. Purification by silica column chromatography (2:3 EtOAc:Hexanes) yielded 80 mg (63%) of the desired product. Hydrazine was added to NMR to prevent oxidation of product. ^1H NMR (500 MHz, CDCl_3) δ 6.95 (d, $J = 8.9$ Hz, 4H), 6.71 (d, $J = 8.9$ Hz, 4H), 6.68 (t, $J = 1.5$ Hz, 2H), 6.64 (d, $J = 1.6$ Hz, 4H), 3.27 (s, 3H), 3.16 (s, 6H), 2.91 (s, 12H). ^{13}C NMR (126 MHz, CDCl_3) δ 147.1, 145.6, 139.8, 138.9, 124.4, 124.0, 116.3, 116.1, 114.0, 113.9, 41.2, 40.9, 35.1; IR (ATR, cm^{-1}): 2933, 2821, 2781, 1515, 1485, 1450, 1326, 1259, 820; HRMS (DART): m/z calc'd for $(\text{M}+\text{H})^+$ [$\text{C}_{31}\text{H}_{36}\text{N}_5\text{S}$] $^+$: 510.2691, found 510.2693.

N³,N⁷-10-trimethyl-N³,N⁷-diphenyl-10H-phenothiazine-3,7-diamine (C2)

1 (743 mg, 2mmol, 1 equiv), RuPhos ligand (9.7 mg, 0.02 mmol, 0.01 equiv), RuPhos Pd G2 precatalyst (15.5 mg, 0.02 mmol, 0.01 equiv), NaOtBu (575 mg, 6 mmol, 3 equiv), and a magnetic stir bar were charged to a flame dried, 20 mL reaction tube and sealed with a Teflon cap. A nitrogen atmosphere was established and *N*-Methylaniline (0.44 mL, 4 mmol, 2 equiv) and dioxane (2 mL) were added via syringe. The reaction was stirred at 80 °C for 16 hrs.

After cooling, the reaction was diluted with DCM and washed with DI water three times. The organic layer was dried with MgSO₄ and concentrated. Purification by silica column chromatography (1:1 DCM:Hexanes) yielded 562 mg (66% yield) of the desired product. ¹H NMR (500 MHz, C₆D₆) δ 7.14 (m, 4H), 6.95 (d, *J* = 2.5 Hz, 4H), 6.84 (d, *J* = 8.3 Hz, 4H), 6.83 – 6.78 (m, 4H), 6.33 (d, *J* = 8.6 Hz, 2H), 2.87 (s, 6H), 2.74 (s, 3H); ¹³C NMR (125 MHz, C₆D₆) δ 149.9, 144.5, 142.2, 129.4, 125.0, 123.2, 123.1, 119.8, 117.6, 114.7, 40.2, 35.0; HRMS (DART): *m/z* calc'd for (M+H)⁺ [C₂₇H₂₆N₃S]⁺: 424.1847, found 424.1845.

10,10'-(butane-1,4-diyl)bis(N³,N⁷-dimethyl-N³,N⁷-diphenyl-10H-phenothiazine-3,7-diamine) (C3)

1,4-bis(3,7-dibromo-10*H*-phenothiazin-10-yl)butane (115 mg, 0.15 mmol, 1 equiv), NaOtBu (96.1 mg, 1 mmol, 6.6 equiv), RuPhos (1.4 mg, 0.003 mmol, 0.02 equiv), RuPhos Pd G2 (2.3 mg, 0.003 mmol, 0.02 equiv), and a magnetic stir bar were charged to a flame dried, 20 mL reaction tube and sealed with a Teflon cap. A nitrogen atmosphere was established and methylaniline (0.1 mL, 0.9 mmol, 6 equiv) and dioxane (1 mL) were added via syringe. The reaction was stirred at 80 °C overnight. The reaction was quenched with Na₂SO₃ and stirred for 30 minutes. Product was extracted into DCM and dried with MgSO₄. The organic layer was concentrated and dried under vacuo. The product was isolated by recrystallization from benzene yielding 78 mg (59% yield) of light green powder. ¹H NMR (500 MHz, C₆D₆) δ 7.11 (dd, *J* = 8.7, 7.2

Hz, 8H), 6.97 (d, $J = 2.5$ Hz, 4H), 6.87 – 6.77 (m, 16H), 6.46 (d, $J = 8.7$ Hz, 4H), 3.39 (m, 4H), 2.86 (s, 12H), 1.71 (m, 4H); ^{13}C NMR (125 MHz, C_6D_6) δ 149.4, 144.3, 141.0, 129.1, 126.4, 122.6, 122.4, 119.7, 117.7, 116.0, 46.4, 39.9, 24.0; IR (ATR, cm^{-1}): 3053, 2919, 2848, 2805, 1593, 1493, 1455, 1250, 1153, 1129, 1088, 748; HRMS (DART): m/z calc'd for $(\text{M}+\text{H})^+$ [$\text{C}_{56}\text{H}_{53}\text{N}_6\text{S}_2$] $^+$: 873.3773, found 873.3787.

Dedication

In honor of Prof. Stephen L Buchwald for his mentorship and leadership in the field of organic chemistry.

7.7 Appendix

Materials and Reagents:

The results of electrochemical experiments on UV-vis spectro-electrochemistry and EQCM were recorded on a VersaSTAT 3 processed with VersaStudio software. Spectro-electrochemical experiments were carried out in a SEC-C thin layer quartz glass spectro-electrochemical cell with 0.5 mm cell length from BASi. Platinum (Pt) mesh working electrode was homemade using Pt mesh and was anchored to a Pt wire. Teflon was used to wrap Pt wire beyond the Pt mesh to avoid further reactions during the electrochemical experiment.

All electrochemical measurements were performed in a three-neck glass cell. A Ag/Ag $^+$ reference electrode and a Pt wire counter electrode were used unless otherwise specified. All potentials are referenced to a Ag/Ag $^+$ reference

electrode, which is 0.50 V vs. NHE. GC electrodes were homemade by wrapping a GC slug in a Teflon casing. Before experimentation, all solutions were subjected to 10 minutes of degassing with Ar or N₂ to prevent undesired side reactions and oxygen reduction in the potential window probed.

The following procedure was taken to clean GC electrodes before use: the electrodes were sonicated in ethanol for 30 seconds before polishing with diamond paste. Upon polishing, the electrode was sonicated in ethanol for an additional 30 seconds and then dried with an infrared lamp before drop-casting the slurry sample or obtaining a CV.

The following procedure was taken to clean the Au QCM electrode before use: any residual organics were removed with acetone using a fine swab that does not scratch surfaces. The Au electrode was then cycled in 0.1 M HClO₄ between -0.2 and 1.4 V vs. Ag/AgCl at 200 mVs⁻¹ until a clean and stable current profile was obtained.

Slurry Preparation:

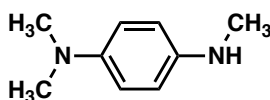
2.0 mg of bulk polymer, 2.5 mg of carbon black and 0.5 mg of PVDF were mixed in a 5 mL vial with 1 mL NMP. Such composition gives a composite loading of 5 mg mL⁻¹. The mixture was sonicated for at least 1 hour until the mixture was homogeneously dispersed in solvent. Then 10 μL of ink was drop-casted onto a GC surface to create a polymer loading of 57 μg cm⁻².

Even though the powder polymers were insoluble in conventional organic solvents, when oxidized the polymers become highly soluble, as the slurry on

GC dissolves as the materials became oxidized. Since the materials were lost during cycling, scan rate dependence and other quantitative analysis was not performed on CVs obtained from slurries.

Synthesis and Characterization:

Polymer **P1**, **P2**, and small molecules 10-methylphenothiazine, 3,7-dibromo-10-methylphenothiazine (**1**), *N,N'*-dimethyl-*p*-phenylenediamine (**2**), *N,N'*-dimethylbenzidine (**3**), *N,N,N'*-trimethyl-*p*-phenylenediamine (**5**), and 1,4-bis(3,7-dibromo-10*H*-phenothiazin-10-yl)butane were synthesized according to literature procedures.¹



N,N,N'-trimethyl-1,4-diaminobenzene (**5**)²

4-Bromo-*N,N*-dimethylaniline (600 mg, 3 mmol, 1 equiv), NaOtBu (432.5 mg, 4.5 mmol, 1.5 equiv), BrettPhos (16.1 mg, 0.03 mmol, 0.01 equiv), BrettPhos Pd G3 (27.2 mg, 0.03 mmol, 0.01 equiv) and a magnetic stir bar were charged to a flame dried, 20 mL reaction tube and sealed with a Teflon cap. A nitrogen atmosphere was established and methylamine (2M in THF) (3 mL, 6 mmol, 2 equiv) and *tert*-butanol (6 mL) were added. The reaction was stirred at 80 °C for 7 hours. The reaction mixture was extracted into EtOAc and washed with water. The organic layer was dried with MgSO₄ and concentrated *in vacuo*. Purification by silica column chromatography (1:1.5 EtOAc:hexanes) yielded

346 mg (77% yield) of the desired product. ^1H NMR (CDCl_3 , 500 MHz): δ 6.77 (d, 2 H), 6.62 (d, 2 H), 2.83 (s, 6 H), 2.81 (s, 3 H) ppm. ^{13}C NMR (CDCl_3 , 126 MHz): δ 144.15, 142.06, 115.99, 113.89, 42.36, 31.74 ppm. IR (ATR, cm^{-1}): 3397, 3022, 2941, 2873, 2799, 1520, 1476, 1447, 1304, 815.

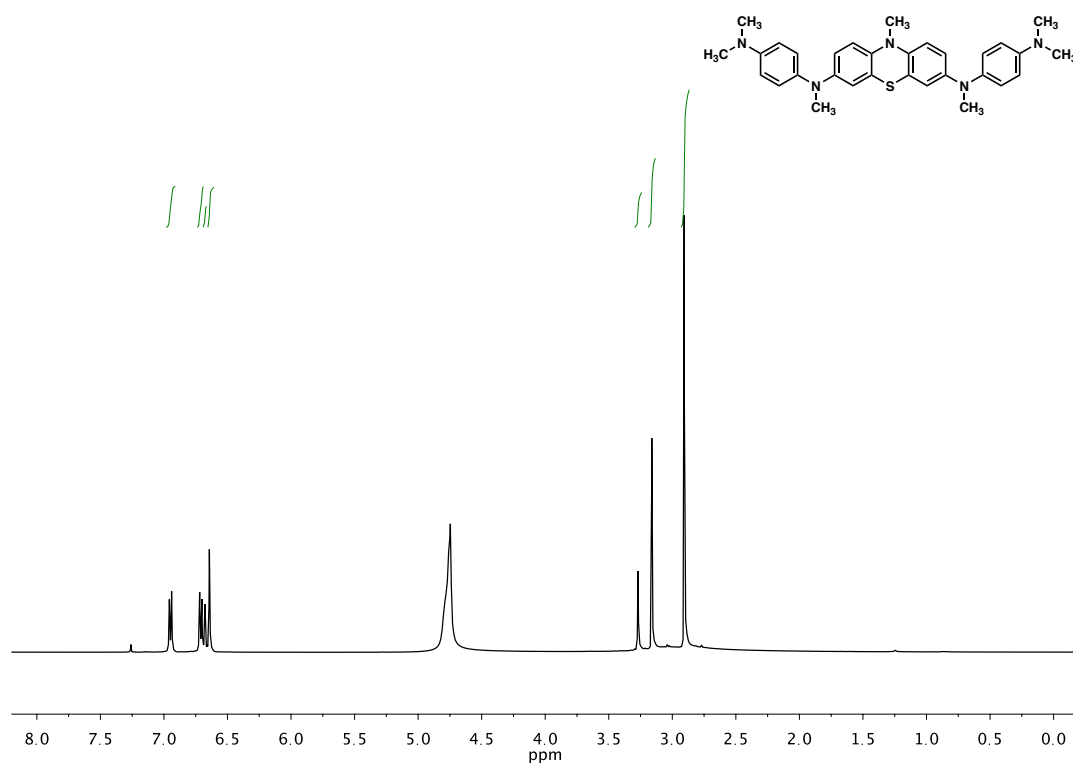


Figure 7.5. ^1H NMR of N_1,N_1' -(10-methyl-10H-phenothiazine-3,7-diyl)bis($\text{N}_1,\text{N}_4,\text{N}_4$ -trimethylbenzene-1,4-diamine) in CDCl_3 with added hydrazine added (C1).

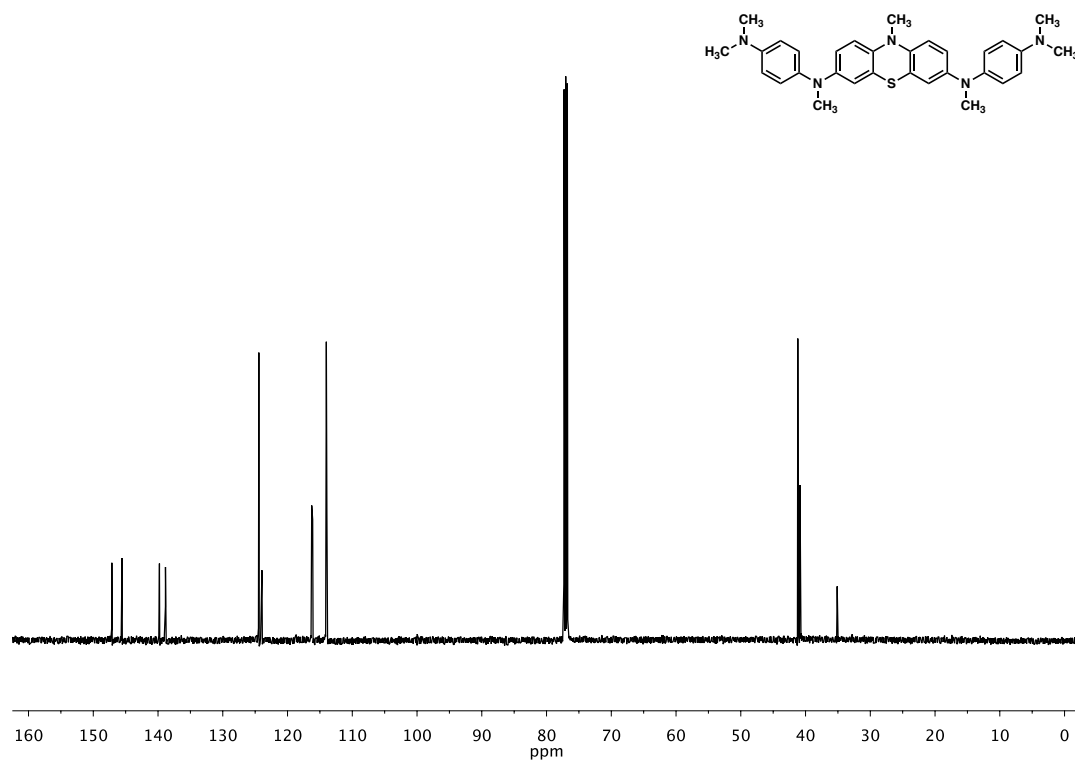


Figure 7.6. ^{13}C NMR of $\text{N}^1, \text{N}^{1'}\text{-}(10\text{-methyl-}10\text{H-phenothiazine-}3,7\text{-diyl})\text{bis}(\text{N}^1, \text{N}^4, \text{N}^4\text{-trimethylbenzene-}1,4\text{-diamine})$ in CDCl_3 (C1).

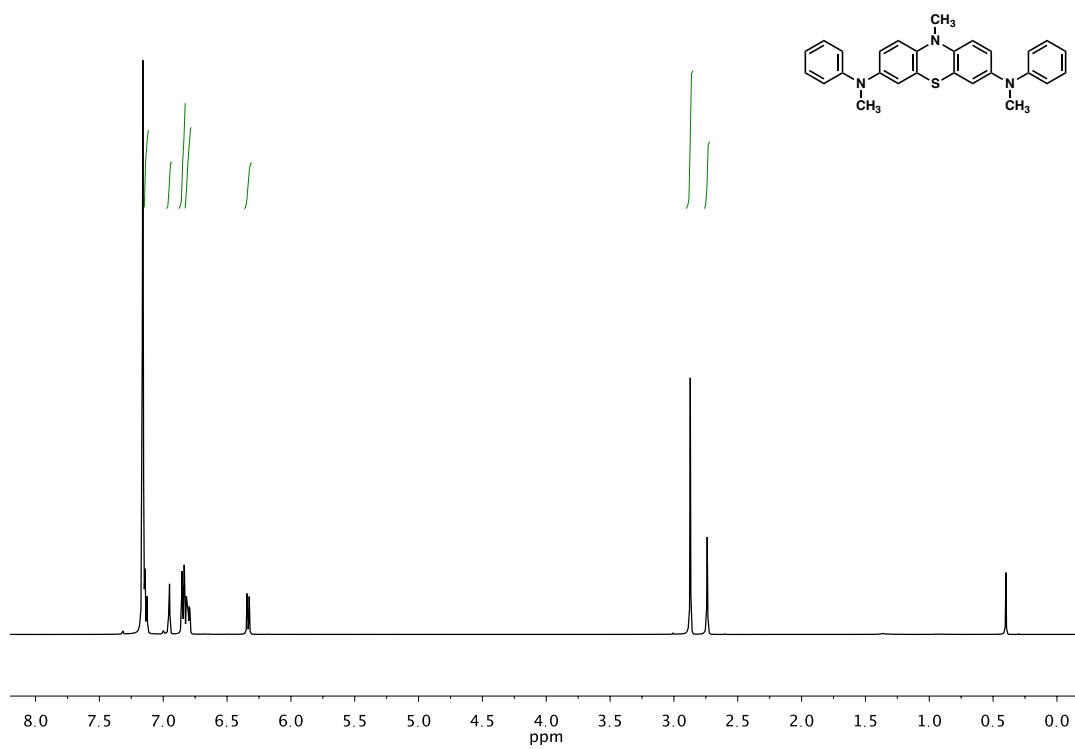


Figure 7.7. ¹H NMR of N3, N7-10-trimethyl-N3,N7-diphenyl-10H-phenothiazine-3,7-diamine in C₆D₆ (C2).

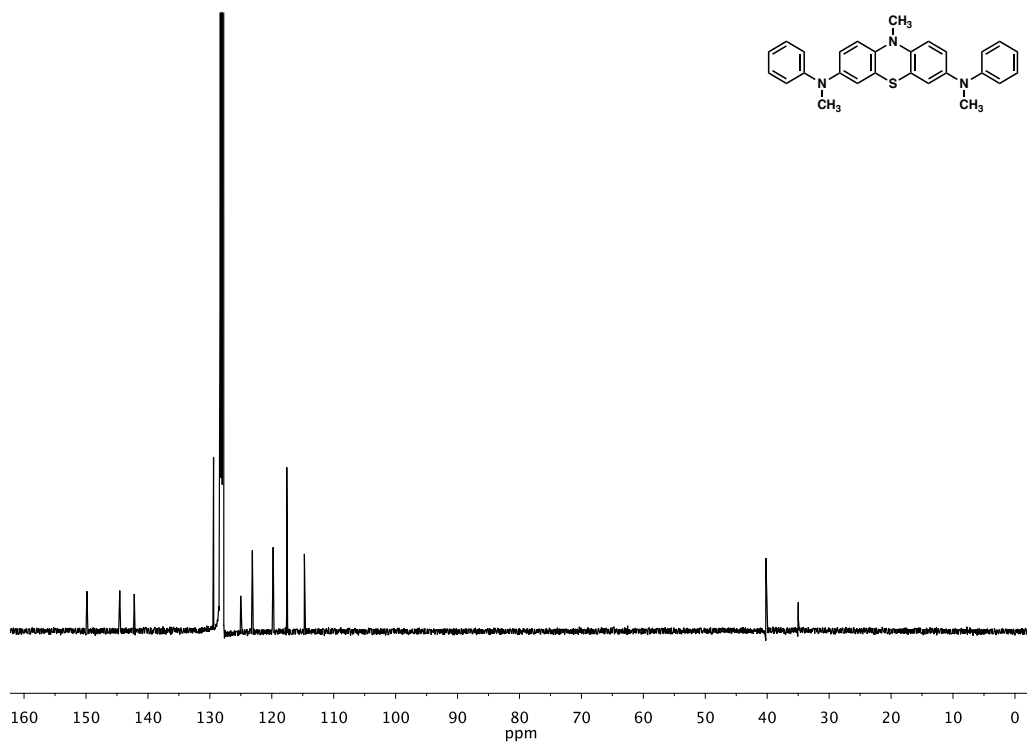


Figure 7.8. ^{13}C NMR of N3, N7-10-trimethyl-N3,N7-diphenyl-10H-phenothiazine-3,7-diamine in C_6D_6 (C2).

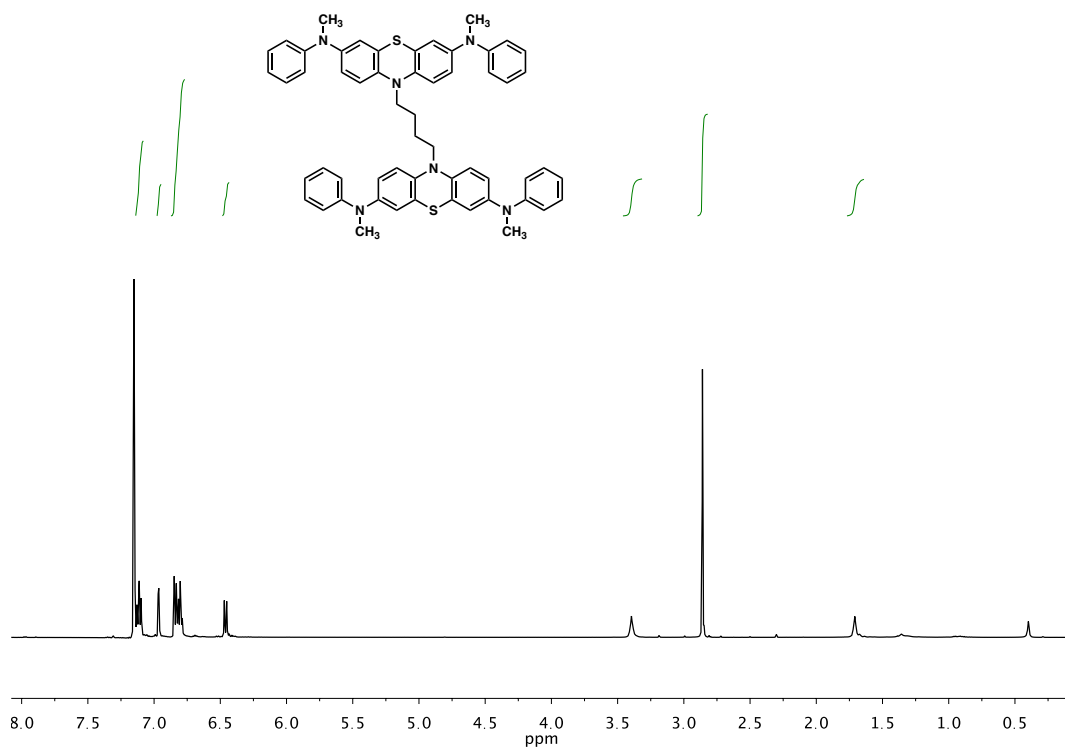


Figure 7.9. ¹H NMR of 10,10'-(butane-1,4-diyl)bis(N3,N7-dimethyl-N3,N7-diphenyl-10H-phenothiazine-3,7-diamine) in C₆D₆ (C3).

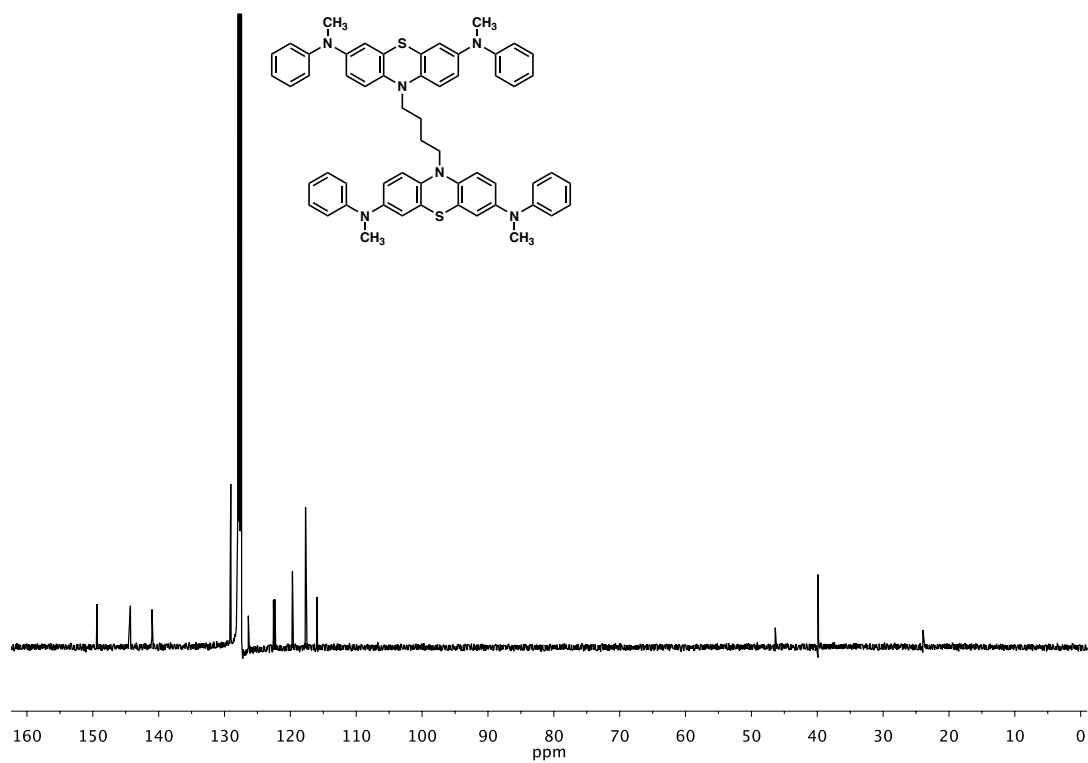


Figure 7.10. ¹³C NMR of 10,10'-(butane-1,4-diyl)bis(N3,N7-dimethyl-N3,N7-diphenyl-10H-phenothiazine-3,7-diamine) in C₆D₆ (C3).

UV-Vis Spectro-electrochemistry

A blank spectrum was taken using 0.1 M TBAP (1:1 MeCN/DCM). 0.5 mM **C1** in the same electrolyte solution was used to fill the spectro-electrochemistry cell. CV was taken at 10 mVs^{-1} , and UV-vis spectra were taken every 10 s (1 spectrum per 100 mV).

The same procedure was used to record the spectro-electrochemistry of the **C2** coupling chemical reaction. 1 mM **C2** in 0.1 M TBAP/MeCN was used as monomer solution, and CV was taken at 10 mVs^{-1} and UV-vis spectra were taken every 10 s (1 spectrum per 100 mV).

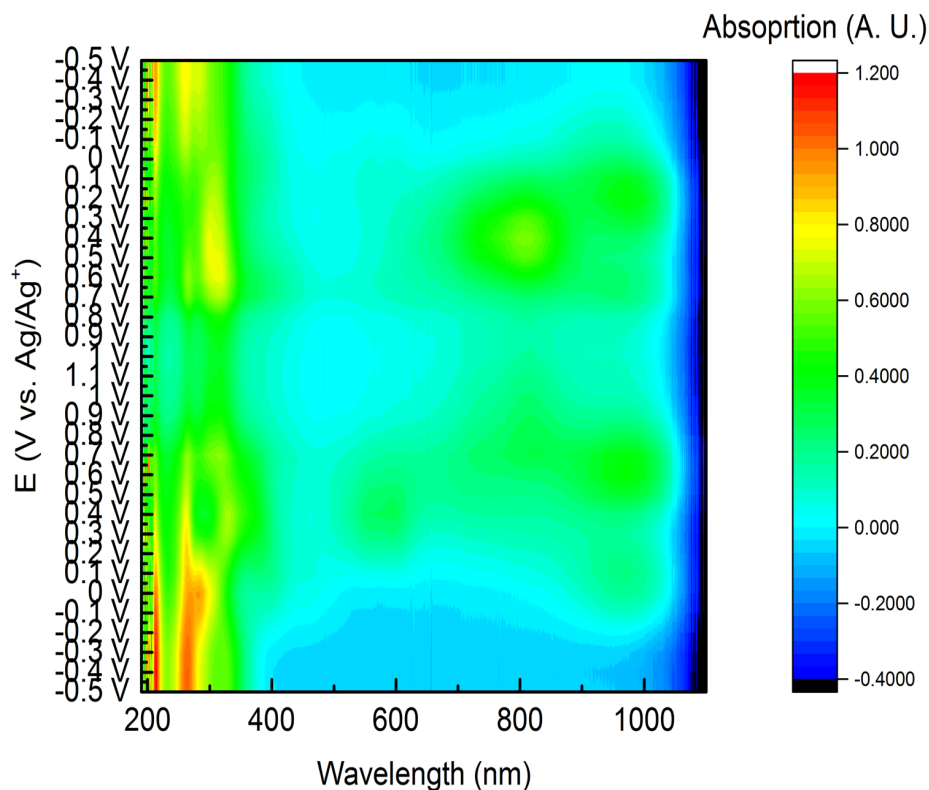


Figure 7.11. UV-vis spectro-electrochemistry contour plot of C1

Electropolymerization of C2

The electropolymerization of **C2** on a GC electrode was carried out in a three-neck glass cell. A 10 mM monomer solution in DCM (1M TBAP) was used; 1 M electrolyte concentration is required in order to minimize solution resistance as the monomer is electrochemically oxidized to the tri-cationic state.

CV was the main method of electropolymerization, and there are two modes of electropolymerization. As shown in Figure 7.3.d, polymerization can be performed by cycling between the full window of electropolymerization, $-0.5 - 1.4$ V, for a desired number of polymerization cycles. Since a large potential window is cycled, this method takes a long time for the polymerization process to finish. For faster electropolymerization, as shown in Figure 7.4.a inset, the potential can be cycled over the third redox couple (between 0.7 and 1.1 V), where polymerization occurs. As a result, the overall time of polymerization is decreased, while maintaining the same film quality.

Upon completion of electropolymerization, all thin-film samples were rinsed with DCM and then acetone to wash away any residual monomer and mobile oligomers on the electrode surface. Subsequently, the clean thin-films were subjected to electrochemical characterization in blank electrolytes.

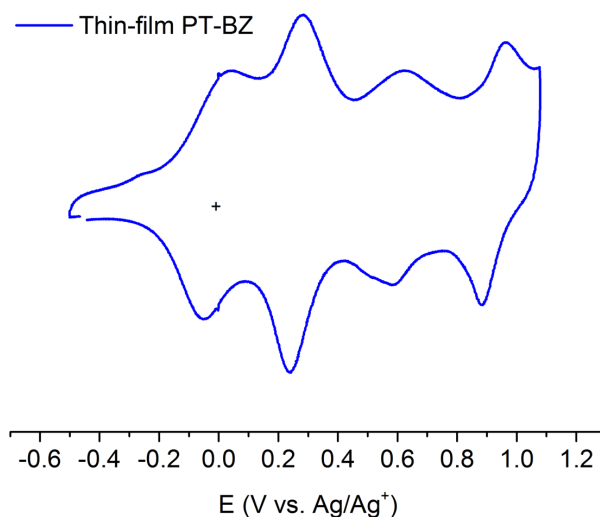


Figure 7.12. CV of P2-TF on GC electrode at 20 mVs^{-1} in 0.1 M TBAP/MeCN.

Electrochemical Quartz Crystal Microbalance

The electrochemical cell used during EQCM experiments are shown in Figure 7.13. A custom-made one chamber electrochemical cell with temperature control was used. A Teflon lid fitted to the chamber, electrodes, and QCM sensors were employed to ensure air-free experimental conditions.

The main objective for the use of EQCM in this manuscript is to confirm two quantities: the mass of deposited film and the mass of charge compensating ions that intercalate through such film. As a result, it is paramount that we determine these quantities with consistency and accuracy.

The system was stabilized with in a one-chamber temperature control glass cell and equipped with a stir bar to maintain the homogeneity of the solution. O-rings in contact with monomer solution was made of Kalrez, which is highly resistant to swelling to organic solvents. Pre-polymerization stabilization is usually established within two hours.

Electropolymerization in QCM starts with a two-cycle stabilization cycle, where the potential is swept between $-0.5 - 0.5$ V, accessing the first two redox couples in the monomer. While significant current is observed for these stabilization cycles, we observed minimal but regular variation in mass and frequency, due to the slight capacitive behavior of monomers as they are oxidized and reduced. Upon establishment of dynamic stabilization, electropolymerization was carried to the third redox couple between $0.70 - 1.15$ V. Cycling about the third redox couple results in a decrease in frequency and an increase in mass as the number of polymerization cycles increases. For twenty cycles of electropolymerization, the increase of mass approaches a linear relationship with the cycle number; after more than twenty cycles of electropolymerization, mass increase starts to slow down due to significant deposition on electrode.

Upon completion of electropolymerization, thin-film samples were cleaned as described in the previous section; thin-film samples are rinsed with DCM and then acetone until a visibly clean and smooth film is obtained. Subsequently, the film is subjected to cycling in 0.1 M TBAP/MeCN. Stabilization pre-cycling

was performed as described for the electropolymerization using QCM until a stable frequency is observed for the system. During cycling, polymer film was cycled between $-0.5 - 0.75$ V, as more positive potential leads to overoxidation of the thin-film on Au substrate, and mass and frequency changes were recorded.

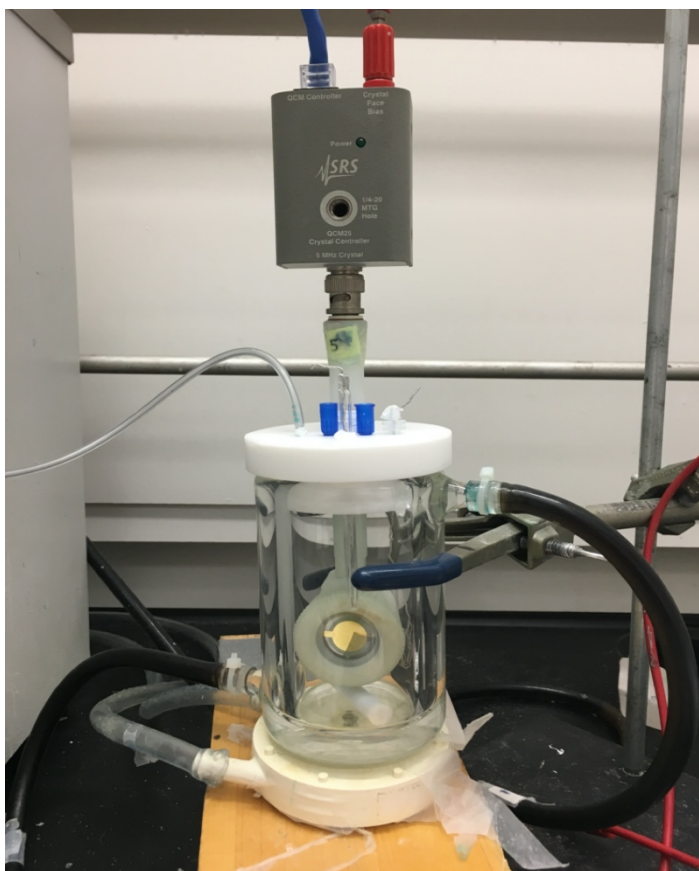


Figure 7.13. EQCM setup for electropolymerization and film cycling of thin-film P2-TF.

Resistance was recorded along with mass and frequency as EQCM experiments were performed. We did not observe resistance changes larger

than ten ohms over the course of all experiments, indicating that the deposition of thin-film and resulting film behave as rigid films without significant viscoelastic changes during these processes. This observation allows for the direct application of the Sauerbrey equation correlating frequency changes to mass changes.

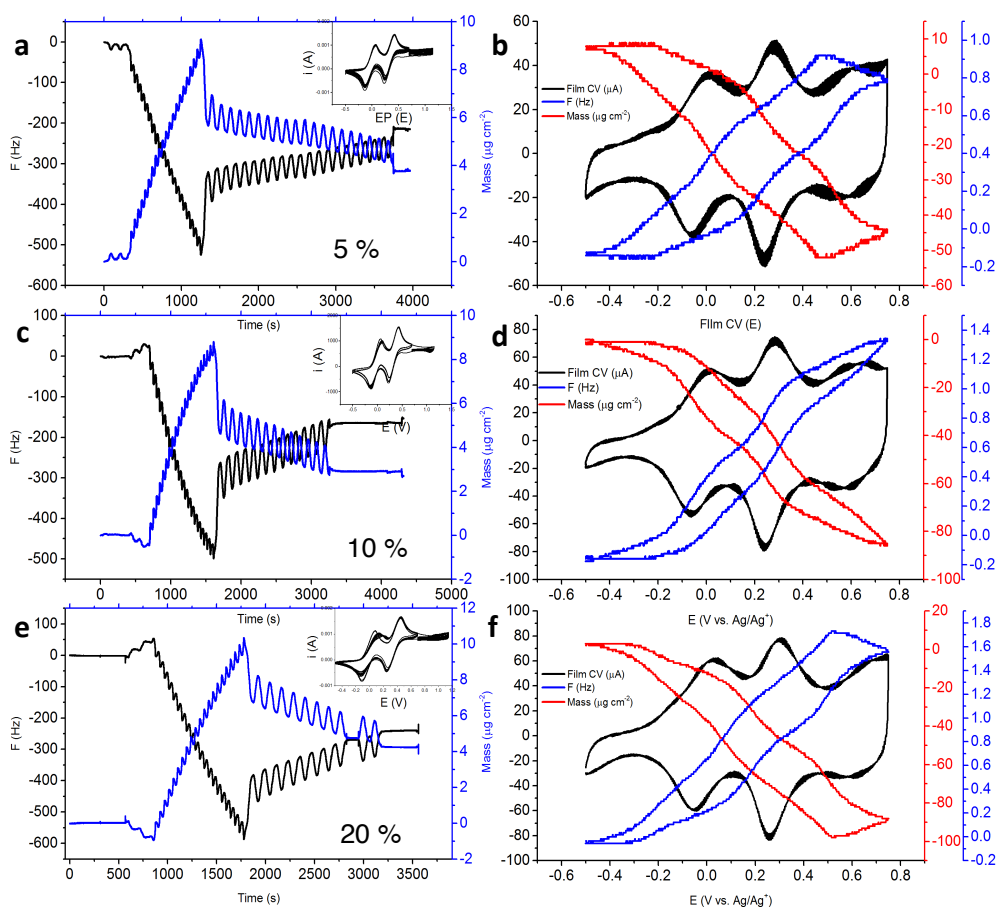


Figure 7.14. Electropolymerization and the resulting film cycling CV and QCM traces. Electropolymerization of **C2** with (a, b) 5%, (c, d) 10%, and (e, f) 20% cross-linker, **C3**. Stabilization of this system is established before and after electropolymerization, as shown in (c) and (e) before and after CV cycling started. Mass difference was taken between the stabilized frequencies in those trials.

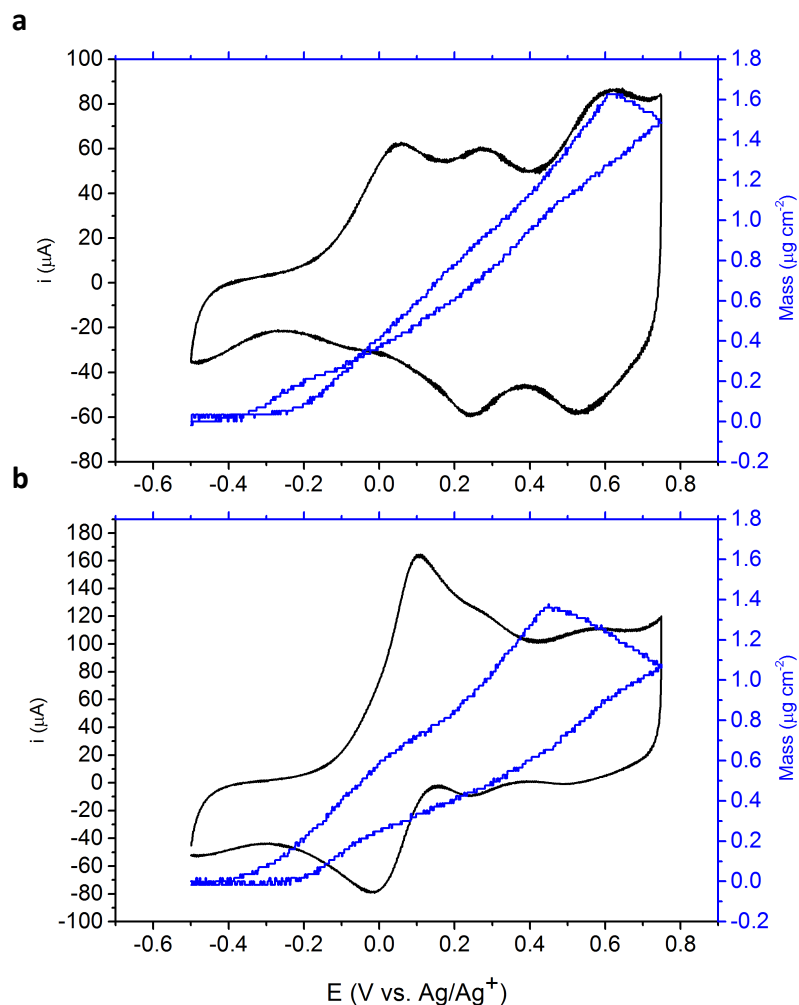


Figure 7.15. Cycling of thin-film P2-TF. Cycling (a) without and (b) with 1 mM of ferrocene (Fc) as a redox shuttle to unlog potentially inaccessible film. The CV trace in (b) shows very different behavior as that in (a), as the response of Fc is confounding the response from the thin-film P2-TF. However, the QCM traces in (a) and (b) do not differ significantly, especially in terms of magnitude (mass change). With Fc in solution, it appears the film expels some species towards the end of the oxidation (decrease in mass between 0.4 – 0.75 V), and this could be due to the incorporation of Fc during oxidation at lower potentials, and as the film becomes more oxidized, they are expelled to accommodate the charge neutrality within the film.

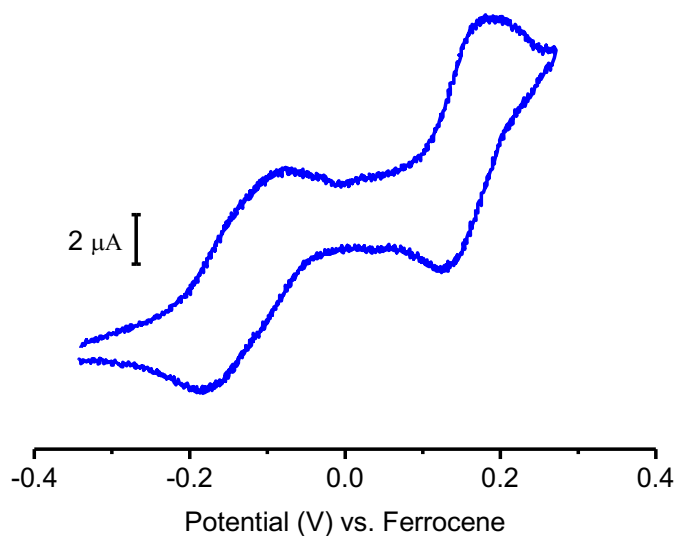


Figure 7.16. CV of 0.5 mM C3 at a GCE (20mVs⁻¹, 0.1 M TBAP in MeCN)

References:

- (1) B. M. Peterson, B. M.; D. Ren, D.; L. Shen, L.; Y.-C. M. Wu, Y.-C. M.; B. Ulgut, B.; G. W. Coates, G. W.; H. D. Abruña, H D.; B. P. Fors. B. P. *ACS Appl. Energy Mater.* **2018**, *1*, 3560.
- (2) A. Ito, A.; D. Sakamaki, D.; H. Ino, H.; A. Taniguchi, A.; Y. Hirao, Y.; K. Tanaka, K.; K. Kanemoto, K.; T. Kato, T. *Eur. J. Org. Chem.* **2009**, *26*, 4441.

CHAPTER 8
CROSS-LINKING EFFECTS ON PERFORMANCE METRICS OF
PHENAZINE-BASED POLYMER CATHODES

8.1 Abstract

Developing cathodes that can support high charge-discharge rates would improve the power density of lithium-ion batteries. Herein, the development of high-power cathodes without sacrificing energy density is reported. *N,N'*-diphenylphenazine was identified as a promising charge-storage center by electrochemical studies due to its reversible, fast electron transfer at high potentials. By incorporating the phenazine redox units in a cross-linked network, a high-capacity (223 mAh g⁻¹), high-voltage (3.45 V vs. Li/Li⁺) cathode material was achieved. Optimized cross-linked materials are able to deliver reversible capacities as high as 220 mAh g⁻¹ at 120 C with minimal degradation over 1000 cycles. The work presented herein highlights the fast ionic transport and rate capabilities of amorphous organic materials and demonstrates their potential as materials with high energy and power density for next-generation electrical energy-storage technologies.

8.2 Introduction

Electrification of transportation is expected to play a critical role in curbing carbon emissions and utilizing renewable energy. Recently, the U.S. Department of Energy has set an initial target of 15 min battery charging times

to advance the market penetration of electric vehicles.¹ Currently, capacitors are the only electrical energy storage systems capable of stably delivering and sustaining these rates, owing to their high rates of charge storage.² However, since capacitors lack faradaic reactions, they have low energy densities compared with batteries, which compromise the range of electric vehicles. State-of-the-art battery materials have seen significant improvements in energy density and lifetime over the past decade. However, the diffusive nature of the energy storage processes continues to limit their rate performance.³ Thus, it is necessary to increase the charge- and ion-transport dynamics to improve the power density of these devices.

During charge and discharge, crystalline inorganic cathodes undergo kinetically slow (de)intercalation events that limit the rate of ion diffusion. In amorphous organic materials, charge-balancing counterion transport can be dramatically enhanced owing to the relatively weak intermolecular forces in the materials.^{4,5} This enables amorphous organic materials to accommodate fast ion transport, resulting in faster charging and discharging rates. However, designing amorphous organic materials that can deliver high power density without sacrificing operating voltage, capacity, or stability has proven challenging.⁶⁻⁸

Cross-linking in binders, electrolytes, and electrode materials increases resistance to dissolution, improves stability, and supports an amorphous nature to increase ion conductivity.⁹⁻¹³ We hypothesized that the morphology of a

redox-active polymer could be optimized by strategically tuning the cross-linking density. Cross-linking can disrupt ordering and restrict polymer mobility to ensure an open, amorphous structure even in the swelled state. Recently, we reported on a cathode material with 3,7-diamino-substituted phenothiazines as charge-storage elements.¹⁴ In that study, cross-linking of a linear energy storage polymer led to improved stability on cycling, higher discharge capacity, and improved rate performance. Unfortunately, the material exhibited poor capacity retention on cycling, a likely consequence of polymer degradation. In an effort to better understand the effects of cross-linking, a polymer containing more stable redox centers was required. Substituted phenazines, specifically *N,N'*-diphenylphenazine (**1**), were identified as a promising class of charge-storage motifs through electrochemical screening/analysis of phenazine-based small-molecule analogues.

In recent years, phenazine has been identified as a promising charge-storage unit in battery cathodes, capacitors, and as a redox-flow catholyte.¹⁵⁻²⁴ Recent work on phenazine-based p-type energy materials has been led by Zhang and co-workers, who became interested in **1** for its ability to improve charge delocalization about the dihydrophenazine unit.^{23,24} In collaboration with Zhou et al., they demonstrated the utility of a crystalline phenazine-based bipolar compound in a dual-ion symmetric battery with full cell capacities as high as 57 mAh g⁻¹. Additionally, they demonstrated the potential of a linear polymer containing phenazine units as a high-voltage cathode material delivering 65

mAh g^{-1} at a discharge rate of 5 C. However, high C-rates were not reported in either study.

Through ternary copolymerizations, we synthesized cross-linked polymers based around substituted phenazines and studied the effects of cross-linking on their electrochemical performance as amorphous cathode materials. These cross-linked phenazine-based polymers delivered energy densities competitive with those of commercial cathodes while providing dramatically enhanced power densities. By optimizing the cross-linking density in these materials, we developed a cathode material that can deliver a remarkable capacity of 220 mAh g^{-1} at 120 C with minimal capacity loss over 1000 cycles.

8.3 Results and Discussion

Electrochemical optimization of the redox storage unit

The electrochemical properties of the redox-active unit in a material can dictate many of the performance metrics of the resulting cathode, including operating voltage, cathode stability, and rate capability. Thus, careful design and electrochemical analysis of the redox unit as a small molecule can enable ideal performance in the material. Alkylation and arylation of phenazine lead to improved kinetic and thermodynamic performance metrics over unsubstituted phenazine. The *N,N'*-disubstituted phenazine units cycle between a neutral and dicationic state and belong to the class of so-called p-type materials.

The p-type materials typically have higher operating voltages than n-type materials (redox centers that undergo reduction and become negatively charged), which are clearly advantageous for cathode applications. Additionally, charge compensation in p-type materials is established by anion transport from the electrolyte. The smaller solvation shell of anions aids in providing higher ionic diffusion and should enable higher charge-discharge rates.²⁶

Analysis of the cyclic voltammograms of phenazine and *N,N'*-diphenylphenazine (**1**) offers insight into their chemical and electrochemical properties. The redox processes of **1** occur at approximately 1500 mV more positive potential than those of phenazine (Figure 8.1). This is ideal behavior for redox units in cathodes, as it extends the operating voltage of the battery. The analysis of peak-to-peak separation, ΔE_{peak} , and the ratio of the anodic peak current to the cathodic peak current, $i_{\text{p,a}}/i_{\text{p,c}}$, of redox events sheds light on the chemical and electrochemical reversibility of the redox centers (Table 8.1 and Chapter 8.6 Appendix, Table 8.4). The first redox couples, that is the transition from the neutral to the -1 state in phenazine and to the $+1$ state in **1**, show ΔE_{peak} values near the ideally reversible value (58 mV). For the second redox couple from the ± 1 to the ± 2 charge state, whereas **1** maintains a low ΔE_{peak} value of only 66 mV, the ΔE_{peak} value of phenazine increases to 216 mV, which indicates an electrochemically irreversible redox couple. Additionally, the $i_{\text{p,a}}/i_{\text{p,c}}$ value of the second redox couple in phenazine decreases with increasing scan

rate, and this again corresponds to electrochemical irreversibility and potentially a coupled chemical reaction (Figure 8.7). Together, this suggests that materials based on **1** will show much higher operating voltages and significantly more

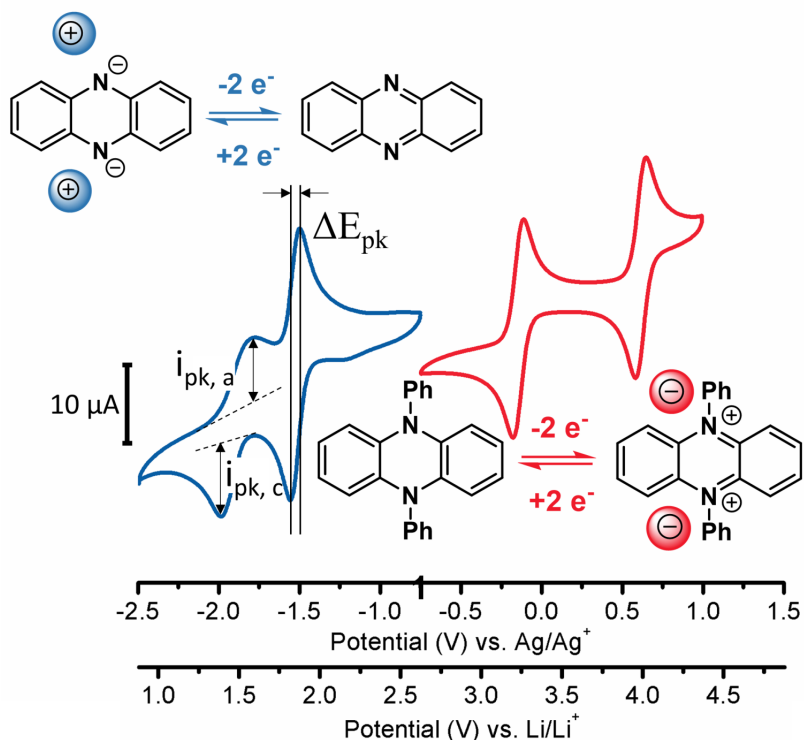


Figure 8.1. The neutral and reduced states of phenazine and the neutral and oxidized states of N,N'-diphenylphenazine (**1**). CV profiles at a glassy carbon electrode of 1 mM solutions of phenazine (blue) and **1** (red) obtained in 0.1 M TBAP in acetonitrile at 50 mV/s.

stable cycling in cathodes than phenazine.

Analysis of the voltammetric profiles of phenazine in the presence and absence of trifluoroacetic acid (TFA, to stabilize the reduced state though binding a proton), **1**, and N,N'-dimethylphenazine (**2**) at a Pt ultramicroelectrode

was used to determine the standard electron-transfer rate constants k^0 (Figure 8.9). In each case, the k^0 values indicated facile and fast charge-transfer kinetics (Table 8.1), which therefore should not be rate-limiting even at high rates.²⁸ This small-molecule study ensures that the rate performance of the reported materials in battery applications will be limited by electronic conductivity or ionic diffusion through the material, and not the rate at which the redox centers can

Table 8.1. Values of peak splitting and standard electron transfer rate constants for phenazine and small molecule derivatives.

Material	ΔE_{peak1} (0 \rightarrow ± 1)	ΔE_{peak2} (± 1 \rightarrow ± 2)	k°_1 (cm/s)	k°_2 (cm/s)
Phenazine (1)	58 mV	216 mV	2.6×10^{-2}	-
Phenazine + 50 mM TFA	107 mV	65 mV	1.4×10^{-2}	1.6×10^{-2}
N,N'-dimethyl- phenazine (3)	86 mV	58 mV	9.3×10^{-3}	8.5×10^{-3}
N,N'-diphenyl- phenazine (2)	65 mV	66 mV	1.1×10^{-2}	9.3×10^{-3}

be oxidized or reduced.

Design and characterization of storage materials

When designing a redox-active polymer for electrochemical energy storage (EES), any atoms that do not contribute to faradaic processes should be limited. We hypothesized that the core structure of **1** could be preserved and incorporated into a partially conjugated polymer framework through cross-coupling of 5,10-dihydrophenazine (**3**) and dichlorobenzene (**4**). Following a

simple reduction of phenazine with sodium dithionite, the newly freed secondary amino groups of 5,10-dihydrophenazine provide excellent handles for Buchwald-Hartwig cross-coupling reactions. Cross-coupling of **3** with **4** yields poly(phenylene-5,10-dihydrophenazine) [poly(Ph-PZ)], an insoluble powder that precipitates from solution (Figure 8.2). The ratio of **3** to **4** is given in Table 8.2, entry 1. It can be seen by comparison of the IR spectra of poly(Ph-PZ) and **1** that the polymer shares a core structure with **1** (Figure 8.10). As expected,

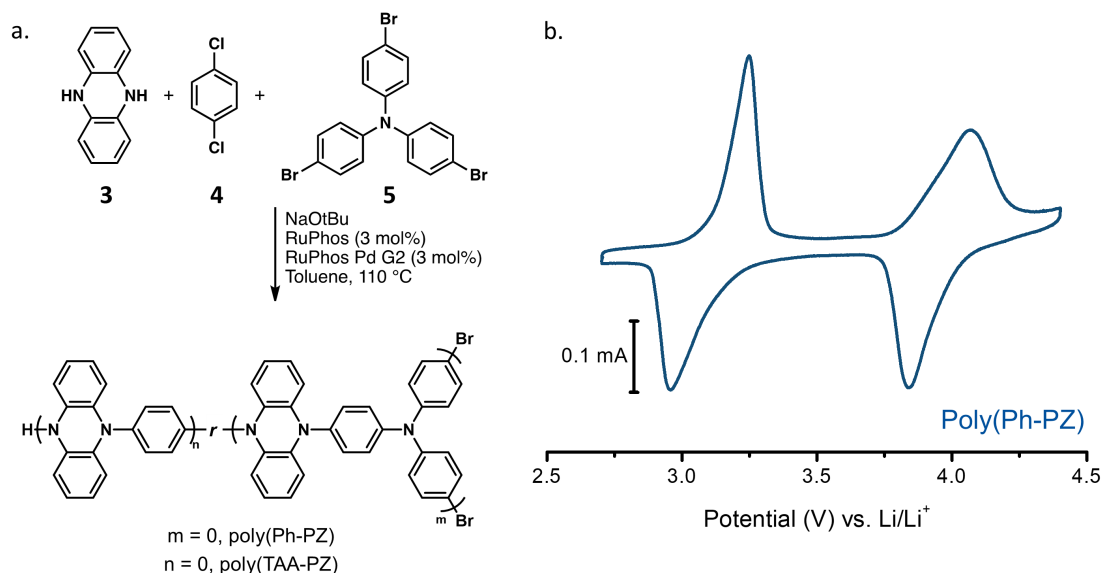


Figure 8.2. (a) Schematic of synthesis of poly(phenylene-5,10-dihydrophenazine) and cross-linked networks, (b) CV of poly(Ph-PZ) in a Li metal coin cell with 1 M LiPF₆ in EC/DEC at 2 mV/s.

the cyclic voltammogram of the material, in a lithium-metal half-cell, exhibits two one-electron oxidations, similar to the CV profile of **1** (Figure 8.2).

Cross-linked networks were synthesized to determine the effect of cross-linking on the electrochemical properties of the cathodes. We envisaged that

tris(4-bromophenyl)amine (**5**) could be copolymerized to cross-link the material (Table 8.2, entry 2) in order to improve stability and disrupt ordering.^{4,27,28}

Table 8.2. Reagent equivalents used in Buchwald-Hartwig cross-coupling step-growth polymerizations to obtain phenazine-based cathode materials.

Entry	Polymer	(4) (equiv)	(5) (equiv)	(6) (equiv)
1	Poly(Ph-PZ)	1.0	1.0	0.0
2	Poly(TAA-PZ)	1.0	0.0	0.76
3	Poly(Ph-PZ)-10	1.0	0.9	0.067
4	Poly(Ph-PZ)-50	1.0	0.50	0.33

Copolymerization of **3** with **5** results in a fully cross-linked material, namely poly(triarylamine-5,10-dihydrophenazine) [poly(TAA-PZ)], which exhibited much more resistance to dissolution in electrolyte solution than poly(Ph-PZ). This was determined by UV/Vis spectroscopy of filtered electrolyte solutions after suspending the cathode material in the electrolyte solution for one week (Figure 8.11). Since any solubility of the active material will result in a loss of capacity on cycling, decreasing the solubility of the material is critical to achieving near-theoretical capacity and stable cycling performance.

In our previous study on cross-linked poly(phenothiazine--dimethylphenylenediamine), we observed that, above a certain threshold of cross-linking density, rate performance declined as a result of lowered ionic transport through the material.¹⁴ Therefore, two molar ratios of **4** and **5** were

examined to determine a cross-linking density that would mitigate dissolution while retaining high ion diffusion (Table 8.2, entries 3 and 4). The molar ratio of poly(Ph-PZ)-10 led to a decrease in solubility in the electrolyte solution in comparison with poly(Ph-PZ) and poly(Ph-PZ)-50. Note that the degree of polymerization of the final polymer also plays a significant role in determining the solubility of the polymer. However, the cross-linked nature of the materials precludes determination of molecular weight by conventional methods.

The incorporation of cross-linker into the material was ensured by taking advantage of the relative rates of monomer cross-coupling reactions in the step-growth polymerization. Owing to the faster rate of cross-coupling of **4** with aryl bromides over aryl chlorides, we hypothesized that **6** would be more rapidly incorporated into the polymer chains than **5** to ensure cross-linked copolymers.^{29,30} When the ratio of **5** to **6** is low, as in poly(Ph-PZ)-10, we expect full incorporation of the cross-linker in the polymer chains, which decreases the solubility of the polymer under battery conditions. This is supported by the elemental analysis of poly(Ph-PZ)-10, which revealed that no aryl bromide end groups were present. By contrast, elemental analysis of poly(Ph-PZ)-50 revealed 0.54% bromine content and 0.67% chlorine content. The presence of bromine in poly(Ph-PZ)-50 and the propensity of poly(Ph-PZ) for dissolution suggest that the copolymer of **3** and **5** exceeded its solubility in toluene and precipitated from the reaction solvent before **4** could be incorporated. This would leave a depleted concentration of **5** remaining in solution and result in

oligomerization between **3** and **4**, as found in poly(Ph-PZ). Therefore, whereas poly(Ph-PZ)-10 is a homogeneously cross-linked material, it is more likely that poly(Ph-PZ)-50 behaves as a mixture of poly(Ph-PZ) and poly(TAA-PZ). The morphology observed by SEM provides additional support for this hypothesis (Figures 8.12-8.14).

The crystallinity of the polymers was investigated by XRD. Diffractograms of the polymers revealed their largely amorphous character (Figure 8.15). At 2θ values of 10° - 25° , four small, broad peaks were observed for poly(Ph-PZ) and poly(Ph-PZ)-10, indicating that some ordering is present in the polymer. As expected, this ordering was lost as the amount of **5** was increased in poly(Ph-PZ)-50 and poly(TAA-PZ). However, no melting or crystallization temperature was observed up to 200°C by differential scanning calorimetry for any of the synthesized polymers (Figure 8.16). Therefore, any ordering observed by XRD is likely due to local interactions between aromatic rings and does not suggest any long-range ordering in the materials.

Coin cell design and cathode conductivity

For high-power applications, fast electron-transfer and ion-transport kinetics are necessary. To singularize the diffusion-limited rate of our materials, we aimed to minimize the rate dependence on electronic transport by making the composite conductivity sufficiently high.³ Cathodes of each polymer were prepared as composites with active material, Super P carbon, CMK-3 mesoporous carbon, and poly(vinylidene difluoride) (PVDF) in 3:3:3:1 ratio. The

partially conjugated π system in these materials is expected to enable fast electron transport through the material,³¹⁻³³ and the high carbon content should provide rapid charge transport through the composite, such that the electronic transport should not be limiting. When not limited electronically, the ability of the materials to transport ions should be rate-limiting during charge and discharge.

Potentiostatic electrochemical impedance spectroscopy (PEIS) and cyclic voltammetry were used to measure the charge-transfer resistance of the cathodes and the ion-diffusion coefficients, respectively (Figures 8.21 and 8.22). The fits for the charge-transfer resistance of each of the plots are listed in Table 8.3 (additional fitting parameters are presented in Table 8.5). As expected, all four polymers exhibited low-charge transfer resistance, enabling fast electron transport. The charge-transfer resistance of poly(Ph-PZ), poly(Ph-PZ)-10, and poly(Ph-PZ)-50 never exceeded 80 Ω throughout charging, indicating fast electron transfer regardless of charge state (Figure 8.23).

Table 8.3. Charge transfer resistances and diffusion coefficients obtained from PEIS data at 2.7 V vs. Li/Li⁺ and CV data, respectively, for poly(Ph-PZ), poly(TAA-PZ), poly(Ph-PZ)-10, and poly(Ph-PZ)-50.

Polymer	R_{ct} (Ω)	D_{pk} (cm²/s)	D_{pk 2} (cm²/s)
Poly(Ph-PZ)	54.0	1.6 X 10 ⁻⁸	1.4 X 10 ⁻⁸
Poly(TAA-PZ)	100.7	4.0 X 10 ⁻⁹	2.5 X 10 ⁻⁹
Poly(Ph-PZ)-10	57.3	1.6 X 10 ⁻⁸	1.5 X 10 ⁻⁸
Poly(Ph-PZ)-50	49.1	5.3 X 10 ⁻⁹	3.9 X 10 ⁻⁹

Cyclic voltammograms of each cathode were taken over a range of scan rates. By applying the Randles-Sevcik equation, the diffusion coefficients of the PF_6^- ions through the electrode were determined. Even at high scan rates, the response remained diffusion-limited, as evidenced by the linear plot of peak current versus the square root of scan rate. The obtained diffusion coefficients of poly(Ph-PZ) and poly(Ph-PZ)-10 are of the order of $10^{-8} \text{ cm}^2 \text{ s}^{-1}$ (Table 8.3). The faster diffusion of PF_6^- observed in poly(Ph-PZ) and poly(Ph-PZ)-10 compared with diffusion through poly(Ph-PZ)-50 and poly(TAA-PZ) is attributed to improved ion transport in the less densely cross-linked materials. For all the polymers presented here, the values of the diffusion coefficient were orders of magnitude higher than those of commercial inorganic oxide cathodes and enable high rate capabilities while maintaining a high degree of utilization of the active material.³⁴⁻³⁷

Material performance in lithium half-cells

The cathodes were cycled in lithium half-cells between 1.5 and 4.3 V at 5 C (Figure 8.3.a), corresponding to a charge-discharge time of 12 min each, shorter than the U.S. Department of Energy target charging time. Poly(Ph-PZ)-10 exhibited the highest discharge capacity of 223 mAh g^{-1} , whereas the capacity of poly(Ph-PZ) on discharge was 209 mAh g^{-1} . This improvement in capacity in poly(Ph-PZ)-10, despite its lower theoretical capacity (203 mAh g^{-1}), is attributed to the aforementioned decrease in solubility over poly(Ph-PZ). Due

to the larger percentage of the inactive cross-linker, poly(Ph-PZ)-50 and

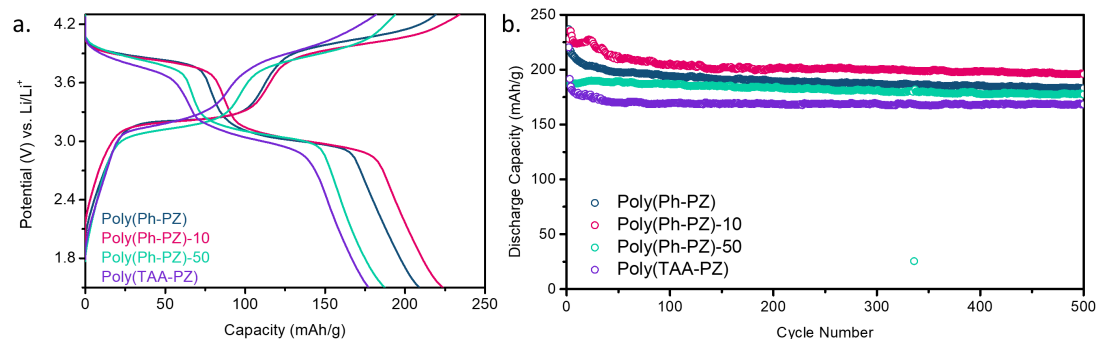


Figure 8.3. (a) Charge-discharge profiles of tenth cycle of poly(Ph-PZ), poly(TAA-PZ), poly(Ph-PZ)-10, and poly(Ph-PZ)-50 at 5 C. (b) Discharge capacity of poly(Ph-PZ), poly(TAA-PZ), poly(Ph-PZ)-10, and poly(Ph-PZ)-50 at 5 C for 500 cycles.

poly(TAA-PZ) delivered capacities of 187 and 177 mAh g⁻¹, respectively.

Since the redox activity of the triarylamine units in the polymers falls outside the electrochemical stability window (4.5 V), they are not able to contribute any charge storage (Figure 8.24). Through analysis of the CV of poly(TAA-PZ), each redox peak in the CV could be attributed to oxidations of the embedded phenazine. Since there are two triarylamine units for every three phenazine units in poly(TAA-PZ), an integral ratio of 2:3 of the areas under the CV peaks would be expected if either peak was due to oxidation of the triarylamine units. However, we observed an approximately 1:1 ratio of the peak areas in the CVs of all of the polymers (Figure 8.25). In all cases, the experimentally measured capacities were slightly higher than the theoretical

capacities of the materials owing to the additional capacity contribution from the carbon in the cathode composite (Figure 8.26).

Continued cycling of poly(Ph-PZ), poly(Ph-PZ)-10, poly(Ph-PZ)-50, and poly(TAA-PZ) at a C-rate of 5 illustrates the prolonged stability of each material (Figure 8.3.b, charge capacities and coulombic efficiencies are shown in Figures 8.27-8.30). All polymers exhibited a modest loss in capacity over the first 50 cycles. Thereafter, they retained at least 92% capacity in the 500th cycle. Notably, poly(Ph-PZ)-10 still delivered a capacity of 196 mAh g⁻¹ in the 500th cycle. It is evident that optimizing cross-linking density to minimize dissolution while minimally affecting capacity is an effective strategy to design a high-energy cathode material. At an average discharge voltage of 3.45 V, poly(Ph-PZ)-10 exhibits one of the highest energy densities (approximately 770 Wh kg⁻¹ of active material) of all polymeric cathode materials reported.

The performance of each polymer at even more demanding discharge rates was further analyzed. Figure 8.4.a plots capacity retention at various discharge rates as a percentage of the initial capacity of the polymer averaged over the first three cycles at 1 C. When discharge rates exceeded 5 C, charging rates were held constant at a C-rate of 5 to ensure a constant initial charge state and isolate the effect of rate on the discharge capacity. Evidently, all of the materials excel under demanding loads, as they maintain the majority of their capacity even when discharged at 60 C. Interestingly, poly(Ph-PZ)-10 had the highest capacity retention at high rates of discharge, followed by poly(Ph-PZ)-

50. All four of the polymers recovered over 90% of their capacity when the

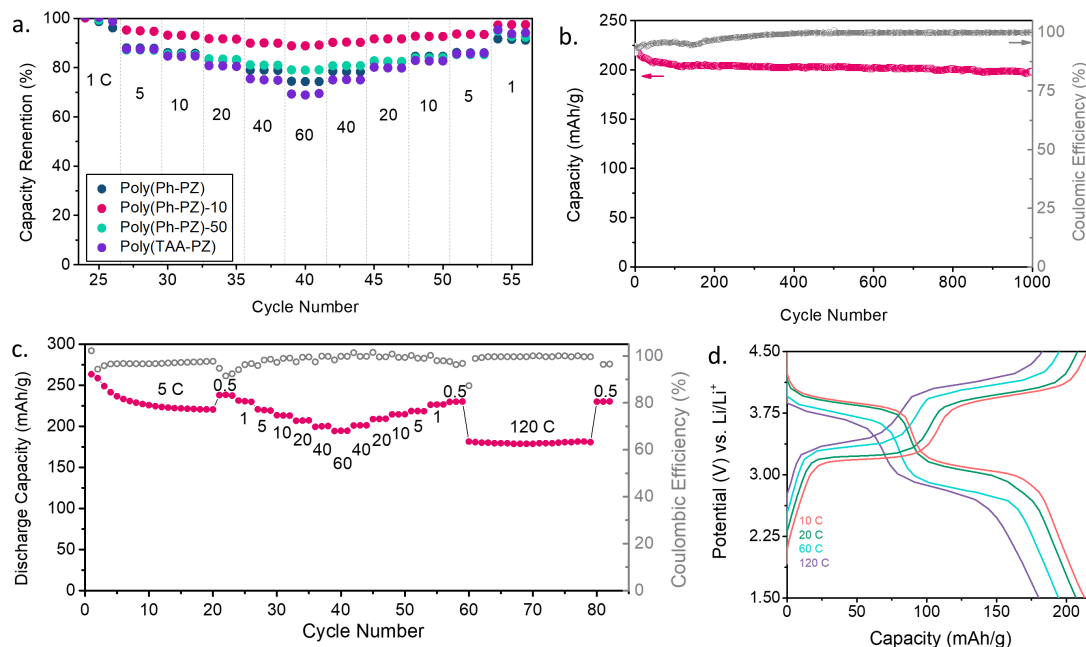


Figure 8.4. (a) Discharge capacity retention of poly(Ph-PZ), poly(Ph-PZ)-10, poly(Ph-PZ)-50, poly(TAA-PZ) when discharged at increasing indicated C-rates. (b) Cycling performance of poly(Ph-PZ)-10, discharged at 120 C, over 1000 cycles. (c) Discharge capacities and coulombic efficiencies of poly(Ph-PZ)-10 charged and discharged at the denoted C-rates. (d) Charge-discharge profile of poly(Ph-PZ)-10 charged and discharged at the indicated C-rates.

discharge rate was returned to 1 C.

Owing to its high capacity, stability, and superior rate performance, poly(Ph-PZ)-10 was cycled at the extraordinary discharge rate of 120 C (Figure 8.4.b). The material delivered a capacity of 220 mAh g⁻¹, corresponding to a power density greater than 27 kW kg⁻¹ when normalized to the mass of the entire cathode composite. With continued cycling, the material stabilized, as

seen in the improved coulombic efficiency with cycling and the delivery of 198 mAh g⁻¹ after 1000 cycles. Further tests were run to probe the performance of poly(Ph-PZ)-10 upon charging and discharging at increasing rates (Figure 8.4.c). The charging voltage was increased to 4.5 V to ensure full charge at high C-rates. The material still delivered 180 mAh g⁻¹ when charged and discharged at 120 C and showed excellent capacity recovery when the charge-discharge rate was returned to 0.5 C. At 120 C, poly(Ph-PZ)-10 still retains its two discrete plateaus, indicative of a faradaic charge storage mechanism (Figure 8.4.d). These high-rate experiments illustrate the ability of amorphous materials to provide fast ion transport and enable high rates of charge-discharge. By tuning the active-mass ratio used in the composite, power and energy density can be optimized for specific applications. The energy density of a cathode composite can be driven higher by increasing the active-mass loading. Cells with 60% active material in the composite were tested at varying discharge rates. At low C-rates (0.5 C) poly(Ph-PZ)-10 was able to deliver a capacity of 182 mAh g⁻¹ (Figure 8.34). When the cell was discharged at progressively higher C-rates (60 C), poly(Ph-PZ)-10 delivered a capacity of 143 mAh g⁻¹. Future work will focus on further understanding ionic transport through amorphous organic materials.

Performance in sodium half-cells

P-type cathode materials lend themselves to be used in alternative ion batteries. Since anions are responsible for the charge compensation of the

oxidized phenazine units, materials based around this redox-active unit are largely unaffected by the metal cations in solution. Therefore, the materials presented here could be used in a range of batteries with anodes such as sodium, magnesium, and potassium without the performance of the cathode being affected. This effect was demonstrated by analyzing the CV profile of poly(Ph-PZ)-10 in a variety of electrolyte salts, as shown in Figure 8.35. The redox peaks of poly(Ph-PZ)-10 retain their shape and magnitude regardless of the nature of the cation in solution.

We sought to determine the efficacy of a poly(Ph-PZ)-10 cathode in a sodium half-cell, as sodium-ion batteries are touted as being a future alternative

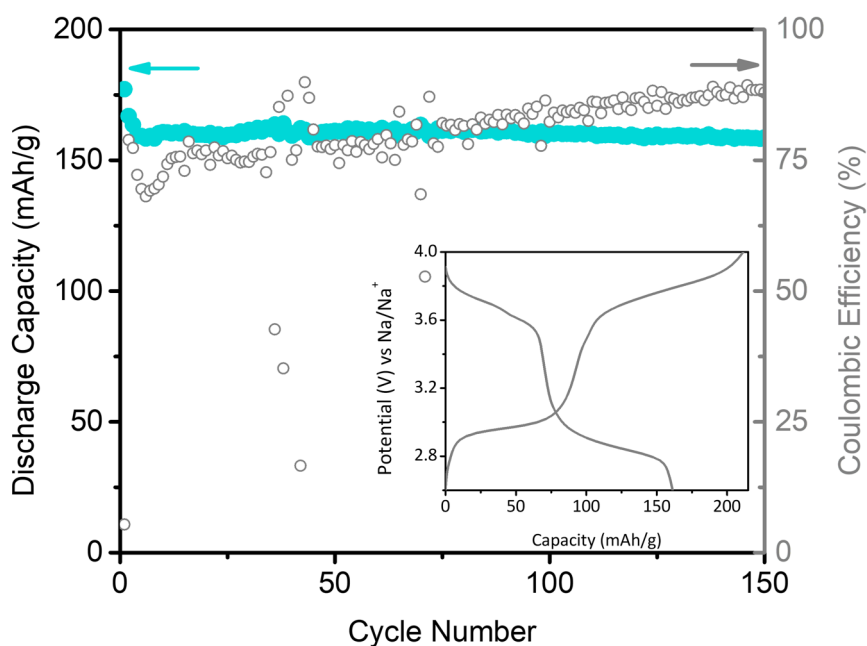


Figure 8.5. Cycling performance of poly(Ph-PZ)-10 in a sodium metal half-cell at 0.5 C. Inset: Charge-discharge profile of sodium metal half-cell.

EES system to lithium ion batteries (Figure 8.5). Coin cells were assembled with a sodium-metal anode and a poly(Ph-PZ)-10 composite as the cathode with 1 M NaPF₆ in ethylene carbonate (EC)/diethyl carbonate (DEC) as the electrolyte. Owing to the high resistance in the sodium cell, the coin cell was tested at a relatively low C-rate. Cycling the cell at 0.5 C provided a steady discharge capacity of greater than 160 mA h g⁻¹ after 100 cycles, comparable to the capacity obtained in a lithium cell. The large charging capacity in the first cycle and the poor coulombic efficiency is attributed to the incompatibility of carbonate-based electrolytes with sodium-metal deposition, which leads to increased resistance in the cell, as observed by PEIS (Figure 8.36).^{38,39} To obtain the same results achieved in the lithium cell, each of the components of the sodium coin cell would require further optimization. Still, these results demonstrate the ability of poly(Ph-PZ)-10 to function in alternative ion batteries.

Experimental Section

General Synthetic Procedures

General information regarding reagents can be found in the Supporting information. N,N'-dimethyl-5,10-dihydrophenazine and N,N'-diphenyl-5,10-dihydrophenazine were synthesized employing previously reported methods.^{40,41}

Fabrication of Coin-Cells

Device measurements were conducted in CR 2032 coin cell casings, which were assembled in an argon filled glove box with oxygen levels below 1

ppm. The anode was lithium metal and the working electrode was fabricated from a slurry of 30 wt% active material ($\sim 0.6 \text{ mg/cm}^2$), 30 wt% Super P carbon, 30 wt% CMK-3, and 10 wt% PVDF as the binder in NMP. The high loading cathode was fabricated with 60 wt% active material, 15 wt% Super P carbon, 15 wt% CMK-3, and 10 wt% poly(vinylidene fluoride) (PVDF) as binder. The slurries were spread onto a carbon paper current collector using the doctor blade method with one layer of scotch tape. The coated electrode was dried for 2 h at 60 °C followed by 14 h at 110 °C in a vacuum oven. A polypropylene separator (Celgard 2300) or a glass microfiber filter (GF/A, Whatman) was used as the separator between the two electrodes. The electrolyte solution was 1:1 by volume of EC (ethylene carbonate) to DEC (diethyl carbonate) with 1 M LiPF₆ (Aldrich). In cells with the celgard separator, 60 μL of electrolyte solution were used, while 80 μL were used in the cells with the fiber glass separators. An Arbin BT2000 battery tester was used to perform galvanostatic charge-discharge experiments on the coin cells at 25 °C.

Procedure for cyclic voltammetric experiments

Benchtop cyclic voltammetry experiments were performed in a three-compartment glass cell with medium porosity glass frits separating the compartments. An Ag/Ag⁺ reference electrode and a Pt wire counter electrode were used. All 3-mm glassy carbon (GC) electrodes were purchased from CH Instruments and used as working electrodes. Prior to the experiment, electrodes were polished using diamond paste and MetaDi Fluid (Buehler). All cyclic

voltammetric measurements were done in 0.1 M TBAP in MeCN unless otherwise specified. The potentials in the CVs were corrected for iR drop using a ferrocene reference at different scan rates.

Synthesis of 5,10-dihydrophenazine

Ethanol and DI water were degassed by sparging with nitrogen for 30 min. 400 mL of water and 100 mL of ethanol were added to a 1 L round bottom flask. Phenazine (4.00 g, 22.2 mmol, 1 equiv) and sodium dithionite (46.6 g, 268 mmol, 12 equiv) were added and the solution was magnetically stirred under a nitrogen atmosphere. The reaction was heated to reflux under nitrogen and allowed to proceed for 4 hrs. The reaction was deemed complete when no solid blue particulate remained. The reaction was allowed to cool, quickly filtered, and washed with deoxygenated water, yielding 3.57 g (88 % yield) of a light green powder. The product was dried and stored under vacuum until use.

General Procedure for Buchwald-Hartwig Cross-coupling Polymerizations

The following method was implemented for the synthesis of poly(Ph-PZ), poly(Ph-PZ)-10, poly(Ph-PZ)-50, and poly(TAA-PZ) (the amount of reagents are detailed for each polymer in the following sections). 5,10-dihydrophenazine, dichlorobenzene, tris(4-bromophenyl)amine, sodium tertbutoxide, RuPhos ligand, and RuPhos Pd G2 precatalyst were charged to a schlenk tube. A nitrogen atmosphere was established and toluene was added. The reaction was

stirred at 110 °C for 16 hours. Upon completion of the reaction time, the polymer was suspended in dichloromethane and washed with water 3 times. After filtration, the polymer was dried at 65 °C under vacuum.

Synthesis of Poly(Ph-PZ)

The general procedure for Buchwald-Hartwig cross-coupling polymerization was followed using 5,10-dihydrophenazine (273 mg, 1.50 mmol, 1 equiv), 1,4-dichlorobenzene (221 mg, 1.50 mmol, 1 equiv), RuPhos (14 mg, 0.03 mmol, 0.02 equiv), RuPhos Pd G2 precatalyst (23 mg, 0.03 mmol, 0.02 equiv), and NaOtBu (346 mg, 3.6 mmol, 2.4 equiv). The polymer (357 mg) was obtained as a tan powder. IR (ATR, cm^{-1}): 3033, 1604, 1503, 1476, 1455, 1329, 1260, 1093, 1061, 1015, 908, 817, 723, 620, 559. Elemental Anal. Found: C, 79.63; H, 4.45; Cl, 2.71.

Synthesis of Poly(Ph-PZ)-10

The general procedure for Buchwald-Hartwig cross-coupling polymerization was followed using 5,10-dihydrophenazine (273 mg, 1.50 mmol, 1 equiv), 1,4-dichlorobenzene (198.5 mg, 1.35 mmol, 0.9 equiv), tris(4-bromophenyl)amine (48.2 mg, 0.1 mmol, 0.067 equiv), RuPhos ligand (14 mg, 0.03 mmol, 0.02 equiv), RuPhos Pd G2 precatalyst (23 mg, 0.03 mmol, 0.02 equiv), and NaOtBu (346 mg, 3.6 mmol, 2.4 equiv). The polymer (394 mg) was obtained as a brown powder. IR (ATR, cm^{-1}): 3033, 1603, 1502, 1476, 1455,

1329, 1259, 1156, 1093, 1061, 1015, 920, 817, 723, 620, 559. Elemental Anal. Found: C, 80.50; H, 4.71; Cl, 1.19.

Synthesis of Poly(Ph-PZ)-50

The general procedure for Buchwald-Hartwig cross-coupling polymerization was followed using 5,10-dihydrophenazine (273 mg, 1.50 mmol, 1 equiv), 1,4-dichlorobenzene (110 mg, 0.75 mmol, 0.5 equiv), tris(4-bromophenyl)amine (241 mg, 0.5 mmol, 0.33 equiv), RuPhos ligand (14 mg, 0.03 mmol, 0.02 equiv), RuPhos Pd G2 precatalyst (23 mg, 0.03 mmol, 0.02 equiv), and NaOtBu (346 mg, 3.6 mmol, 2.4 equiv). The polymer (439 mg) was obtained as a brown powder. IR (ATR, cm^{-1}): 2079, 1605, 1499, 1479, 1455, 1333, 1280, 1259, 1156, 1093, 1061, 1015, 820, 730, 617, 555. Elemental Anal. Found: C, 79.96; H, 4.69; Br, 0.54; Cl, 0.67.

Synthesis of Poly(TAA-PZ):

The general procedure for Buchwald-Hartwig cross-coupling polymerization was followed using 5,10-dihydrophenazine (273 mg, 1.50 mmol, 1 equiv), tris(4-bromophenyl)amine (482 mg, 1.0 mmol, 0.67 equiv), RuPhos ligand (14 mg, 0.03 mmol, 0.02 equiv), RuPhos Pd G2 precatalyst (23 mg, 0.03 mmol, 0.02 equiv), and NaOtBu (346 mg, 3.6 mmol, 2.4 equiv). The polymer (414 mg) was obtained as a brown powder. IR (ATR, cm^{-1}): 3028, 1606, 1497, 1479, 1456, 1310, 1282, 1256, 1158, 1099, 1060, 1013, 822, 817, 732, 616, 553. Elemental Anal. Found: C, 76.83; H, 4.59; Br, 1.49.

8.4 Conclusion

The performance metrics of the phenazine-based materials described herein as cathodes are among the highest reported for organic cathode materials. Careful design of cross-linked copolymer poly(Ph-PZ)-10 resulted in improved capacity, stability, and rate performance over the linear poly(Ph-PZ). At an average operating voltage of 3.45 V versus Li/Li⁺, poly(Ph-PZ)-10 delivers 223 mAh g⁻¹ and 220 mAh g⁻¹ at 5 C and 120 C, respectively. Addition of the cross-linker was shown to enable a higher active-material fraction to be used in the cell while maintaining a high percentage of the material's capacity. The family of materials studied here exhibited excellent ionic transport kinetics that resulted in extraordinary capacity retention at very high C-rates. Although comparison with commercial batteries is difficult, these materials exhibit competitive energy densities while providing power densities comparable to those of commercial capacitors, demonstrating the viability of organic cathodes in EES devices. Specifically, this work demonstrates the impact of fast ionic diffusion through amorphous materials on rate capability.

8.5 References

- (1) Howell, D. et. al., Enabling Fast Charging: A Technology Gap Assessment, 2017, DOI: <https://doi.org/10.2172/1416167>, accessed: September, 2019.

- (2) Schütter, C.; Pohlmann, S.; Balducci, A. *Adv. Energy Mater.* **2019**, *9*, 1900334.
- (3) Tian, R.; Park, S. H.; King, P. J.; Cunningham, G.; Coelho, J.; Nicolosi, V.; Coleman, J. N. *Nat. Commun.* **2019**, *10*, 1933.
- (4) Yao, M.; Kuratani, K.; Kojima, T.; Takeichi, N.; Senoh, H.; Kiyobayashi, T. *Sci. Rep.* **2014**, *4*, 3650.
- (5) Armand, M. *Solid State Ionics* **1983**, *9-10*, 745.
- (6) Nevers, D. R.; Brushett, F. R.; Wheeler, D. R. *J. Power Sources* **2017**, *352*, 226.
- (7) Häupler, B.; Wild, A.; Schubert, U. S. *Adv. Energy Mater.* **2015**, *5*, 1402034.
- (8) Bryan, A. M.; Santino, L. M.; Lu, Y.; Acharya, S.; D'Arcy J. M. *Chem. Mater.* **2016**, *28*, 5989.
- (9) Ma, Y.; Ma, J.; Cui, G.; *Energy Storage Mater.* **2019**, *20*, 146.
- (10) Tan, S. J.; Zeng, X. X.; Ma, Q.; Wu, X. W.; Guo, Y. G. *Electrochem. Energy Rev.* **2018**, *1*, 113.
- (11) Dirlam, P. T.; Glass, R. S.; Char, K.; Pyun, J. *J. Polym. Sci. Part A* **2017**, *55*, 1635.
- (12) Muench, S.; Wild, A.; Friebe, C.; Häupler, B.; Janoschka, T.; Schubert, U. S. *Chem. Rev.* **2016**, *116*, 9438.
- (13) Lopez, J.; Mackanic, D. G.; Cui, Y.; Bao, Z. *Nat. Rev. Mater.* **2019**, *4*, 312.

- (14) Peterson, B. M.; Ren, D.; Shen, L.; Wu, Y.-C. M.; Ulgut, B.; Coates, G. W.; Abruña, H. D.; Fors, B. P. *ACS Appl. Energy Mater.* **2018**, *1*, 3560.
- (15) Lee, M.; Hong, J.; Lee, B.; Ku, K.; Lee, S.; Park, C. B.; Kang, K. *Green Chem.* **2017**, *19*, 2980.
- (16) Yang, S.-Y.; Chen, Y.-J.; Zhou, G.; Fu, Z.-W. *J. Electrochem. Soc.* **2018**, *165*, A1422.
- (17) Wang, J.; Tee, K.; Lee, Y.; Riduan, S. N.; Zhang, Y. *J. Mater. Chem. A* **2018**, *6*, 2752.
- (18) Matsunaga, T.; Kubota, T.; Sugimoto, T.; Satoh, M. *Chem. Lett.* **2011**, *40*, 750.
- (19) Hollas, A.; Wei, X.; Murugesan, V.; Nie, Z.; Li, B.; Reed, D.; Liu, J.; Sprenkle, V.; Wang, W. *Nat. Energy* **2018**, *3*, 508.
- (20) Peng, C.; Ning, G.-H.; Su, J.; Zhong, G.; Tang, W.; Tian, B.; Su, C.; Yu, D.; Zu, L.; Yang, J. *Nat. Energy* **2017**, *2*, 17074.
- (21) Wang, J.; Chen, C. S.; Zhang, Y. *ACS Sustainable Chem. Eng.* **2018**, *6*, 1772.
- (22) Kwon, G.; Lee, S.; Hwang, J.; Shim, H. S.; Lee, B.; Lee, M. H.; Ko, Y.; Jung, S. K.; Ku, K.; Hong, J.; Kang, K. *Joule* **2018**, *2*, 1771.
- (23) Dai, G.; Wang, X.; Qian, Y.; Niu, Z.; Zhu, X.; Ye, J.; Zhao, Y.; Zhang, X. *Energy Storage Mater.* **2019**, *16*, 236.
- (24) Niu, Z.; Wu, H.; Liu, L.; Dai, G.; Xiong, S.; Zhao, Y.; Zhang, X. *J. Mater. Chem. A* **2019**, *7*, 10581.

- (25) Xu, K. *Chem. Rev.* **2004**, *104*, 4303.
- (26) Weber, A. Z.; Mench, M. M.; Meyers, J. P.; Ross, P. N.; Gostick, J. T.; Lui, Q. *J. Appl. Electrochem.* **2011**, *41*, 1137.
- (27) Le Nest, J. F.; Callens, S.; Gandini, A.; Armand, M. *Electrochim. Acta* **1992**, *37*, 1585.
- (28) Garcia-Calvo, O.; Lago, N.; Devaraj, S.; Armand, M. *Electrochim. Acta* **2016**, *220*, 587.
- (29) Barrios-Landeros, F.; Carrow, B. P.; Hartwig, J. F. *J. Am. Chem. Soc.* **2009**, *131*, 8141.
- (30) Fors, B. P.; Buchwald, S. L. *J. Am. Chem. Soc.* **2009**, *131*, 12898.
- (31) Castillo-Martínez, E.; Carretero-González, J.; Armand, M. *Angew. Chem. Int. Ed.* **2014**, *53*, 5341; *Angew. Chem.* **2014**, *126*, 5445.
- (32) G. P. Evans in *Advances in Electrochemical Science and Engineering* (Eds.: H. Gerischer, C. Tobias), VCH, Weinheim, 1990, pp. 3 – 8. [33]
- (33) Wang, X.; Hao, H.; Liu, J.; Huang, T.; Yu, A. *Electrochim. Acta* **2011**, *56*, 4065.
- (34) S. B. Tang, S. B.; M. O. Lai, M. O.; L. Lu, L. *Mater. Chem. Phys.* **2008**, *111*, 149.
- (35) Yang, S.; Wang, X.; Yang, X.; Bai, Y.; Liu, Z.; Shu, H.; Wei, Q. *Electrochim. Acta* **2012**, *66*, 88.
- (36) Cui, Y.; Zhao, Z.; Guo, R. *Electrochim. Acta* **2010**, *55*, 922.

- (37) Kim, H.; Hong, J.; Park, Y. U.; Kim, J.; Hwang, I.; Kang, K. *Adv. Funct. Mater.* **2015**, *25*, 534.
- (38) Yan, G.; Alves-Dalla-Corte, D.; Yin, W.; Madern, N.; Gachot, G.; Tarascon, J.-M. *J. Electrochem. Soc.* **2018**, *165*, A1222.
- (39) Sugimoto, A.; Kotani, T.; Tsugimoto, J.; Yoneda, S. *J. Heterocycl. Chem.* **1989**, *26*, 435.
- (40) Theriot, J. C.; Lim, C.-H.; Yang, H.; Ryan, M. D.; Musgrave, C. B.; Miyake, G. M. *Science* **2016**, *352*, 1082.

8.6 Appendix

Experimental Information

General Reagent Information

Toluene and dichloromethane (DCM) were purchased from J.T. Baker and purified by vigorous purging with argon for 2 hours, followed by passing through two packed columns of neutral alumina under argon pressure. RuPhos (95%), RuPhos Pd G2, sodium *tert*-butoxide (NaOtBu), 1,4-dichlorobenzene (>99%), tris(4-bromophenyl)amine (98%), LiPF₆ (1M in EC/DEC (1:1 v/v) (battery grade), LiClO₄ (99.99%), MgClO₄ (ACS grade), and trifluoroacetic acid (reagent plus, 99%) were purchased from Millipore Sigma and used as received. Phenazine (99%) and 1,4-dibromobenzene (98%) were purchased from Alfa Aesar and used as received. NaClO₄ (98+%) was purchased from Fluka Chemical Corporation and used as received. Sodium dithionite was

purchased from Oakwood Chemicals and used as received. Tetrabutylammonium Perchlorate (TBAP) (98%, TCI) was purified by recrystallization from ethyl acetate three times and dried under reduced pressure at 60 °C for 12 hours. Acetonitrile (MeCN) (HPLC Grade) was purchased from Fisher Chemical and dried over activated 4 Å molecular sieves (Mallinckrodt Chemicals) for at least two days before use. 1-Methyl-2-pyrrolidinone (NMP) (anhydrous 99.5%) was purchased from Sigma-Aldrich and used as received. Microcloth PSA (polishing paper) was purchased from Buehler. Ordered mesoporous carbon, CMK-3, was purchased from ACS materials and used as received. Super P carbon (Imerys Graphite& Carbon) and poly(vinylidene fluoride) (PVDF) (Kynar Flex) were dried overnight in a vacuum oven at 60 °C and stored in a desiccator.

Cyclic Voltammetry Procedures

Benchtopy cyclic voltammetry experiments were performed in a three-compartment glass cell with medium porosity glass frits separating the compartments. An Ag/Ag⁺ reference electrode and a Pt wire counter electrode were used, unless otherwise specified. All 3-mm glassy carbon (GC) electrodes were purchased from CH Instruments. Prior to the experiment, electrodes were polished using diamond paste and MetaDi Fluid (Buehler). All cyclic voltammetry measurements were done in 0.1 M TBAP in MeCN unless otherwise specified. The potentials in the CVs was corrected for iR drop using a ferrocene reference at different scan rates.

Device Testing

Device measurements were conducted in CR 2032 coin cell casings which were assembled in an argon filled glove box with oxygen levels below 1 ppm. The anode was lithium metal and the working electrode was fabricated from a slurry of 30 wt% active material ($\sim 0.6 \text{ mg/cm}^2$), 30 wt% Super P carbon, 30 wt% CMK-3, and 10 wt% PVDF as the binder in NMP. The high loading cathode was fabricated with 60 wt% active material, 15 wt% Super P carbon, 15 wt% CMK-3, and 10 wt% poly(vinylidene fluoride) (PVDF) as binder. The slurries were spread onto a carbon paper current collector using the doctor's blade method with one layer of scotch tape. The coated electrode was dried for 2 h at 60 °C followed by 14 h at 110 °C in a vacuum oven. The thickness of the cathode composite (active material + carbon + binder + current collector) ranged from 100 to 125 μm . A measurement of the thickness of the slurry alone was impossible due to penetration of the slurry into the carbon paper current collector during deposition. The typical mass loading of the active material on the cathode was $\sim 0.34 \text{ mg/cm}^2$, but also varied due to the nature of the carbon paper. A polypropylene separator (Celgard 2300) or a glass microfiber filter (GF/A, Whatman) was used as the separator between the two electrodes. The electrolyte solution was 1:1 by volume of EC (ethylene carbonate) to DEC (diethyl carbonate) with 1 M LiPF_6 (Aldrich) or 1 M NaPF_6 (Alfa Aesar). In cells with the celgard separator, 60 μL of electrolyte solution were used, while 80 μL were used in the cells with the fiber glass separator. An Arbin BT2000 battery

tester was used to perform galvanostatic charge-discharge experiments on the coin cells with a constant charge-discharge current rate of 5 C, over a voltage range of 1.5 V to 4.3 V vs. Li/Li⁺ at 25 °C in order to evaluate the cycling performance. For rate measurements, the coin cell was charged at 5 C and discharged at the indicated C-rate. The cells were first cycled at 5 C to prevent the initial cycles, when the electrode-electrolyte interfaces are forming, from affecting the results of the rate testing.

The theoretical capacities of poly(Ph-PZ), poly(Ph-PZ)-10, poly(Ph-PZ)-50, and poly(TAA-PZ) were calculated using Eq. (1):

$$C_{theor} = \frac{nF}{3600 \left(\frac{M_w}{1000}\right)} \quad (1)$$

where *n* is the number of electrons that can be stored per a redox active unit, *F* is Faraday's constant (96485 C mol⁻¹), and *M_w* is the molar mass of the repeating unit. The C-rate is the amount of current required to charge-discharge a battery in a specified time, where 1 C is the necessary current to pass the entire charge of *C_{theor}* in 1 hour.

CV studies were conducted using assembled coin cells of each of the four polymer electrodes to obtain diffusion coefficients of the PF₆⁻ ions through the solid-state electrode material. A range of scan rates was employed, and for each experiment, the peak cathodic current of the two redox couples were obtained. From plots of the peak current versus the square root of scan rate,

the slope was extracted and used to calculate diffusion coefficients according to Eq. 2, the Randles-Sevcik equation:¹

$$i_p = 2.69 \times 10^5 n^3/2 AD_o^{1/2} C v^{1/2} \quad (2)$$

Where n is the number of electrons transferred, A is the surface area of the electrode in cm^2 , C is the concentration of the diffusing species in mol/cm^3 , v is the scan rate in V/s , i_p is the peak current in Amperes, D is the diffusion coefficient in cm^2/s .

Ultramicroelectrode Studies

Phenazine, phenazine with 50 mM trifluoroacetic acid, N,N'-dimethylphenazine, and N,N'-diphenylphenazine were each dissolved at a 1 mM concentration in solutions with 0.1 M TBAP supporting electrolyte in acetonitrile. A 10 μm platinum electrode was used as the working electrode in a three-compartment cell with a platinum wire as the counter electrode and a Ag/Ag^+ reference electrode. Cyclic voltammograms were obtained at 20 mV/s and used to obtain a steady state response for the redox events for each of the small molecules due to convergent flux.

The limiting current at steady state, following each redox event, was used to calculate the diffusion coefficient, D , by Eq. (3):

$$D = \frac{i_L}{2\pi FdC} \quad (3)$$

where i_L is the limiting current, d is the diameter of the electrode, and C is the concentration of the analyte (1 mM), and F is Faraday's constant. To determine the standard heterogeneous rate constant, k^0 , Eq (4)² was employed:

$$\left(\frac{4D_R}{\pi k^0 r_0}\right) \exp[-(1 - \alpha)nf(E - E^{0'})] = \frac{i_L - i}{i} - \frac{D_R}{D_0} \exp[-nf(E - E^{0'})] \quad (4)$$

By assuming that $D_0 = D_R = D$, the equation can be simplified to Eq. (5) for reductions and Eq. (6) for oxidations:

$$\ln\left(\frac{i_L - i}{i}\right) = \alpha nf\left(E - E^{1/2}\right) + \ln\left(\frac{4D}{\pi k_s r_0}\right) \quad (5)$$

$$\ln\left(\frac{i_L - i}{i}\right) = (1 - \alpha)nf\left(E - E^{1/2}\right) + \ln\left(\frac{4D}{\pi k_s r_0}\right) \quad (6)$$

where i is the current at a given potential, α is the transfer coefficient, n is the number of electrons transferred, E is the potential, $E^{1/2}$ is the potential at half the limiting current, and r_0 is the radius of the electrode (5 μm). A plot of $\ln\left(\frac{i_L - i}{i}\right)$ vs. $E - E^{1/2}$ will give an intercept of $\ln\left(\frac{4D}{\pi k^0 r_0}\right)$ from which the rate constant was determined. The calculated D and k^0 values are found in Tables S1 and 8.1, respectively.

Ultraviolet-Visible Light Spectroscopy Studies

The UV-Vis experiments were conducted on a Hewlett Packard spectrophotometer (model 8453). A semi micro rectangular quartz spectrophotometer cell with a path length of 10 mm was used for the UV-Vis measurements. The absorbance was measured over a range from 190 to 1100 nm.

Scanning Electron Microscopy Studies

Images were obtained using a Zeiss Gemini 500 scanning electron microscope. The samples were sonicated in NMP to disperse the polymers in solution and then drop cast onto a clean silicon wafer substrate for analysis. A working voltage of 1.0 keV was used for imaging with a 20.0 μm aperture. A high efficiency secondary electron detector was mixed with the in-lens detector to improve topographical imaging while maintaining a high resolution.

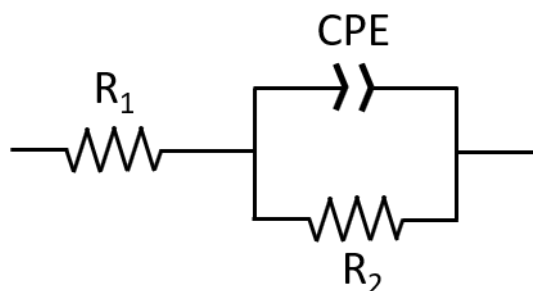
X-ray Diffraction Spectroscopy (XRD)

Powder XRD spectra were taken using a Rigaku Ultima IV X-ray diffractometer. Measurements were taken using a 40 kV operating voltage with a 44 mA current at a scan speed of 5.0 degrees per minute.

Electrochemical Impedance Spectroscopy (EIS)

Potentiostatic electrochemical impedance spectroscopy (PEIS) measurements were carried out using a BioLogic SP-150 potentiostat on assembled coin cells. Impedance measurements were obtained at six steady state potentials after the cells had been allowed to sit fully assembled for at least 24 hours. The cell was cycled once at 1 mV/s to 4.3 V vs. Li/Li⁺ and reversed to 2.7 V. The cell was held at each potential for 600 seconds prior to each PEIS measurement to obtain a steady state in the system and swept between the tested potentials at 1 mV/s. The measurements were taken over a frequency range of 0.001-1000000 Hz with an AC amplitude of 10.0 mV.

A Nyquist plot for each of the polymers was made to compare the charge transfer kinetics and electric responses of each of the polymers. Using BioLogics's Z-fit software, the semicircle region at high and middle frequencies of the Nyquist plots at 2.7 V were fit with the following circuit:



R_1 corresponds to the solution resistance, R_2 represents in charge transfer resistance, and CPE is the constant phase element accounting for the capacitance associated with the double layer formed between the electrode and the electrolyte. The obtained fit values are printed in Table S2.

Energy and Power Density Calculation

Based on the rate data for poly(Ph-PZ)-10 from this work and data on a commercial LiNMC³, the energy density and power density of the active material and of the cathode composite material were calculated based on Eq. (7) and Eq. (8), respectively:

$$\text{Energy density} = C_{sp} \times V \quad (7)$$

$$\text{Power Density} = C_{sp} \times V \times (C \text{ rate}) \quad (8)$$

where C_{sp} is the specific capacity, V is the average discharge potential versus a lithium metal anode, and C-rate is the C-rate the coin cell was discharged at.

Supplementary Figures

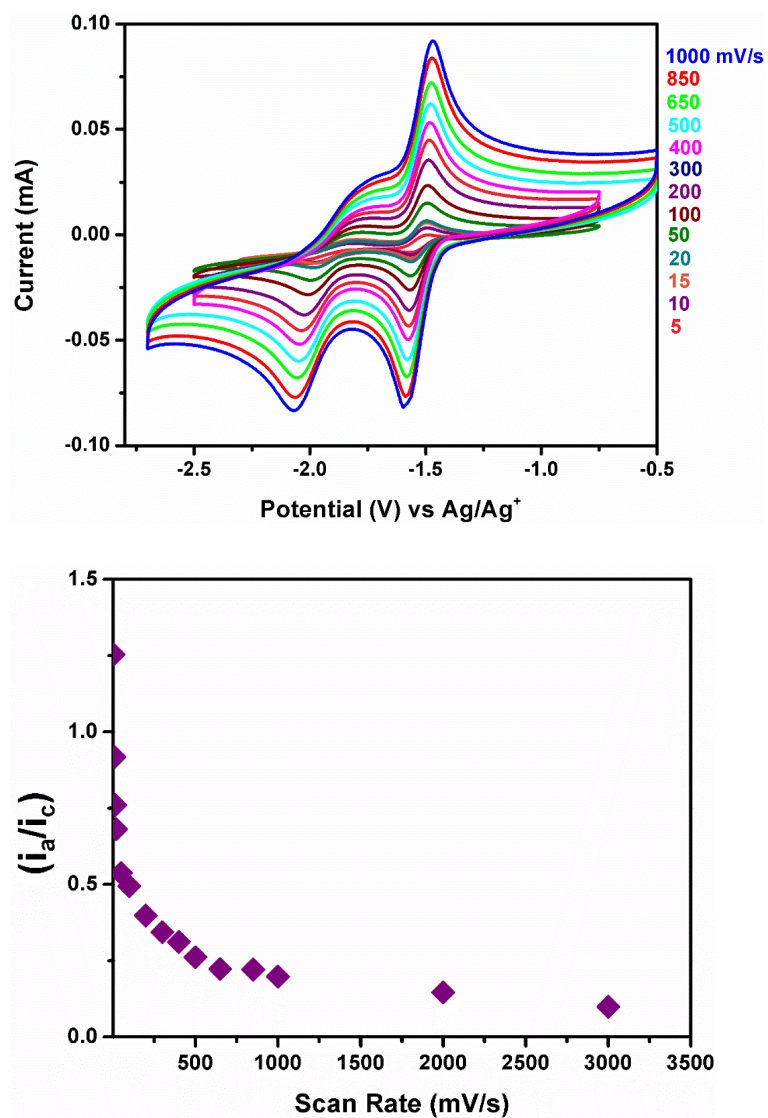


Figure 8.6. (a) Cyclic voltammograms at various scan rates for a solution of 1 mM phenazine in 0.1 M TBAP in MeCN and (b) plot of peak anodic current/peak cathodic current of the second redox couple ($E_{1/2} = -1.92$ V) versus scan rate.

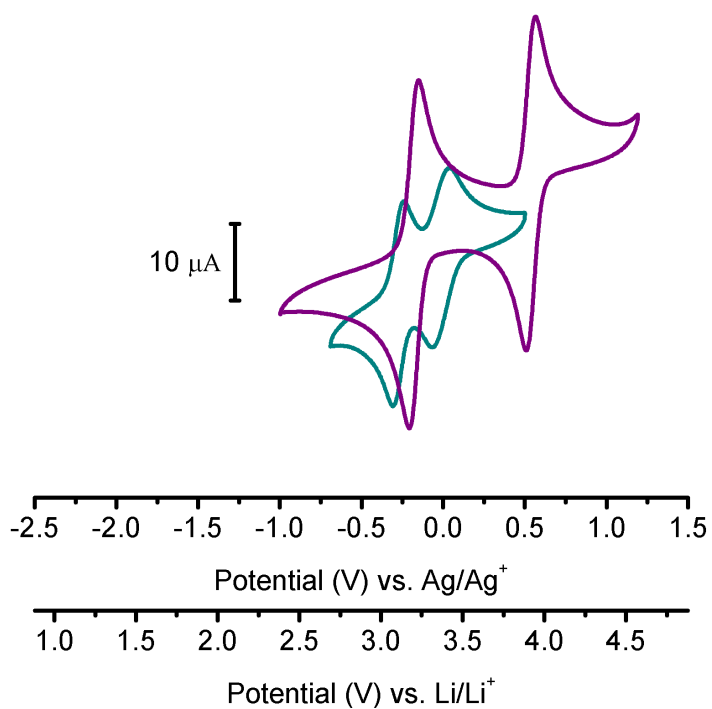


Figure 8.7. CV profiles in 0.1 M TBAP in MeCN at a glassy carbon electrode for 1 mM phenazine with the addition of 50 mM TFA to the electrolyte solution (green) and 1 mM N,N'-dimethylphenazine (purple) at 50 mV/s.

Table 8.4. Diffusion coefficients obtained from the limiting currents at an ultra-microelectrode and ratio of peak anodic current/peak cathodic current from cyclic voltammetry at a glassy carbon electrode for phenazine small molecules at 50 mV/s.

Small Molecule	$D_{0 \rightarrow \pm 1}$ (cm²/s)	$D_{\pm 1 \rightarrow \pm 2}$ (cm²/s)	$i_{pk,a}/i_{pk,c}$ (0$\rightarrow\pm 1$)	$i_{pk,a}/i_{pk,c}$ ($\pm 1 \rightarrow \pm 2$)
Phenazine	6.3×10^{-6}	6.4×10^{-6}	1.01	0.54
Phenazine + 50 mM TFA	1.1×10^{-5}	1.2×10^{-5}	1.14	0.80
N,N'-dimethyl-phenazine	7.1×10^{-6}	6.7×10^{-6}	0.98	1.02
N,N'-diphenyl-phenazine	8.0×10^{-6}	7.1×10^{-6}	0.99	0.89

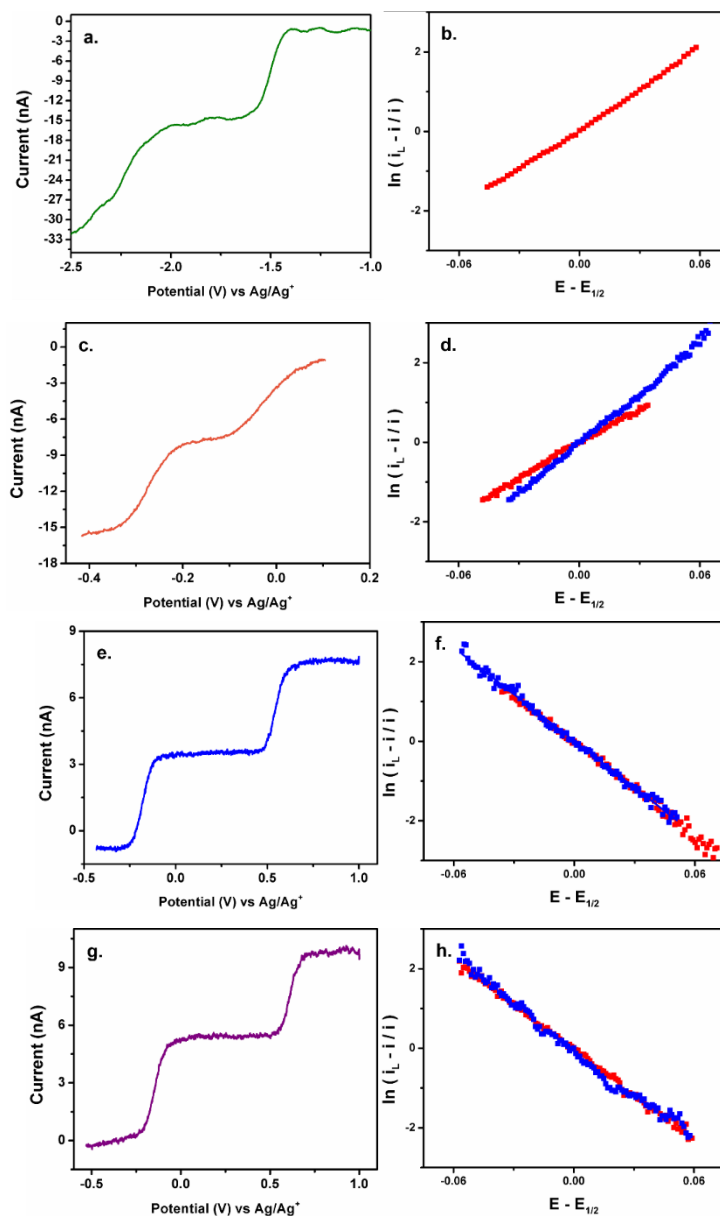


Figure 8.8. Steady state profiles (a,c,e,g) at 20 mV/s and linear fits for determining k^0 (b,d,f,h) for the first electron transfer (red) and the second electron transfer (blue) obtained at a 10 μ m electrode for phenazine (a,b), phenazine with 50 mM TFA (c,d), N,N'-dimethyl-phenazine (e,f), and N,N'-diphenyl-phenazine (g,h).

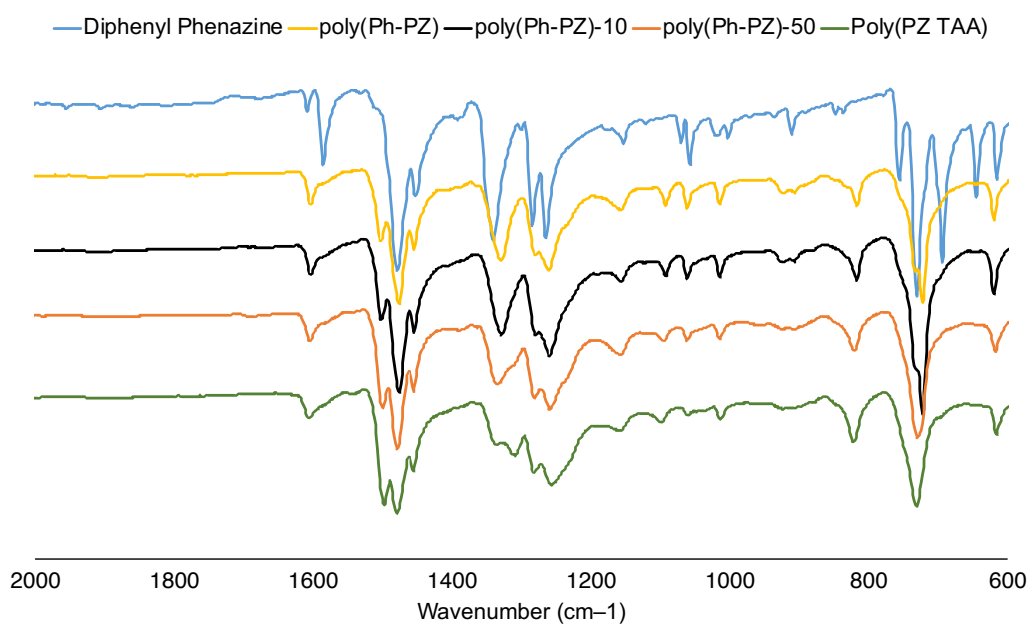


Figure 8.9. Infrared spectra of N,N'-diphenyl-5,10-dihydrophenazine, poly(Ph-PZ), poly(Ph-PZ)-10, poly(Ph-PZ)-50, poly(TAA-PZ)

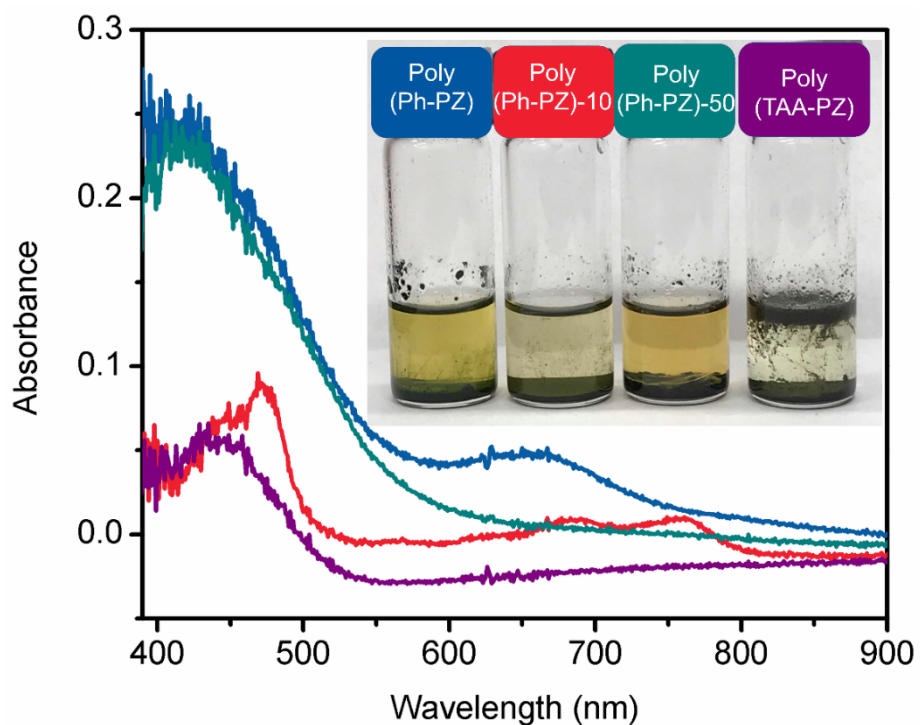


Figure 8.10. Absorbance spectra of solutions of 1 M LiPF_6 in EC/DEC obtained after 10 mg of poly(Ph-PZ) (blue), poly(Ph-PZ)-10 (pink), poly(Ph-PZ)-50 (green) and poly(TAA-PZ) (purple) were suspended in solutions for 1 week. All solutions were filtered before obtaining UV-Vis spectra. Inset shows a picture of the solutions immediately before the absorbance spectra was obtained.

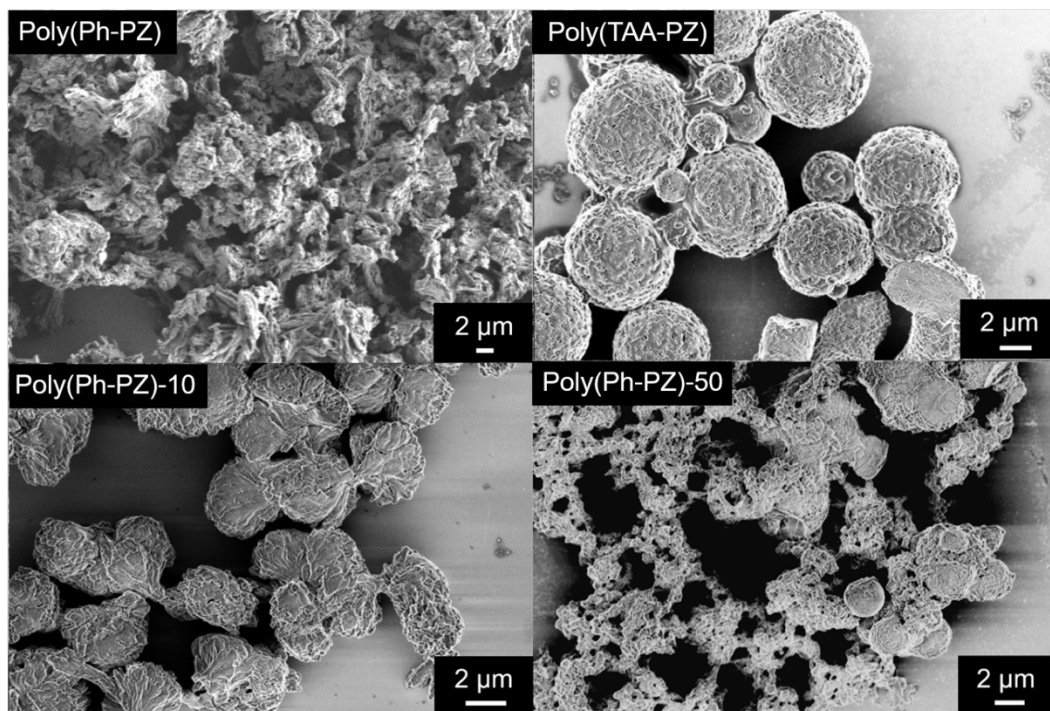


Figure 8.11. SEM images of poly(Ph-PZ), poly(TAA-PZ), poly(Ph-PZ)-10, and poly(Ph-PZ)-50. While poly(Ph-PZ), poly(TAA-PZ), and poly(Ph-PZ)-10 all appear to possess unique morphology, poly(Ph-PZ)-50 appears as a combination of the morphologies present in poly(Ph-PZ) and poly(TAA-PZ).

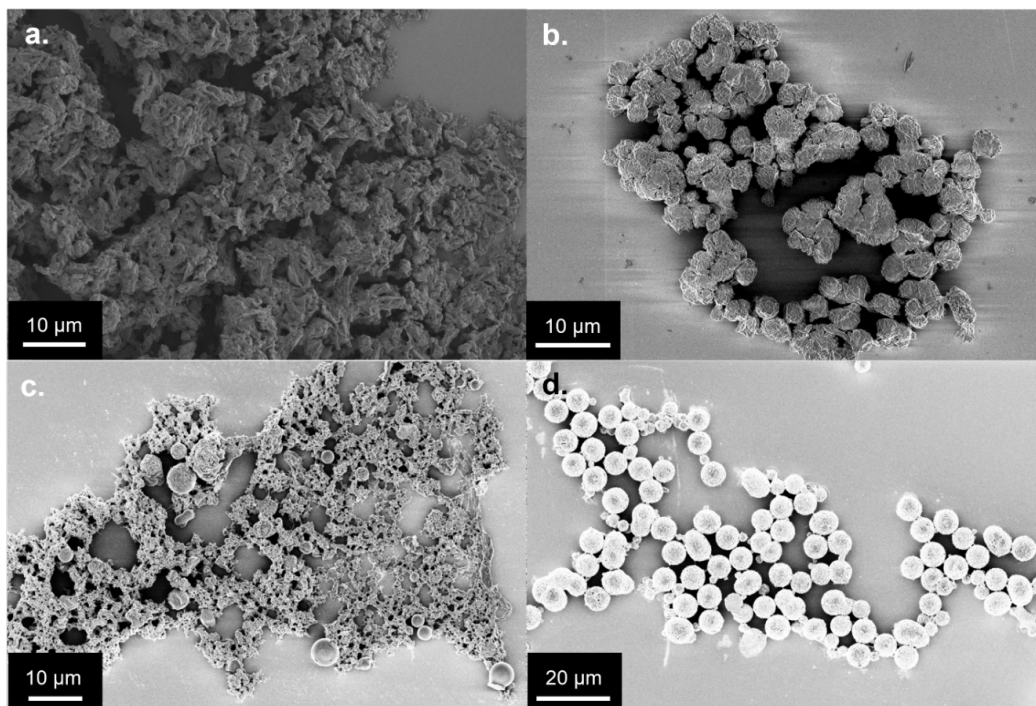


Figure 8.12. SEM images of (a) poly(Ph-PZ), (b) poly(Ph-PZ)-10, (c) poly(Ph-PZ)-50, and (d) poly(TAA-PZ). These images exhibit the unique morphologies of poly(Ph-PZ), poly(TAA-PZ), and poly(Ph-PZ)-10 while poly(Ph-PZ)-50 appears as a combination of the morphologies present in poly(Ph-PZ) and poly(TAA-PZ). This suggests that early in the reaction, 5,10-dihydrophenazine couples with tris(4-bromophenyl) amine so poly(TAA-PZ) precipitates out and later in the reaction, when the concentration of tris(4-bromophenyl) amine is depleted, polymer chains of 5,10-dihydrophenazine coupled mostly with the dichlorobenzene form.

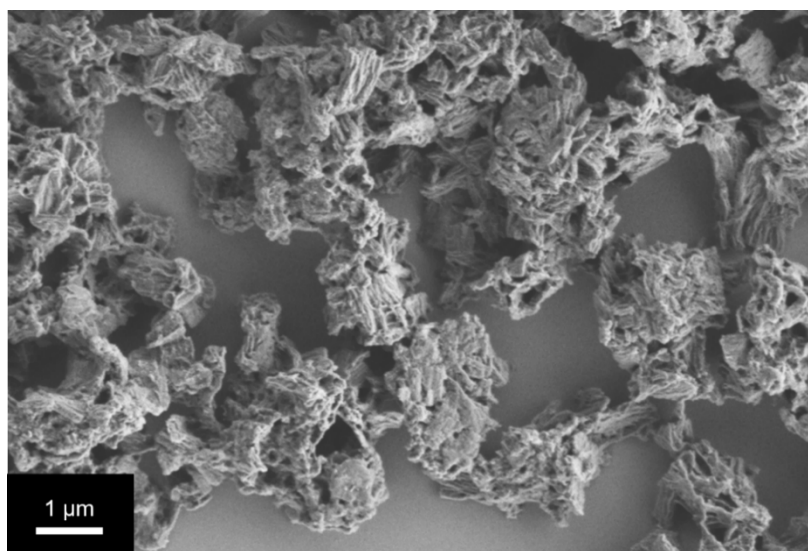


Figure 8.13. SEM image of poly(Ph-PZ)-10 made from cross coupling 9,10-dihydro-phenazine (1.0 equiv.) with dibromobenzene (0.90 equiv.) and tris(4-bromophenyl) amine (0.067 equiv.). The unique morphology observed in this polymer compared to poly(Ph-PZ)-10 made with dichlorobenze suggests that the rate at which the cross-coupling with the different monomer units occurs has a significant effect on the obtained morphology of the final polymer which we would expect to also impact other properties of the material as well.

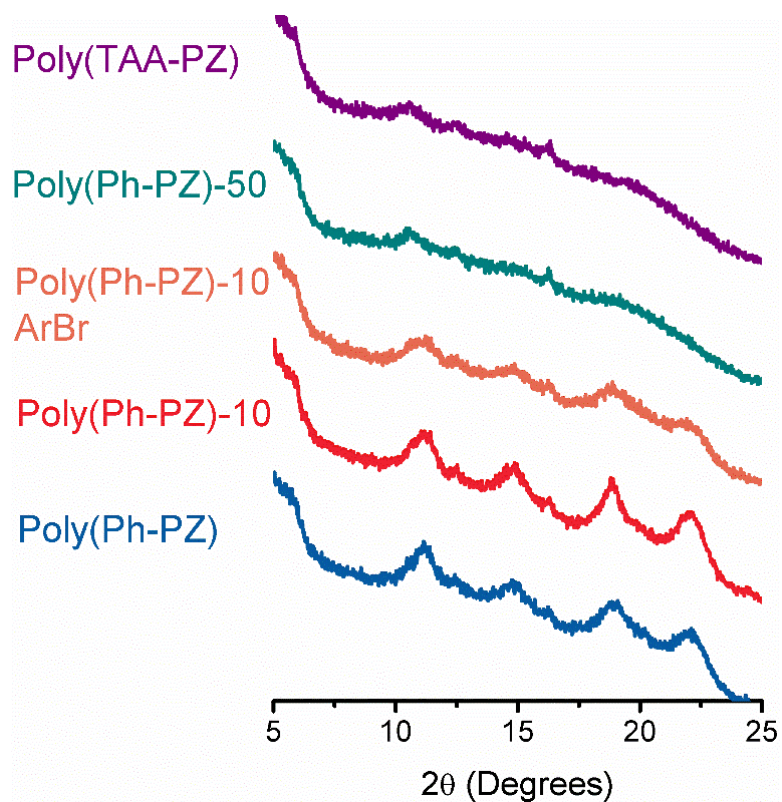


Figure 8.14. Powder X-ray diffraction (XRD) spectra for poly(Ph-PZ) (blue), poly(Ph-PZ)-10 (red), poly(Ph-PZ)-10 synthesized from cross-coupling with dibromobenzene (orange), poly(Ph-PZ)-50 (green), and poly(TAA-PZ) (purple). The four peaks visible in poly(Ph-PZ) and poly(Ph-PZ)-10 are lost with the increasing molar equivalents of tris(4-bromophenyl amine) in poly(Ph-PZ)-50 and poly(TAA-PZ), as well in poly(Ph-PZ)-10 synthesized from cross-coupling with dibromobenzene in place of dichlorobenzene.

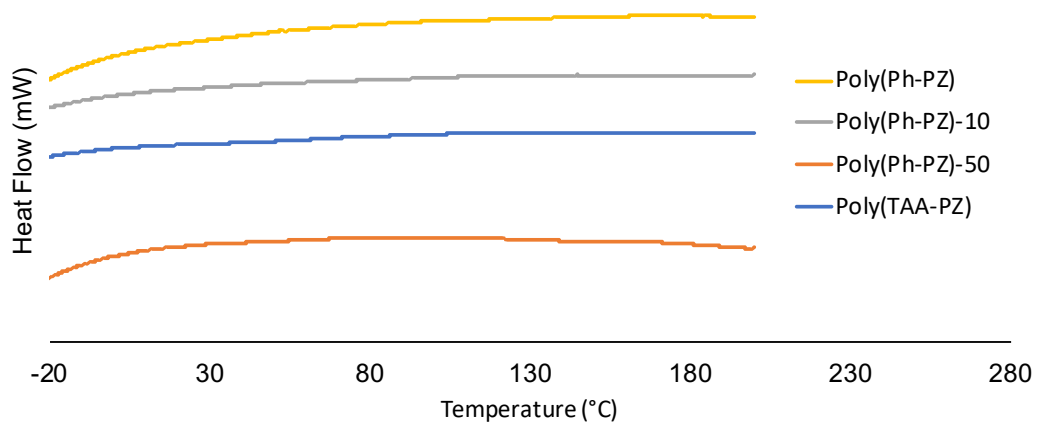


Figure 8.15. Differential Scanning Calorimetry (DSC) traces of the second heat of poly(Ph-PZ), poly(Ph-PZ)-10, poly(Ph-PZ)-50 and poly(TAA-PZ). No T_g or T_c were observed up to 200 °C in any of the polymers, supporting their amorphous structures.

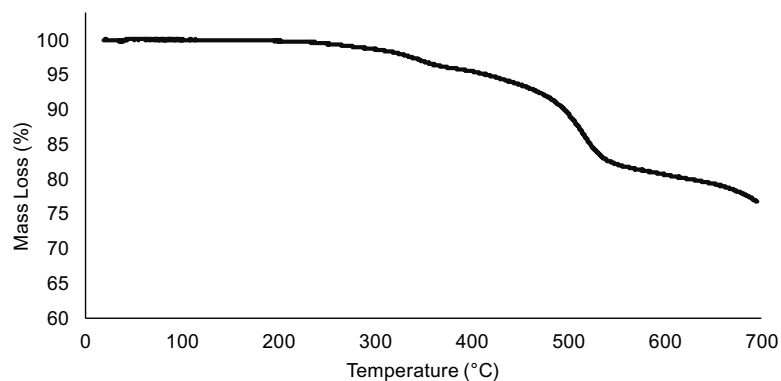


Figure 8.16. Thermogravimetric Analysis (TGA) of poly(Ph-PZ).

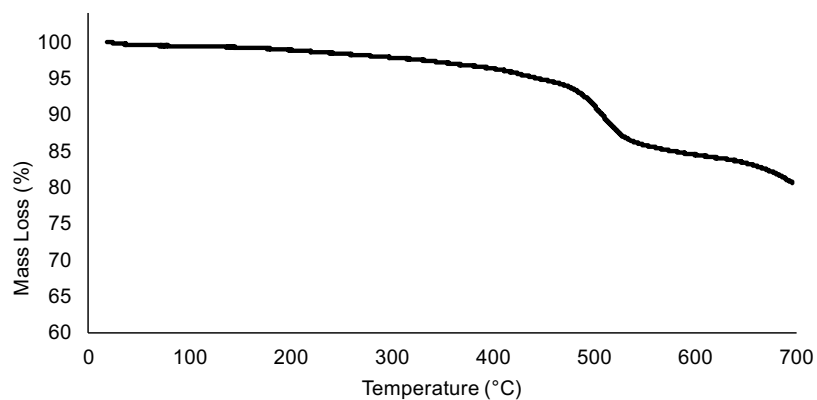


Figure 8.17. TGA of poly(Ph-PZ)-10

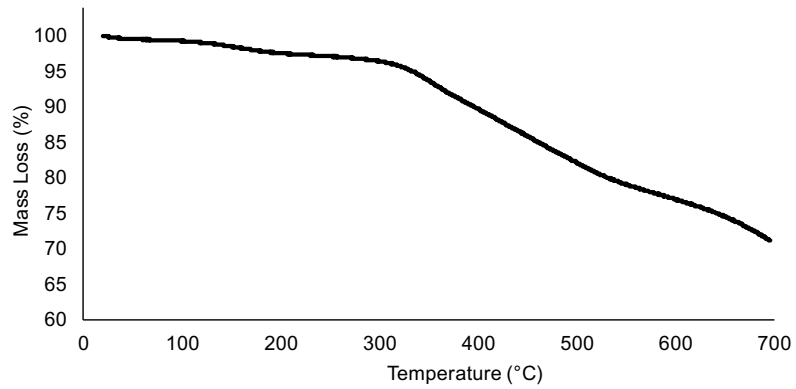


Figure 8.18. TGA of poly(Ph-PZ)-50.

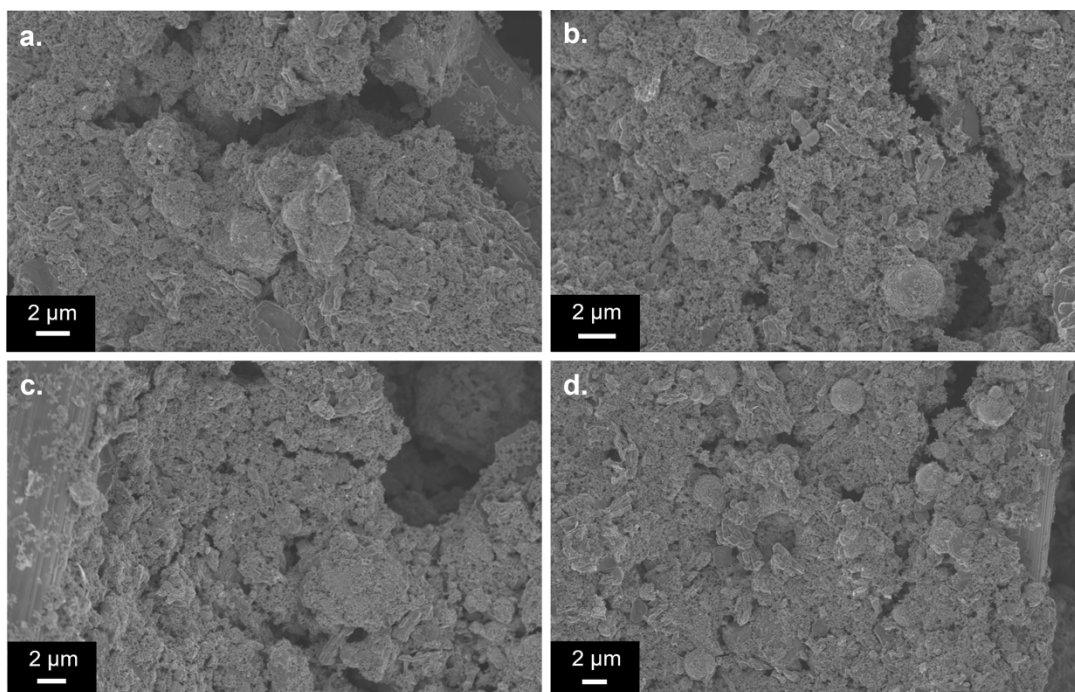


Figure 8.19. SEM images of pristine cathode composites (active material + carbon + binder on carbon paper current collector) of (a) poly(Ph-PZ), (b) poly(PH-PZ)-10, (c) poly(Ph-PZ)-50, and (d) poly(TAA-PZ).

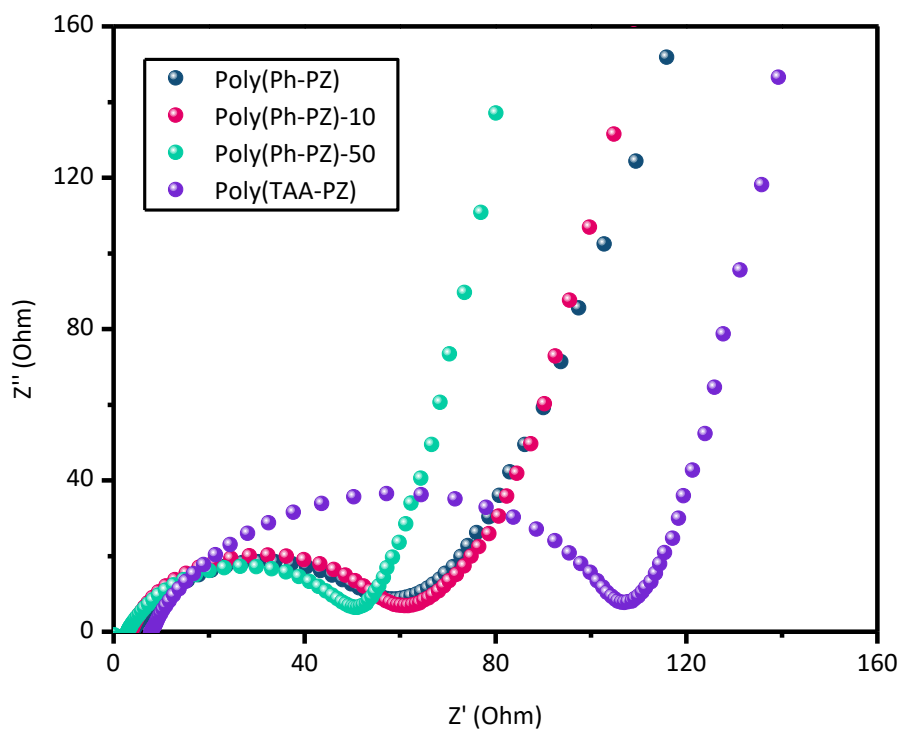


Figure 8.20. Potentiostatic electrochemical impedance spectra at 2.7 V vs. Li/Li⁺ of poly(Ph-PZ), poly(TAA-PZ), poly(Ph-PZ)-10, and poly(Ph-PZ)-50.

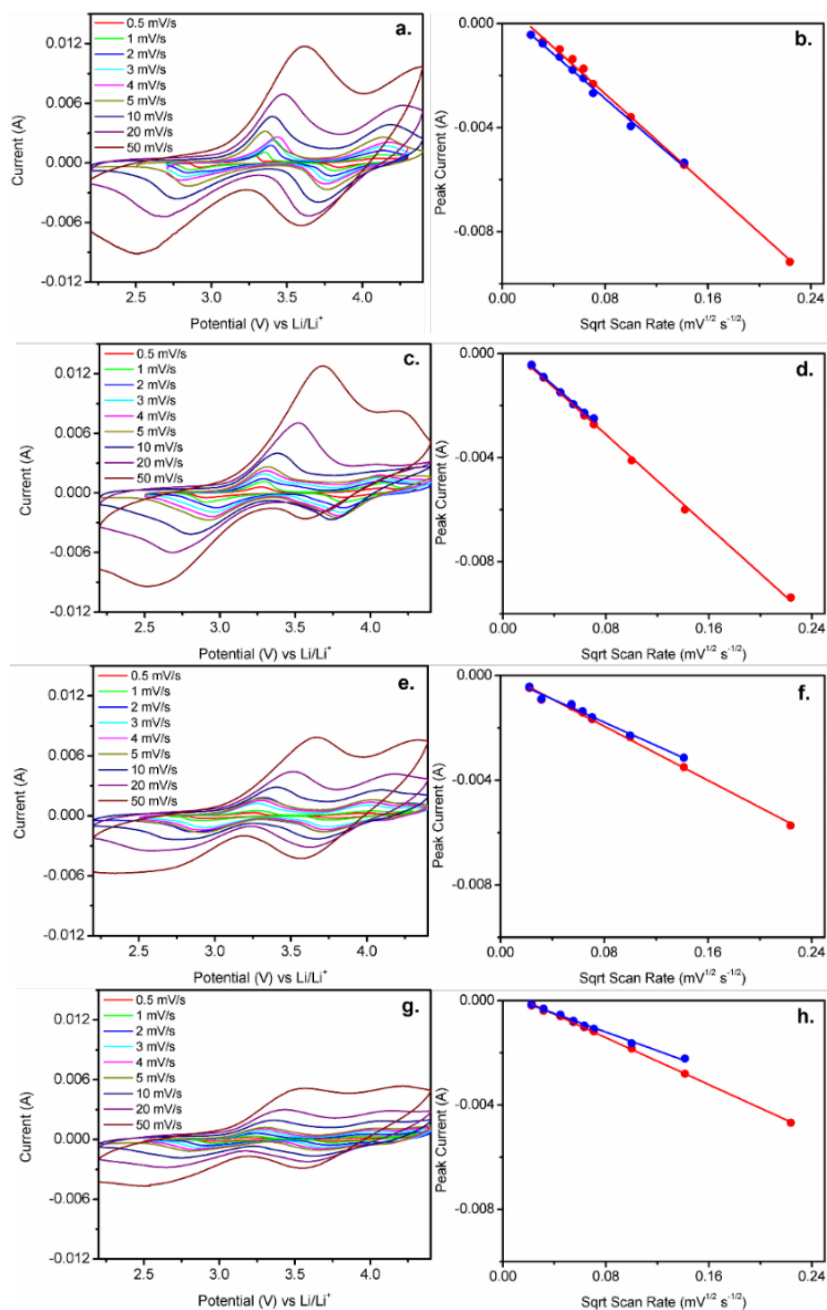


Figure 8.21. Cyclic voltammograms (a,c,e,g) and linear fits of the peak reduction current versus the square root of scan rate (b,d,f,h) for poly(Ph-PZ) (a,b), poly(Ph-PZ)-10 (c,d), poly(Ph-PZ)-50 (e,f), and poly(TAA-PZ) (g,h). The first redox peak (+1→0) fit is shown in red and the second (+2→+1) is shown in blue. The slope of the fit was used to determine the diffusion coefficient of PF₆⁻ in each polymer.

Table 8.5. Fitted values from PEIS at 2.7 V vs. Li/Li⁺.

Active Material	R ₁ (Ω)	CPE(F·s ^(a-1))×10 ⁻⁶	a	R ₂ (Ω)
Poly(Ph-PZ)	4.07± 0.39	45.65 ± 11.86	0.76 ± 0.55	54.00 ± 0.04
Poly(Ph-PZ)-10	3.36 ± 0.37	25.01 ± 6.01	0.80 ± 0.55	57.27 ± 0.66
Poly(Ph-PZ)-50	2.95 ± 0.36	59.34 ± 15.30	0.78 ± 0.55	49.12 ± 0.48
Poly(TAA-PZ)	7.95 ± 0.28	21.77 ± 2.36	0.79 ± 0.52	100.70 ± 0.55

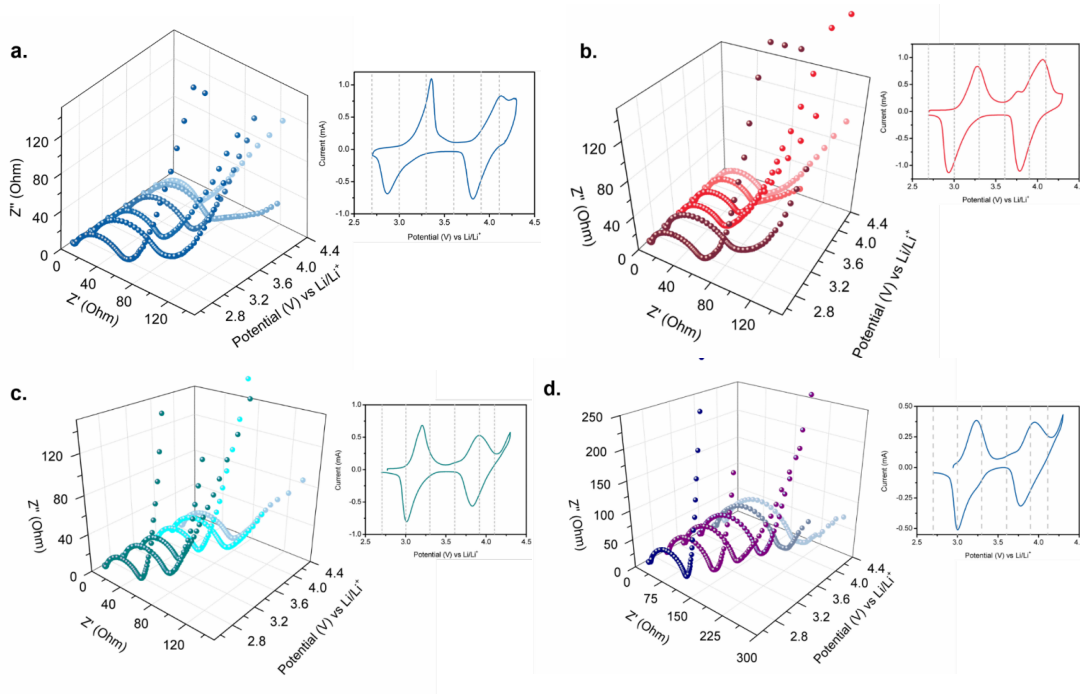


Figure 8.22. PEIS spectra at different depths of discharge for (a) poly(Ph-PZ), (b) poly(Ph-PZ)-10, (c) poly(Ph-PZ)-50, and (d) poly(TAA-PZ). Grey lines on corresponding CV show the potentials at which the impedance spectra were obtained.

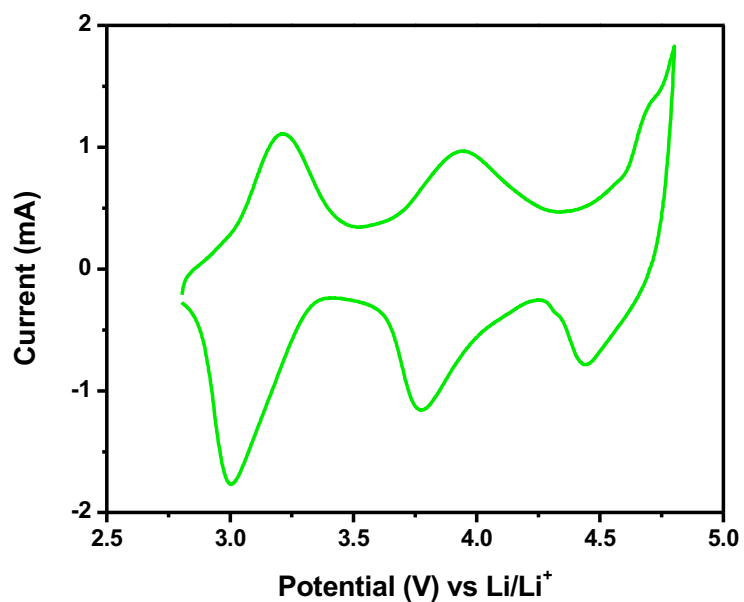


Figure 8.23. CV of poly(TAA-PZ) in a lithium half cell with 1 M LiPF₆ in 1:1 (v/v) tetramethylsulfolatne : ethyl methyl carbonate at 2 mV s⁻¹. The third redox couple, resulting from the oxidation of the triarylamine cross-linking unit, lies outside the electrochemical stability of EC/DEC.

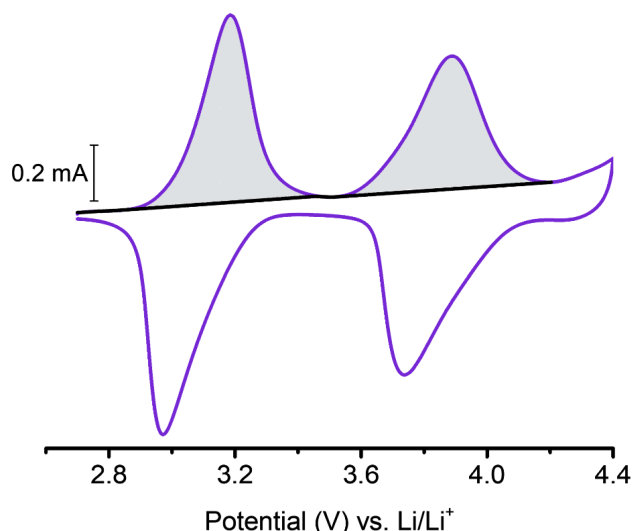


Figure 8.24. CV of Li half cell with poly(TAA-PZ) at 1 mV/s used for integration of the two oxidation peaks. The integrated peaks areas are 0.13046 and 0.12083 for the first and the second peaks, respectively. The ratio of the peaks were 1 : 0.93. Since the tertiary amine in the cross-linking unit would be expected to contribute only 2/3 of an electron for every one electron of each of the amine groups in phenazine, the two observed peaks of poly(TAA-PZ) must be from the nitrogens of phenazine.

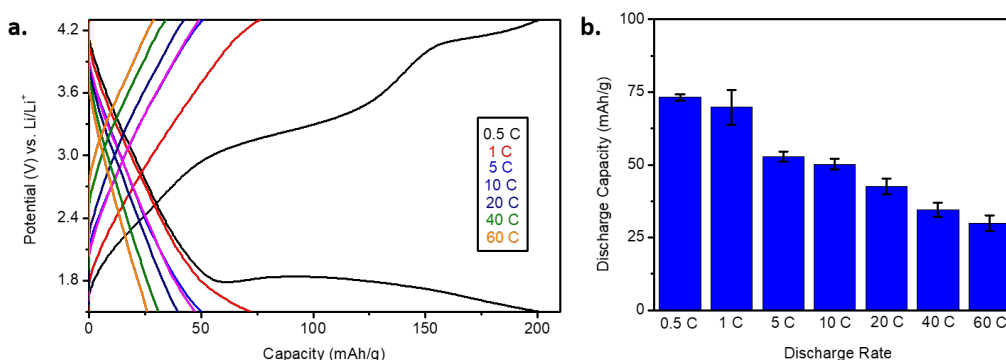


Figure 8.25. (a) Charge-discharge curves from a carbon cell, composed of a 3:3:1 ratio of Super P carbon : CMK-3 : PVDF binder on carbon paper cathode with a lithium metal anode at various rates of discharge. Capacity is normalized to the mass of the equivalent amount of active material that would be present in a typical coin cell (see Device Testing). (b) The average capacity contribution after three carbon cells. Error bars represent one standard deviation.

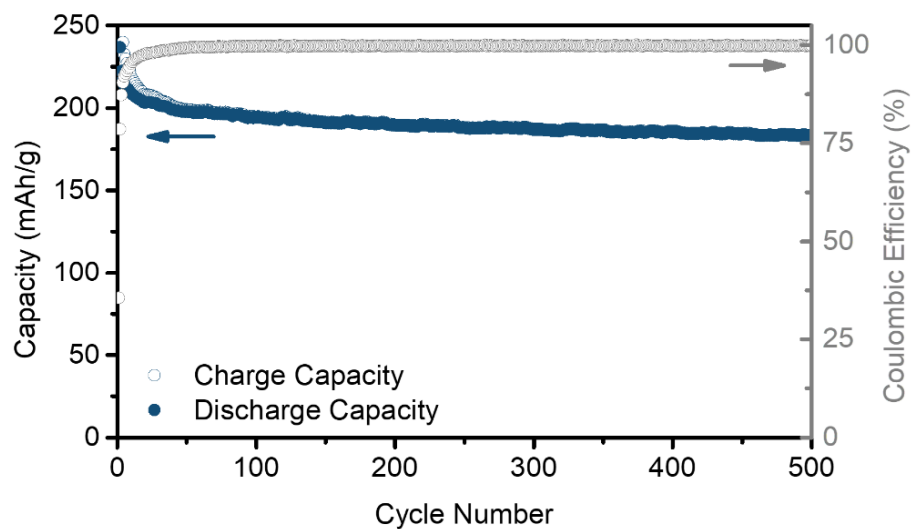


Figure 8.26. Charge capacity, discharge capacity, and coulombic efficiency of poly(Ph-PZ) for 500 cycles being charged and discharged at 5 C.

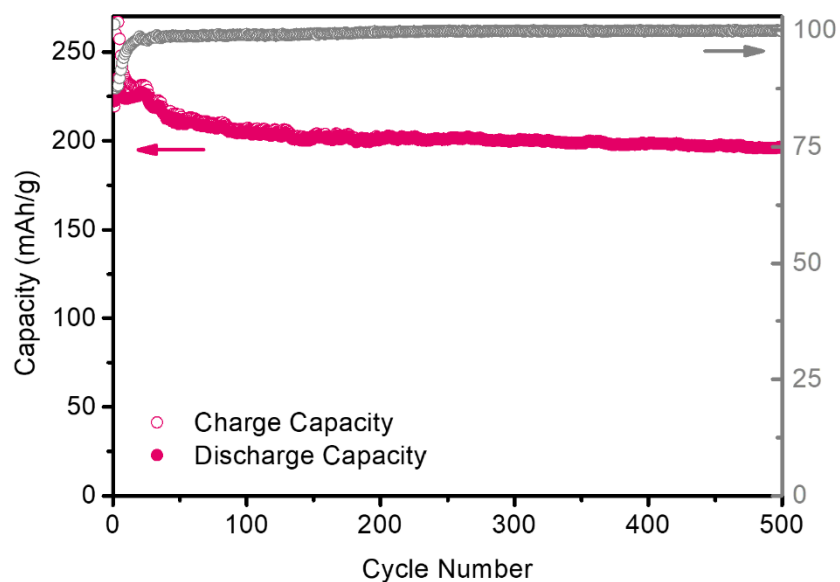


Figure 8.27. Charge capacity, discharge capacity, and coulombic efficiency of poly(Ph-PZ)-10 for 500 cycles being charged and discharged at 5 C.

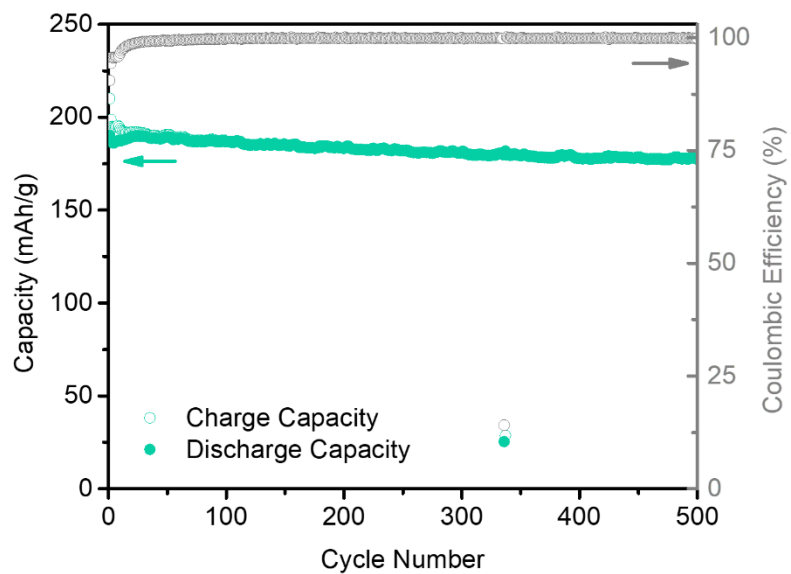


Figure 8.28. Charge capacity, discharge capacity, and coulombic efficiency of poly(Ph-PZ)-50 for 500 cycles being charged and discharged at 5 C.

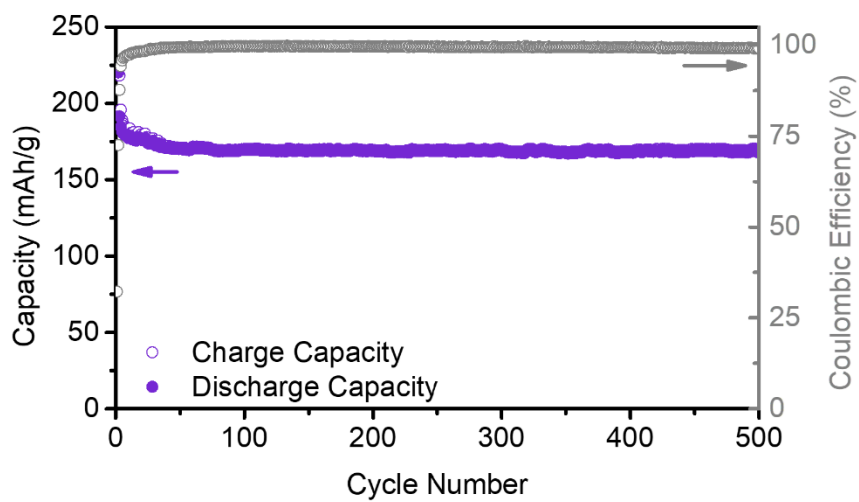


Figure 8.29. Charge capacity, discharge capacity, and coulombic efficiency of poly(TAA-PZ) for 500 cycles being charged and discharged at 5 C.

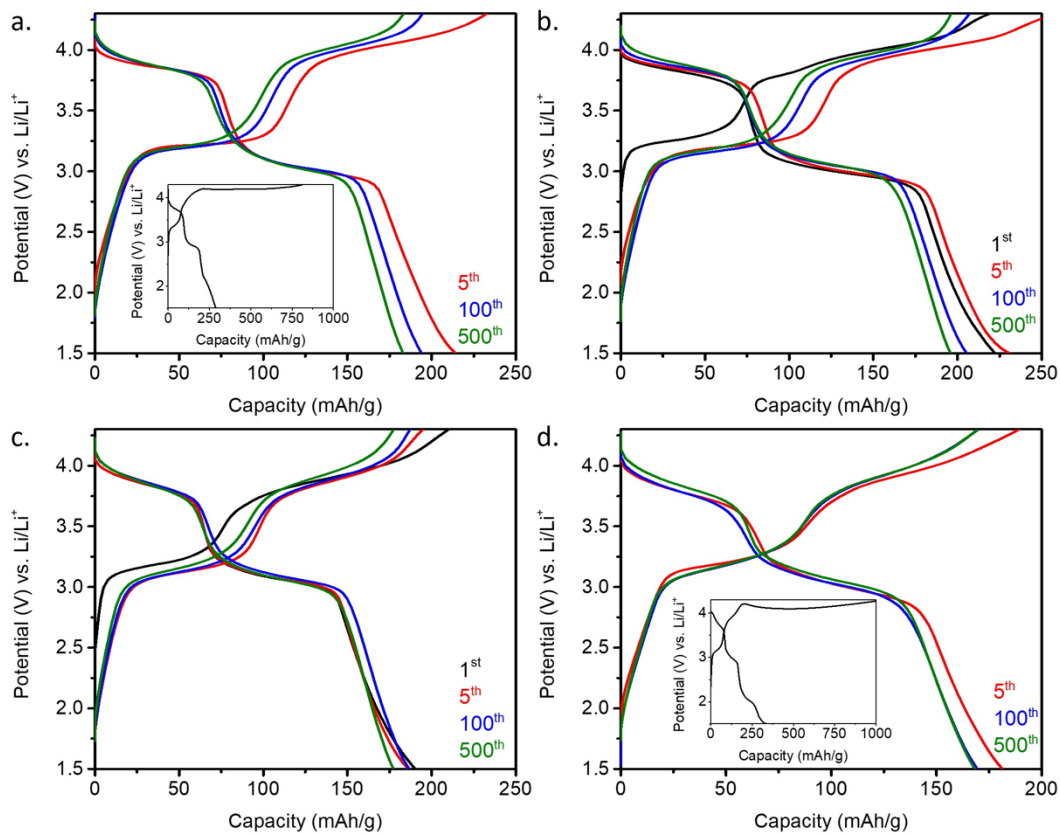


Figure 8.30. Charge-discharge profiles of (a) poly(Ph-PZ), (b) poly(Ph-PZ)-10, (c) poly(Ph-PZ)-50, and (d) poly(TAA-PZ) of the 1st, 5th, 100th, and 500th cycle of the 5 C charge-discharge experiment. The first cycle of poly(Ph-PZ) and poly(TAA-PZ) are shown in the insets due to a large overpotential associated with their first charging cycle.

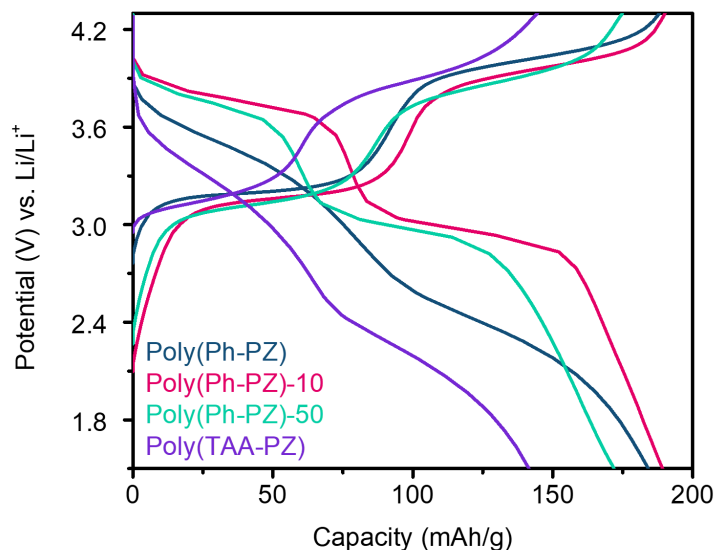


Figure 8.31. Charge-discharge profiles of poly(Ph-PZ), poly(Ph-PZ)-10, poly(Ph-PZ)-50, and poly(TAA-PZ) when charged at 5 C and discharged at 60 C. All four polymer exhibit retention of faradaic events even at high rates of discharge, while the terpolymers (poly(Ph-PZ)-10 and poly(Ph-PZ)-50) are able to retain sharp, flat plateaus.

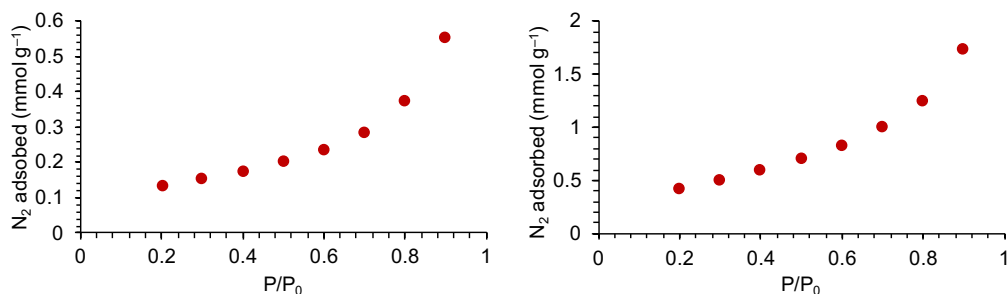


Figure 8.32. Nitrogen adsorption isotherms at 77 K of poly(Ph-PZ)-10 synthesized using dichlorobenzene (left) and dibromobenzene (right). All other analyzed polymers showed no appreciable nitrogen adsorption

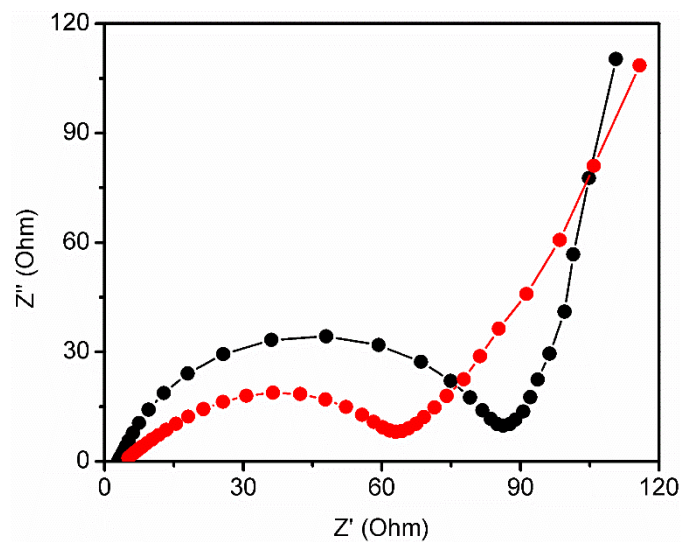


Figure 8.33. PEIS spectra of poly(Ph-PZ)-10 coin cell before (black) and after (red) ten CV cycles, where the potential was swept between 2.7 V and 4.3 V vs. Li/Li⁺ at 1 mV/s. Both spectra were taken at 2.7 V vs. Li/Li⁺. The decrease in charge transfer resistance after cycling is attributed to the formation of stable, electronically conductive interfaces in the cell.

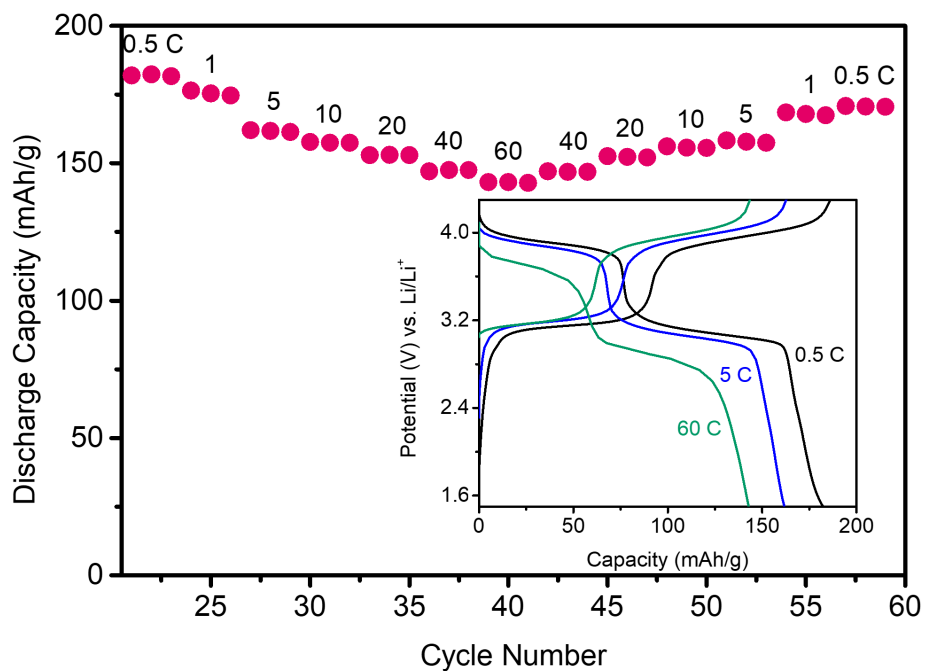


Figure 8.34. Discharge capacity of high active mass loading (6:3:1 poly(Ph-PZ)-10: conductive carbon: PVDF) cell when discharged at increasing rates. Inset: Charge-discharge curves of high mass loading cell of poly(Ph-PZ)-10 at 0.5, 5, and 60 C.

Table 8.6. Energy and power density poly(Ph-PZ), poly(Ph-PZ)-10, and commercial LiNMC (data from ref. 5) calculated with the weight of the cathode composite (active material + conducting additives + binder) and the average discharge potential vs. Li/Li⁺.

Cathode	Capacity (mAh/g)	C-Rate	Voltage vs. Li/Li⁺	Wt%^a	Energy density (Wh/kg)	Power Density (W/kg)
Poly(Ph-PZ)	209	5	3.45	0.3	216	1080
Poly(Ph-PZ)-10	223	5	3.45	0.3	230	1150
Poly(Ph-PZ)-10	220	120	3.45	0.3	227	27200
Poly(Ph-PZ)-10	167	1	3.45	0.6	340	340
Poly(Ph-PZ)-10	143	60	3.45	0.6	296	17800
Commercial LiNMC ⁵	178	0.5	3.75	0.9	601	300
Commercial LiNMC ⁵	129	5	3.75	0.9	435	2180
Commercial LiNMC ⁵	54	20	3.75	0.9	182	3650

^a Weight percent of active material in the cathode composite.

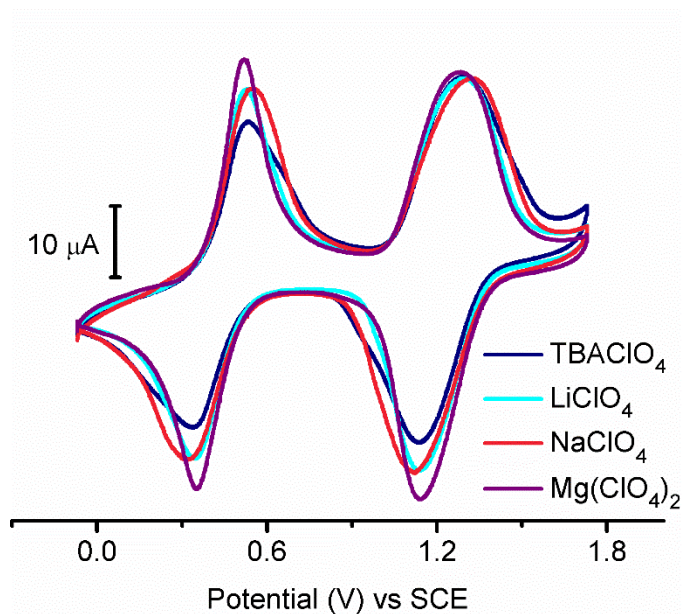


Figure 8.35. CV's of poly(Ph-PZ)-10 slurry on a glassy carbon electrode in degassed MeCN with various perchlorate electrolyte salts (0.1 M) at a scan rate of 10 mV/s. The slurry consisted of 1.5 mg of poly(Ph-PZ)-10, 3 mg of Super P carbon, and 0.5 mg of PVDF dissolved in 1 mL of NMP. The mixture was sonicated for approximately one hour until the particulates were homogeneously dispersed. 2.0 μL of the slurry were drop-cast on a polished glassy carbon electrode for a polymer loading of 0.042 mg/cm^2 . CV's were obtained in a three-compartment cell with a platinum counter electrode and Ag/Ag^+ reference electrode.

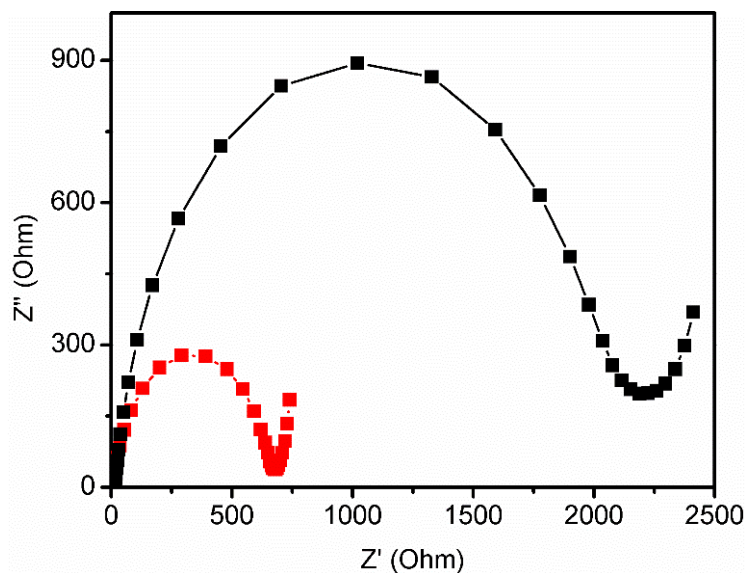


Figure 8.36. PEIS spectra of poly(Ph-PZ)-10 in a sodium half-cell before (black) and after (red) eleven CV cycles, where the potential was swept from 2.5 V to 4.0 V vs. Na/Na⁺ at 1 mV/s. Both spectra were taken with the potential held at 2.5 V vs. Na/Na⁺.

CHAPTER 9

THE EFFECTS OF ORDERING AND MORPHOLOGY ON CHARGE STORAGE MECHANISM IN ORGANIC CATHODE MATERIALS

9.1. Introduction

Electrochemical energy storage (EES) is a necessary element in utilizing energy generated from renewable sources at both mobile and grid level platforms. Lithium (Li)-ion batteries are the most widely implemented EES system, because they offer high energy densities and extended (greater than 1000) cycle lifetimes. However, there remains a challenge in designing battery systems which can be charged on the order of seconds rather than hours. Electric vehicles need rapidly charging energy storage to compete with the convenience of traditional combustion engine automobiles. In order to improve charge rates, the kinetic limitation of slow ion diffusion in the electrodes needs to be addressed.

Two approaches have been applied to improve ion diffusion and rate performance: decreasing particle size (thin films, nanowires, nanoparticles, and porous materials), and alleviating stresses from ion intercalation.¹⁻³ The former has been more thoroughly studied. Through nanoengineering battery materials, ion diffusion path lengths can be minimized and mitigate the dependence of charging and discharging on solid state diffusion. However, nano materials

introduce new challenges, including cost, increased resistivity, and increased surface area for undesirable side reactions.⁴⁻⁶

Alternatively, intercalation pseudocapacitors, amorphous materials, and crystalline materials with designed defects have all shown improved rate performance in half-cell experiments. In each, a case can be made that the improved performance is attributed to more facile ion diffusion, by one or some combination of the following approaches: reduced strain upon intercalation, eliminating phase change, providing multiple diffusion pathways, and lowering the activation barrier to ion diffusion. In all cases, when the dependence on ion diffusion has been alleviated, a more pseudocapactive response has followed, exhibiting the following features: (1) current that scales with sweep rate over potential scans, (2) narrowing of ΔE_{peak} in cyclic voltammetry response, (3) sloping galvanostatic charge discharge curves.

Improved ionic transport in these systems resulted in improved kinetics of the electrochemical reaction and improved performance. Thus, we were inspired to investigate if ion transport and electrochemical signature (pseudocapacitive or battery-type) could be controlled in organic redox active materials by tuning the morphology. While many inorganic materials have been structurally altered in order to exhibit pseudocapacitor type behavior, to the best of our knowledge no report has demonstrated a relationship between an organic material's morphology and the resulting charge storage mechanism. Herein, we

demonstrate the ability to alter charge storage mechanism by tuning the structure and morphology surrounding a shared redox active unit.

Owing to the weaker intermolecular forces in organic compounds than in inorganic compounds, many crystalline organic electrodes can tolerate high charge-discharge rates. Ion diffusion coefficients in organic-based electrodes can be improved by multiple orders of magnitude over crystalline inorganic cathodes. Additionally, ion transport in amorphous materials can often follow multiple pathways, tolerate stress of ion transport, and support even higher rates of diffusion. Therefore, we sought to determine the influence that ordering in an organic structure has on the charge storage mechanism of the electrode material.

In this study, N,N'-diphenyl-phenazine (Ph_2PZ) was selected as the charge storage unit because it exhibits fast and reversible electron transfer kinetics at high potentials, and is stable in the cationic and dicationic state, making it an ideal candidate for this study. Additionally, Ph_2PZ has demonstrated excellent performance as a charge storage unit in many different organic cathode materials.⁷⁻¹² By comparing an insoluble, crystalline molecule, $(\text{Ph-PZ})_{2.5}$, and two macromolecules, poly(Ph-PZ) and poly(135- Ph-PZ), with decreasing degrees of crystallinity, we are able to study the effect of molecular packing on the kinetics of charge storage mechanism.

9.2. Experimental Section

General Synthetic Procedures

(Ph-PZ)_{2.5} was synthesized according to previous reports.¹²

Synthesis of poly(135-Ph-PZ)

5,10-dihydrophenazine (273 mg, 1.50 mmol, 1 equiv), 1,3,5-tribromobenzene (315 mg, 1.00 mmol, 1 equiv), RuPhos (9.3 mg, 0.01 mmol, 0.01 equiv), RuPhos Pd G2 precatalyst (15.5 mg, 0.01 mmol, 0.01 equiv), and NaOtBu (346 mg, 3.6 mmol, 2.4 equiv) were added to a schenk reaction tube, evacuated and backfilled with nitrogen three times. Following, toluene (5 mL) was added via syringe. The reaction was stirred at 110 °C for 16 hours. The reaction was cooled suspended in dichloromethane (100 mL) and extracted with water (100 mL) five times, or until all sodium bromide was removed. The polymer (312 mg) was obtained as a brown powder. IR (ATR, cm⁻¹): 3033, 1573, 1478, 1440, 1319, 1279, 1243, 732, 704, 618. Elemental Anal. Found: C, 77.87; H, 10.28; N, 10.90; Br, 2.01.

Synthesis of poly(Ph-PZ)

5,10-dihydrophenazine (273 mg, 1.50 mmol, 1 equiv), 1,4-dibromobenzene (356 mg, 1.50 mmol, 1 equiv), RuPhos (7 mg, 0.01 mmol, 0.01 equiv), RuPhos Pd G2 precatalyst (11.7 mg, 0.01 mmol, 0.01 equiv), and NaOtBu (346 mg, 3.6 mmol, 2.4 equiv) were added to a schenk reaction tube, evacuated and backfilled with nitrogen three times. Following, toluene (5 mL)

was added via syringe. The reaction was stirred at 110 °C for 16 hours. The reaction was cooled suspended in dichloromethane (100 mL) and extracted with water (100 mL) five times, or until all sodium bromide was removed. The polymer (357 mg) was obtained as a tan powder. IR (ATR, cm^{-1}): 3033, 1604, 1503, 1476, 1455, 1329, 1260, 1093, 1061, 1015, 908, 817, 723, 620, 559. Elemental Anal. Found: C, 81.49; H, 4.61; N, 10.28, Br, 0.97.

Characterization

Powder X-ray diffraction measurements were recorded on a Rigaku Ultima IV X-ray diffractometer. Measurements were taken using a 40 kV operating voltage with a 44 mA current at a scan speed of 5.0 degrees per minute over a 2θ range of 5–60°. Infrared spectra were recorded on a Bruker Tensor II with an ATR attachment. Differential scanning calorimetry (DSC) measurements were acquired on a TA Instruments Q1000 with a heat/cool/heat at 10 °C/min when heating and 5 °C/min when cooling. Thermogravimetric analysis was acquired on a TA Instrument Q500 at a rate of 10 °C/min. Cyclic voltametry and potentiostatic electrochemical impedance spectroscopy (PEIS) measurements were carried out using a BioLogic SP-150 potentiostat on assembled coin cells. Galvanostatic charge/discharge experiments were conducting on a Neware battery test station. Surface area measurements were acquired with a Micromeritics 3-Flex gas sorption analyzer.

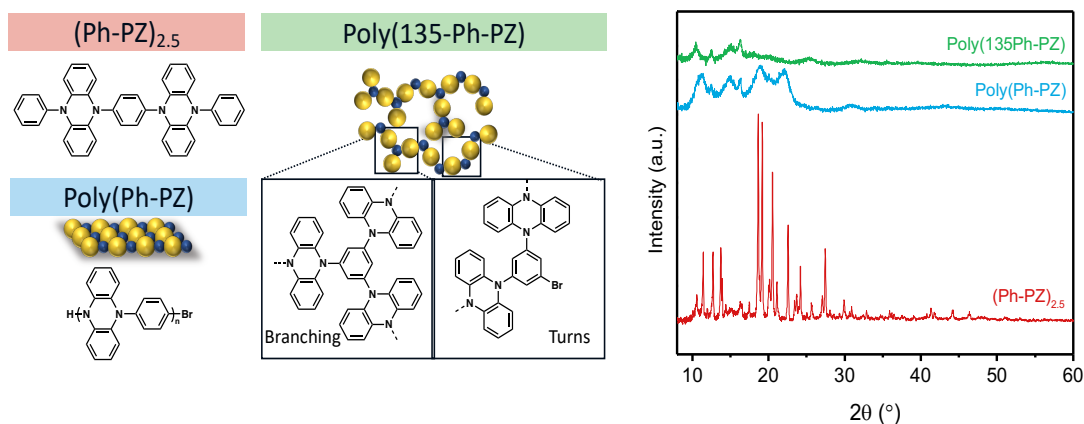


Figure 9.1. Schematic representations of the chemical structure $(\text{Ph-PZ})_{2.5}$, poly(Ph-PZ), and poly(135Ph-PZ) and their corresponding XRD spectra demonstrating the ordering of their structures.

9.3 Results and Discussion

The chemical structures of the three materials investigated are shown schematically in Figure 1a-c. The three materials display different degrees of crystallinity owing to the size of the molecules and the presence or absence of branching in the macromolecules. Poly(Ph-PZ) and poly(135Ph-PZ) lacked melting or crystallization transitions observed by DSC measurements, indicating an amorphous morphology (Figure 9.2). The XRD patterns of the three materials are shown in Figure 9.1. Poly(Ph-PZ) displayed four peaks at low angles, suggesting the presence of strongly ordered aggregates of the polymer chains. The two broad 19 and 24 degrees commonly attributed to π - π stacking between chains.¹⁰ Unlike linear poly(Ph-PZ), poly(135-Ph-PZ) contains 1,3,5 substitution about phenylene linkers which generates kinks and branches along the polymer chain. This regio-irregularity can be expected to disrupt short range

ordering and pi-pi stacking. The expected disruption of pi-pi stacking is supported by the disappearance of the peaks at 19 and 24 in the powder diffraction pattern of poly(135Ph-PZ). Although, (Ph-PZ)_{2.5} was recrystallized from toluene and displays sharp crystalline peaks in the x-ray diffraction pattern, it would be advisable to obtain a x-ray crystal structure to confirmed the packing structure within this material. With three materials containing Ph₂PZ, one crystalline and two largely amorphous materials with varying degrees of crystalline domains, we can begin to probe the influence of crystallinity on the electrochemical signature of each material.

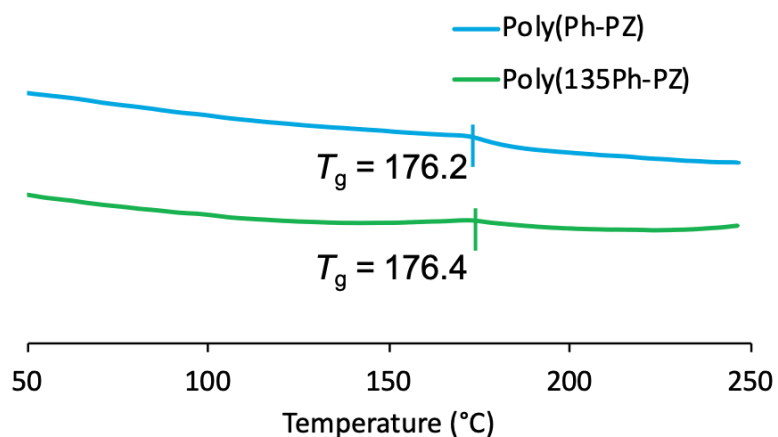


Figure 9.2. The differential scanning calorimetry traces of poly(Ph-PZ) (blue) and poly(135Ph-PZ) (green). The samples were subjected to a heat/cool/heat cycle, heated at 5 °C/min and cooled at 10 °C/min. Shown is the second heat.

Charge storage in the Ph₂PZ unit occurs by two discrete one electron oxidations at 3.2 V and 4.0 V vs. Li/Li⁺.¹¹ During the charging process, Ph₂PZ is oxidized and anions present in the electrolyte solution diffuse through the material to charge compensate the electron deficient material. The electrochemical properties of each material were determined as composites, consisting of active material (60%), conductive carbon (30%), and polyvinylidene difluoride (PVDF)(10%) in a two-electrode Li-metal half-cell with 1 M LiPF₆ in ethylene carbonate/diethyl carbonate (EC/DEC 1:1 by volume) electrolyte solution. Figure 9.3 shows the cyclic voltammograms for each of the materials when swept at 0.25 mV/s.

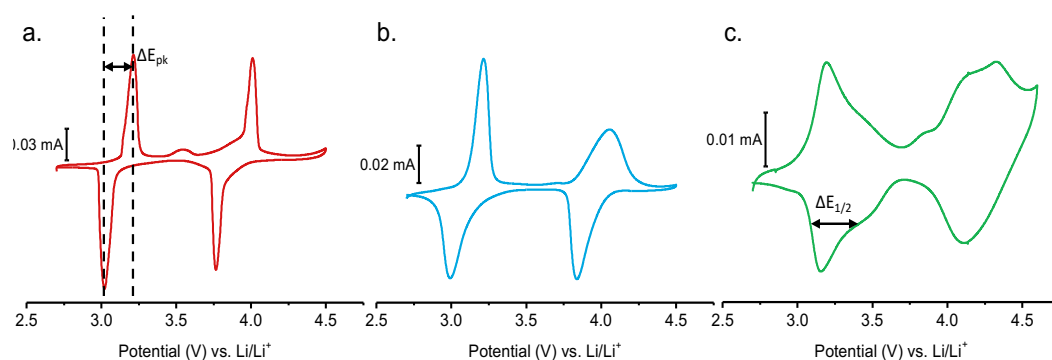


Figure 9.3. Voltammetric profiles at 0.25 mV/s of (a) (Ph-PZ)_{2.5}, (b) poly(Ph-PZ), and (c) poly(135Ph-PZ).

Large peak splitting is observed in crystalline (Ph-PZ)_{2.5} at slow scan rates in each of the redox couples. Peak splitting of the first redox and second redox couple is 210 mV and 250 mV. A large difference in the anodic and cathodic peak potentials corresponds to a significant free energy differences between the oxidized and reduced species. This likely arises from structural

changes occurring in (Ph-PZ)_{2.5} to relieve strain occurring upon insertion/removal of counterions. Structural changes can be accompanied by volumetric expansion or contraction during charge and discharge, and negatively affect device cyclability. Slowly scanning (Ph-PZ)_{2.5} at 0.05 mV/s, half-height peak widths ($\Delta E_{1/2}$) of 36 and 48 mV for each redox couple were observed (Table 9.1). Narrow $\Delta E_{1/2}$, like those of (Ph-PZ)_{2.5}, are often attributed to attractive interactions associated with the kinetics of nucleation and phase change.¹³

Table 9.1. Half-height peak widths ($\Delta E_{1/2}$) of (Ph-PZ)_{2.5}, poly(Ph-PZ), and poly(135Ph-PZ) at 0.05 mV s⁻¹ each redox

Material	Peak 1, anodic (mVs⁻¹)	Peak 1, cathodic (mVs⁻¹)	Peak 2, anodic (mVs⁻¹)	Peak 2, cathodic (mVs⁻¹)
(Ph-PZ)_{2.5}	40.2	48.1	43.1	36.3
Poly(Ph-PZ)	60.4	116	252	91.6
Poly(135Ph-PZ)	350	405	394	484

The $\Delta E_{1/2}$ of redox events in both polymers increase as crystallinity decreases relative to (Ph-PZ)_{2.5}. Broadening of the $\Delta E_{1/2}$ can be attributed to repulsive interactions between redox centers. The $\Delta E_{1/2}$ of Poly(Ph-PZ) fall between 60.4 – 252 mV (Table 9.1). Polymers are expected to have greater spatial variation than crystalline materials, therefore electron density of the PH₂PZ redox unit can vary significantly and broaden $\Delta E_{1/2}$. The first oxidation of poly(Ph-PZ) displays much more narrow $\Delta E_{1/2}$ similar to (Ph-PZ)_{2.5}, while the

peak widths of poly(135Ph-PZ) range from 350 to 484 mV. The peak width is expected to increase in poly(135Ph-PZ) due to chemical distinct redox centers at kinks and branching events, yielding a distribution of standard redox potentials throughout the material.¹⁴ This increase in $\Delta E_{1/2}$ can also be attributed to the suppression of crystalline domains by branching in the material. The peak splitting of poly(135Ph-PZ) is significantly smaller than either (Ph-PZ)_{2.5} and poly(Ph-PZ), approaching 0 mV in the second redox couple. With fewer regions of crystallinity, the energetic cost of ion pairing is alleviated, phase transitions are minimized, and the kinetics of redox events are improved. The reduced peak splitting further indicates a redox reaction not limited by ion diffusion. When redox reactions are not limited by ion diffusion, they can imitate surface controlled processes and give rise to pseudocapacitive behaviors.

Monitoring the current response over a range of scan rates offers a better understanding of the charge storage mechanism and the limiting process in these materials. Redox reactions limited by semi-infinite linear diffusion are governed by the Randles-Sevcik equation, and peak current, i_p , is proportional to the square root of sweep rate, $v^{1/2}$. Alternatively, in systems where the redox reactions are surface-controlled (not limited by diffusion), the i_p will scale with sweep rate, v . Plotting the current response, normalized to sweep rate, of potential sweeps at increasing rates between 0.25 mVs⁻¹ and 5 mVs⁻¹ allows us to visually probe the limitations of diffusion on charge storage (Figure 9.4). The profile of poly(135Ph-PZ) remains relatively constant with increasing sweep

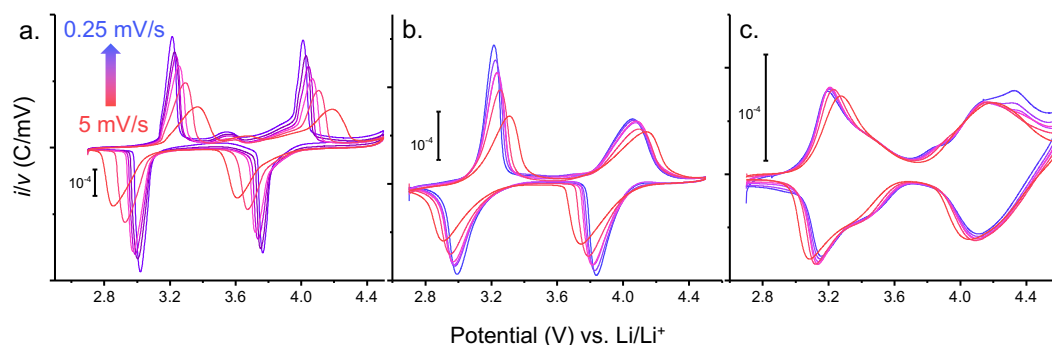


Figure 9.4. Cyclic voltammograms normalized to sweep rate for (a) (Ph-PZ)_{2.5}, (b) poly(Ph-PZ), and (c) poly(135Ph-PZ). Diffusion limitations lead to decreasing peak current at faster sweep rates in (Ph-PZ)_{2.5} and poly(Ph-PZ)

rate, indicating the reaction kinetics are not limited by ion diffusion and the process appears surface controlled. In this range of scan rates, neither ionic nor electronic diffusion through the material is the rate limiting step for charge storage. In contrast, the profiles of poly(Ph-PZ) and (Ph-PZ)_{2.5} show decreased normalized peak currents with increasing scan rate. This implies that portions of the observed response are limited by diffusion. An increase in peak splitting and $\Delta E_{1/2}$ were also observed in the profiles of poly(Ph-PZ) and (Ph-PZ)_{2.5}. This likely indicates diffusion limitations arising from the structural changes associated with the redox reactions in these materials.

The contributions of diffusion- and surface-limited processes to the total current can be quantitatively determined using the following power law¹⁶:

$$i = av^b \quad (1)$$

where a and b are adjustable parameters. A b value of 1 indicates a surface controlled process while a b value of $\frac{1}{2}$ indicates a diffusion-controlled process. Values for b are determined from plots of $\log(\text{peak current})$ vs. $\log(\text{sweep rate})$ and are displayed in Figure 9.5a. The redox processes of Poly(135Ph-PZ) are all almost entirely surface controlled, having b values of approximately 1 for each of the redox peaks. Poly(Ph-PZ) and $(\text{Ph-PZ})_{2.5}$ both possess b values between 0.5 and 1, indicating a mixture of diffusion-limited and surface controlled mechanisms. Many materials display complex charge storage mechanisms which stem from concurrent diffusion-controlled and surface-controlled contributions. The first oxidation in $(\text{Ph-PZ})_{2.5}$ displays a b value of 0.64, quantifying the high degree of diffusion limitations in the crystalline material. As crystallinity is disrupted in poly(Ph-PZ) and poly(135Ph-PZ), b values increase. The b values of poly(Ph-PZ) fall between 0.77 and 0.94.

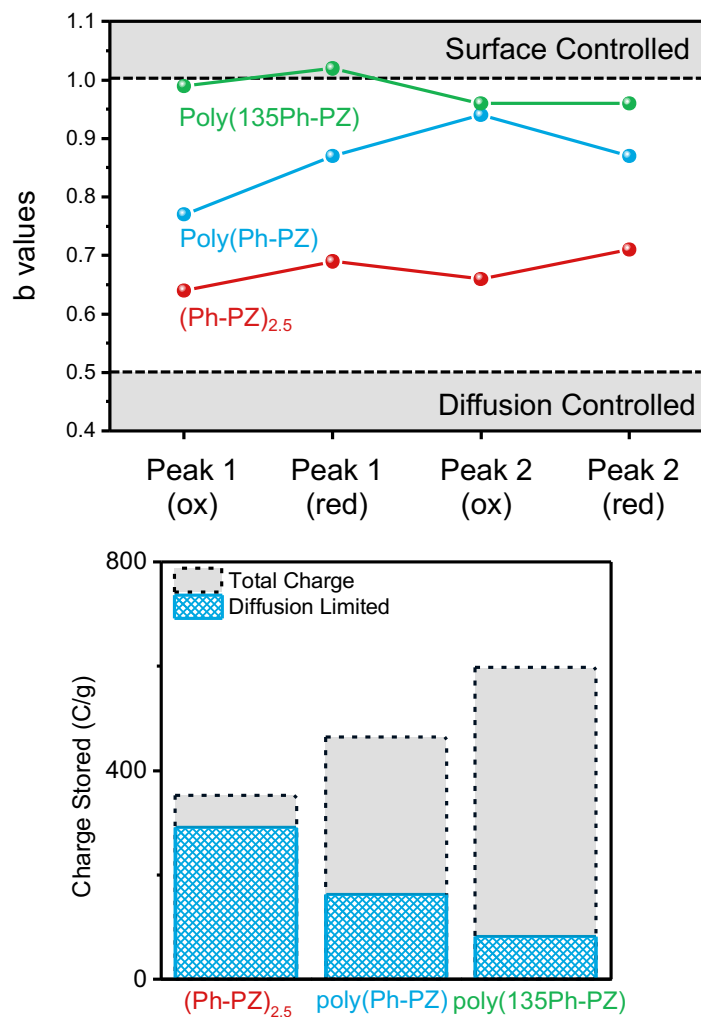


Figure 9.5. (a) The b values of $(\text{Ph-PZ})_{2.5}$, poly(Ph-PZ), poly(135Ph-PZ) for the 0 to +1 (first redox couple) and +1 to +2 (second redox couple) redox events. (b) the contribution of diffusion-limited faradaic charge processes to the total amount of charge stored when cycled at 0.05 mV/s for each of the materials.

Poly(135Ph-PZ) displays the most surface controlled charge storage mechanism with b values near 1 for each redox event. Values near 1 are commonly observed in pseudocapacitive materials with minimized ion diffusion or in structures that support facile ion transport.

Further breakdown of the charge storage mechanism, diffusive or surface-controlled, can be achieved using the following equation:

$$i = k_1\nu + k_2\nu^{1/2} \quad (2)$$

If the total current is assumed to derive from either diffusive or surface controlled faradaic processes, then k_1 and k_2 are constants corresponding to the surface-controlled and diffusion-controlled currents at a given potential, respectively. Inspection of these profiles illustrates a shift in charge storage mechanism from a diffusion-controlled process to a surface-controlled process with decreasing ordering in the cathode materials. The current delivered by either mechanism is depicted in the bar graph in Figure 9.5b. Almost all charge stored in (Ph-PZ)_{2.5} arises from diffusion-controlled processes, except for small contributions arising from the formation of an electric double layer. In stark contrast, charge storage in poly(135Ph-PZ) is dominated by surface-controlled processes.

Galvonastatic intermittent titration technique (GITT) was used to determine the diffusion coefficient of each material throughout the charging and discharging processes. The limiting diffusion coefficients of poly(Ph-PZ) and poly(135Ph-PZ) differ by nearly 2 orders of magnitude. This supports the analysis of peak splitting and $\Delta E_{1/2}$, which suggested that diffusion is improved

in the less ordered material. While the diffusion coefficients of each polymer are nearly the same at potentials where no faradaic reactions occur, the coefficient of diffusion in poly(Ph-PZ) dropped by over an order of magnitude during the charge and discharge of the first redox event, between 3.0 to 3.2 V vs Li⁺/Li. This decrease in diffusion is not observed in poly(135Ph-PZ), indicating that the disruption of ordering in the branched polymer facilitates fast ion diffusion even at moments of high ion flux during faradaic reactions. A less pronounced drop in diffusion coefficient is observed over the charging of the second redox event in both poly(Ph-PZ) and poly(135Ph-PZ). The first redox event of poly(Ph-PZ) is the most limited by diffusion, indicated by a b value of 0.77 and supported by the decrease in diffusion coefficient observed during this redox event. The diffusion limited kinetics observed of this redox couple likely rises from structural rearrangements associated with swelling the neutral polymer with counter ions and the accompanying solvent molecules. The swelled and ionic polymer, is more suited to support ionic transport leading to faster ion diffusion and more pseudocapactive charge storage over the second redox event.

Lastly, the electrochemical signature of the galvanostatic charge/discharge (GCDC) traces of (Ph-PZ)_{2.5}, poly(Ph-PZ), and poly(135Ph-PZ) can provide insight into the charge storage mechanism (Figure 9.6). Each material exhibits electrochemical signatures consistent with those observed by cyclic voltammetry. Consistent with the peak splitting in the CV, the materials with less ordered domains exhibit less polarization when charged and

discharged at 1 A/g (~5C). Flat plateaus were observed GCD profiles of $(\text{Ph-PZ})_{2.5}$, while sloping arose in poly(Ph-PZ) and poly(135Ph-PZ). Flat plateaus and charge storage at a constant potential, as observed in the more ordered materials, is characteristic of a battery-type material. Conversely, sloping plateaus and a nearly linear relationship between potential and capacity is an electrochemical signature of a pseudocapacitor. Poly(135Ph-PZ) exhibits more sloping plateaus, its electrochemical signatures indicate a charge storage mechanism with significantly decreased diffusion control and increasingly pseudocapacitive nature when compared to its more ordered counterparts.

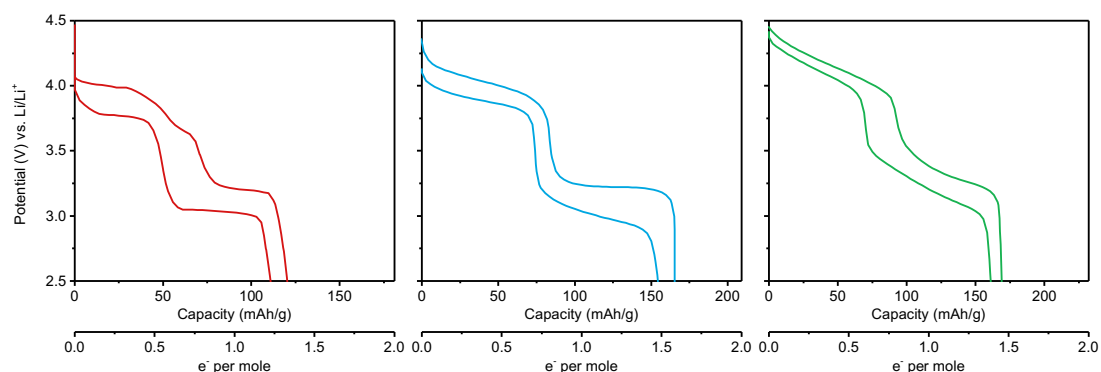


Figure 6. The galvanostatic charge discharge traces of $(\text{Ph-PZ})_{2.5}$ (left, red), poly(Ph-PZ) (center, blue), and poly(135Ph-PZ) (right, green).

9.4 Conclusion

Thus, we have shown that the charge storage mechanism in organic materials can be dictated through manipulation of the materials morphology. The redox active unit Ph_2PZ was embedded in 3 materials displaying varying degrees of ordering. Within crystalline $(\text{Ph-PZ})_{2.5}$, charge storage was limited by

diffusion of ions, due in large part to the energetic cost of reorganization within the crystalline domains. By disrupting the ordering in poly(Ph-PZ) and poly(135Ph-PZ), it is possible to support ion diffusion and alleviate diffusion-limitations associated with the charge storage mechanism. Facilitating ion diffusion within poly(135Ph-PZ) lead to an electrochemical signature more consistent with pseudo capacitive energy storage, characterized by broadened $\Delta E_{1/2}$ and sloping discharge curves. This approach to organic cathode design could be used as a template to develop new materials with high energy density and excellent rate capabilities.

9.5 References

- (1) Tanh-Tam, T.; Coates, G. W.; Abruña, H. D. *Chem. Commun.* **2015**, *51*, 14674.
- (2) Nisula, M.; Karppinen, M. *J. Mater. Chem. A* **2018**, *6*, 7027.
- (3) Koshika, K.; Sano, N.; Oyaizu, K.; Nishide, H. *Chem. Commun.* **2009**, *7*, 836.
- (4) Zhang, Q.; Uchaker, E.; Candelariuz, S. L.; Cao, G. *Chem. Soc. Rev.*, **2013**, *42*, 3127.
- (5) Maier, J. *Nat. Mater.* **2005**, *4*, 805.
- (6) Levi, M. D.; Salitra, G.; Markovsky, B.; Teller, H.; Aurbach, D.; Heider, U.; Heider, L. *J. Electrochem. Soc.* **1999**, *146*, 1279.

- (7) Dai, G.; He, Y.; Niu, Z.; He, P.; Zhang, C.; Zhao, Y.; Zhang, X.; Zhou, H. *Chem. Int. Ed.* **2019**, *58*, 9902.
- (8) Dai, G.; Liu, Y.; Niu, Z.; He, P.; Zhao, Y.; Zhang, X.; Zhou, H. *Matter* **2019**, *1*, 945.
- (9) Obrezkov, F. A.; Ramezankhani, V.; Zhidkov, I.; Traven, V. F.; Kurmaev, E. Z.; Stevenson, K.J.; Troshin, P.A. *J. Phys. Chem. Lett.* **2019**, *10*, 5440.
- (10) Dai, G.; Wang, X.; Qian, Y.; Niu, Z.; Zhu, X.; Ye, J.; Zhao, Y.; Zhang, X. *Energy Storage Mater.* **2019**, *16*, 236.
- (11) Gannett, C. N.; Peterson, B. M.; Shen, L.; Seok, J.; Fors, B.P.; Abruña, H. D. *ChemSusChem* **2020**, *13*, 2428.
- (12) Lee, M.; Hong, J.; Lee, B.; Ku, K.; Lee, S.; Park, C. B.; Kang, K. *Green Chem.* **2017**, *19*, 2980.
- (13) Lukatskaya, M. R.; Dunn, B.; and Gogotsi, Y. *Nat. Commun.* **2016**, *7*, 1.
- (14) Peerce, P.J.; Bard, A.J. *J. Electroanal. Chem. Interf. Electrochem.* **1980**, *114*, 89.
- (15) Laviron, E. *J. Electroanal. Chem. Interf. Electrochem.* **1979**, *101*, 19.
- (16) Lindström, H.; Södergren, S.; Solbrand, A.; Rensmo, H.; Hjelm, J.; Hagfeldt, A.; Lindquist, S. E. *J. Phys. Chem. B.* **1997**, *101*, 7717.